
Digital Waveguide Mesh Topologies in Room Acoustics Modelling

Damian Thomas Murphy

A thesis submitted in partial fulfilment of the requirements for the degree of
Doctor of Philosophy in Music Technology

THE UNIVERSITY *of York*



DEPARTMENT OF ELECTRONICS

FEBRUARY 2000

Abstract

All sounds have associated with them an environmental context related to the acoustic space within which they are heard. Composers have long used and manipulated these properties of sounds in space as a fundamental part of their music. Many methods have been used to simulate the acoustics of an enclosed space, and recently digital waveguide mesh models have provided an accurate and efficient method of modelling this physically complex system. Current waveguide models used in the field of room acoustics are based on a rectilinear mesh topology and are limited to providing only a partial solution to an accurate Room Impulse Response (RIR).

This thesis examines the use of 2-D digital waveguide mesh structures in room acoustics modelling. It is hypothesised that the limitations and accuracy of such models can be improved upon by using a mesh topology based on a triangular decomposition of the 2-D plane. The *WaveVerb* System has been developed to allow RIRs to be generated from a 2-D representation of a room using both rectilinear and triangular mesh topologies, with an emphasis on its use as a high level creative tool for the computer musician.

Results from both mesh topologies are analysed. In the first instance wave propagation through the modelled room can be observed visually through an animated graphical representation. The spectral content of the measured RIRs from both models is also analysed and further comparisons are made against standard room acoustic parameters. Audio samples are convolved with measured RIRs in order to evaluate the subsequent environmental context. All of these results point to the fact that the triangular mesh topology offers a significant improvement in terms of quality and accuracy over that of the more commonly used rectilinear waveguide mesh.

Finally, possible future developments for the *WaveVerb* system are presented. These include methods to improve execution time and extend the model to three dimensions, as well as investigating its potential use as a teaching aid.

Contents

Abstract.....	ii
Contents.....	iii
List of Tables.....	ix
List of Figures.....	x
Acknowledgements.....	xv
Declaration.....	xvi
Chapter 1 Introduction	1
1.1 Background.....	1
1.1.1 Composing With Space.....	1
1.1.2 Room Acoustics.....	4
1.1.3 Room Acoustics Modelling.....	5
1.2 Aims of Research.....	6
1.2.1 Motivation.....	6
1.2.2 Statement of Hypothesis.....	7
1.2.3 Thesis Structure.....	8
1.2.4 Contribution to the Field.....	9
1.3 Summary.....	10
Chapter 2 The Soundfield in an Enclosed Space	11
2.1 Introduction.....	11
2.2 The Room as a System.....	11
2.3 Sound in an Enclosed Space.....	11
2.3.1 The Direct Sound.....	12
2.3.2 Early Reflections.....	14
2.3.3 The Reverberant Sound.....	15
2.4 Room Modes.....	15
2.4.1 Calculation of Room Modes.....	16
2.4.2 Influence of Modes on the Acoustics of a Room	18
2.5 Frequency Regions.....	18
2.6 The Room Impulse Response.....	19
2.6.1 RIR Measurement.....	20
2.6.2 Time Delay Spectrometry, (TDS).....	21

2.6.3	Maximum Length Sequence Signal Analysis, MLSSA.	21
2.7	Acoustic Measurements and Preference Criteria.....	21
2.7.1	Reverberation Time, (RT_{60}).....	22
2.7.2	Early Decay Time, (EDT).....	24
2.7.3	Initial Time Delay Gap, (ITDG).....	24
2.7.4	Early to Late Sound Index, (C_{80}).....	25
2.7.5	Centre Time, (T_s).....	26
2.7.6	Sound Strength, (G).....	26
2.7.7	Early Lateral Energy Fraction, (LF).....	26
2.7.8	Inter-Aural Cross-Correlation, (IACC).....	26
2.8	Aural and Visual Cues.....	27
2.9	Summary.....	31
Chapter 3 Artificial Reverberation		34
3.1	Introduction.....	34
3.2	Electro-Mechanical Reverberation.....	34
3.2.1	Reverb Chambers.....	34
3.2.2	Duct Reverbs.....	35
3.2.3	Spring Reverbs.....	36
3.2.4	Plate Reverbs.....	36
3.3	Digital Reverb.....	37
3.3.1	Building Digital Rooms – Unit Reverberators.....	38
3.3.2	Combining Unit Reverberators.....	40
3.3.3	Reverberation Using Convolution.....	41
3.4	Auralization.....	43
3.4.1	Fully Computer Auralization.....	43
3.4.2	Computed Multiple-Loudspeaker Auralization.....	44
3.4.3	Direct Acoustic Scale-Model Auralization.....	44
3.4.4	Indirect Acoustic Scale Model Auralization.....	44
3.4.5	Some Potential Uses of Auralization Techniques.....	45
3.5	Summary.....	45
Chapter 4 Acoustic Modelling Techniques		48
4.1	Introduction.....	48
4.2	Geometrical Models.....	49
4.2.1	Overview.....	49
4.2.2	Ray-Tracing Method.....	49

4.2.3	Image-Source Method.....	51
4.3	Finite Element Analysis.....	52
4.3.1	The Finite Element Method, (FEM).....	52
4.3.2	The Boundary Element Method, (BEM).....	54
4.3.3	Suitability of the FEM and BEM.....	55
4.4	Finite Difference Time Domain (FDTD) Models.....	56
4.5	Waveguide Modelling Techniques.....	57
4.5.1	The Basic Digital Waveguide Element.....	57
4.5.2	Signal Scattering.....	59
4.5.3	Finite Difference and DSP Formulations.....	62
4.5.4	Applications and Limitations.....	64
4.6	Summary.....	69
 Chapter 5 Mesh Construction and Implementation		75
5.1	Introduction.....	75
5.2	Unit Scattering Junctions.....	76
5.3	Mesh Construction.....	77
5.3.1	Boundary Conditions – The General Case.....	77
5.3.2	Boundary Conditions – Exceptional Cases.....	82
5.4	Mesh Excitation.....	85
5.5	Mesh Output.....	90
5.6	Dispersion Error.....	93
5.7	Software Design and Implementation.....	96
5.7.1	Memory Usage.....	97
5.7.2	Description of Program Structures.....	98
5.8	Program Flow.....	105
5.8.1	Initialisation.....	106
5.8.2	Scattering Pass.....	108
5.8.3	Delay Pass.....	108
5.9	Output Formats.....	109
5.10	Mesh Animation and Visualisation.....	110
5.10.1	Double Buffering.....	110
5.10.2	Viewing and Modelling.....	110
5.10.3	Testing and Verificiation.....	111
5.11	Summary.....	112

Chapter 6 Results	115
6.1 Introduction.....	115
6.2 Observation of Standard Wave Phenomena.....	116
6.2.1 Mesh Excitation and Observation of Wavefront.....	116
6.2.2 Reflection.....	117
6.2.3 Diffraction and Interference.....	119
6.2.4 Further Interference Effects.....	121
6.2.5 Discussion.....	122
6.3 Case Study.....	124
6.4 Modal Analysis.....	127
6.4.1 Room A.....	128
6.4.2 Room B.....	129
6.4.3 Room C.....	130
6.4.4 Room D.....	131
6.4.5 Discussion.....	132
6.5 Frequency Response Analysis.....	133
6.5.1 Room A – Abs0.9.....	135
6.5.2 Room A – Abs0.4.....	136
6.5.3 Room A – AbsComplex.....	137
6.5.4 Room B – Abs0.9.....	138
6.5.5 Room B – Abs0.4.....	139
6.5.6 Room B – AbsComplex.....	140
6.5.7 Room C – Abs0.9.....	141
6.5.8 Room C – Abs0.4.....	142
6.5.9 Room C – AbsComplex.....	143
6.5.10 Room D – Abs0.9.....	144
6.5.11 Room D – Abs0.4.....	145
6.5.12 Room D – AbsComplex.....	146
6.5.13 Discussion.....	147
6.6 Acoustic Parameter Analysis.....	151
6.6.1 RT_{60} – Abs0.9.....	153
6.6.2 RT_{60} – Abs0.4.....	154
6.6.3 RT_{60} – AbsComplex.....	155
6.6.4 Spatial Average RT_{60} – For Each Room.....	156
6.6.5 Spatial Average RT_{60} - For Each Absorption Condition	157
6.6.6 C_{80} – Abs0.9.....	158
6.6.7 C_{80} – Abs0.4.....	159

6.6.8	C_{80} – Abscomplex.....	160
6.6.9	EDT – Abs0.9.....	161
6.6.10	EDT and RT_{60} – Spatially Averaged – Abs0.9.....	162
6.6.11	Discussion.....	163
6.7	Audio Examples.....	165
6.7.1	Discussion.....	167
6.8	Summary.....	169
Chapter 7 Conclusions		173
7.1	Summary and Conclusions.....	173
7.1.1	Hypothesis.....	173
7.2	The Future.....	179
7.3	Further Work.....	179
7.3.1	Boundary Conditions and Air Absorption.....	179
7.3.2	Three Dimensions and Parallel Implementation.....	180
7.3.3	Surround Sound.....	181
7.3.4	User Interface.....	181
7.4	Publications.....	182
Appendix A Mathematical Derivations		183
A.1	The General Scattering Equation.....	183
A.2	Finite Difference Formulation of Scattering Equations.....	185
A.3	Finite Difference Formulation of Boundary Conditions.....	187
Appendix B Octave Band Acoustical Parameters		190
B.1	Room A – Abs0.9.....	190
B.2	Room A – Abs0.4.....	192
B.3	Room A – AbsComplex.....	194
B.4	Room B – Abs0.9.....	196
B.5	Room B – Abs0.4.....	198
B.6	Room B – AbsComplex.....	200
B.7	Room C – Abs0.9.....	202
B.8	Room C – Abs0.4.....	204
B.9	Room C – AbsComplex.....	206
B.10	Room D – Abs0.9.....	208
B.11	Room D – Abs0.4.....	211

B.12	Room D – AbsComplex.....	213
Appendix C	Guide to Audio CD	216
Appendix D	Guide to Data CD	219
Appendix E	CD-1, Audio	222
Appendix F	CD-2, Data	223
Glossary		224
References		229

List of Tables

2.1	Sepmeyer rectangular room dimension ratios for favourable mode distribution..	17
3.1	Real time convolution performance limits of a Pentium MMX 200MHz CPU...	42
5.1	The ten distinct junction types that could arise in the rectilinear mesh.....	84
5.2	The twenty distinct junction types that could arise in the triangular mesh.....	86
6.1	Direct source to listener distances for the four variable listener positions used in each room.....	125
6.2	The three different sets of absorption conditions used to vary the absorption ratios at the walls for each room.....	126
6.3	Dimensions of each of the four rooms for each mesh, in number of junctions....	126

List of Figures

1.1	A 17 th Century room attributed to Athanasius Kircher (1601-1680).....	4
2.1	Block diagram of the room as a system.....	11
2.2	Plan view of an enclosed space with source and listening positions marked.....	12
2.3	The direct sound caused by an impulse arrives at the listening position.....	14
2.4	Early reflections arrive at the listening position.....	14
2.5	The exponentially decaying reverberant sound.....	15
2.6	The first three pressure standing waves between two rigid reflective walls.....	16
2.7	A rectangular room L m long, W m wide and H m high.....	17
2.8	The audio spectrum divided up into four regions.....	18
2.9	(a) Ideal reverberation time. (b) A measure of Early Decay Time.....	24
2.10	The Early to Late Sound Index, also known as Clarity, C_{80}	25
2.11	Visualising sound wave propagation in a model of New Theatre, New York.....	30
3.1	An acoustic reverberation chamber.....	35
3.2	A duct type reverb.....	35
3.3	Cross section of a spring reverb system.....	36
3.4	Cross section of a plate reverb system.....	37
3.5	Comb filter unit reverberator.....	38
3.6	Modified comb filter giving an allpass unit reverberator.....	39
3.7	Combinations of unit reverberators making a full reverberation simulation.....	40
4.1	A simple two-dimensional ray-tracing model.....	50
4.2	Improvements on ray-tracing. (a) Cone tracing. (b) Pyramid tracing.....	51
4.3	Demonstration of the image-source method.....	52
4.4	A general mechanical system with one degree of freedom.....	53
4.5	(a) 20-node pressure based acoustic finite element. (b) Resulting 3-D mesh.....	53
4.6	The definition of the derivative, $df(x)/dx$, of the function $f(x)$	56
4.7	Digital waveguide implemented using a pair of bi-directional delay lines.....	58
4.8	A general scattering junction J with N connected waveguide for $i = 1, 2, \dots, N$	59
4.9	A 2-D waveguide mesh constructed from linked parallel 1-D “strings”.....	61
4.10	Possible topological arrangements of scattering junctions.....	62
4.11	General 4-port scattering junction used in the 2-D rectilinear waveguide mesh..	62
4.12	Directional dispersion error on a typical section of the 2-D rectilinear mesh.....	66
4.13	2-D waveguide mesh topologies with associated dispersion analysis measures..	67
5.1	(a) 4-port scattering junction. (b) 6-port scattering junction.....	76
5.2	Termination of a waveguide mesh due to a boundary resulting in a reflection...	78

5.3	Signal-flow representation of the junction between two lossless tubes.....	81
5.4	A corner of the rectilinear mesh noting that the corner element is not connected	82
5.5	A more complex room resulting in different types of boundary junctions.....	82
5.6	Rectilinear and triangular mesh constructions based on the room in Fig. 5.4.....	83
5.7	Mesh excitation using a one way waveguide element to input a signal.....	88
5.8	Mesh excitation signals. (a) Dirac Impulse. (b) Gaussian Impulse.....	90
5.9	A soundfield can be decomposed into four spherical harmonic components.....	91
5.10	Measuring the B-format X-component from (a) rectilinear, (b) triangular mesh.	92
5.11	Dispersion error as measured on the rectilinear mesh.....	95
5.12	Dispersion error as measured on the triangular mesh.....	95
5.13	Typical data structure used to define the triangular mesh and how it is interpreted by the program.....	100
5.14	Valid connections are made between junctions using pointers to their neighbours on the mesh according to the corresponding junction types.....	101
5.15	Passing a signal from junction to junction involves setting the output value to the input value of neighbouring junctions according to connections that are valid.....	102
5.16	Iterative two-pass computation algorithm describing program flow and model execution.....	105
5.17	Camera analogy showing how a computer deals with rendering and viewing an object.....	111
6.1	Wavefronts visible due to rectilinear mesh being excited with a Gaussian impulse applied over 6 time steps.....	116
6.2	Wavefronts at the same time step on (a) rectilinear mesh, (b) triangular mesh...	117
6.3	Reflection at a wall (a) with reversal of phase, (b) with preservation of phase...	117
6.4	Graphical interface for <i>WaveVerb</i> System demonstrating anechoic conditions..	118
6.5	Diffraction and interference effects on the rectilinear mesh.....	119
6.6	A ray-tracing example of the situation shown in Fig 6.5.....	120
6.7	Diffraction and reflection due to an object being placed in the room.....	120
6.8	Demonstrating the principle of speaker delay towers.....	121
6.9	A room with slightly concave ends demonstrating a focal point.....	122
6.10	The four different sized rooms used as part of the case study.....	125
	Modal Analysis: Room A: Output Point 1.....	128
	Modal Analysis: Room A: Output Point 2.....	128
	Modal Analysis: Room A: Output Point 3.....	128
	Modal Analysis: Room A: Output Point 4.....	128
	Modal Analysis: Room B: Output Point 1.....	129

Modal Analysis: Room B: Output Point 2.....	129
Modal Analysis: Room B: Output Point 3.....	129
Modal Analysis: Room B: Output Point 4.....	129
Modal Analysis: Room C: Output Point 1.....	130
Modal Analysis: Room C: Output Point 2.....	130
Modal Analysis: Room C: Output Point 3.....	130
Modal Analysis: Room C: Output Point 4.....	130
Modal Analysis: Room D: Output Point 1.....	131
Modal Analysis: Room D: Output Point 2.....	131
Modal Analysis: Room D: Output Point 3.....	131
Modal Analysis: Room D: Output Point 4.....	131
Frequency Response Analysis: Room A – Abs0.9: Output Point 1.....	135
Frequency Response Analysis: Room A – Abs0.9: Output Point 2.....	135
Frequency Response Analysis: Room A – Abs0.9: Output Point 3.....	135
Frequency Response Analysis: Room A – Abs0.9: Output Point 4.....	135
Frequency Response Analysis: Room A – Abs0.4: Output Point 1.....	136
Frequency Response Analysis: Room A – Abs0.4: Output Point 2.....	136
Frequency Response Analysis: Room A – Abs0.4: Output Point 3.....	136
Frequency Response Analysis: Room A – Abs0.4: Output Point 4.....	136
Frequency Response Analysis: Room A – AbsComplex: Output Point 1.....	137
Frequency Response Analysis: Room A – AbsComplex: Output Point 2.....	137
Frequency Response Analysis: Room A – AbsComplex: Output Point 3.....	137
Frequency Response Analysis: Room A – AbsComplex: Output Point 4.....	137
Frequency Response Analysis: Room B – Abs0.9: Output Point 1.....	138
Frequency Response Analysis: Room B – Abs0.9: Output Point 2.....	138
Frequency Response Analysis: Room B – Abs0.9: Output Point 3.....	138
Frequency Response Analysis: Room B – Abs0.9: Output Point 4.....	138
Frequency Response Analysis: Room B – Abs0.4: Output Point 1.....	139
Frequency Response Analysis: Room B – Abs0.4: Output Point 2.....	139
Frequency Response Analysis: Room B – Abs0.4: Output Point 3.....	139
Frequency Response Analysis: Room B – Abs0.4: Output Point 4.....	139
Frequency Response Analysis: Room B – AbsComplex: Output Point 1.....	140
Frequency Response Analysis: Room B – AbsComplex: Output Point 2.....	140
Frequency Response Analysis: Room B – AbsComplex: Output Point 3.....	140
Frequency Response Analysis: Room B – AbsComplex: Output Point 4.....	140
Frequency Response Analysis: Room C – Abs0.9: Output Point 1.....	141
Frequency Response Analysis: Room C – Abs0.9: Output Point 2.....	141

Frequency Response Analysis: Room C – Abs0.9: Output Point 3.....	141
Frequency Response Analysis: Room C – Abs0.9: Output Point 4.....	141
Frequency Response Analysis: Room C – Abs0.4: Output Point 1.....	142
Frequency Response Analysis: Room C – Abs0.4: Output Point 2.....	142
Frequency Response Analysis: Room C – Abs0.4: Output Point 3.....	142
Frequency Response Analysis: Room C – Abs0.4: Output Point 4.....	142
Frequency Response Analysis: Room C – AbsComplex: Output Point 1.....	143
Frequency Response Analysis: Room C – AbsComplex: Output Point 2.....	143
Frequency Response Analysis: Room C – AbsComplex: Output Point 3.....	143
Frequency Response Analysis: Room C – AbsComplex: Output Point 4.....	143
Frequency Response Analysis: Room D – Abs0.9: Output Point 1.....	144
Frequency Response Analysis: Room D – Abs0.9: Output Point 2.....	144
Frequency Response Analysis: Room D – Abs0.9: Output Point 3.....	144
Frequency Response Analysis: Room D – Abs0.9: Output Point 4.....	144
Frequency Response Analysis: Room D – Abs0.4: Output Point 1.....	145
Frequency Response Analysis: Room D – Abs0.4: Output Point 2.....	145
Frequency Response Analysis: Room D – Abs0.4: Output Point 3.....	145
Frequency Response Analysis: Room D – Abs0.4: Output Point 4.....	145
Frequency Response Analysis: Room D – AbsComplex: Output Point 1.....	146
Frequency Response Analysis: Room D – AbsComplex: Output Point 2.....	146
Frequency Response Analysis: Room D – AbsComplex: Output Point 3.....	146
Frequency Response Analysis: Room D – AbsComplex: Output Point 4.....	146
6.11 Section from the rectilinear mesh with an input point and two output points labelled, and potential paths from input to output marked.....	148
6.12 Close up view of RIR measurement taken from the rectilinear mesh with Dirac pulse used as the excitation signal.....	148
6.13 Path lengths on the triangular mesh.....	149
Acoustic Parameter Analysis: RT_{60} – Abs0.9: Room A.....	153
Acoustic Parameter Analysis: RT_{60} – Abs0.9: Room B.....	153
Acoustic Parameter Analysis: RT_{60} – Abs0.9: Room C.....	153
Acoustic Parameter Analysis: RT_{60} – Abs0.9: Room D.....	153
Acoustic Parameter Analysis: RT_{60} – Abs0.4 Room A.....	154
Acoustic Parameter Analysis: RT_{60} – Abs0.4 Room B.....	154
Acoustic Parameter Analysis: RT_{60} – Abs0.4 Room C.....	154
Acoustic Parameter Analysis: RT_{60} – Abs0.4 Room D.....	154
Acoustic Parameter Analysis: RT_{60} – AbsComplex: Room A.....	155
Acoustic Parameter Analysis: RT_{60} – AbsComplex: Room B.....	155

Acoustic Parameter Analysis: RT_{60} – AbsComplex: Room C.....	155
Acoustic Parameter Analysis: RT_{60} – AbsComplex: Room D.....	155
Acoustic Parameter Analysis: Spatial Average RT_{60} – For Each Room: Room A	156
Acoustic Parameter Analysis: Spatial Average RT_{60} – For Each Room: Room B	156
Acoustic Parameter Analysis: Spatial Average RT_{60} – For Each Room: Room C	156
Acoustic Parameter Analysis: Spatial Average RT_{60} – For Each Room: Room D	156
Acoustic Parameter Analysis: Spatial Average RT_{60} – For Each Absorption Condition: Abs0.9.....	157
Acoustic Parameter Analysis: Spatial Average RT_{60} – For Each Absorption Condition: Abs0.4.....	157
Acoustic Parameter Analysis: Spatial Average RT_{60} – For Each Absorption Condition: AbsComplex.....	157
Acoustic Parameter Analysis: C_{80} – Abs0.9: Room A.....	158
Acoustic Parameter Analysis: C_{80} – Abs0.9: Room B.....	158
Acoustic Parameter Analysis: C_{80} – Abs0.9: Room C.....	158
Acoustic Parameter Analysis: C_{80} – Abs0.9: Room D.....	158
Acoustic Parameter Analysis: C_{80} – Abs0.4: Room A.....	159
Acoustic Parameter Analysis: C_{80} – Abs0.4: Room B.....	159
Acoustic Parameter Analysis: C_{80} – Abs0.4: Room C.....	159
Acoustic Parameter Analysis: C_{80} – Abs0.4: Room D.....	159
Acoustic Parameter Analysis: C_{80} – AbsComplex: Room A.....	160
Acoustic Parameter Analysis: C_{80} – AbsComplex: Room B.....	160
Acoustic Parameter Analysis: C_{80} – AbsComplex: Room C.....	160
Acoustic Parameter Analysis: C_{80} – AbsComplex: Room D.....	160
Acoustic Parameter Analysis: EDT – Abs0.9: Room A.....	161
Acoustic Parameter Analysis: EDT – Abs0.9: Room B.....	161
Acoustic Parameter Analysis: EDT – Abs0.9: Room C.....	161
Acoustic Parameter Analysis: EDT – Abs0.9: Room D.....	161
Acoustic Parameter Analysis: EDT and RT_{60} , Spatially Averaged – Abs0.9: Room A.....	162
Acoustic Parameter Analysis: EDT and RT_{60} , Spatially Averaged – Abs0.9: Room B.....	162
Acoustic Parameter Analysis: EDT and RT_{60} , Spatially Averaged – Abs0.9: Room C.....	162
Acoustic Parameter Analysis: EDT and RT_{60} , Spatially Averaged – Abs0.9: Room D.....	162
A.1 Termination of a waveguide mesh due to a boundary resulting in a reflection...	187

Acknowledgements

Thanks are due first of all to my supervisor, Professor David Howard, for enabling me to embark upon this research and take it in whatever direction I saw fit. His advice, enthusiasm and encouragement have helped considerably, and his general drive in delivering and developing Music Technology at York has been an inspiration. I would also like to thank James Angus, Tony Tew and Chris Shadle (in advance) for the time spent reading and discussing this thesis, particularly to Tony for stepping in at the last minute. To the support staff in the Department of Electronics, especially Brenda, Steve Tate and Ross Oliver. To Paul Modler for never complaining about the Origin being a touch on the slow side due to all the simulations I was running. To Lauri Savioja at the Helsinki University of Technology, whose work initially got me hooked on this waveguide mesh thing, and whose help at a couple of points in the past few years has been invaluable. Similarly invaluable have been the discussions with fellow York research student and waveguide modeller Guilherme Campos; and thanks also to Angelo Farina of the University of Parma for allowing me to use his *Aurora* Acoustical Parameters module. To my research colleagues, particularly John Tuffen, Tim Brookes and Mark Hildred, not to mention Barry and Mike - despite their best efforts to get me to waste valuable time on “network deathmatch” it would still seem that I’ve managed to hand in on time. I have also spent some considerable time over the past four years in various teaching posts: to Rodney Marsh at LMU for letting me spend much of my time writing up this thesis; Tim Ward at LMU for selling me his CD burner at *the* most opportune moment – I couldn’t have done this thesis without it! Tim Banks at Bretton Hall; Liz Jones and all the staff at Harrogate College, particularly Ann Pearson who again has been so inspirational to work with. I should not forget all those “miscellaneous hangers-on” who’ve had to put up with me going on about getting this thesis done for what must seem like an eternity. To Greg (English) for putting up with me taking over the house over the last months; Greg (Irish) for dodgy free gig-going on the basis that he is the only ex-MusTecher that I’ve known to become a *bone fide* rock star; Rob and James for help in compiling many a fantasy musical equipment list; Ben for helping me in the quest for the best “free” music software; Steve and Lynne for the promise of a night in the, “best hotel in York”; Joanne for putting up with my constant persistence in asking her to come and do some singing for me, some of which has been captured as part of this thesis; and to Kathryn, John and Gary back home whose friendship and support is comfortable, old and so very much appreciated. To my family, especially my Mother for persevering all these years, and hey I’ve finally got a “proper” job. And to the last and most definitely least (!) of all, The Dorward – Queen of Evil, Empress of the Seven Galaxies, Mistress of the Invisible Table and the use thereof (highly recommended for a contents page I can tell you), and to whom I owe so much...

Declaration

I hereby declare that this thesis is entirely my own work and all contributions from outside sources, through direct contact or publications, have been explicitly stated and referenced.

I also declare that some parts of this program of research have been presented previously, at conferences and in journals. These publications are listed as follows:

1. D.T. Murphy and D.M. Howard, “A multi-channel spatial simulation system for computer music applications”, *Proceedings of the 1998 Institute of Acoustics Conference, Reproduced Sound 14*, Oct 22-25, 1998, Windermere, England, Vol 20: Part 5, pp 161-168, (1998).
2. D.T. Murphy, D.M. Howard and A.M. Tyrrell, “Multi-channel reverberation for computer music applications”, *Proceedings of the 1998 IEEE Workshop on Signal Processing Systems*, pp 210-219, Oct 8-10, 1998, Boston, USA.
3. D.T. Murphy and D.M. Howard, “Modelling and directionally encoding the acoustics of a room”, *Electronics Letters*, Vol 34, No 9, 1998, pp 864-865.
4. D.T. Murphy and D.M. Howard, “Physically modelling the acoustics of a room using a digital waveguide mesh”, *Proceedings of the 25th Euromicro Conference*, pp 82-89, Milan, Italy, Sept. 8-10, 1999.
5. D.T. Murphy and D.M. Howard, “The WaveVerb Multi-Channel Room Acoustics Modelling System”, *Proceedings of the International Computer Music Conference*, pp 472-475, Hong Kong, Oct. 22-27, 1999.

In addition, elements of this research have also featured in:

6. D.G. Malham, “Sound Spatialisation”, *1998 Workshop on Digital Audio Effects (DAFX98)*, pp 62-70, November 19-21, 1998, Barcelona, Spain.

Chapter 1

Introduction

1.1 Background

The purpose of this chapter is to present an introduction to the principal field of research to which this thesis aims to contribute. From this it will be possible, via the statement of a hypothesis, to identify specific goals for, and potential benefits from, the proposed developments in this field, and to define a plan of action through which to achieve the goals set out.

1.1.1 Composing With Space

Composing with sound in space, the art of sound spatialisation, has become particularly important within the domain of computer music and the recording studio in the latter half of this century, to the point that it has assumed a similar position today as the art of orchestration had in the nineteenth century [Roads, 1995]. Spatialisation as a whole can be divided into the *virtual* and the *physical*.

In the virtual reality of the studio a composer or recording engineer can create the illusion of sounds within an imaginary environment. These sounds can be altered and controlled within this environment as if it were some actual reality, to the point that the listener may be so immersed that what they perceive is, to them, completely real. This is all done via the use of delays, panning, filters, and most importantly, reverberation. It is also possible to model acoustic spaces that would be impossible to realise architecturally using these techniques.

In the area of physical spatialisation, sounds can be projected over a multi-channel, multi-speaker sound system from positions completely surrounding the listener, including above and below or even within the audience. It is also possible to actively control the acoustics of the hall using electro-acoustic systems.

Sound spatialisation has become an even more important aspect of composition in recent years with the advent of powerful and relatively cheap computer platforms and Digital Signal Processing (DSP) hardware. Surround sound has started to become commonplace in the domestic market, and 3-D audio applications have started to appear in a range of diverse applications, from studio effects processors, through to computer audio cards and widescreen

televisions. The virtual and physical acoustic soundfields projected around the audience or listener can be treated as a landscape on which the constituent sound sources can be placed and “viewed”. Composer Trevor Wishart uses the term *landscape* to describe the *virtual acoustic space* that is the source of the sounds we hear [MacDonald, 1995], [Wishart, 1996]. This landscape has a foreground and background, fixed and moving sources, and it can be fixed in playback or controlled, manipulated and performed from some form of control surface or via human gesture [Todoroff, 1995]. Therefore acoustic space can be used in a manner similar to the cinematic use of camera angle, lens perspective or width, focus and depth of field [Roads, 1995].

The use of space in music composition is not a new concept. In the sixteenth century composers at the Basilica San Marco in Venice - notably Adrian Willaert and Andrea Gabrieli - produced works for two or more choirs situated in different parts of a hall [Roads, 1995]. A verse would be first heard from a choir at one side of the hall, and a response would come from the choir at the other side. This arrangement was facilitated by two facing organs in the basilica. Wolfgang Amadeus Mozart wrote compositions for two spatially separated orchestras and Hector Berlioz and Gustav Mahler wrote works for multiple orchestras and choruses, some of which were offstage. After these experiments, however, there is little documented evidence of the use of spatial techniques in composition until the electronic era and the advent of the loudspeaker.

The first musical use of electronic sound spatialisation was Walt Disney’s *Fantasia* [Malham and Myatt, 1995], produced in 1939. The orchestra on the sound track was recorded using 33 microphones, and mixed by orchestral section onto six audio tracks. A seventh track held a mono mix, an eighth recorded the ambient sound from a distant microphone and a ninth held a metronome click track. For cinema playback, a three-channel version of the eight-channel original was played back from an optical recorder that was synchronised to the film. The original intention was to reproduce this over 90 speakers spread behind the screen and around the cinema, although this was rarely done in practice. As the film was being shown, sounds would be positioned and moved around the audience as part of the soundtrack.

There is a rich history of the use of spatial techniques in the various forms of electronically based music that originated in the 1950s. These include Karlheinz Stockhausen’s *Gesang der Jünglinge* in 1956, Edgar Varèse’s *Poème Electronique* in 1958 - this involved 15 tape recorders and 400 loudspeakers, and was experienced by up to 2 million people at the Brussels World Fair [Malham and Myatt, 1995] - and Iannis Xenakis’ *Hibiki Han Ma* in 1970. This latter piece was a twelve-channel electroacoustic composition performed on a system of 800

loudspeakers distributed around the audience, over their heads and under their seats [Roads, 1995].

Popular music still relies heavily on 2-channel stereo playback presentation, so the use of spatial techniques has usually been limited to the use of stereo panning, delays, and reverberation. However, the demand for high quality reverberation in the field of modern popular recording has led to very powerful, and often very expensive, spatial processors, far beyond the specifications and ideas behind the first digital reverberation algorithms. For instance the Lexicon 480L is probably the recording industry's most well-renowned, and most impressive high quality reverberation processor currently available [Riley, 1994]. More recent advances in technology have resulted in the first commercially available standalone reverberation unit based on convolution processing [Robjohns, 1999], with the user being supplied with the impulse responses of real concert halls on CD-ROM for loading into the device.

The recent developments in cinema based surround-sound have brought the discipline of sound spatialisation and composition to the awareness of a whole new audience. This technology is also finding its way into the domestic market via DVD and home cinema systems coupled with the wish to re-create the cinematic experience in one's own living room. This advancement and access to sound spatialisation technology has been paralleled in the growth of the use of the Personal Computer (PC) in the home, with many commonly available soundcards providing multi-speaker outputs for surround-sound enhanced games, music and multimedia. Associated with this has been the more widespread use of 3-D audio techniques to re-create the immersive, physical soundfield virtually using only headphones or two speakers. For instance the QSound system [White, 1995a], originally implemented in hardware, is now available in software to run on a standard PC fitted with some appropriate DSP cards, as well as a plug-in module for popular hard disk recording systems. The QSound system has been used extensively in popular music, with credits on Madonna's *The Immaculate Conception*, Sting's *The Soul Cages* and Pink Floyd's *Pulse*.

Sound spatialisation by electronic means has infiltrated almost all musical composition and production through many different ideas and techniques. As the technology to allow the exploration and use of these methods becomes more readily available, with an associated increase in the flexibility and user control inherent in such systems, the use of space can be integrated into all forms of music and musical composition in the same way that pitch, timbre and timing are currently used and accepted.

1.1.2 Room Acoustics

In order to successfully manipulate and control sound spatialisation it is necessary to have an understanding of the underlying acoustic principles, both of how sound behaves in an enclosed space and of the properties of the space itself, be it virtual or physical. As with the use of space in composition, the study of room and concert hall acoustics is by no means a new field. The history of room acoustics, or architectural acoustics as it is sometimes termed, can be traced back to the Roman architect Vitruvius, the first to record advice on acoustics [Barron, 1993], and even to the ancient Chinese scholars several centuries B.C. [Wang, 1994]. Similarly the sixteenth century composers at the Basilica San Marco in Venice must have had at least a conceptual understanding of how sound behaves in a space - what sounds “good” or “bad” in a particular venue - if they were to incorporate it as a significant compositional part in their music. There have been a number of works on the properties of sound and its behaviour over the generations, such as the work of Boyle and Newton on sound in the seventeenth century, and Lord Rayleigh’s *Theory of Sound* in 1877, although the latter’s comments on room acoustics are limited to generalities [Barron, 1993].

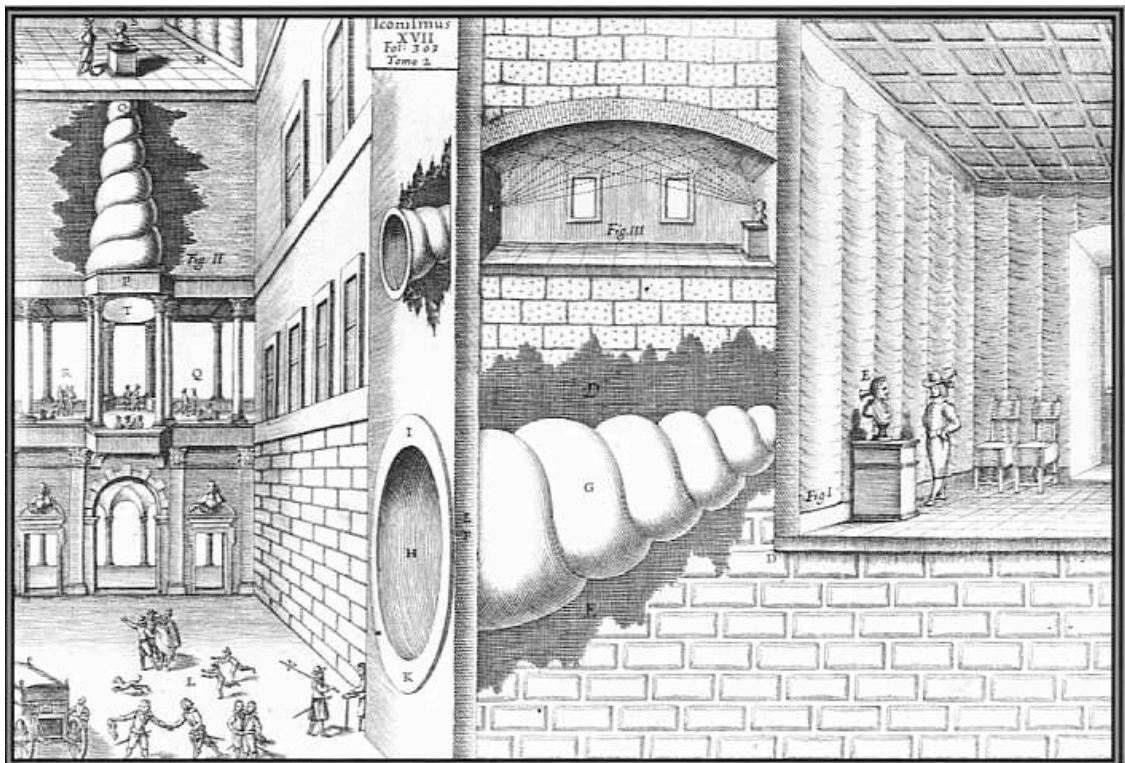


Figure 1.1 A 17th Century room design attributed to Athanasius Kircher (1601-1680), demonstrating how giant conch shells and - more usefully - arched ceilings can be used to reflect and focus sound. From [Physics Review, 1996a].

Consider also the work of Athanasius Kircher (1601-1680), a Jesuit priest and professor of physics and mathematics. In 1650 he published a work entitled *Acoustics, Musurgia Universalis – Acoustics, the Universal Expression of Music* [Physics Review, 1996a], which

discussed the reflection and diffusion of sound and whether sound can be transmitted in a vacuum. This included the design of an imaginary building (Figure 1.1), designed to allow concealed listeners to eavesdrop on the conversations of other people in neighbouring rooms. This early example of acoustic espionage was facilitated by the use of giant conch shells built into the walls that acted to reflect and focus the sound to listening posts hidden in statues. Despite this rather curious and perhaps ridiculous premise the design clearly demonstrates how sound could be reflected and focused using an arched ceiling.

Even in the early years of the 20th Century, opinions were often misguided as to what constituted a “good” acoustic space for music:

“In 1912 an eminent Viennese architect was asked for his opinion on a famous concert hall in Vienna. As a result, he wrote a quaint essay entitled ‘The Mystery of Acoustics’, determined that the secrets of the subject should not go with him to the grave. He concluded that concert halls become acoustically excellent when fine music played in them is gradually absorbed by the walls. The music of the symphony orchestras and the voices of singers impregnate the building materials, causing mysterious changes in the molecular structure. But brass instruments, he warned, have a bad effect and military music played in a fine hall could ruin its acoustics within a week. ‘In the mortar’, he said, ‘live the sounds of great composers’.”

[Physics Review, 1996b]

However it is with the pioneering works of Wallace Clement Sabine, begun in 1895 [Sabine, 1964], that room acoustics finally became established as a serious scientific discipline.

1.1.3 Room Acoustics Modelling

Once the principles and properties of room acoustics had started to be understood in a more rigorous fashion it was only a matter of time before musicians and engineers would want to simulate the characteristics of acoustic spaces, with particular regard to the reverberant sound. The development of spatial simulation in this manner within the field of computer music was due to an interest on the part of post World War II composers in the placement of sound sources within an acoustical environment [Dodge and Jerse, 1985]. In the recording studio, with the advent of multi-track tape in the 1950s, instruments and vocalists could be individually captured using a microphone in close proximity to them in order to achieve more control over the final sound on tape. Although all natural sounds are heard in the context of the environment which surrounds them, the use of these methods meant that only the direct sound would be captured

and the ambience of the performance space would be lost. Therefore it was required to somehow restore this - or even another - environmental context to the original recorded sound.

Initial attempts at modelling the soundfield in a room used a variety of electro-mechanical devices that often seemed crude but were highly successful. This included the use of reverberation chambers and large steel plates (see Chapter 3.2). The success of such models was primarily due to the continuous, physical mediums that were used as an analogue to the air within an enclosed space. However it is the age of digital electronics and the work of Schroeder [Schroeder and Logan, 1961], and [Schroeder, 1962] that has paved the way for the advanced, high quality, DSP-based room acoustics processors that are in common use today.

1.2 Aims of Research

1.2.1 Motivation

Currently, the acoustic characteristics of a room are, in the main, modelled using one of three methods:

- generically, using an all-purpose reverberation algorithm, with additional specific early reflections
- explicitly, based on the geometrical features present in the room
- exactly, using convolution and a measurement from a real space

Digitally implemented generic methods are the most commonly used, with even the most basic algorithms imparting a high quality and realistic reverberant effect to a sound source. However they are not capable of modelling an acoustic space with specific geometrical and acoustic features and source and listener locations, as might be required by the computer musician or architectural acoustician. If this level of detail and accuracy is required an explicit model must be used, the most common being those grouped under the heading of geometrical models (see Chapter 4.2). However these models are limited in a number of ways. They are complex to implement, with prohibitively excessive computation times if a long Room Impulse Response (RIR) is required. They are also only valid for high frequencies where reflections are specular, and as such cannot take account of low frequency wave phenomena such as diffraction and interference. In general, geometrical models are best suited to modelling the direct sound and early reflections of the characteristic RIR, with reverberation being added using a generic method. Exact methods are the most accurate as they are capable of completely recreating the acoustic characteristics of the modelled space. However they are limited to recreating a limited set of spaces in which measurements have been made and are often expensive to implement due to the fast convolution processing required.

If a musician or composer wishes to define a specific spatial environment, with sound sources and listening positions, room size, geometry and absorption characteristics, it will usually be conceived of at a high level, with a physical idea of what this space should look and sound like. If this space does not already exist then an exact model is clearly not feasible. Generic modelling may give a working impression of what this landscape will sound like, but can never hope to be truly accurate without a specific algorithm designed for the purpose, requiring expert DSP and acoustics knowledge on the part of the composer. It would seem that the best way of realising - or auralizing - this compositional idea would be to design an explicit model based on the easily conceptualised geometrical measurements. However, as has already been discussed, the most common methods of generating an explicit model of an enclosed space are far from ideal.

If a specific model is required that can be seen to offer some of the realism of generic and exact models yet offer the flexibility of geometrical models then the solution usually exists in a direct time domain model of wave motion within the space. Digital waveguide models have been used in this manner and are an accurate and efficient method of modelling a physically complex medium, such as that which exists within the boundaries of an enclosed acoustic space. 2-D and 3-D waveguide mesh structures have been used to model plates, membranes, and acoustic spaces as well as more abstract sound objects. Current waveguide models used in the field of room acoustics, based on a rectilinear arrangement of waveguide elements, are limited to providing only a partial solution to an accurate RIR, as they are only valid for low frequencies. These models are further limited due to frequency and directional dependent dispersion, an inherent problem in lattice type structures. This dispersion error can be minimised by using a different topological arrangement of the waveguide elements and scattering junctions in the underlying waveguide mesh structure.

1.2.2 Statement of Hypothesis

The triangular digital waveguide mesh is a paradigm applicable to the problem of successfully modelling the acoustics of an enclosed space, offering a significant improvement in quality and accuracy over that of the more commonly used rectilinear digital waveguide mesh.

This hypothesis is supported in three ways:

1. Theoretically, by examining the underlying principles and properties of the triangular and rectilinear waveguide mesh topologies, with particular emphasis on their dispersion error characteristics.
2. Practically, using a wide variety of both visual and audio examples showing how the waveguide mesh structures behave, and how measured RIRs can be used successfully or otherwise to impart an environmental context on the source material.
3. Analytically, by comparing the measured RIRs from both mesh topologies against theoretical expectation and standardised acoustical parameters.

1.2.3 Thesis Structure

The remainder of this thesis describes the program of research that has been undertaken to prove, or otherwise, the hypothesis stated above. The chapters are organised and presented as follows:

Chapter 2 begins by considering a general room and examining the characteristic growth of sound within it, introducing the concepts of direct sound, early reflections, reverberation and room modes. The Room Impulse Response is also introduced and how it can be used as the basis for examining the acoustic properties of the room in which it has been measured. Some of the more commonly used acoustical parameters are also discussed as is the importance of aural and visual cues in our interpretation of sounds in the space around us.

Chapter 3 examines the methods that have been used to create a generic reverberant effect, including the use of electro-mechanical devices and digital reverberation based on combinations of unit reverberators as well as the principles of convolution and auralization that are used in exact models of particular acoustic spaces.

Chapter 4 introduces the main methods that can be used to model a more specifically defined room. Geometrical models are covered as are finite and boundary element methods and the finite difference time domain technique. Waveguide models are introduced and the theory behind their use is covered, including applications and limitations. Dispersion error is examined across a range of mesh topologies and the triangular waveguide mesh is presented as offering an improvement over the rectilinear mesh. It is through this that a specification is arrived at for the model that will be used to test the hypothesis, and a number of implementation issues are identified and discussed, including the development platform to be used.

Chapter 5 covers in some detail the theory behind the rectilinear and triangular waveguide mesh structures. This includes how the mesh is terminated at a boundary and the concept of

scattering junction types is introduced. The scattering equations for each junction type across both mesh structures are presented. Mesh input and output is examined and a detailed analysis of the dispersion error present in both meshes is offered for comparison. The *WaveVerb* digital waveguide mesh reverberation system is introduced and a number of software design considerations are covered, including pertinent elements of code, the basic algorithm used and how the waveguide mesh is animated and visualised.

Chapter 6 presents a series of results based on the current implementation of the *WaveVerb* System. Initially the model is tested for observation of standard wave phenomena with actual still screenshots of the animated model being presented, in addition to MPEG animations. A case study is discussed involving the modelling of four different sized rooms with varying absorption and source-listener combinations for both mesh topologies. The RIR measurements taken from each of these cases are examined in a number of ways. This includes low frequency response and modal analysis, spectral analysis, comparison of acoustical parameters and convolution processing with a range of audio examples.

Finally Chapter 7 summarises the main body of the thesis, draws conclusions from the results with relevance to the hypothesis and indicates directions in which the work may usefully be extended in the future.

Supporting details are presented in the appendices. These include a data CD containing RIR measurements, MPEG animations and source code, and an audio CD containing examples of sampled audio convolved with a variety of measured RIRs.

1.2.4 Contribution to the Field

In the course of research presented in this thesis as outlined above, original contributions have been made to knowledge and understanding in the fields of waveguide mesh techniques, and the musical application of room acoustics modelling. Briefly, these contributions are as follows:

The implications of implementing a bounded waveguide mesh in terms of the range and number of scattering junction types required (Chapter 5.3).

Ambisonic B-format encoding of the output from the waveguide mesh (Chapter 5.5).

The practical implications of implementing a large scale waveguide mesh in software (Chapter 5.7).

The first serious study and analysis of a waveguide mesh structure as a full audio bandwidth room acoustics model including evaluation of frequency response, acoustical parameters according to ISO3382 and processed music and audio (Chapter 6.3 - 6.7).

The benefits offered by the triangular waveguide mesh topology over a corresponding rectilinear mesh as a suitable room acoustics model (Chapter 6.8 and Chapter 7).

1.3 Summary

A brief history and appreciation of the use of sound spatialisation in music, room acoustics and room acoustics modelling has been presented. Given that a musician or composer may conceptualise a sound landscape at a high level based on physical measurements and ideas, it is required to render this space as a physical or virtual reality using a suitable model or simulation. The three main classes of acoustic model that have been identified all fall somewhat short of dealing with this problem in an accurate and realisable manner. Digital waveguide models provide an accurate and efficient method of modelling a physically complex medium such as that which exists within the boundaries of an enclosed room. Current waveguide models used in the field of room acoustics are based on a rectilinear mesh topology and are limited to providing only a partial solution to an accurate RIR. It is thought that the limitations and accuracy of such models can be improved upon by using a different topological arrangement of the underlying waveguide mesh structure.

Based on this idea, an hypothesis has been stated together with how it will be supported. In order to prove this hypothesis a program of research has been planned and outlined, over the course of which original contributions were made to knowledge and understanding in the fields of waveguide mesh techniques, and the musical application of room acoustics modelling. These contributions have been identified and summarised.

Chapter 2

The Soundfield in an Enclosed Space

2.1 Introduction

The purpose of this chapter is to provide background information on the behaviour of sound in an enclosed space and how its properties can be quantified and analysed. It should be possible to observe behaviour in the model analogous to sound propagating within a room, and make measurements comparable with actual standardised quantities from any output generated. This chapter examines the detailed characteristic propagation and growth of sound within an enclosed space, how particular acoustic properties can be measured and the manner in which pertinent physical quantities can be extracted from these measurements. Finally, this chapter discusses the role of visual cues in our understanding of the behaviour of sound and how they work in tandem with our hearing mechanism to reveal information about the acoustic environment within which we are placed.

2.2 The Room as a System

An enclosed space can be considered in general terms as a system where a given input signal results in a corresponding output. This output signal is the result of a transformation due to the characteristics of the system itself. In this case the input to the system is a sound wave provided by an appropriate acoustic stimulus, such as a voice, an instrument or pre-recorded sound from a loudspeaker. The output from the system is a specific point or points in the room where the resultant pressure variations due to the input and its interactions with the room are monitored - either by the listener or by an appropriate electronic measurement device. The room, or system, transforms the input according to its physical properties, such as the dimensions, the number of surfaces, and how absorptive these surfaces are.

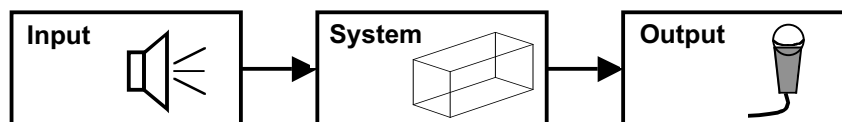


Figure 2.1 Block diagram of the room as a system. The input signal is transformed by the physical properties of the room to give the output.

2.3 Sound in an enclosed space

An enclosed space is defined as an acoustic environment that is bounded by physical objects such as walls, floor, and ceiling differentiating it from the situation existing outdoors in a free

field. Sound intensity (power per unit area) is inversely proportional to the square of the distance from the source. Intensity is proportional to the square of sound pressure so the inverse square law for intensity becomes the inverse distance law for sound pressure. That is, sound pressure is inversely proportional to distance. The behaviour of sound in an ideal free field is determined only by these properties whereas in an enclosed space reflections and interactions at the boundaries also have to be considered in addition to these inverse square and inverse distance properties.

A room or hall can be considered as a typical enclosed space. Every room will have an individual set of physical properties that determine its acoustic characteristics and just how it will transform an input signal. However in general the build up of sound in a room due to an acoustic event at a given point is the same in all cases. This soundfield can be examined by considering a fixed *source*, which emits a short impulsive sound - the input to the system - and a fixed *listener* who hears the resultant effect of this sound being emitted - the output from the system. Note that in this case the term listener is used very generally and can be equally applied to the ear of a real person or the input to an electronic measuring device. Consider the simple plan view of a room in Figure 2.2 with marked source **S**, and listener position **L**. At a time $t = 0$ the source emits a short, impulsive sound at a level high enough to excite the soundfield in the room across the whole audible frequency spectrum. The sound wave generated by the input signal will arrive at the listener position via an infinite number of paths, and can be divided into three distinct stages.

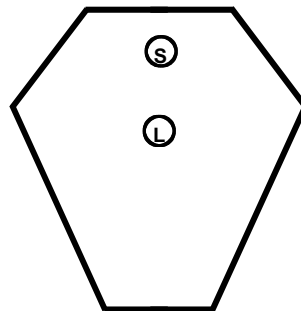


Figure 2.2 Plan view of an enclosed space with a sound source marked at **S** and an output at listening position **L**. At the time $t = 0$ the source emits a short impulsive sound.

2.3.1 The Direct Sound

The velocity of sound can be calculated by considering the adiabatic (no transfer of heat) gas law:

$$PV^\gamma = \text{constant} \quad (2.1)$$

where P is the pressure of the gas (in Nm^{-2}), V is the volume of the gas (in m^3) and $\gamma = 1.4$ is the ratio of the specific heats of air at constant pressure and constant volume respectively. This gas law is appropriate as the pressure variation caused by a sound moves so quickly that there is no time for heat to transfer between areas of high and low pressure. The velocity of sound in a solid can be calculated from:

$$v = \sqrt{\frac{E}{\rho}} \quad (2.2)$$

where v is the velocity of sound (in ms^{-1}), ρ is the density of the material (in kgm^{-3}) and E is the Young's modulus of the material (in Nm^{-2}), being a measure of the elasticity of the material in question. This equation can also be used to calculate the velocity of sound in air, using the equivalent to Young's modulus for air which is given by:

$$E_{\text{air}} = \gamma P \quad (2.3)$$

The density of a gas is given by:

$$\rho_{\text{gas}} = \frac{PM}{RT} \quad (2.4)$$

where M is the molecular weight of the gas in question (in kg mole^{-1}), R is the gas constant ($8.31 \text{ JK}^{-1} \text{ mole}^{-1}$) and T is the absolute temperature (in K). Substituting Equations (2.3) and (2.4) in (2.2) gives the velocity of sound in a gas:

$$v_{\text{gas}} = \sqrt{\frac{\gamma RT}{M}} \quad (2.5)$$

Therefore the finite velocity of sound is highly dependent upon the absolute temperature and the molecular weight of the gas. The molecular weight of air is affected by the presence of water vapour also known as the humidity of the atmosphere, with very humid conditions effectively reducing the velocity of sound. From Equation (2.5) it is possible to calculate that sound travels at approximately 343 metres per second (ms^{-1}) for a room temperature of 18°C . This finite measurement implies that there will be a slight delay before the listener registers any sound from the source. This delay is dependent upon the distance the sound has to travel and the shortest path between the two positions is a straight line. This is called the *direct sound* and will be heard first of all. It will occur at time t_d after $t = 0$ as shown in Figure 2.3. The direct sound carries the original signal with only a slight degradation in quality due to energy being dissipated by the medium it is travelling through.

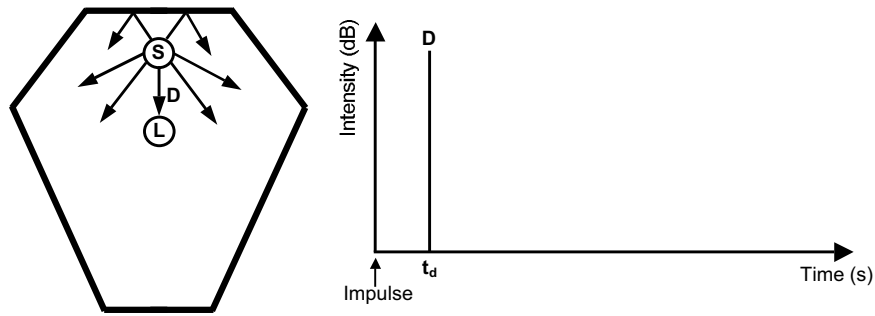


Figure 2.3 The Direct Sound arrives at listening position L at time $t = t_d$ after $t = 0$.

2.3.2 Early Reflections

Clearly there will only be one of these infinite number of paths that travel directly to the listener. The next set of shortest paths, resulting in sounds arriving just after the direct sound, are those that have been reflected off one or more of the surfaces present in the room. The set of discrete sounds arriving at the listener after following these paths are called *early reflections* and they are separated by time, level and direction from the direct sound and each other. No matter where the source and listener are located relative to each other, the level of the direct sound will change only slightly. The Early Reflections however will vary considerably according to the relative positions of source and listener and the geometry of the room. We use them to supply us with information about the size and shape of the room and the location of the sound source within it. If these early reflections are separated by about 30ms from each other then they will be perceived as discrete echoes [Howard and Angus, 1996]. Similarly if the room is large enough to result in the first early reflection arriving 30ms after the direct sound a difference will be perceived as the ear resolves the two sounds into two distinct events. The total length of travel affects the intensity level of an early reflection in a similar manner to the direct sound. However there will be a further drop in level due to some of the sound energy being absorbed at the reflecting surface. The precise time distribution of these early reflections will vary according to the exact size and shape of the enclosed space.

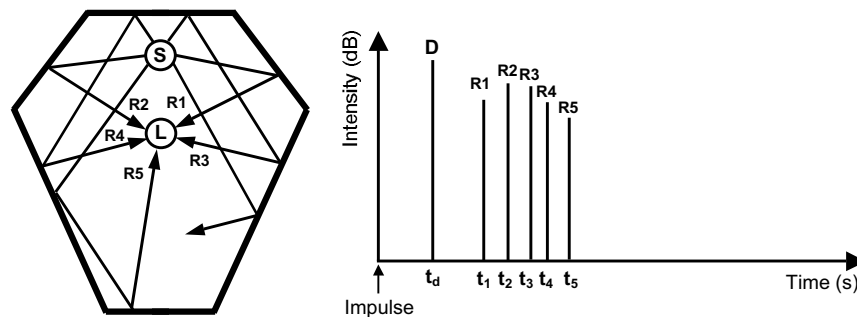


Figure 2.4 Early reflections R1,...,R5 arriving at listening position L at times t_1, t_2, \dots, t_5 after $t = 0$.

2.3.3 The Reverberant Sound

After the early reflections, sound continues to be received at the listener's position from an ever-increasing number of multiple-reflection paths. Each individually arriving impulse is weaker on average than those that have arrived previously, due to the ever increasing number of reflections it has undergone, each of which absorbs some of its initial energy. All of these components merge together densely in a continuously decaying *reverberant sound*, which is perceived as a stretching out and gradual decay of the original impulsive event. The reverberant sound behaves differently from the direct sound and early reflections in that it is *diffuse*. Therefore it will visit all parts of the room with equal probability and so remain constant as the position of the listener varies. If the sound source is continuous, the reverberant sound will build up until it reaches an equilibrium level where the sound power input is equal to the power lost due to absorption. This only occurs after some time sufficient for many reflected waves to arrive - this being after the early reflections - and so is dependent upon the amount of absorption in the room and its size. When the sound stops, the sound level decreases at a rate determined by the size of the space and the amount of sound energy absorbed at each reflection.

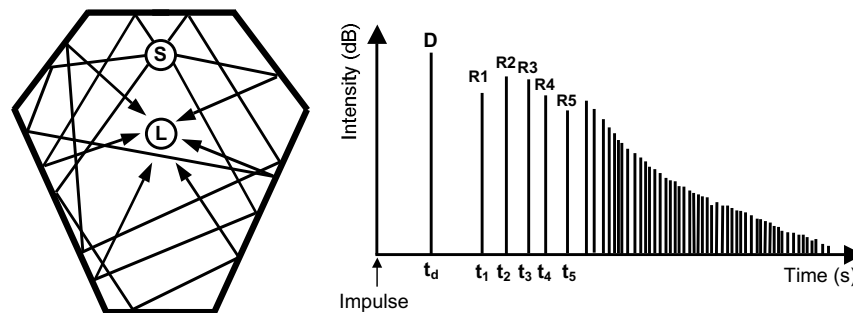


Figure 2.5 The exponentially decaying reverberant sound

2.4 Room Modes

If a sound source is between two reflective (ie they absorb only a minimal amount of sound energy at each reflection) parallel walls a *standing wave* can occur with the pressure component of the wave at a maximum and the velocity component at a minimum at the boundary walls [Howard and Angus, 1996]. This results in the reinforcement or resonance of sound energy at certain frequencies. The lowest frequency wave that can fit these boundary conditions has a wavelength equal to double the distance between the two walls. This is the lowest resonant frequency and is known as the fundamental, f_0 . Other similar resonances occur at multiples of this fundamental, $2f_0$, $3f_0$, and are referred to as natural frequencies, resonant frequencies, room resonances or room modes. Two walls 5 m apart will generate room modes at frequencies 34.4Hz, 68.8Hz, 103.2Hz (with speed of sound = 343ms^{-1}). Pressure antinodes (maximum pressure) are always created at each wall and pressure nodes (zero pressure) exist halfway between two antinodes.

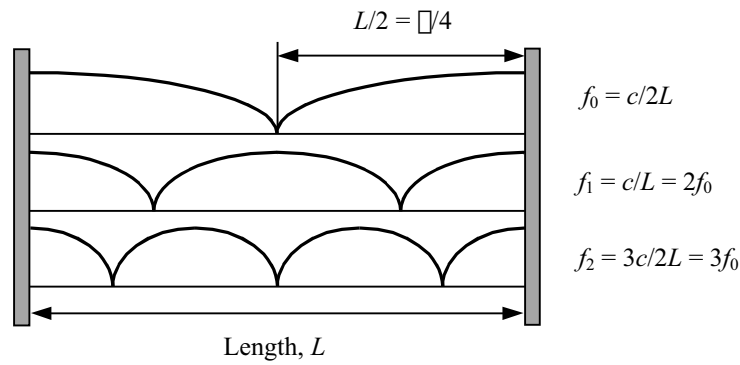


Figure 2.6 The first three pressure standing waves and calculated resonant frequencies between two rigid reflective walls

Adding two more pairs of mutually perpendicular walls to form a simple 3-D rectangular enclosure adds two more resonance systems each with its own fundamental and modal series. These modes involving the reflections between two opposite and parallel walls are known as axial modes. There are also further sets of modes involving reflections between four surfaces - the tangential modes - and all six surfaces - the oblique modes.

These standing waves behave differently to the rest of the sound present in the room [Howard and Angus, 1996]. In the ideal case there should be an equal probability of a sound wave being reflected from any surface and in this way energy is reflected in a random fashion and a diffuse field is the result. With a room mode the sound wave travels a path involving only a limited set of the surfaces in the room. This involves the wave striking a wall at a particular angle of incidence that will remain constant resulting in a cyclic path back to the original surface it was reflected from. It is the length of this cyclic path as discussed above that results in a particular prominent frequency. Room modes will therefore exist for discrete frequencies that are a function of the geometry of the room, and as these modes are spatially static - that is they will not change until all the energy in the wave has been absorbed at the surfaces involved - there will be considerable variation in sound pressure level as the listener moves about the room.

2.4.1 Calculation of Room Modes

One of the solutions of the wave equation leads to a straightforward method of calculating the room modes that are present in a rectangular enclosure [Rayleigh, 1945]. Consider such a rectangular room as placed within the mutually perpendicular x , y , z axes of the Cartesian coordinate system as shown in Figure 2.7.

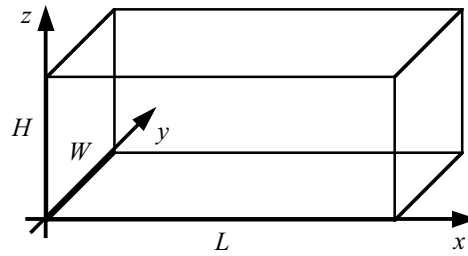


Figure 2.7 A rectangular room L m long, W m wide and H m high.

The x axis is defined to be parallel to the longest dimension of the room L , (generally the length), the y axis is defined to be parallel to the next longest dimension W , (width), and the z axis is defined to be parallel to the smallest dimension H , (height). Using Equation (2.6) as stated by Rayleigh in 1869 it is possible to calculate the frequencies that correspond to the modes present in the room due to its geometry.

$$f_{pqr} = \frac{c}{2} \sqrt{\frac{p^2}{L^2} + \frac{q^2}{W^2} + \frac{r^2}{H^2}} \quad (2.6)$$

Where:

f_{pqr} = mode (p, q, r) in Hz

c = speed of sound ($= 343\text{ms}^{-1}$)

L, W, H = Room Length, Width and Height, in m.

p, q, r = the number of half wavelengths between the surfaces, $0, 1, 2, \dots$

Note that, for example, mode $(1,0,0)$ would correspond to the first axial mode along the length of the room, and mode $(1,1,0)$ would correspond to the first tangential mode between the four walls. If any of the dimensions of the room are multiples of each other then some of the resonant frequencies will coincide leading to more prominent and problematic room modes. When designing an acoustically sensitive rectangular room it is desirable to select dimensions that lead to an even distribution of room modes so that this “stacking” of the resonant frequencies is avoided. A number of studies have resulted in favourable ratios for the three dimensions. The Sempeyer results from 1965 quoted in [Everest, 1994] are presented in Table 2.1:

	HEIGHT	WIDTH	LENGTH
Ratio Set A	1.0	1.14	1.39
Ratio Set B	1.0	1.28	1.54
Ratio Set C	1.0	1.6	2.33

Table 2.1 The Sempeyer rectangular room dimension ratios for favourable mode distribution.

2.4.2 Influence of Modes on the Acoustics of a Room

Clearly the modal frequencies play an important role in the acoustics of a room, being an unavoidable consequence of the design. The number of modes will increase with frequency and they are often unevenly distributed, with considerable gaps between the lower order modes. If a musical note were to be pitched in one of these gaps it would sound abnormally weak in comparison with other notes. A standing wave is not absorbed as easily as sound waves that travel in a more random manner, visiting all of the available surfaces, and in an untreated room this will lead to a longer decay time at these particular frequencies. The decay of sound energy in the room can no longer be considered as a single exponential decay dependent upon the average absorption present, as prominent modes will take longer to die away. Speech quality can be particularly deteriorated in small rooms due to the presence of strong axial modes spaced approximately 20Hz or more apart, or from any coincident or very closely distributed modes [Everest, 1994].

2.5 Frequency Regions

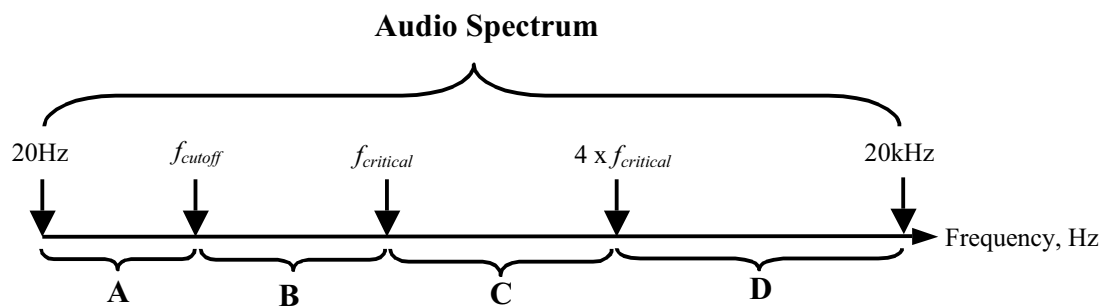


Figure 2.8 The audio spectrum divided up into four regions, each characterised by a different acoustic property.

When considering the acoustics of small rooms the audible frequency spectrum can be divided into four regions as shown in Figure 2.8 across which the dominant acoustic factor will vary. Region A – *the cut-off region* – is the range of frequencies below the lowest axial room mode. Frequencies below this cut-off point will still propagate through the room although they will not be supported or boosted by the presence of any room resonances. The cut-off point can be calculated from:

$$f_{cut\ off} = \frac{c}{2L} \quad (2.7)$$

where:

- c = Speed of sound, in ms^{-1} ($= 343\text{ms}^{-1}$)
- L = Longest dimension, in m.

Above f_{cutoff} , in region B, the dimensions of the room are comparable to the wavelength of sound being considered and the behaviour of the room modes is the dominant acoustic feature. In this region the acoustic field in the room can no longer be considered as diffuse and the concept of reverberation time (see Section 2.7.1) is somewhat false with an examination of modal decay in the room being a more applicable measure.

In Region D the diffuse field dominates, reverberation time is a valid quantity, the effects of room modes are minimal and the listener should perceive an even reverberant sound throughout the space. It is also in this region that the wavelength of sound is short enough so that geometric acoustic modelling techniques apply, reflections can be considered specular, and sound can be conceived as travelling in “rays” (see Section 4.2).

The boundary between regions B and D is somewhat blurred and in this treatment is considered as the transition region C where both diffraction and diffusion can be observed. The wavelengths involved are often too long for geometric acoustic methods but too short for approaches using wave acoustics. The lower boundary of region C is often called the critical frequency $f_{critical}$ and can be calculated in an approximate manner using Equation (2.8), where d is the smallest room dimension. The upper bound is approximately $4 \times f_{critical}$.

$$f_{critical} = \frac{3c}{d} \quad (2.8)$$

The critical frequency helps to determine whether a room is acoustically “large” or “small”. In a large room $f_{critical}$ is less than the lowest frequency of a typical sound that will be heard in the room. For small rooms $f_{critical}$ is within the frequency range of the sounds heard [Howard and Angus, 1996].

2.6 The Room Impulse Response

In the general case of a *linear time invariant* (LTI) system, the *output signal* can be obtained by performing the *convolution* of the *input signal* with the system’s *impulse response*. The properties of an LTI system do not vary with time, and it will obey the principle of linear superposition which is stated as follows:

“if an input consisting of a number of signals is applied to a linear system, then the output is the sum, or superposition, of the system’s responses to each signal considered separately”.

[Lynn and Fuerst, 1996]

Note that this is analogous to the principle of linear superposition for waves. The discrete *unit impulse*, or *Dirac delta function* $\delta[n]$ is the input signal used to determine the system's impulse response. It is defined as:

$$\begin{aligned}\delta[n] &= 0 & n < 0 \\ \delta[n] &= 1 & n = 0\end{aligned}$$

where the integer value n , denotes the discrete sample number and $n = 0$ corresponds to some convenient time origin or reference. If this signal is applied to a system the excitation will apply for the instant $n = 0$. Any output signal observed after $n = 0$ must therefore be characteristic of the system itself, since the input signal has since stopped. For this reason, this impulse response is often referred to as the natural response of the system.

Convolution allows the output signal of any LTI system to be found in response to any given input signal. The output signal is found by *convolving* its input signal with the impulse response of the system in question. Convolution is a form of superposition, relying upon the fact that any input signal can be built up by summing the weighted, shifted impulses. Since the system is by definition Linear Time Invariant and so obeys the principle of superposition, the output signal must equal the summation of its responses to all such impulses considered separately.

Referring to (2.2), if an acoustic space can be considered as an LTI system then it should be possible to determine the output at the listener position given only the input signal and the room's measured impulse response. Therefore the acoustic properties of a real enclosed space can be uniquely defined by measuring the Room Impulse Response (RIR) at a specific listening point for a unit impulse input signal applied at a given sound source location. If the listening point is defined to be at the entrance to the ear canals or at the surface of the ear drums of the listener's head then the result is a pair of unique measurements known as the Binaural Room Impulse Response (BRIR). This RIR/BRIR measurement will contain all the information required to artificially recreate - via convolution - the effect of placing a listener and any arbitrary sound source within the actual room at the given measurement locations. Note that there is a unique RIR/BRIR for each different sound source/listener position combination.

2.6.1 RIR Measurement

A loud impulsive sound source is often used in the measurement of RIRs in a room or hall, examples being blank firing pistols, spark generators, small cannons or balloons being pricked [Everest, 1994]. In all cases they are approximations to the Dirac impulse as it is impossible to physically create an infinite short pulse with an infinite amplitude. Such sound sources must

excite the space across the whole spectrum and so allow decays to be measured that are sufficiently high enough above the noise floor level inherent in both the space and measurement system. This is particularly difficult at low frequencies as such sources often have insufficient energy to excite the room to usable levels.

In an effort to improve these rudimentary methods different source signals have been used including tone burst and modulated noise. The current, most commonly used RIR measurement techniques are Time Delay Spectrometry (TDS) [Everest, 1994] and Maximum Length Sequence Signal Analysis (MLSSA) [Rife and Vanderkooy, 1989].

2.6.2 Time Delay Spectrometry, (TDS)

TDS was born out of a requirement to measure the transient response of loudspeakers accurately and dates back to 1967 [Everest, 1994]. The excitation signal used is a variable frequency sine wave sweep. A receiver is tuned to sweep in synchronisation with the excitation signal, and operates together with a time delay offset due to the relatively slow speed of sound. This time delay is set so that it corresponds exactly to the time taken for the sound from the excitation source to travel the measured distance to the receiver so that the two are in perfect step with each other. This technique also allows distinct reflections to be measured and examined. For instance a first reflection from a wall will take a specific amount of time to reach the receiver via the reflected path. By setting the receiver offset equal to this time it will measure only that specific reflected component, rejecting all other noise, reflections and reverberation.

2.6.3 Maximum Length Sequence Signal Analysis, (MLSSA)

In a MLSSA system a Maximum Length Sequence (MLS) is used as the system input. A binary MLS is a periodic two-level pseudo-random sequence of length $L = 2^N - 1$, where N is an integer, which yields essentially an impulse under circular auto-correlation [Rife and Vanderkooy, 1989]. An analogue version of an MLS is applied to the system, and the resulting response is sampled, and cross-correlated with the original sequence. The result of the cross-correlation is essentially the system impulse response, and hence yields the required RIR.

2.7 Acoustic Measurements and Preference Criteria

The previous section discussed how sound behaves in an enclosed space and has already suggested possible measurements that are pertinent in describing more objectively the acoustic characteristics therein, an obvious example being the “amount” of reverberant sound present in the room. However, as the psychoacoustic evaluation by the listener of the sound within the room plays an equally important role in deciding its properties, it becomes clear that the more subjective criteria - what makes a room sound “good” for some types of music but not for

others, and what it is exactly that makes it sound “good” or “bad” - are also important acoustic design considerations.

For instance, reverberation is an important and desirable acoustic property of rooms and halls as it reinforces musical sounds and adds a rich texture to their timbre. It helps to integrate the varying directional and timbral components of a sound source into a uniform event. However, too great a level of reverberant sound can result in reduced intelligibility of speech. To counter this, a high intensity level of direct sound compared with reverberated sound is important to allow the listener to hear clear sound with good speech intelligibility. Further, early reflections can reinforce the original sound but are more likely to cause interference effects that will result in reduced intelligibility of speech and timbral variation of general sounds.

Some of the more important objective parameters have been identified and clearly defined by various authors such as Beranek [Beranek, 1962], Ando [Ando, 1985] and Barron [Barron, 1993] as well as the ISO [ISO3382, 1997]. Given that a RIR theoretically contains all of the information regarding the acoustic characteristics of the room in which it has been measured, it is also possible to derive these specific objective parameters from the RIR. Clearly this adds to the importance of the role of the RIR in acoustic modelling. Not only can it be used to recreate the sonic properties of a space but it can also be used to provide specific information relating to clearly defined objective criteria. Although a RIR is specific to a particular combination of source and listener positions it is possible to average these objective criteria over a number of different positions for a number of different RIRs to arrive at a general figure for the whole space.

2.7.1 Reverberation Time, (RT_{60})

At one time reverberation was considered the single most important characteristic of an enclosed space for speech or music and the concept and measurement of reverberation time was introduced by Sabine at the turn of the century. It is defined formally as the time expressed in seconds that would be required for the sound pressure level to decrease by 60dB, at a rate of decay given by the linear least squares regression of the measured decay curve from a level 5dB below the initial level to 35dB below [ISO3382, 1997]. When the decay rate used is measured from 5dB below the initial level to 35dB below, RT_{60} is sometimes be referred to as T_{30} . However, it is often difficult to obtain an accurate measure for RT_{60} due to decay curves being non-monotonic - perhaps due to prominent, high amplitude or near-coincident modes - or because of a high level of background noise. In such cases an RT_{60} value based on the decay rate over a smaller dynamic range can be used, with a minimum range of 20dB, extending from 5dB down to 25dB down, being allowable and referred to as T_{20} .

Clearly it should be possible to calculate RT_{60} from a well measured RIR. However, it is also possible to derive a value from the architectural features present in the room based on the Sabine reverberation equation which is defined as follows:

$$RT_{60} = \frac{0.161V}{S\bar{\alpha}} \quad (2.9)$$

where:

$$\begin{aligned} V &= \text{Volume of the enclosed space, in m}^3 \\ S\bar{\alpha} &= \text{Total absorption, in sabins.} \end{aligned}$$

The total absorption can be calculated by considering the individual absorption contributed by each type of surface present in the room, and is effectively the sum of all the surface areas in the hall multiplied by their *absorption coefficients*. This absorption coefficient, as defined by Sabine, expresses the ratio between the absorbed and incident energy of a sound wave at a surface. This is because no surface is completely reflective and an incident sound wave will lose some of its energy on impact. If 40% of the incident sound energy is absorbed at a surface the absorption coefficient is said to be 0.4. One square metre of this material would contribute 0.4 sabins to the total absorption in a room. The value of the coefficient ranges from 0 to 1 with an open window being the perfect absorber - an absorption coefficient of 1.0 - as sound passing through it never returns to the room. The absorption coefficient of a material varies with frequency and with the angle of incidence of the sound wave (or ray). Due to the random and infinite nature of sound travelling around a room interacting with all of the surfaces therein, it is desirable to measure sound absorption coefficients averaged over all possible angles of incidence. It is standard practice to publish the coefficients for various materials to be used in these types of calculations. The standard frequencies used, due to the frequency dependent variance of the absorption coefficients, are 125, 250, 500, 1000, 2000 and 4000Hz.

The formula is limited in its use to non-absorbent halls with an average value of $\bar{\alpha}$ less than about 0.3 and becomes less accurate as the average value for $\bar{\alpha}$ increases. For instance if all the surfaces in a room were open windows with $\bar{\alpha} = 1$, RT_{60} , from Equation (2.9), is still non-zero, essentially giving a reverberation effect outdoors in the free field. It is also required that the reverberant field be diffuse and effectively constant for all positions so absorption coefficients valid for all angles of incidence are appropriate quantities.

A reverberant hall is called *live*, as opposed to a *dead* or *dry* space that reflects little sound back to the listener. It has a large volume compared with the size of the audience and highly reflective surfaces. A live hall, “imparts fullness of tone to music” [Beranek, 1962] and this sense of *liveness* is directly related to RT_{60} values for frequencies at about 500Hz.

The optimum reverberation time depends upon the volume of the venue and its desired use [Howard and Angus, 1996]. For large churches or cathedrals where choral and/or organ music are commonly used the suggested optimum RT_{60} is greater than 2.0s and less than 4.0s. At the other end of the scale for recording studios, suggested values for RT_{60} range from about 0.3s to 0.5s. However a large RT_{60} is often achieved at the cost of poor intelligibility of speech. For example, in smaller churches where talking is emphasised over music a correspondingly lower RT_{60} value would be required.

In general if the reverberation time is too long it will hinder the clarity of both speech and music with the important transient sounds being masked. Diffuse fields are more desirable as they will lead to a smooth decay of reverberant sound, as is a slight increase in low frequency reverberation time. This will help to compensate for the lack of sensitivity of the ear to low frequency sounds and the relatively low levels of sound energy radiated by some low range instruments. However at such low frequencies interference due to room modes may be a more pertinent problem.

2.7.2 Early Decay Time, (EDT)

Early Decay Time (EDT) is the time, in seconds, taken for the reverberant sound to decay 10dB. ISO3382 states that EDT, like RT_{60} , should be measured from the slope of the octave band integrated impulse response curves. The slope of this decay curve is determined from the slope of the best fit linear regression line to the appropriate part of the actual decay curve. The EDT is obtained from the initial 10dB of the decay. It is subjectively more important than RT_{60} and is related to *perceived* reverberance. RT_{60} relates more to the actual physical properties of the space.

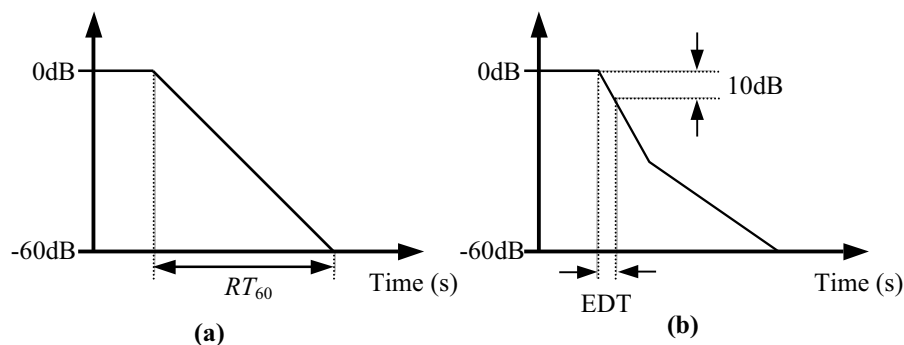


Figure 2.9 (a) Theoretical reverberation time, RT_{60} ; (b) Irregular reverberation slope and a measure of Early Decay Time, EDT.

2.7.3 Initial Time Delay Gap, (ITDG)

The Initial Time Delay Gap (ITDG) was originally defined by Beranek [Beranek, 1962] and is the time delay in seconds or milliseconds from the direct sound until the first reflection. It is usually calculated directly from the RIR. ITDG is related to a sense of intimacy of the music performed within the hall. If a space is small then it has a visual intimacy. Similarly if the music played in a hall sounds as if it is being played in a small space then it has acoustical intimacy. The main acoustical cue used by the listener to determine the size of a space is this ITDG. Halls that are described as intimate have an ITDG of less than 20ms [Beranek, 1962] with a direct sound that is not too low in level relative to the level of reverberant sound.

2.7.4 Early to Late Sound Index, (C_{80})

The early to late sound index, more commonly known as *Clarity*, relates to the time distribution of the reverberant energy, in particular the significance of the direct sound and early reflections compared with the reflections of the diffuse sound field. It is a measure of the ratio of the energy contained in the first 80ms of sound compared with the energy from 80ms onwards until extinction and is expressed in decibels [ISO3382, 1997].

C_{80} is associated with the perception of music and there is a similar definition for the perception of speech, C_{50} , with a measure over the first 50ms. C_{80} is more formally defined as:

$$C_{80} = 10 \log \frac{\int_0^{80} p^2(t) dt}{\int_{80}^{\infty} p^2(t) dt} \quad (2.10)$$

where $p(t)$ is the measured RIR. It is similarly possible to measure an early to *total* sound energy ratio, for example D_{50} , known as *Definition*, which is sometimes used for speech conditions. *Definition* is directly related to C_{50} as follows:

$$C_{50} = 10 \log \frac{D_{50}}{1 - D_{50}} \quad (2.11)$$

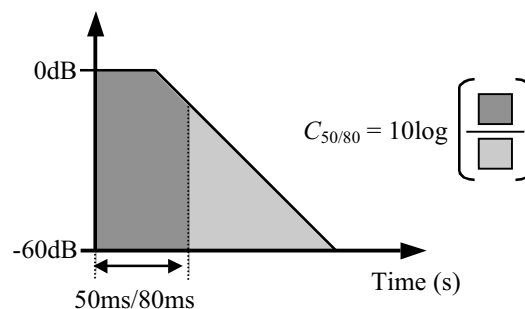


Figure 2.10 The Early to Late Sound Index, also known as Clarity C_{80} , with the early sound defined as either the first 50ms or the first 80ms of sound according to whether the result is associated with the perception of music (80ms) or speech (50ms).

2.7.5 Centre Time, (T_s)

Centre Time (T_s) measured in seconds is the time of the centre of gravity of the squared impulse response, and avoids the discrete division of the RIR into early and late periods. It is defined in Equation (2.12):

$$T_s = \frac{\int_0^{\infty} t p^2(t) dt}{\int_0^{\infty} p^2(t) dt} \quad (2.12)$$

C_{80} , C_{50} , D_{50} and T_s , as well as relating to speech intelligibility, relate to perceived definition and clarity or the balance between clarity and reverberance. As already discussed this is an important compromise and will have direct significance as to what a room may be successfully used for.

2.7.6 Sound Strength, (G)

The Sound Strength G is the difference, in decibels, between the squared and integrated sound pressure level of the measured impulse response and the squared and integrated sound pressure level produced by the same omni-directional source in a free field, measured 10m from its centre. It is defined as follows:

$$G = 10 \log \frac{\int_0^{\infty} p^2(t) dt}{\int_0^{\infty} p_{10}^2(t) dt} \quad (2.13)$$

where $p(t)$ is the instantaneous sound pressure of the impulse measured at the measurement point, and $p_{10}(t)$ is that measured at a distance of 10m in the free field.

2.7.7 Early Lateral Energy Fraction, (LF)

This is the fraction of energy (LF) arriving from lateral directions within the first 80ms and can be measured from impulse responses obtained from an omni-directional and figure-of-eight pattern microphones [ISO3382, 1997]. It is defined as:

$$LF = \frac{\int_{0.005}^{0.08} p_L^2(t) dt}{\int_0^{0.08} p^2(t) dt} \quad (2.14)$$

where $p_L^2(t)$ is the instantaneous sound pressure in the auditorium impulse response measured with a figure-of-eight pattern microphone. Note that there are other similarly defined early lateral energy measures, for instance [ISO3382, 1997] and [Hugonnet and Walder, 1998].

2.7.8 Inter-Aural Cross-Correlation, (IACC)

Inter-aural cross-correlation (IACC) is associated with binaural listening and measures the degree of correlation between the first 50ms of the pressure impulse responses received at each ear [Tronchin and Farina, 1997]. Ando [Ando, 1985] states that IACC is a significant factor in determining the subjective diffuseness, or lack of a particular directional impression, of a soundfield and it depends mainly on the directions from which reflections arrive at the listener and on their associated amplitudes. Subjective diffuseness is perceived when there is a low degree of IACC with a well defined direction being perceived if the IACC has a strong peak for $|\tau| < 1\text{ms}$. The normalised inter-aural cross-correlation function, IACF, is defined in Equation (2.15):

$$IACF_{t_1, t_2}(\tau) = \frac{\int_{t_1}^{t_2} p_L(t) \cdot p_R(t + \tau) dt}{\sqrt{\int_{t_1}^{t_2} p_L^2(t) dt \int_{t_1}^{t_2} p_R^2(t) dt}} \quad (2.15)$$

where $p_L(t)$ is the impulse response at the entrance to the left ear canal and $p_R(t)$ is similarly the impulse response for the right ear canal. The inter-aural cross-correlation coefficients, IACC, are given by:

$$IACC_{t_1, t_2} = \max |IACF_{t_1, t_2}(\tau)|, \quad \text{for } |\tau| < 1\text{ms} \quad (2.16)$$

IACC and LF measures relate to the subjective qualities of *spatial impression*. The state of diffusion of the reverberant sound field relates to *envelopment* in the room or hall and the measure of IACC. The perceived width of the sound source relates to *spaciousness* and the measure of LF.

2.8 Aural and Visual Cues

Clearly the most important feedback we have as to the behaviour of sound within a space is via our hearing mechanism. Using the ear/brain combination we can ascertain all the information we need to give us an impression of the space within which we are placed. This spatial impression is a fundamental aspect of all sound events. Every sound we hear has associated with it a particular acoustic characteristic in terms of the environment it occurs in - an environmental context. Even an anechoic or purely artificial synthesized sound has an environmental context - that of no environment at all. This is very unnatural to our hearing as we are so used to hearing sounds placed within a space. At the most primitive level this environmental information helps us to survive in the world by providing us with information as to where a sound source is located. This enables us to react accordingly whether the sound heralds potential danger - the engine of the car racing towards us as we cross the road, the siren

on the ambulance about to drive through a red light - or signifies safety and security - the mother calling to a lost child. As animals that essentially live on the “flat” surface of the world, our ears are situated on either side of our head. This helps us to more easily differentiate between sounds from the left or right, hence enabling us to locate a source on the horizontal plane even if we cannot see it [Begault, 1994]. The pinna point slightly forwards and present a very different profile from the rear than they do from the front enabling us to differentiate between sounds from the front and the rear. This effect is easily demonstrated by facing a noisy sound source and cupping your hands behind your ears, a noticeable timbral difference being the result as the cupped hands essentially increase the size of the pinna, emphasising the difference between the front and rear profile. Humans use a combination of interaural differences in time and intensity to locate a source on the horizontal plane. Contrast this with the hearing mechanism of the barn owl [Begault, 1994]. Barn owls primarily use time differences to locate a source on the horizontal plane and intensity differences for vertical localisation. This is due to the ears being placed asymmetrically with the left ear pointing down and the right ear pointing up hence giving an additional interaural cue for elevation that humans do not have. From an evolutionary standpoint this would appear to be related to the fact that owls usually hunt their prey from above.

Our hearing has so developed from a primitive survival mechanism that when listening to sounds in the environment around us we are able to detect the very smallest of changes. Trained listeners can effectively measure the size of a room or the distance to a wall by the length of time between the direct sound and the first early reflection. The balance of direct to reverberant sound can help the listener ascertain the distance of the source from them. Of particular note are the abilities of the visually impaired who receive all their cues about the environment around them through senses other than the eye. This ability was remarked upon as early as 1795 by Erasmus Darwin who wrote:

“The late blind Justice Fielding walked for the first time into my room, when he once visited me, and after speaking a few words said, ‘This room is about 22 feet long, 18 feet wide and 12 high;’ all of which he guessed by the ear with great accuracy.”

Erasmus Darwin, *Zoonomia*, Vol II, p 487, as referenced in [Beranek, 1962].

This skill is not limited to the visually impaired as musicians, acousticians, and experienced listeners of music can often gain a sense of the space in question simply from listening to a sound within it, be this a simple hand clap or a full orchestra playing a musical work.

However, it would be foolish to overlook the fact that we are animals that rely on vision as our primary sense of the world. Vision and hearing usually work together to allow us to fully

appreciate what is going on around us - upon hearing the car racing towards us we will locate its position using our eyes *and* ears and then *see* if it is likely to be a potential danger requiring further action. Multi-speaker surround sound is now commonplace in cinema and home entertainment systems. However no matter to what extent sounds are positioned around the listener in order to enhance the spatial impression of the subject matter, the dialogue will always be reproduced from the centre channel speaker (or reproduced equally from both left and right front stereo speakers either side of the screen, therefore effectively locating the sound at the mid point between them), due to the picture being located front and centre. If the sound from an actor's mouth were to be perceived as emanating from a position other than the screen area it would seem unnatural - what we hear would not agree with what we see. In contrast to this it remains true that in a typical cinema the centre speaker used for dialogue *is* usually displaced somewhat from the screen - perhaps behind, above or below. However we still perceive the words as coming from the actors' mouths as our ear/eye/brain combination link the sound events with the visual cues and hence compensate for the slight auditory localisation error.

It is this reliance on vision to confirm what we hear that leads many audio-only 3-D and surround sound systems to be limited in the results that they produce. A visual fix on an audio event greatly helps our ability to perceive it as intended [Begault, 1991]. We will always attempt to search out the source of a sound visually - provided this sense is available to us - in order to more quickly identify its location. When creating or controlling sounds within a space from a compositional viewpoint this visual feedback becomes particularly important for the user when more abstract or non-ideal acoustic spaces are involved - spaces that our ears have not listened to and hence have no prior experience of for reference purposes [Ballan et al, 1994].

Wave propagation is a phenomenon common in many physical media and this has often resulted in the properties of sound waves being more easily demonstrated using a medium other than air. Water undulation models - perhaps more commonly known as "ripple tanks" in secondary school science - are particularly simple analogues of sound wave propagation, being limited however to only two dimensions. It is also possible to analyse the reflection paths of sound within a scale model using lasers. Light models have also been used to investigate sound level distributions by photography of a ground glass screen at audience seating positions [Barron, 1993]. Such methods are limited to high frequencies only where sound can be considered to behave as a ray rather than a wave. In these models the propagation speed of light is effectively infinite and hence timing information can not be ascertained. This is obviously a severe limitation when looking at the properties of sound within a room.

For the first time in 1912 sequences of photographs were taken by Sabine of actual sound propagating through a model. Figure 2.11 shows the propagation of a single sound wave and its

reflections in the vertical plane from the sides of the proscenium arch in the New Theatre, New York. Sabine described this method as a modification of the Toepler-Boys-Foley method of photographing air disturbances [Sabine, 1964], also known as the Schlieren technique [Barron, 1993]. Essentially the method involves building a scale model of the space, removing two parallel sides and as sound is passing through it illuminating it instantaneously by the light from a very fine and distant electric spark. A photographic plate is placed at a short distance on the other side of the model, with light being refracted by the sound waves as it passes through them essentially acting as their own lenses in the production of the image.

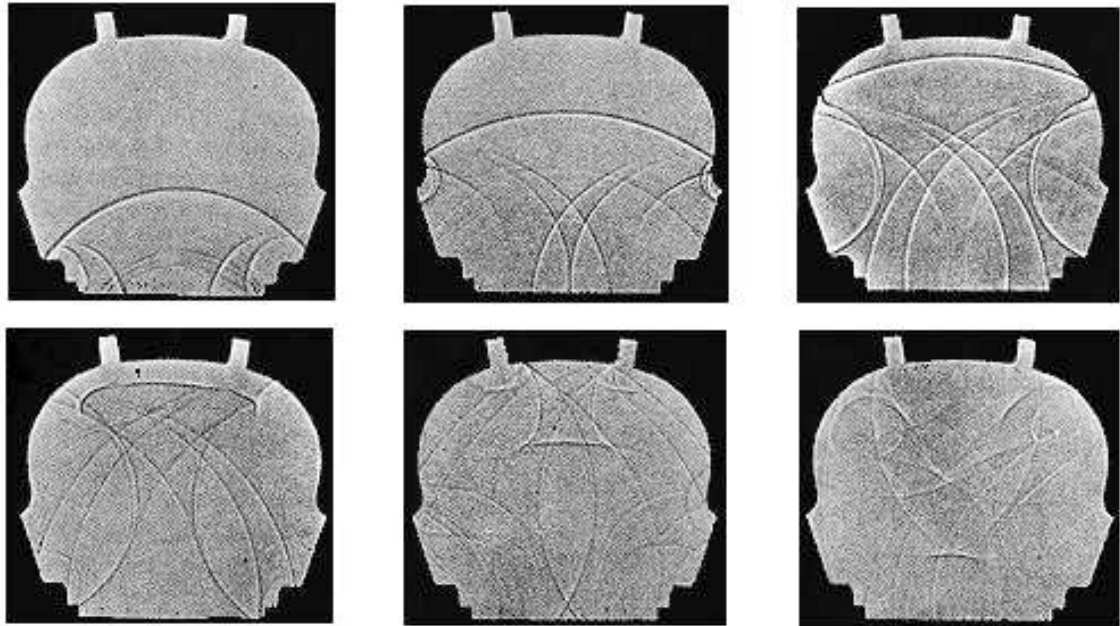


Figure 2.11 Photographing Sound - Visualising sound wave propagation in a model of New Theatre in New York. The sequence of propagation runs from the top left frame to the bottom right [Sabine, 1964].

Although limited to two dimensional qualitative information about a relatively short time interval after the initial sound, the results were impressive and their detailed discussion by Sabine reveals a great deal of important information. For instance using the photographs of New Theatre, Sabine demonstrates how even relatively small architectural details contribute important diffraction effects to the acoustics of the hall. Acoustic analysis using sound rays cannot account for these effects and if used in this particular example would have resulted in an erroneous conclusion as to the acoustic quality in certain areas of the theatre. An analysis of the examples in Figure 2.11 and other photographs enabled the architects to change the design of the theatre and so eliminate some of the problematic acoustic effects before the building was constructed.

The behaviour of sound is often a difficult concept to grasp both for the novice and the expert and clearly a visualisation of sound propagation can lead to an increased understanding of the

principles involved, as evidenced in Sabine's work described above. Similarly, as stated in [Ballan et al, 1994] visual feedback from a space created by the composer will allow more intuitive control of the sound within, and perhaps aid sound source localisation if audio is produced in synchronisation with video. It is often said that a *picture paints a thousand words* so it must surely be the case that a moving picture or animation will convey more information than a static snapshot. Animations are easily realisable on even the most basic current PC systems, and are becoming more commonplace with a number of established standard file formats and the use of the Internet as a distribution medium. Companies such as Celestion have been using animations since 1980 to analyse the vibrations of loudspeakers [Wright, 1998] and the existence of wave phenomena such as diffraction in a small enclosed space is a clear case for their use in the study of room acoustics.

2.9 Summary

It is possible to consider the acoustics of an enclosed space as a generic system with an input and an associated output that is transformed in some manner according to the properties of the space itself. If the input signal applied to an enclosed space and to a comparable analogous system of non-specific origin is the discrete unit impulse, and the resultant output signal is the same for both, then the original room can effectively be replaced with this equivalent system. The impulse response of the room, or equivalent system, for given source and listener positions is a unique measure of its physical properties. By examining this RIR it should be possible to determine the characteristic features of sound propagation in an enclosed space. These features have been identified as:

- The Direct Sound

- Early Reflections

- Reverberant Decay

- Dominant Resonant Frequencies – Room Modes

The RIR can be used directly in an appropriate convolution signal processing operation that results in a system equivalent to the original room. It can also be used as an analysis tool from which relevant well-defined, objective acoustical parameters can be extracted. In general these parameters also correlate to some of the more perceptually important measures of acoustic performance that are perhaps more difficult to quantify and interpret without non-trivial statistical analysis. The importance of visual feedback in understanding the detailed behaviour of sound propagation has also been identified.

For any model to be successful there must be adequate provision for testing, with resultant measures correlating to relevant criteria that are readily understood. Within the broader context of this thesis this chapter has helped to identify two important analysis methods:

Visual Analysis

The concept of controlling spatial parameters as an increasingly important and integral part of musical composition was discussed in Chapter 1. However, as musicians are not usually experienced in theoretical acoustics, it is possible that there exists a mismatch or lack of understanding between the compositional/perceptual intent and the corresponding physical quantities and acoustic result. However it cannot be ignored that the musician or composer will often have an intimate, higher level understanding of musical sound. The composer knows what a resultant spatial effect should sound like but may not understand how it is achieved, or how it might exist as a physical reality. It therefore seems evident that a system or model designed for musical control of space would benefit from some form of graphical control, with feedback from the space itself and the sound within it. This visual feedback gives the first potential method of analysing any such wave propagation model. As examined in Chapter 2.8 there is a rich history of successfully using visual analogues of wave propagation to demonstrate acoustic principles. Such a mechanism would give a number of potential benefits as follows:

- Immediate visual feedback as to whether the model is behaving as expected.

- A clear and valid method of evaluating the properties of the model.

- A method of defining a room together with input and output location using physical quantities corresponding directly to a graphical representation.

- A clear and valid method of evaluating the aural effect of a room/source/listener combination.

- Provision of visual cues as to the acoustic environment and to how it is behaving.

RIR Analysis

The second analysis method is clearly evident in the form of the measured RIR. As stated, its use is twofold. From the point of view of what is required of any musically useful model of wave propagation in an enclosed space, the RIR, when implemented in a convolution signal processing routine, becomes the digital realisation of the physical reality of the space itself. This therefore allows sounds to be auditioned as if they had been placed in the modelled room and an aural analysis of the quality of the resultant spatial effect.

Secondly, more qualitative analysis using measured RIRs is also possible. A frequency domain representation should reveal information about room modes and allow a comparison with those predicted using Equation (2.6). Using the criteria for analysing RIRs as set in ISO3382 and described in Section 2.7, additional acoustic parameters can be calculated including those measures associated with reverberation. Using one of the modules from *Aurora* - a software processing and analysis toolkit for RIRs [Farina and Righini, 1999] (see also Section 3.3.3) - a number of acoustic parameters can be readily calculated according to ISO3382 guidelines from

RIRs in WAV audio file format. These include RT_{60} , EDT, Clarity C_{50} and C_{80} , Definition, and Centre Time. According to the software designer the impulse response is octave-band filtered by means of Infinite Impulse Response (IIR) IEC-compliant filters, then it is squared, so obtaining the acoustic energy, and processed. For calculation of reverberation time, the squared impulse response is backward-integrated, with an optional noise-removal algorithm, and a linear regression is performed over the appropriate dB range.

However no matter how close this equivalent system may come to what is theoretically expected, the most revealing form of analysis, as with any perceptually important musical event, will still involve the informal auditioning of sounds processed by the model. Can such an equivalent system impart and relate a detailed, realistic and convincing spatial effect?

Chapter 3

Artificial Reverberation

3.1 Introduction

The reverberant sound is the most prominent acoustic feature perceived when we listen to sound within a space. Indeed it was long considered the most important acoustic characteristic of a room or hall. As such, when processing an audio signal with a system considered to be an equivalent to the acoustics of an enclosed space, it has often been the case that only this general reverberant effect is reproduced and not the actual exact soundfield. Artificial reverberation processing, or *reverb* as it is more generally known, is a technique widely used to enhance recorded and synthesized sounds and a number of methods have been used with varying degrees of success in the search for a convincing effect. This chapter looks at some of these methods. This includes the traditional but at times crude electro-mechanical models that substitute the room system with electrical and mechanical components, digital reverberation using algorithms based on networks of simple filters, and modern auralization and convolution processing techniques.

3.2 Electro-Mechanical Reverberation

3.2.1 Reverb Chambers

Before the use of electronic reverberation systems, one of the only ways to add reverberation to a pre-recorded signal was to construct an acoustic reverberation chamber consisting of a room with highly reflective surfaces. The most natural effect was obtained with walls built at irregular angles and coated with hard plaster or tile [Woram, 1989]. Figure 3.1 shows a diagram of an acoustic reverberation chamber. A pre-recorded signal is fed to the loudspeaker and picked up by one or more microphones. Highly reflective surfaces present within the chamber produce a diffuse and reverberant soundfield. The resulting sound, as recorded through the microphones, will therefore contain the acoustic characteristics of the chamber, as if the original sound had been recorded within it.

Although this method is very effective in its production of a reverberation effect, it is not a practical option in most cases. Reverb chambers are expensive to build, especially as they must be suitably isolated from outside noise. They require high quality speakers and microphones so as not to colour the original sound in an adverse way, and they are inflexible in that once the

room is built, changing the reverb characteristics is not easy without the use of movable drapes or acoustic barriers. However, reverb chambers provide the only true reverberation of all artificial systems with even the best quality digital units being unable to copy the three-dimensional feel or physical impact a chamber can add to powerful percussive sounds.

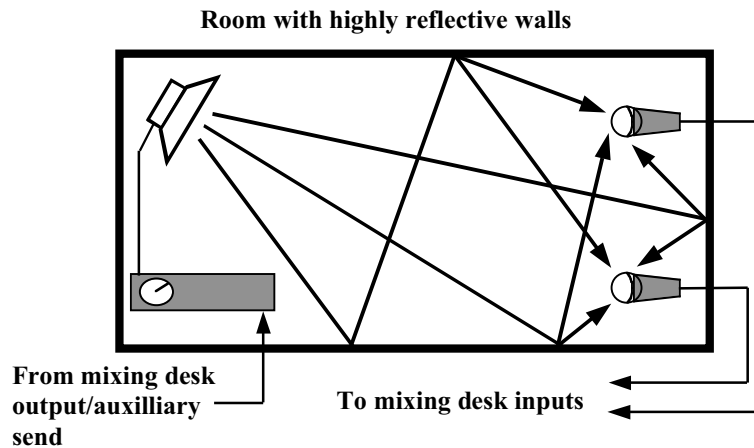


Figure 3.1 An acoustic reverberation chamber. A signal is introduced to the chamber via a power amp and loudspeaker and output using the pair of microphones.

3.2.2 Duct Reverbs

It was found that attaching a small loudspeaker to one end of a common garden hose and a microphone to the other produced a reverberant effect with some echo. This idea was developed further to use larger sections of solid pipe (see Figure 3.2). An example of a commercially available reverb unit of this type was the *Cooper Time Cube* [Wadhams, 1990], which consisted of a rack mountable chassis containing the driving electronics and microphone preamp and a box containing the tubing. These types of system were limited in both their frequency response and dynamic range and could only produce one kind of basic sound. However they did work to some extent and had the advantage of being relatively compact and portable.

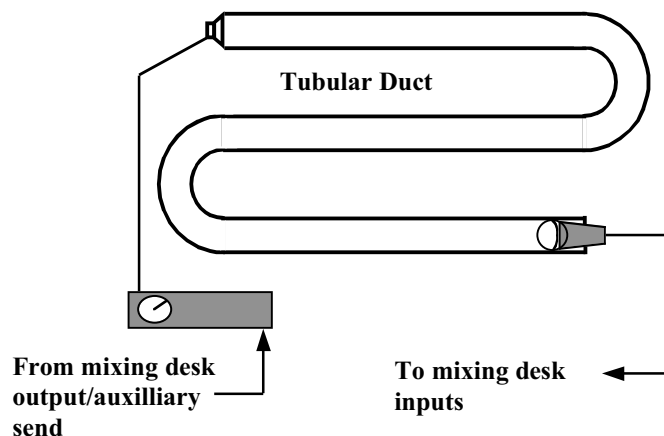


Figure 3.2 A duct type reverb. A signal is introduced to the duct via a power amp and loudspeaker at one end and output using a microphone at the other.

3.2.3 Spring Reverbs

A simple and inexpensive way of producing a reverberation effect is by using a spring coupled between two transducers as shown in Figure 3.3 [Wadhams, 1990]. A signal input to the sending transducer makes the spring vibrate in a torsional mode. This signal travels back and forth along the spring, reflecting at the ends until it falls below the residual noise level. This mechanical energy is converted back into an electrical signal at the receiving transducer at the other end of the spring. This method is analogous to a loudspeaker and microphone with the spring transmission line being the propagating medium rather than the normal air molecules. Two springs are usually used and their sound is determined by the thickness of the wire, the number of turns per inch and the overall length. In some cases, more springs are used, each having different characteristics, varying in length, mass or stiffness, so as to obtain a richer reverb texture through more random reflections. Some spring reverbs also have an adjustable damping mechanism that changes either the actual damping applied to the spring or alters its length in order to achieve the required reverb decay time.

The resulting effect in early spring reverb systems did not turn out to give a good approximation of natural reverberation. They can produce a very noticeable metallic glitch when a sharp edged transient waveform is applied and are subject to mechanical feedback from the soundfield exciting the springs directly. Springs are also generally deficient in transient and high frequency response. However, this method is still in use in many modern guitar amplifiers because of the desirable resonant decaying characteristic it imparts to the sound.

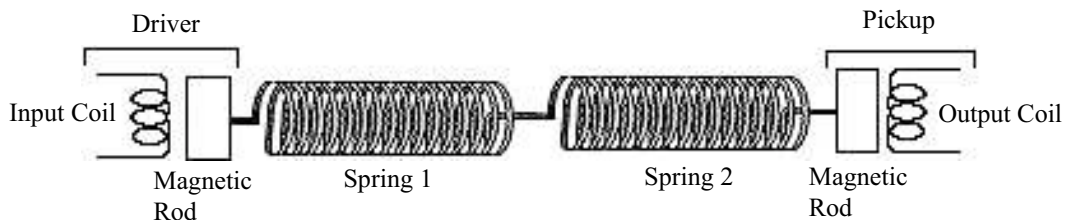


Figure 3.3 Cross section of a spring reverb system [Wadhams, 1990].

3.2.4 Plate Reverbs

What may well be the most popular pre-digital reverberation device was developed by Dr. Walter Kuhl of the Rundfunktechnisches Institut (Institute of Broadcasting Technology) in Hamburg, Germany in 1957 [Woram, 1989]. It consisted of a large rectangular steel plate suspended at its four corners, excited with an audio signal via a transducer. At the edges of the plate, the bending waves created by this radiating signal are reflected in a manner similar to the way in which sound waves are reflected at the surfaces present in a room. This original device became a widely used tool in recording studios worldwide although was superseded in 1971 by a smaller device, based on the same principles, which used a 30cm x 30cm sheet of gold foil

instead of a large steel plate. This was to be much more useful than the inconveniently large plates and produced a better effect with an improved high frequency response due to the thinness of the gold foil. The heavier the material used to make the plate, the more the high frequencies have to be boosted in order drive it with a corresponding increase in the residual noise level. A single transducer would pick up the bending waves and output a signal that simulated quite closely the reverberant nature of a large room. Later models used two transducers at the output to give a stereo effect. A damping system was also used to adjust the reverberation time of the plate/foil. The success of these devices is still in evidence today with most off-the-shelf digital reverb units having an algorithm emulating the plate reverb effect.

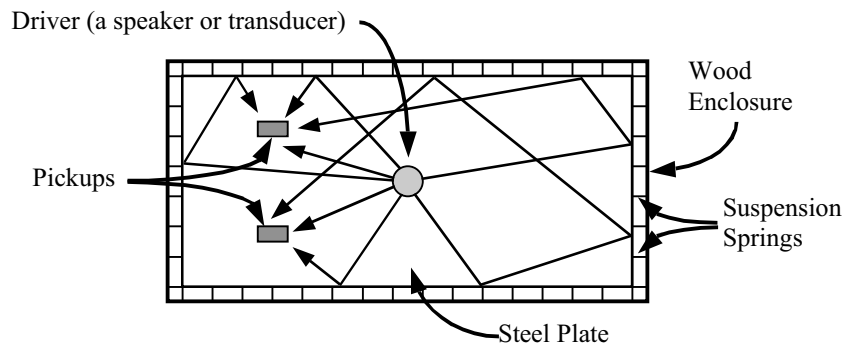


Figure 3.4 Cross section of a plate reverb system, [Wadhams, 1990].

3.3 Digital Reverb

The purpose of digital reverb is to model the reverberant sound in a generic manner using a combination of digital signal processing, time delays, filters and mixers, to simulate the effect of a room or hall when applied to an arbitrary sound source. Ideally, the impulse response of the final filtering scheme resembles the impulse response of the modelled room. One of the main advantages of digital reverb systems is their flexibility. The type of reverb available can be changed easily by selecting another algorithm from a list of preset programs. Often these presets can be further tailored to individual needs by altering some of the internal parameters of the algorithm in question such as the decay time of the reverberant sound. Another helpful feature, remote control, is also often provided, usually via the industry standard Musical Instrument Digital Interface (MIDI) or Society of Motion Picture and Television Engineers (SMPTE) protocols, enabling reverb parameters to be controlled from other pieces of equipment, such as a synthesizer or sequencer. This inherent flexibility and the fact that the reverb algorithms are based around the use of a digital delay line enables dedicated reverb units to produce other delay based special effects for musical use such as phasing, flanging and chorusing.

In architectural acoustics, the study of digital reverberation can aid in the design of buildings - especially important in the case of concert halls and recording studios. In digitally synthesised

music, the reverb unit can be seen to be part of the instrumental ensemble, adding a controllable element over the perceived sound quality so that composers can imagine their music being heard and enriched by virtually any sound space they might imagine or program into such a unit. However, even digital reverberation, with all its inherent flexibility and quality, is not without its particular drawbacks. The reverb unit can only emulate a real RIR as typical listening spaces are inherently high order systems which cannot be precisely simulated in real time using commonly available computing techniques. The requirement for full audio bandwidth processing with an increased dynamic range and signal-to-noise ratio places a heavy demand on the memory size in these application-specific digital signal processors - particularly if long decay times are to be implemented - and on the quality of the input/output converters.

3.3.1 Building Digital Rooms – Unit Reverberators

Digital reverb algorithms have been a standard post-synthesis sound enhancement tool for digital music creation since Schroeder’s classic papers in 1961 [Schroeder and Logan, 1961] and 1962 [Schroeder, 1962]. These original computer simulations of room reverberation were composed of combinations of *allpass filters* and *comb filters*. These two basic building blocks were called *unit reverberators*.

Comb Filters

The input to a comb filter enters a delay line and upon reaching the output this delayed signal is fed back to the input after being multiplied by some gain factor g . The time taken to circulate once through the delay line is called the loop time, T , and the filter will therefore sound, or “ring”, at the frequency corresponding to the inverse of this loop time, $F = 1/T$. This is the natural frequency of the filter. The response of the filter decays exponentially as determined by the values of the loop time and the amplitude gain factor. Values of g near unity give the longest decay times, but g must also be less than unity for the filter to be stable.

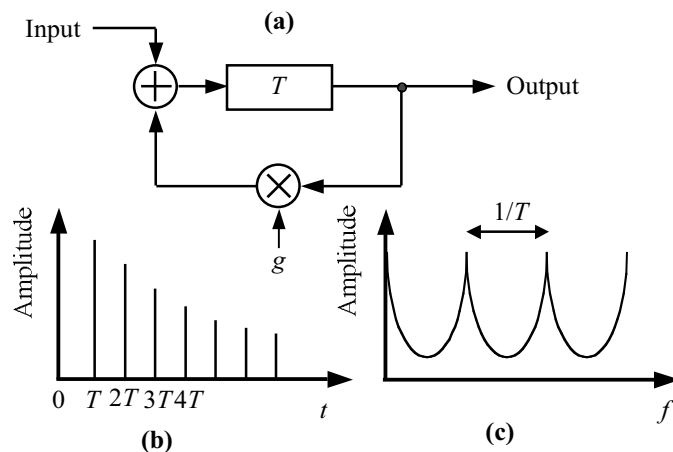


Figure 3.5 Comb filter unit reverberator; (a) Filter design with delay T , and feedback gain g ; (b) Impulse response of filter; (c) Frequency response.

The decay time of the filter is often defined to be the -60dB point of the decay relating directly to the definition of reverberation time. Note from Figure 3.5 there is also a delay in the onset of the first impulse of the impulse response, which obviously corresponds to the loop time. The comb filter is so called because its steady state frequency amplitude response resembles the teeth of a comb. The spacing between the maxima of the teeth of this comb equals the natural frequency and the amplitude difference between these maxima and the interspaced minima is a measure of the value g . As g approaches unity, the maxima and minima become more pronounced.

Allpass Filters

The allpass filter is similar in implementation to the comb filter but involves the addition of a suitably amplified undelayed path through to the output. It has a flat amplitude response with no attenuation in the steady state with the relative amplitudes of the spectral components of the input signal remaining unaltered at the output. However, there is a substantial effect on the phase of individual components, and its transient response can impart colour to a sound during a sharp attack or after a sharp decay. As with the comb filter the length of the delay line is called the loop time T , and a factor g specifies the decay time, which again must be set to less than unity for stability.

The impulse response of an allpass filter, like that of a comb filter, is an exponentially decaying pulse train although in this case there is no delay between the start of the input and the appearance of an output. The first impulse in the response is also of negative magnitude whereas the others are positive as before. This is due to the mixing proportions of $(-g)$ gain for the undelayed signal, and $(1 - g^2)$ gain for the delayed signal.

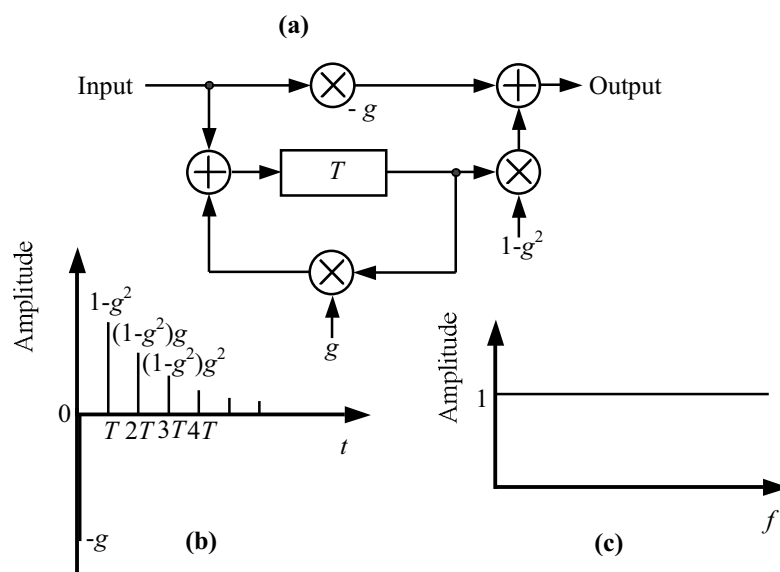


Figure 3.6 Modified comb filter giving an allpass unit reverberator; (a) Filter design with delay T ; (b) Impulse response of filter; (c) Frequency response.

3.3.2 Combining Unit Reverberators

Schroeder's original designs using interconnections of these two unit reverberators, as shown in Figure 3.7, have formed the basis of many digital reverberators since. Figure 3.7(a) represents a parallel connection of four comb filters followed by two allpass, with some proportion, k , of the original signal added in at the output. Figure 3.7(b) shows a series connection of allpass filters, again with some proportion of the original signal added in at the output. The idea with both of these combinations is to use the unit reverberators to generate the effect of wall reflections and the time of travel of the wave-front as it passes from one wall to the other. The addition of some of the original signal simulates the closeness of the source to the listener.

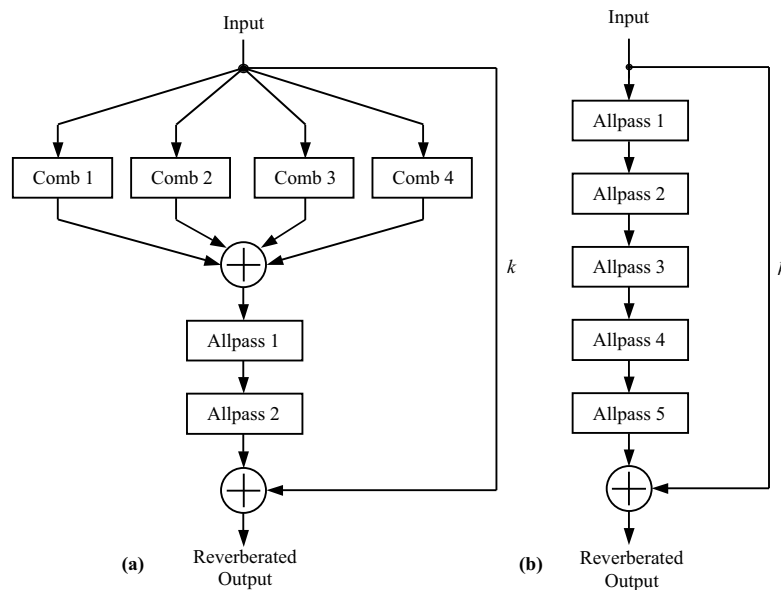


Figure 3.7 Combinations of unit reverberators to make a functioning filter reverberation simulation system

The characteristic sound of a reverb system based upon these designs depends upon the choice of the loop times, T - determining the impulse distribution over time - and the amplitude gain factors, g - determining the reverberation time - for each of the component unit reverberators. In modelling a large concert hall reverberator (a) uses comb filter loop times of around 50ms with a ratio of longest:shortest delay of 1.7:1 [Roads, 1995]. The allpass filters have relatively short loop times of about 5ms or less. The purpose of the allpass filters is not to lengthen the decay time but to increase the density of the reverberation. Hence the reverberation time of these filters should be kept short, to about 100 ms or less. It is also important for natural sounding reverberation to choose loop times that are relatively prime to one another [Moorer, 1979]. This ensures that none of the impulses in the filter responses are spaced at common multiples to one another in such a way as to coincide causing large peaks in the otherwise smooth decay of the overall response.

Several improvements have been made to Schroeder's two original designs. For instance, with a fixed source and listener, the early reflections can be modelled using a tapped delay line and the late reverberant "tail" can be qualitatively modelled using a combination of allpass chains, comb filters, and low pass filters [Moorer, 1979]. A lowpass filter in the feedback loop of a comb filter can be used to simulate air absorption and non-specular reflection. It is also important that the sounds presented in each ear should be mutually incoherent [Roads, 1995]. That is, the reverberation algorithm should be slightly different - decorrelated - for each channel of processing, in order to give a more realistic effect.

3.3.3 Reverberation Using Convolution

An accurate but computationally intensive means of simulating the reverberation in an acoustic space is to convolve the RIR of the actual space with the signal to be reverberated. The RIR of the space can be modelled approximately using delay lines and unit reverberators or more exactly using one of the methods described in Chapter 4. Alternatively the RIR of the space to be modelled can be measured directly as discussed in Section 2.6. This RIR can then be convolved with the signal required to be reverberated by implementing the impulse response as a Finite Impulse Response (FIR) filter. This FIR filter replaces the actual room - if the RIR has been obtained directly - effectively giving an equivalent system. All the properties of the original system - the room - including brightness, diffusion and reverberation decay time will be preserved by the FIR filter model [Reilly and McGrath, 1995].

Direct convolution in the time domain is not practical for reverberation because of the large number of computations involved. For example, consider a 2s long RIR sampled at a rate of 48kHz. Each sample of each channel of the input signal must be multiplied and summed 48,000 x 2 times. So, for two seconds of audio input:

$$\begin{array}{rclcl}
 48,000 \times 2 & \times & 96,000 & = & 9,216,000,000 \\
 \text{Multiply/adds} & & \text{Samples} & & \text{Multiply/adds per} \\
 \text{per sample} & & \text{per second} & & \text{second for two channels}
 \end{array}$$

Therefore to reverberate one second of stereo sound by direct convolution requires 9.216 billion multiply/adds [Roads, 1995] and carrying out this number of operations in real time requires computer performance that is still not commonly available. Reverberation by convolution can be implemented more efficiently using the Fast Fourier Transform. In general, for an RIR N samples long, fast convolution takes on the order of $N \times \log_2 N$ operations. So the example above would require less than 1,500,000 operations, giving a speedup by a factor of 6100. Alternatively, if a fast convolution carried out on a specific processor takes 1 second, it would take the same processor 101 minutes to calculate the same via direct convolution. Therefore for most applications, it is more practical to implement reverberation using multiplication in the

frequency domain via the FFT, rather using than the equivalent convolution operation in the time domain.

Companies such as Lake DSP have for some time been producing hardware to allow accurate aural rendering of acoustic spaces using multi-channel convolution in real time [Lake Technology Ltd, 1999]. However this technology is effectively out of reach of most potential users due to the high cost of development and the application-specific hardware involved. With ever-increasing speeds in standard PC processor technology real-time convolution is slowly becoming more commonplace, making this method of reverberation a more practical reality.

Aurora is a software tool for measuring, filtering and convolving the RIRs of acoustic spaces with arbitrary audio signals [Farina and Righini, 1999]. It is designed to operate as 14 plug-in extensions to the *Cool Edit* range of PC based software audio editors [Syntrillium, 1999]. One of these plug-in modules is *Convolver* which is capable of executing single precision floating point frequency domain convolution in real time on the CPU of the host PC. Table 3.1 shows the real-time performance limits of a (now obsolete) Pentium MMX 200 MHz working with waveforms at a sample rate of 44.1kHz:

DESCRIPTION	NO. OF CHANNELS IN SOURCE SIGNAL:	NO OF CHANNELS IN IMPULSE RESPONSE:	IMPULSE RESPONSE LENGTH (TAPS):
Mono Input/ Mono IR	1	1	1,000,000
Mono Input/ Stereo IR	1	2	64,000
Stereo Input/ Stereo IR	2	2	16,000
Stereo Input/ 2 Stereo IRs	2	4	4,000

Table 3.1 Real time convolution performance limits of a Pentium MMX 200Mhz CPU working with 44.1kHz sample rate waveforms.

Although there are some other commonly available hardware and software effects units that use convolution as part of the reverberation process, it would seem that the forthcoming Sony DRE S777 Sampling Reverb will be the first unit to use real time convolution as the engine to accurately recreate the reverberation effect of real rooms and halls [Robjohns, 1999]. In this prototype machine actual RIRs are stored on CD-ROMs and loaded using the built in CD-ROM drive. A small amount of editing by the user of the reverb characteristics is allowed although

not as much as on current algorithm-based reverb units. Currently the measurements of 10 venues in Japan and Europe have been made with more to follow including, it has been stated, more uncommon acoustic environments such as forests, domestic spaces and submarines. The processing is state of the art with application-specific DSP chips capable of executing 256,000 point convolutions, 24-bit I/Os as standard, sampling rates of 44.1kHz or 48kHz with an optional DSP upgrade to 96kHz. Four-channel surround sound will also be an option, with four discrete output points in the venues at the measurement stage taking this into consideration. The cost of this technology is suggested to be somewhere between £3500 and £6000 depending on fitted options; this is still cheaper than the current state of the art industry standard reverb unit, the Lexicon 480L. It should only be a relatively short time before second generation products are available to the semi-professional and consumer markets spreading research and development costs over a much wider product base. This has already been the case with advanced physical modelling synthesis and processing as developed by companies such as Yamaha and Roland.

3.4 Auralization

One of the aims in the field of audio and acoustics has been to recreate a particular recording or listening environment exactly. *Auralization* is another step in this direction. The term is introduced to be used in analogy with visualization to describe rendering audible (imaginary) sound fields [Kleiner et al, 993]. It is defined as follows:

“Auralization is the process of rendering audible by physical or mathematical modelling, the sound field of a source in space, in such a way as to simulate the binaural listening experience at a given position in the modelled space.”

[Kleiner et al, 1993].

The main aim is not to recreate the sensation of the sound itself, but to recreate the aural impression of the acoustic characteristics of a space within which the sound is required to be heard. The theory of auralization has been well understood for many years; however it is only relatively recently, with improved measurement techniques and faster DSP, that it has become a practical reality. There are four basic techniques in current use within the field of auralization, all of which are based upon approximations of the properties of the sound source, the acoustic space and the listener.

3.4.1 Fully Computed Auralization

The acoustic properties of modelled rooms are examined by software designed to predict the BRIR. Firstly the RIR is found, often using a more refined version of the Ray Tracing or Image

Source modelling methods (see Section 4.2) together with additional techniques to take account of the absorption, scattering and diffraction properties of sound waves propagating through the space. This RIR is then processed to arrive at the BRIR. This process could be a simple stereo representation of the sound field achieved by having receiving points at approximately interaural distance or, for greater accuracy, it could involve a more complicated fully binaural representation by measurement of the free-field to ear drum pressure transfer functions for a particular listener's head. This is known as the Head Related Transfer Function (HRTF). The particular properties of these models can then, using a convolution process to filter an audio signal, be monitored binaurally over headphones or transaurally over stereo speakers.

3.4.2 Computed Multiple-Loudspeaker Auralization

This is very similar to fully computed auralization except for the final method of presentation to the listener, which is in this case over a multiple loudspeaker array. A multi-channel convolution system is also required. The greatest advantage of this method over fully computed auralization techniques is the natural directionality of the soundfield produced by the loudspeaker array; sounds coming from behind the listener really do originate from behind. However, for total accuracy, the array must be located in an anechoic chamber so that the listening room itself does not further colour the sound.

3.4.3 Direct Acoustic Scale-Model Auralization

In this method a scaled down three-dimensional model of the space is used, complete with acoustic absorption, with frequency-scaled audio signals actually being played within it. The signals are then converted to full scale for presentation to the listener. The advantage of this system is that it does not rely upon a mathematical model for accuracy. Therefore all the natural properties of an acoustic wave propagating through a space are inherent in the output, as this is what is actually happening. Problems arise in that the scale models are not always an accurate representation of reality due to the difficulties in building them at such a reduced size. This is especially the case with scaled down absorbers, microphones and dummy listening heads. This is also probably the oldest technique of modelling an acoustic space out of the four described, with methods dating back as far as 1965 [Kleiner et al, 1993].

3.4.4 Indirect Acoustic Scale-Model Auralization

With this method the BRIR of the scale model is calculated and convolution is used for processing and presentation. This offers a number of improvements over the direct acoustic scale model technique including a higher signal-to-noise ratio, less distortion and the convenience of being able to store the BRIR, rather than the actual scale model, as the representation of the characteristics of the room.

3.4.5 Some Potential Uses of Auralization Techniques

Auralization techniques and the construction and realisation of virtual acoustic spaces in this way have a number of varied potential uses as follows:

- Training of architects, acoustic engineers and audio engineers.
- Training of musicians.
- Training of the visually impaired.
- Factory noise prediction and noise quality assessment.
- Studies in psychoacoustics.
- Studies in reverberation enhancement, and the room-loudspeaker interface.
- Investigation into microphone response patterns and placement.
- Virtual reality systems.
- Cinema sound systems.
- Effects in video games.
- Improvement of binaural sound for in-flight entertainment.
- Subjective assessment of concert hall acoustics.
- Acoustic design and simulation of new concert halls.

Auralization is still a relatively new tool although some of the techniques - with particular reference to the HRTF - are being used as the basis for “3-D surround sound enhancement” in commonly available multimedia products such as computer soundcards and home entertainment systems. Demonstrations of full auralization systems have been made and are becoming more commonplace. However verification of their accuracy in the reproduction of the desired aural effect is still lacking, rather limiting the use of these methods as a serious acoustic design tool [Kleiner et al, 1993].

3.5 Summary

A number of methods have been used in the search for a detailed, realistic and convincing reverberation effect. Although they vary significantly in how they are implemented each model introduced in this chapter is essentially an “equivalent system” to the enclosed space with its own particular physical properties determining how close it is to reality. Electro-mechanical methods may seem somewhat archaic in the digital age but their legacy remains. Spring reverbs are still found in guitar amplifiers and the plate reverb algorithm is a staple preset of modern digital reverb units. It is the inherent physicality and analogue nature of these models that make them - in some cases - so successful. They are not limited by the necessary simplifications imposed by the discrete nature of the digital domain and chambers and plate models are possibly the closest equivalent systems to real enclosed spaces. The effect they produce however has often been subject to the relatively poor quality of the driving electronics and

output transducers and they are also expensive to produce and inconvenient to use. Both chambers and plates are inflexible when compared with the range of simulations produced by even the cheapest off-the-shelf reverb units. However the principle of a reverb chamber is still used in some Auralization techniques with a scale model of an actual hall being used as a replacement physical medium

The most successful systems to date are those based around digital reverberation filter algorithms. These methods are cheap, robust, flexible and of the highest quality. However they are often very general in their approach and are not usually designed to model a specific room or hall or take account of fine architectural details. Although easy to use, editing the preset algorithms can be involved with user-definable parameters bearing little or no relation to the reality they hope to emulate.

Auralization and convolution reverberation techniques are clearly the most accurate of those discussed so far, capable of recreating exactly the properties of a particular hall. However these virtual reality audio systems come with significant overhead. Extreme care has to be taken with the accuracy of the measurement process, convolution processing is still relatively expensive in terms of the computational power required, and in the case of auralization, a special non-standard playback system is often required. More importantly from the user's point of view there are severe limitations in terms of the flexibility and editing allowed in such systems, although the quality of the simulation implies there should perhaps be no need to edit. At the heart of the process is an actual RIR from a real space there is little that can be done to alter its properties in a straightforward manner. Therefore the user is limited to the RIRs supplied with the unit at the discretion of the manufacturer. Flexibility has been sacrificed for accuracy and audio quality, and we have effectively returned to the concept of the reverb chamber. However this "virtual reverb chamber" is a significant improvement, being considerably smaller and more convenient to use, and being capable of accurately reproducing any acoustic space if an appropriate RIR measurement is available.

It would seem that what is required from a general, ideal model of acoustic space, is the accuracy of a convolution system - already identified as being desirable when used in conjunction with the RIR in Section 2.9 - together with the flexibility of traditional digital reverb algorithms. It should be possible however to generate this RIR based only on a description of the physical characteristics of the modelled space. The RIR is directly related to the acoustic properties of the model with a simple change in the specific architectural features of the virtual space resulting in a corresponding direct change in the RIR. The methods examined so far do not fall into this category. They either model a particular space or equivalent system

exactly or approximate a range of typical spaces in a very general manner. An alternative acoustic modelling paradigm has to be considered.

Chapter 4

Acoustic Modelling Techniques

4.1 Introduction

The previous chapter introduced some of the methods that have been used to model the acoustics of a room, with particular emphasis on the reverberant sound. The earliest electro-mechanical models of the room system replace the actual room with a physical medium having wave propagation properties analogous to those of a 3-D space, the plate model being a particularly successful example. Digital reverberation models use a topology of simple filters and delay lines as a more abstract but accurate replacement system. Reverberation via convolution and auralization techniques yield the most accurate and convincing results but often at the cost of increased complexity and expensive processing power. The methods examined so far have usually been limited to producing either very general results - for instance digitally modelling a reverberant decay that, with simple editing, can be used to approximate the characteristics of many different spaces - or very exact results suitable only for modelling a specific hall - the Sony Sampling Reverb. A method of accurately modelling the acoustics of a general room or hall given only its architectural characteristics is still required.

The purpose of this chapter is to introduce and assess the techniques currently applicable to room acoustics modelling in order to identify that which might be most suitable to the problem highlighted by the previous chapter. This is the requirement to have the accuracy of a convolution based reverberation model combined with the flexibility of traditional digital reverberation algorithms based only on the physical characteristics of the space. A number of potential modelling paradigms are available to tackle this problem, examples being geometrical room acoustics models, finite element and boundary element methods, time domain finite difference models and the related waveguide mesh approach. Each model will be introduced in this chapter and the relative merits and disadvantages discussed with a view to arriving at a suitable solution to the room acoustics modelling problem.

4.2 Geometrical Models

4.2.1 Overview

Geometric acoustic models provide a much simplified yet intuitive and - within limitations - accurate method of modelling sound propagation. The principle has already been mentioned in passing in the previous two chapters and essentially conceptualises a sound wave as a ray. In this way the path of a propagating wave can be examined with considerable clarity and rigour. Specular reflections at a surface can be considered where the angle of incidence is equal to the angle of reflection. Absorption can also be accounted for where the ray loses a percentage of its energy in a frequency dependent manner according to the absorption coefficient of the reflecting surface in question. Absorption due to the propagating medium proportional to the distance travelled by the sound ray can also be modelled.

Geometric models are based on the assumption that the surfaces involved are essentially flat and large compared to the wavelength of sound being considered. This implies that these models are only valid for high frequencies. The full audio spectrum, generally considered, ranges from 20Hz to 20kHz, with corresponding wavelengths ranging from approximately 17m down to 1.7cm. This implies that geometric models are only really applicable for larger acoustic spaces. They are further limited as they do not in general take account of other wave phenomena. Diffraction effects cannot be accounted for as propagation in straight lines is an inherent part of the model. Similarly, interference effects are disregarded as there are no phase components to superimposed rays, as is diffusion due to all reflections being considered as specular. Therefore in the low frequency regions where these effects are particularly noticeable and in spaces where the physical dimensions are comparable to the wavelength of the sound source being investigated, the ray approach becomes invalid.

There are two main geometric models – the *ray-tracing* method and the *image-source* method – and although they are essentially variations on a theme they differ in terms of computation speed, flexibility, and how they may each be extended to consider scattering and diffraction effects [Stephenson, 1990].

4.2.2 Ray-Tracing Method

Ray-tracing was first applied to concert hall acoustics by Krokstad, Strøm, and Sørsdal in 1968 and was essentially the first attempt to arrive at a digitally modelled RIR [Krokstad et al, 1968]. A sound source is imagined to release a number of sound rays in all directions at a certain moment in time. The path of each ray, taking into account all reflections at walls or objects, is followed, and when it arrives at a previously designated point, its energy, arrival time, direction and any other relevant information is calculated and recorded. This can be plotted as a

histogram showing the temporal distribution of the energy received, and can be seen as an approximation to the impulse response of the acoustic space. This is not, however, the actual impulse response of the space due to its approximate nature depending upon the number of particle paths calculated, and the time resolution achieved.

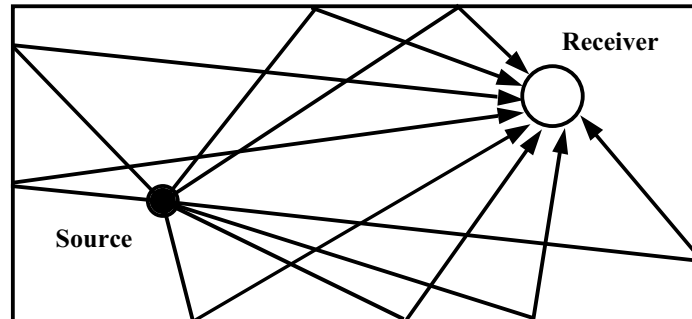


Figure 4.1 A simple two-dimensional ray-tracing model with a number of ray paths emitted from the source and followed up, taking into account all reflections, until they arrive at the receiver.

There are a number of limitations associated with ray tracing techniques. For instance the size of the detector has to be considered as it is not possible to model it as a point. This is because an infinitely small detector cannot detect an infinitely small sound ray. Therefore detectors and/or rays have to be given finite dimensions with the usual detector shape being a sphere [Dhillon, 1994]. Variable size detectors dependent on the number of rays and their individual length can also be used to improve detection accuracy due to the path length of the rays increasingly becoming more divergent.

In simple rooms the number of rays required for accuracy is not too high but as reflection orders and the complexity of the room geometry increase then the number of rays required to successfully model a RIR also increases by a significant amount. Due to the angle between adjacent rays emitted from the point source remaining approximately constant, as the ray length becomes longer, the model becomes less exact [Krokstad et al, 1968]. This has been improved upon by using diverging beam techniques such as pyramid and cone tracing [Farina, 1995]. With standard ray tracing it is important to ensure an even distribution of sound rays over the surface of the sphere acting as the sound source. To cover the sphere in a cone tracing method it is necessary to allow adjacent cones to overlap as shown in Figure 4.2(a). This can result in the problem of the same path being detected a number of times unless there is a non-uniform distribution of energy within the cone allowing multiple reflection paths to add up correctly. Pyramid tracers offer an improvement over this method as the source sphere is completely covered without beams overlapping as shown in Figure 4.2(b). There is a further problem in that as beams are traced and reflected according to the path of their central axis, reflections from multiple surfaces cannot be accounted for leading to detection errors.

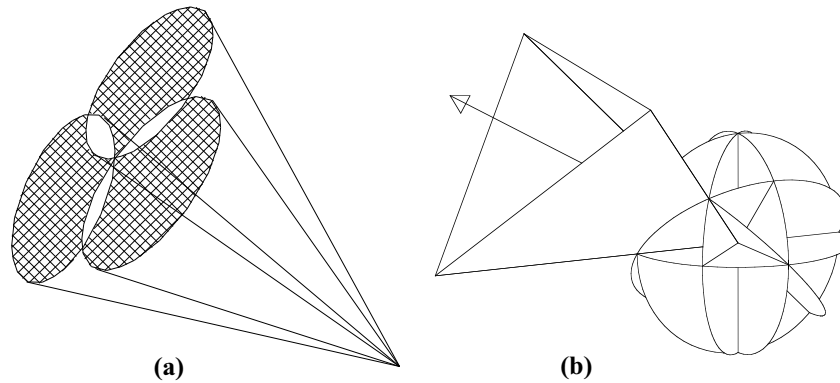


Figure 4.2 Improvements on the basic ray-tracing technique; (a) Cone tracing - note how the cones overlap; (b) Pyramid tracing - a variation on cone tracing that avoids overlapping edges [Farina, 1995].

All ray or beam tracing methods are based on the premise that the space is diffuse which is often an invalid assumption. They are also usually computationally intensive due to the large number of rays that are required for accurate results [Begault, 1994], particularly if the entire RIR is to be calculated complete with the all important reverberant field component. This situation can be improved upon by using ray tracing to calculate the early reflections together with a digital reverberation technique to add a more general reverberant tail for the space in question. Other methods correct the later soundfield component of a limited ray-tracing result with a time varying multiplicative or additive factor based on statistical analysis [Farina, 1995]. However ray-tracing methods are still very useful, particularly as they can be adapted to include important frequency dependent scattering and diffraction effects. Stephenson further states that these methods offer an appropriate compromise as required between accuracy, length of RIR, spatial resolution and calculation time with no particular increase in this time as the number of sources increases [Stephenson, 1990].

4.2.3 Image-Source Method

The Image-Source method is based on the idea that a sound ray reflected from a plane wall can be imagined as originating from an *image source*. This is the mirror image of the original sound source formed by the wall, the wall being the plane of reflection. Clearly as shown in Figure 4.3, the distance via the reflected route is equivalent to the direct line between the image-source and the listener. As there will be more than one wall in an enclosed space, this mirroring process has to be carried out to image sources already constructed, leading to second-order images, third-order images and so on. The final pattern of image sources, which is basically infinite, represents the original acoustic space. Rather than having to trace the individual ray paths, the contributions of all the individual image sources taking into account the $1/r^2$ law, wall absorption and air attenuation are merely added together. For a given source/listener combination each source will emit only one ray in a direction defined by the point where the

listener is located. This is clearly an improvement over ray-tracing methods as there is no need to consider ray emission directions or detector size and shape.

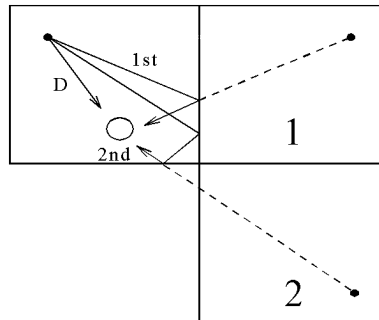


Figure 4.3 Demonstration of the image-source method. Reflections are calculated by constructing a straight-line path from an equivalent source - created by mirroring the actual source in the reflecting wall - to the receiver. The 1st reflection is first order (hence labelled 1) as the associated image is constructed by mirroring the source in one wall only. The 2nd reflection is second order (hence labelled 2) as the associated image has been constructed by two mirroring processes: in this case being the mirror image of the 1st reflection's image-source.

This process is relatively straightforward for simple rectangular shaped rooms, although rapidly becomes non-trivial for more complex geometries. Even for rectangular rooms the number of image sources increases exponentially with the number of reflections, giving an associated rise in computation time. With more complex spaces there is a further rise in computation time associated with the need to perform visibility checks on each image-source. Not all of the image-sources created due to the planes of reflection constructed by the room's geometry can physically exist. It is not always possible to follow up an equivalent ray path from actual source to listener using the walls involved in the mirroring process. This is because real walls are limited by edges, and are not infinite planes, and it is possible that the geometrically constructed reflection points may lie outside of the actual limited wall area. A further limitation of the image-source model is that it can only model specular reflections and cannot take account of most physical wave phenomena. However the image-source method is more accurate than the ray-tracing method. If an RIR is to be constructed with the requirement that only the early reflections are accurately modelled the image-source method is often preferable as the computation time for the first few orders of reflection will not be too prohibitive.

4.3 Finite Element Analysis

4.3.1 The Finite Element Method, (FEM)

The Finite Element Method (FEM) is an iterative numerical method for calculating the resonant frequencies present in an enclosed space. Consider a general mechanical system with one degree of freedom as shown in Figure 4.4 where a body of mass M is coupled to an inert point

by a stiffness K and caused to move by an external force F . The motion is damped by a factor C . The equation of motion for this system for a displacement x of the mass over time is given in Equation (4.1):

$$M \frac{d^2x}{dt^2} + C \frac{dx}{dt} + Kx = F \quad (4.1)$$

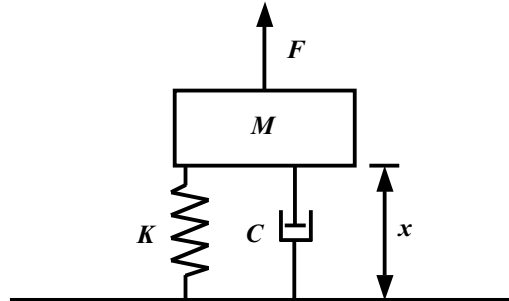


Figure 4.4 A general mechanical system with one degree of freedom: A body of mass M is coupled to an inert point by a stiffness K and caused to move by an external force F . The motion is damped by a factor C .

Setting F and C to zero allows the natural frequency of vibration of the system to be found assuming sinusoidal motion:

$$x = |x| e^{i\omega t} \quad (4.2)$$

In a general mechanical system there will be many degrees of freedom with multiple alternatives for F , M , K and C . The finite element method breaks down the system into discrete component elements of finite size. The surface of an element is defined by nodes or junctions and the effective result is a mesh representing the entire system. Figure 4.5 gives an example of a 20-node pressure-based acoustic finite element together with the way in which it could be used to cover the whole volume of a room, resulting in a 3-D mesh.

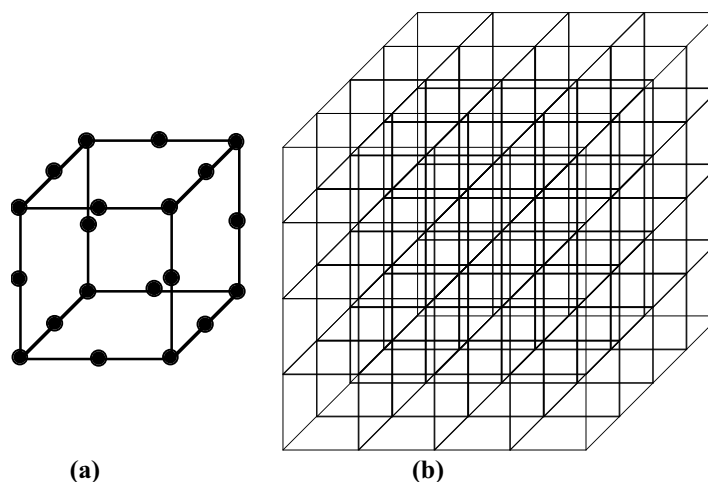


Figure 4.5 The Finite Element Method relies upon a system being broken down into discrete component elements of finite size; (a) a 20-node pressure-based acoustic finite element; (b) its use in modelling a room resulting in a 3-D mesh.

This essentially produces a large number of simultaneous equations which can be represented as matrix forms of Equations (4.1) and (4.2). The equations of motion are therefore:

$$[M]\ddot{x} + [C]\dot{x} + [K]x = [F] \quad (4.3)$$

And the equivalent equations for the natural frequencies are:

$$([K] - \omega^2 [M])x = 0 \quad (4.4)$$

Where ω represents a series of frequencies, ω_n . Therefore the FEM when used to model a structure (or acoustic space) will consist of the following steps:

1. Divide the structure into sections – elements with nodes.
2. Describe the behaviour of the physical quantities in/on each element.
3. Connect the elements together at the nodes to form a series of equations approximating the whole structure.
4. Solve the system of equations for unknown quantities at the nodes, for example, displacement values.
5. Calculate desired quantities at selected elements, for example, pressure values.

The FEM is well suited to solving Equation (2.1), the analytical expression for the modal frequencies of a rectangular room. Results showing the successful application of the method to this problem can be found in [Wright, 1995], [Savioja et al, 1995], and [Savioja et al, 1996a]. The latter two studies involve the use of commercial FEA software called ABAQUS [Hibbitt et al, 1999]. It was found in [Wright, 1995] that for successful identification of near-coincident modes a non-uniform graded mesh was required. For a full model of a sound source in space the FEM is less appropriate due to the very high mesh density in the area around the source required to represent the large pressure gradient [Wright, 1995], leading to prohibitively long processing times.

4.3.2 The Boundary Element Method, (BEM)

The Boundary Element Method (BEM) is perhaps more applicable for modelling a sound source within a space and hence obtaining the RIR. A boundary is approximated by a continuous mesh of surface elements in a similar manner to the way in which the space itself is modelled using the FEM. This helps to reduce the dimensionality of the problem, requiring only that a mesh be generated over the boundary of the space. Consider the basic linear wave equation for acoustic wave propagation through an elastic medium:

$$\nabla^2 u = \frac{1}{c^2} \frac{\partial^2 u}{\partial t^2} + b \quad (4.5)$$

where $u(x,t)$ is the velocity potential, c is the speed of sound, $b(x,t)$ is the sound source and x and t are the position and time. Equation (4.5) can be transformed to the frequency domain resulting in the Helmholtz Equation:

$$\nabla^2 u + k^2 u = b \quad (4.6)$$

where $k = \omega/c$ is the wave number and ω is the angular frequency. It is possible to express Equation (4.6) in a boundary element matrix formulation [Niku et al, 2000]:

$$[H][P] = [G][V] + [B] \quad (4.7)$$

where P and V are the pressure and velocity and B is a body source vector. H and G are frequency dependent and there is one row or column for each boundary element node in the model [Adey et al, 2000]. Therefore having computed the acoustic field within the space, the acoustic variables are known at all the node points on the boundary and can in turn be evaluated at any point inside the space. Examples of the BEM in room acoustics problems can be found in [Wright, 1995] and [Savioja et al, 1996a]. Extensions to the basic premise are possible including adding mechanical finite elements coincident in space with the boundary elements to model specific structural materials at the walls with associated absorption properties [Wright, 1995].

4.3.3 Suitability of the FEM and BEM

Although both the FEM and BEM have been used to partially model the acoustics of a room it would seem clear that they are still far from the ideal choice. These models are accurate in their results and with ever increasing computer speeds are becoming more realisable to implement. However they are still generally used only for small rooms and low frequencies. This is due to the very fine element size required to accurately model across the whole frequency range. Around seven nodes, or six elements, per wavelength are required as a sufficient spatial sampling rate [Geest and McCulloch, 1998]. If an element is 0.5m long, with $c = 343\text{ms}^{-1}$ the maximum frequency that can be calculated with any reasonable accuracy is $343/0.5 \times 6 \approx 114\text{Hz}$. Doubling the frequency halves the element size quadrupling the number of elements for a 2-D structure with an associated rise in processing time. Even for very small spaces such as vehicles there is an upper useful frequency limit of 300-500Hz. Further problems include the inability of these methods to model incoherent sound sources and diffusion successfully [Geest and McCulloch, 1998] and inaccuracies for large scattering angles at high frequencies [Dhillon, 1994].

4.4 Finite Difference Time Domain (FDTD) Models

In this method all calculations are carried out in the time domain using acoustical equations that are discretized locally. This discretization introduces some numerical phase error but wave amplitude is modelled accurately making this method suitable for the measurement and study of long transients in sound pressure level [Botteldooren, 1995]. Time domain calculation has the benefit of processing speed but the construction of frequency dependent boundary conditions is more difficult than with the FEM and BEM. The method is generally faster than the FEM even though a denser mesh is required to obtain results of a similar accuracy [Savioja, 1995]. The model itself is based on a finite difference approximation for both the time and space derivatives in the wave equation. The spatial sampling positions are usually related to a Cartesian grid placed across the space to be modelled. The finite difference method is based upon an approximation of the definition of a mathematical derivative. For an arbitrary continuous function $f(x)$, its derivative can be defined as:

$$\frac{df(x)}{dx} = \lim_{h \rightarrow 0} \frac{f(x+h) - f(x)}{h} \quad (4.8)$$

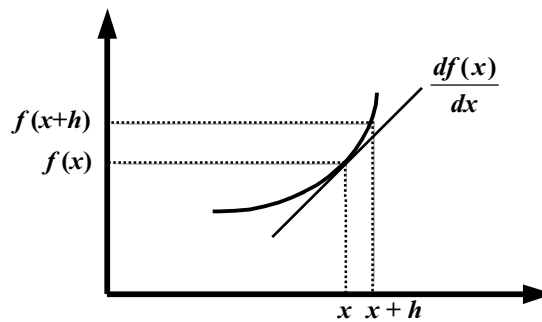


Figure 4.6 The definition of the derivative, $df(x)/dx$, of the function $f(x)$.

This becomes exact as h tends to 0. For finite calculations, h cannot tend to zero and so is a parameter of the system being approximated. Therefore, a derivative can be calculated as follows:

$$\frac{df(x)}{dx} = \frac{f(x+h) - f(x)}{h} \quad (4.9)$$

This is known as the *forward difference formula*. By applying this expression twice it is possible to arrive at the standard difference scheme approximation for the second derivative:

$$\frac{d^2f(x)}{dx^2} = \frac{f(x+h) - 2f(x) + f(x-h)}{h^2} \quad (4.10)$$

The finite difference method has been used to model acoustic wave propagation by providing a numerical and computable solution to the 2-dimensional wave equation [Van Duyne and Smith, 1993]. It has also been used in room acoustics problems ([Savioja et al, 1996a] and [Botteldooren, 1995]) where it has provided a realisable and accurate method for modelling low frequency regions in small rooms.

4.5 Waveguide Modelling Techniques

Digital waveguide models are an accurate and efficient method of modelling a physically complex system. They provide a suitable alternative to traditional modelling methods based around a direct solution of the wave equation and have proved successful in the fields of acoustic modelling particularly in the area of digital sound synthesis [Smith, 1992]. Delay lines, junctions and filters are used to construct acoustic models, with a basic waveguide element consisting of two delay lines capable of carrying a signal in opposite directions. It is also possible to synthesise sound by creating objects built just from networks of interconnected waveguide elements. These waveguide networks can form a one or two-dimensional mesh structure that not only parallels the behaviour of its real world counterpart, but also, if visualised, bears a physical resemblance. These waveguide mesh structures have been used successfully to model the properties of strings, membranes and plates. It would therefore seem to be the case that, more generally, waveguide meshes are an appropriate method of modelling wave propagation through any medium. Extending the simple mesh to three dimensions allows the creation of more abstract sound objects and, more importantly from the point of view of this thesis, demonstrates the potential of modelling sound propagation through a 3-D acoustic space.

4.1.1 The Basic Digital Waveguide Element

The theory of digital waveguides is based around the general d'Alembert solution of the one dimensional wave equation giving the transverse velocity $v(x,t)$, in this case at time t and position x on an ideal vibrating string. The solution is the sum of two velocity waves v^+ and v^- travelling at speed c in opposite directions:

$$v(x,t) = v^+(x - ct) + v^-(x + ct) \quad (4.11)$$

By discretizing time and space this travelling wave solution to the one-dimensional wave equation may be implemented digitally with a pair of bi-directional delay lines as shown in Figure 4.7. The discrete time formulation of Equation (4.11) can be obtained by letting $t = nT$ with $n = 0,1,2,\dots$, with time sample T and x being defined at the discrete set of positions, $\{x_0 \pm cnT, n = 0,1,\dots\}$, with x_0 being an arbitrary set position. The wave value at any discrete point m

along the waveguide, with $0 \leq m \leq n$, is the sum of the velocity waves in the upper and lower delay lines.

$$v(x, mT) = v^+(x - cmT, mT) + v^-(x + cmT, mT) \quad (4.12)$$

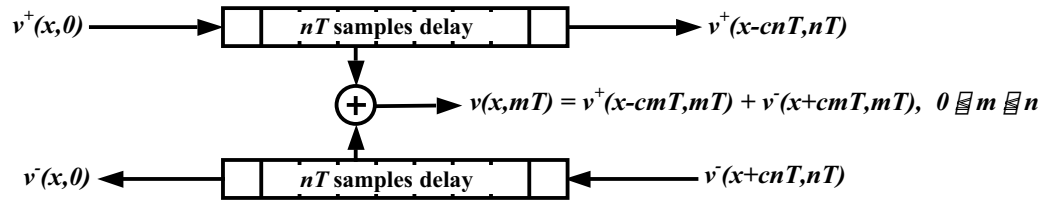


Figure 4.7 The Digital Waveguide implemented using a pair of bi-directional digital delay lines.

The upper delay line propagates a signal travelling to the right and the lower delay line propagates a signal to the left and these two signals are independent of one another. This structure is the basic digital waveguide element. The actual signal or wave value at any point may be obtained by summing the data held in the two digital delay lines.

The variables used in the wave equation depend upon the physical properties of the medium to which it is being applied. Note that there is also a large degree of commutability between travelling wave variables as discussed in [Smith, 1992]. Velocity (first order time derivative of displacement), acceleration (first order time derivative of velocity) or slope (first order time derivative of acceleration) waves can also be used, as can spatial derivatives of the travelling wave solution to the one-dimensional wave equation. For vibrating strings or membranes the most convenient choice is *force*, f and *velocity*, v . For vibrating columns of air, *volume velocity*, v (also called *flow*), and *pressure*, p are the variables usually considered. There is also a direct correspondence between these pairs of variables and those considered in electrical transmission lines, *current*, I and *voltage*, V . As the wave phenomena being considered in each medium are effectively equivalent then so are the travelling wave expressions within the limits of the particular variables being used. Also of particular relevance are the *wave impedance* or *characteristic impedance* relations between the travelling wave components of force and velocity, pressure and volume velocity, or current and voltage. In general travelling waves propagate along a digital waveguide unchanged as long as this characteristic impedance is constant. The characteristic impedance is the geometric mean of the two sources of resistance to motion. In the case of a one dimensional string this is the inertial resistance of the string due to its mass and the spring force or tension of the displaced string due to its elasticity. There are equivalent variables for both the electrical and air column analogues.

4.5.1 Signal Scattering

A signal will propagate in opposite directions through a waveguide element until the characteristic impedance changes, resulting in signal scattering. These points are called *scattering junctions* and when a signal is incident upon such a discontinuity, part of it is reflected back along the waveguide element and part of it is transmitted on to the next element in such a way that energy is conserved. Scattering junctions have a number of important functions in digital waveguide models. Short cylindrical sections of varying diameter can be connected together via scattering junctions and used to model the vocal tract [Markel and Gray, 1976]. Guitar strings can be coupled together at a bridge in a similar manner. Scattering junctions can also be used to input energy from a physical object into the waveguide system, one example being a model of a piano hammer [Van Duyne et al, 1994]. Conversely, scattering junctions may be used to control the energy output from a system, one example being a model of finger holes in a wind instrument [Välimäki et al, 1996].

It is also possible to connect together a number of waveguides at a scattering junction, possibly each of a different impedance. This junction may be lossless, loaded with an impedance of its own or driven by an external force. Consider the general case of a scattering junction J with N connected waveguides for $i = 1, 2, \dots, N$:

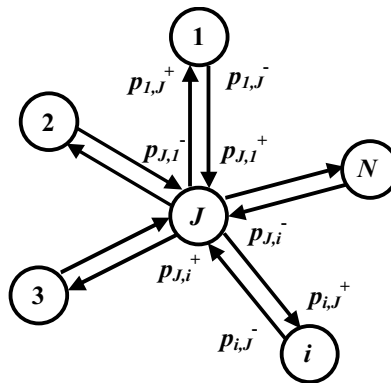


Figure 4.8 A general scattering junction J with N connected junctions for $i = 1, 2, \dots, N$.

The sound pressure in a waveguide when considered as a column of air is represented by p_i , the volume velocity by v_i and the impedance of the waveguide by Z_i . The input to a waveguide is termed p_i^+ and the output p_i^- . The signal $p_{i,J}^+$ therefore represents the incoming signal to junction i along the waveguide from the opposite junction J . Similarly, the signal $p_{i,J}^-$ represents the outgoing signal from junction i along the waveguide to the opposite junction J . Note that in this case the volume velocity is equal to pressure divided by the characteristic impedance:

$$v_i = p_i / Z_i \quad (4.13)$$

The delay elements are bi-directional and so the sound pressure in one waveguide element is defined as the sum of its input and output:

$$p_i = p_i^+ + p_i^- \quad (4.14)$$

As the waveguides are equivalent to bi-directional unit-delay lines, the input to a scattering junction is equal to the output from a neighbouring junction into the connecting waveguide at the previous time step. This can be expressed as:

$$p_{J,i}^+ = z^{-1} p_{i,J}^- \quad (4.15)$$

where z^{-1} is defined as a unit delay. If a number of strings intersect at a junction without loss of energy it is required that all the velocities of all the strings are equal so that they move together at that single point, and that all the forces exerted by all the strings must sum to zero so that they balance each other [Van Duyne and Smith, 1993]. These conditions can be expressed explicitly for an air column waveguide element using wave variables based on volume velocity and pressure as follows:

1. The sum of the input volume velocities, v^+ , equals the sum of the output volume velocities, v^- - the flows add to zero - at a junction:

$$\sum_{i=1}^N v_i^+ = \sum_{i=1}^N v_i^- \quad (4.16)$$

2. The sound pressures in all crossing waveguides are equal at the junction:

$$p_1 = p_2 = \dots = p_i = \dots = p_N \quad (4.17)$$

These two conditions together with Equation (4.13), the acoustic impedance relation, lead to an expression for the sound pressure p at the lossless scattering junction J as a function of the sound pressures of the incident travelling waves, p_i^+ :

$$p_J = \frac{2 \sum_{i=1}^N \frac{p_i^+}{Z_i}}{\sum_{i=1}^N \frac{1}{Z_i}} \quad (4.18)$$

Further, the waves emerging from the junction and travelling back along the waveguide in the opposite direction due to this scattering effect can be expressed as follows:

$$p_i^- = p_J - p_i^+ \quad (4.19)$$

These two expressions are known as the *scattering equations* for the interconnection of several waveguides at a point [Van Duyné and Smith, 1993]. Essentially these equations determine that for a wave incident upon a junction some fraction of its energy is reflected so that it travels back along the waveguide in the opposite direction from which it came and the remainder enters the junction where it is divided between the outgoing connected waveguide elements. Note that according to these equations the relative proportions of this scattering effect are determined only by the associated impedances of the connected waveguides. The derivation of these scattering equations is included in Appendix A.

The general nature of these scattering equations imply that it is a trivial matter to extend a simple chain of waveguide elements to two or three dimensions. For instance as shown in Figure 4.9 four parallel “string” type waveguides can be linked together to form a simple mesh structure by replacing the 2-port scattering junctions with corresponding four port junctions that effectively link across the parallel rows to form a 2-dimensional construct.

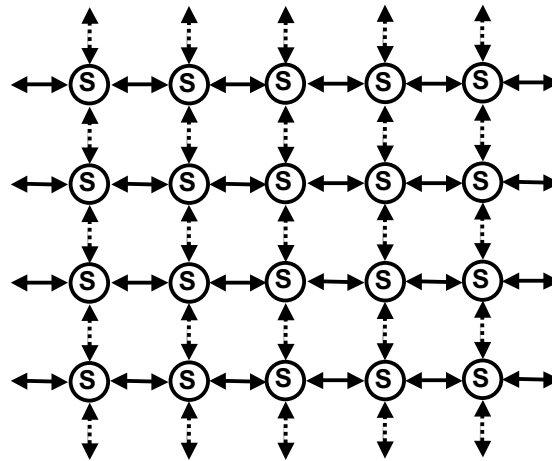


Figure 4.9 A 2-dimensional waveguide mesh constructed from parallel 1-dimensional “strings” linked together with 4-port scattering junctions replacing the usual 2-port junctions. Note that the scattering junctions are represented using “S” and the waveguides are represented using the double headed arrows.

The only change in the scattering equations is that there are now four inputs and outputs per junction rather than two - there is no particular notion of increased complexity in the basic model. The scattering equations remain essentially the same except they now deal with an increased number of junctions. In a similar fashion, 2-dimensional constructs can be layered on top of one another to form 3-dimensional objects, with the 4-port junctions being replaced by 6-port scattering junctions.

Similarly, the flexibility and simplicity of the scattering equations allows different 2-dimensional and 3-dimensional topological arrangements of the scattering junctions to be constructed. Some examples are shown in Figure 4.10.

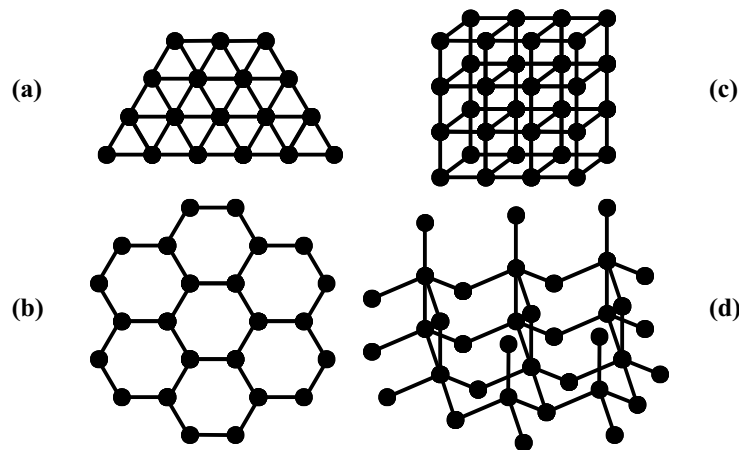


Figure 4.10 Possible topological arrangements of scattering junctions; (a) The 2-D Triangular Mesh (6-port junctions); (b) The 2-D Hexagonal Mesh (3-port junctions); (c) The 3-D Rectilinear Mesh (6-port junctions); (d) The 3-D Tetrahedral Mesh (4-port junctions).

An example of the simplicity of these scattering equations can be demonstrated by examining the 2-dimensional rectilinear mesh and the 3-dimensional tetrahedral mesh. In both cases the number of neighbouring scattering junctions is four, leading to the same scattering equations for both models. However the difference is obviously in the connectivity of the junctions and the topological arrangement of the mesh. From the perspective of implementing these models the problem becomes one of memory management - how such an array of variable elements is created and managed and how propagating signals are passed between these elements. Clearly a 2-dimensional rectilinear arrangement, conceived as a simple $m \times n$ matrix, would be easier to implement than the corresponding 3-dimensional tetrahedral model.

4.5.2 Finite Difference and DSP Formulations

In a general waveguide mesh model all impedances $1/Z_i$ are set to be equal. The case of a 2-dimensional rectilinear mesh with 4 neighbours is shown in Figure 4.11.

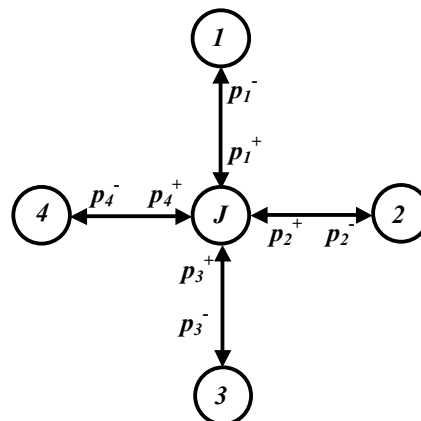


Figure 4.11 The general 4-port scattering junction as used in the 2-D rectilinear waveguide mesh, with all impedances $1/Z_i$ set to be equal.

The scattering equations can be reduced to:

$$p_j(n) = \frac{p_1^+(n) + p_2^+(n) + p_3^+(n) + p_4^+(n)}{2} \quad (4.20)$$

$$p_i^- = p_j^- p_i^+ \quad (4.21)$$

Note also that the sum of the inputs to a scattering junction equals the sum of the outputs:

$$\sum_{i=1}^4 v_i^+ = \sum_{i=1}^4 v_i^- \quad (4.22)$$

Using Equations (4.20)-(4.22) and Equation (4.15) it is possible to arrive at a difference equation expression equivalent to the scattering equations (see derivation in Appendix A):

$$p_j(n) - 2p_j(n-1) + p_j(n-2) = \frac{1}{2} [p_1(n-1) - 2p_j(n-1) + p_3(n-1)] + \frac{1}{2} [p_2(n-1) - 2p_j(n-1) + p_4(n-1)] \quad (4.23)$$

Comparing Equation (4.23) with the 2-dimensional wave equation:

$$\frac{\partial^2 u}{\partial t^2} = c^2 \left[\frac{\partial^2 u}{\partial x^2} + \frac{\partial^2 u}{\partial y^2} \right] \quad (4.24)$$

Shows that it is the standard second-order difference scheme for the 2-dimensional hyperbolic partial differential wave equation. Wave propagation speed $c = 1/\sqrt{2}$ and time and spatial sampling intervals are set to be equal [Van Duyne and Smith, 1993]. Therefore it can be seen that there is an equivalence between traditional finite-difference methods and these waveguide mesh structures. The difference in these methods lies in the approach to the solution. Finite-difference methods discretize the wave equation appropriate for the object being modelled whereas waveguide models originate from a discretization of the general solution to this wave equation [De Poli and Rocchesso, 1998]. Similar difference relations have been shown to exist for the 2-dimensional triangular waveguide mesh [Fontana and Rocchesso, 1995] and the 3-dimensional tetrahedral waveguide mesh [Van Duyne and Smith, 1996].

The finite difference expression in Equation (4.23) can be more conveniently rearranged as:

$$p_j(n) = \frac{1}{2} \sum_{i=1}^4 p_i(n-1) - p_j(n-2) \quad (4.25)$$

Or alternatively:

$$p_j = \frac{z^{-1} \cdot \frac{1}{2} \sum_{i=1}^4 p_i}{1 + z^{-2}} \quad (4.26)$$

This is an equivalent expression to the difference scheme more suited to a digital signal processing implementation of a waveguide model and is known as the *transfer function* of the scattering junction [Savioja et al, 1996b].

4.5.3 Applications and Limitations

Digital waveguide structures have been used extensively to model string and wind instruments. 2-dimensional waveguide meshes are well suited to modelling the properties of plates and membranes used in the construction of percussion instruments. The 2-D rectilinear mesh was originally used for this purpose [Van Duyne and Smith, 1993] and has also been used successfully to model gongs [Van Duyne et al, 1994]. Improvements have been made over this original implementation by using different mesh topologies including a 2-D triangular mesh, [Laird et al, 1998] and [Fontana and Rocchesso, 1995], and an interpolated formulation of the 2-D rectilinear mesh [Savioja and Välimäki, 1996]. 3-D meshes enable sound propagation to be modelled in any arbitrary 3-D medium, allowing full physical models of instruments to be constructed. However 3-D models, as already explained, although relatively simple to construct in terms of the scattering equations used, introduce difficulties in implementation due to the complexity and connectivity of the resulting structures. As such these techniques have only been used to model virtual abstract sound objects that have simple topologies, using 2-D rectilinear meshes layered and connected to form 3-D objects [Rossiter et al, 1996]. However this opens many possibilities for sound synthesis exploration and experimentation. 3-D mesh structures are also applicable to room acoustics problems. Implementations based on both the difference approach [Savioja et al, 1994] and the DSP formulation [Savioja et al, 1996b] have proved successful in this respect. Again these results are based on a simple 3-D rectilinear mesh. Work has also been carried out on analysing the properties of the 3-D tetrahedral mesh [Van Duyne and Smith, 1995] and [Van Duyne and Smith, 1996]. Although it generally proves to be more accurate and efficient it has not as yet been used to model a specific propagation medium, possibly due to the complexities involved in implementation as discussed above.

There are a number of limitations associated with using a waveguide mesh for modelling an enclosed acoustic space, the most pertinent being *sampling rate considerations* and *dispersion error*.

Sampling Rate

The scattering junctions in a waveguide mesh effectively correspond to spatial sampling points. Therefore the sampling rate of the mesh, and hence the highest frequency that can propagate through it, depends upon the distance between the junctions and their topological arrangement. A wave travelling along a one-dimensional chain of scattering junctions connected using unit-

delay waveguide elements will propagate one unit distance in one time unit. In a 2-D or 3-D rectilinear mesh the speed of wave propagation is found in the diagonal direction. For an N -dimensional system one diagonal junction to junction movement corresponding to \sqrt{N} unit distances requires N unit delays. Therefore it can be shown, according to [Savioja et al, 1996b] that the update frequency, f_{update} , of a rectilinear N -dimensional mesh is:

$$f_{update} = \frac{c\sqrt{N}}{d} \quad (4.27)$$

where c represents the speed of sound in the medium and d is the distance between two junctions. The implication is that in order to propagate an arbitrary audio signal with a 20kHz bandwidth, the distance between junctions must be correspondingly small. For example, in a 2-D mesh if $c = 343\text{m/s}$, and an f_{update} of 44.1kHz (standard CD sampling rate) is required, the physical distance between junctions should be set at about 0.011m. Therefore for a 2-D representation of a physical medium of the size of a typically small room, a highly dense mesh consisting of many scattering junctions has to be constructed. For example, a 2-D waveguide mesh representation of a room 4.4m wide and 6.0m long would require in excess of 55,000 scattering junctions. Clearly, even though waveguide techniques are often an efficient method of implementing a physical model, this is a significant overhead in terms of the processing time and memory required for data storage.

The implications of using a 3-D waveguide mesh for modelling the acoustics of a room have been considered in [Campos, 1999] based upon the limitations of the mesh density/sampling rate. For comparisons between computing platforms the following expression can be used:

$$T_M \approx 0.42 \times 10^6 \times V \times RT_{60} \times f_{sn}^4 \times t_n \quad (4.28)$$

where:

T_M	Total model computation time in s
V	Volume of Acoustic Space to be modelled in m^3
RT_{60}	Reverberation Time measurement in s
f_{sn}	Normalised sampling rate = $f_{update}/44100$
t_n	Average computation time per junction per 44100 iterations, in s .

An example cited in [Campos, 1999] offers a comparison between modelling a large reverberant cathedral with a Volume of $100000m^3$ and $RT_{60} = 9s$, and a small acoustically dead room with a Volume of $50m^3$ and $RT_{60} < 1s$. For the same level of computing power and audio quality the ratio between the T_M values is more than 18000. Reducing the sampling rate of the mesh offers considerable savings in computation time. However it is often the case that in order to take account of other limiting factors the mesh actually has to be oversampled, resulting in an even denser mesh and a much higher execution time.

Dispersion Error

The other principal limitation of waveguide mesh models is the phenomenon known as *dispersion error*. A dispersive medium is one for which the velocity of a propagating wave is dependent upon its frequency [Brillouin, 1953]. Many examples of wave propagation can be shown to be non-dispersive such as Maxwell's equations of electromagnetism, in which light is defined to travel with a constant velocity [Brillouin, 1953]. Similarly the equations relating to the propagation of sound in air yield a constant velocity value. [Van-Duyne and Smith, 1993] first considered dispersion in waveguide mesh structures by comparing what happens in an ideal membrane with the behaviour of the corresponding waveguide based model. Clearly in the ideal membrane the speed of wave propagation is independent of frequency as the solution of the 2-D wave equation is an integral sum of plane waves all moving at constant speed c . Hence an ideal membrane is a non-dispersive medium. The dispersive properties of the 2-D waveguide mesh can be examined by carrying out a Von Neumann analysis of the finite difference equation using the discrete Fourier Transform. A Von Neumann analysis of the finite difference approximations to a partial differential equation is based on the use of Fourier transform theory to compare the evolution over time of the spatial spectrum in both the continuous and discrete formulations [Van Duyne and Smith, 1993]. This results in a 2-D surface plot of normalised wave speed against spatial frequency, examples of which are presented in Figure 4.13 and in the following chapter (Chapter 5.6). The result of this analysis is that for the 2-D rectilinear mesh there is no dispersion at any frequency when travelling in a direction diagonal to the mesh coordinate system. However there is a considerable drop in speed for higher frequencies propagating vertically and horizontally along the actual waveguide elements corresponding to the axes of the coordinate system (see Figure 4.12).

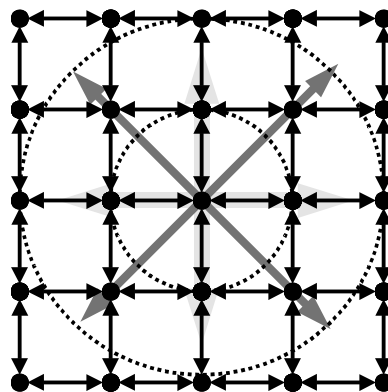


Figure 4.12 A typical section from a 2-dimensional rectilinear waveguide mesh. The dotted circular lines represent perfect wavefronts as would be expected in a continuous medium. Waves travelling diagonally along the mesh, indicated by the darker thinner arrows, travel at the same speed for all frequencies. Waves travelling along the coordinate axes, indicated by the thicker lighter arrows, exhibit frequency dependent dispersion.

The effect of this in a small bounded mesh is that there is a mis-tuning of the resonant nodes [Van Duyne and Smith, 1994]. Possible solutions to this problem include applying all-pass filtering at the boundaries or over-sampling the mesh and low-pass filtering. The authors also suggest that as the high frequency modes are so densely distributed this error may not be considered so important in an audio context. However this dispersion error is not just frequency dependent but also dependent upon the topology of the mesh structure. This can be minimised to some extent by using a different arrangement of scattering junctions and waveguide elements. A number of possible topological arrangements have been considered and analysed [Van Duyne and Smith, 1996] and the results are presented in Figure 4.13.

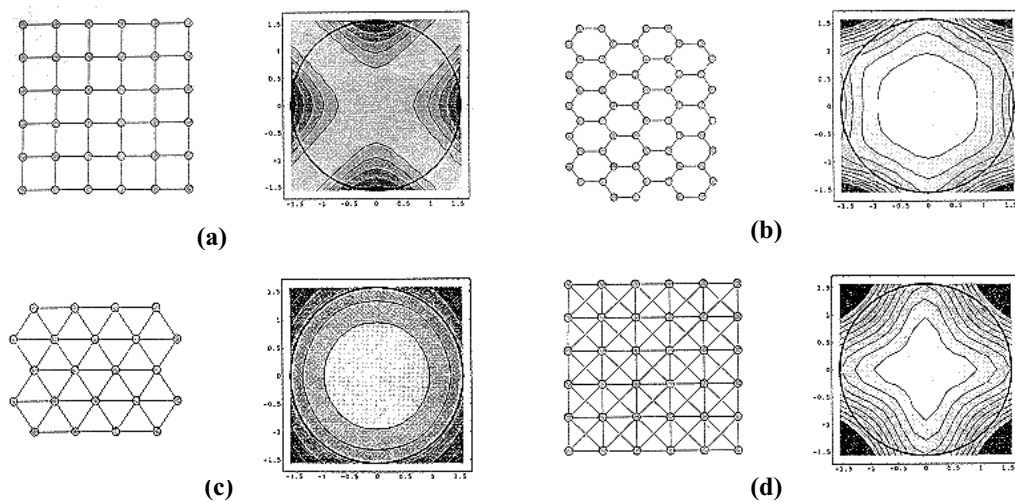


Figure 4.13 Some possible 2-D waveguide mesh topologies with their associated dispersion analysis measurements. (a) the rectilinear 4-port mesh; (b) the hexagonal 3-port mesh; (c) the triangular 6-port mesh; (d) an 8-port rectilinear mesh. Note that in all cases the x and y axes correspond to the angular frequency components and range from $-\pi/2$ to $\pi/2$. From [Van Duyne and Smith, 1996].

The plots in Figure 4.13 display contours of normalized wave speed on the associated waveguide mesh against plane wave speed and direction. The centre region of the plot corresponds to low plane wave frequencies and the outer regions correspond to high frequencies. The angular position on the plot relative to the centre, being the frequency plane origin, corresponds to the direction of plane wave travel on the mesh. The x and y axes correspond to the angular frequency components and range from $-\pi/2$ to $\pi/2$ in all cases. Therefore it can be seen that Figure 4.13(a) is in agreement with the claim made above that on the rectilinear mesh there is no dispersion when travelling diagonally relative to the mesh coordinate system but that there is a considerable drop in wave speed for high frequencies when travelling along the coordinate axes themselves. Clearly from these plots the triangular waveguide mesh (Figure 4.13(c)) gives the best results with dispersion error minimised so that is almost totally independent of the direction of propagation. A waveguide mesh arranged in

such a fashion reduces the dispersion error inherent in such systems to being dependent *only* on the frequency of the wave rather than the frequency *and* the direction of travel.

It has been suggested that an output from such a mesh could be post-processed using appropriate filtering methods to correct this frequency dependent dispersion error so it would be consistent across all angular directions of wave propagation [Savioja and Välimäki, 1999b]. This filtering has been termed *Frequency Warping* and involves post-processing the output signal from the mesh using a warped FIR filter which effectively introduces frequency shifting to reduce the dispersion error. The FIR filter structure used involves replacing every delay element with a first-order allpass filter with the transfer function:

$$A(z) = \frac{z^{-1} + \alpha}{1 + \alpha z^{-1}} \quad (4.29)$$

The extent of the warping effect is determined by the coefficient α , which is the same for all the allpass filters in the chain and the tap coefficients are set equal to the signal samples to be post-processed. It then becomes a matter of finding the optimal value for α for the frequency bandwidth required. If this technique is to be used the input signal first has to be warped using the coefficient $-\alpha$, and the spatial sampling interval of the mesh has to be multiplied by a factor $D = (1-\alpha)/(1+\alpha)$. This scaling compensates for the downshift of low frequencies caused by the warping process. Finally, the output signal from the mesh is warped with a coefficient value of α . Results obtained in [Savioja and Välimäki, 1999b] state that in order to achieve the same accuracy as in the warped triangular mesh, the standard triangular mesh would have to use a spatial sampling interval one-third the size, increasing both the memory requirements and the execution time of the model.

A similar result to that of the triangular mesh can be obtained by using a rectilinear mesh that effectively inserts additional unit delays between junctions diagonally apart. Interpolation is then used to correct for the fact that this extra set of junctions would have to be placed between actual mesh nodes [Savioja and Välimäki, 1996]. However recent results have shown that a triangular topology is still an improvement over this interpolated rectilinear mesh [Savioja and Välimäki, 1999a].

In three dimensions similar reductions in dispersion error have been made by using alternative topologies with the tetrahedral waveguide mesh offering a significant improvement over the basic rectilinear model [Van Duyne and Scott, 1995] and [Van Duyne and Smith, 1996].

4.6 Summary

There are a number of methods that could be used to model the acoustic properties of an enclosed space. Geometrical models have proved to be very successful to date. The ray-tracing method plus its associated variations has proved to be reliable and adaptable and is the basis of a number of room modelling packages [Naylor, 1993]. However it can be complex to implement with a large number of paths required for an accurate simulation, and lengthy RIRs can take a prohibitively long time to compute. The image-source method can be more accurate than ray-tracing as it is not dependent on ray emission directions, detector size or shape. Further, it is straightforward to implement for rooms based on a simple geometry although it can only deal with specular reflections. However it rapidly becomes non-trivial for rooms based on a non-rectangular design with visibility checks having to be performed on each image-source. As with ray-tracing there is an associated rise in computation time as the length of the required RIR increases and both methods are limited to being valid only for high frequencies. In general these methods are most applicable and suitable for accurately modelling the direct sound and early reflections in a room, with the reverberant sound being added using a more qualitative model.

Finite Element Analysis methods (FEM and BEM) are well suited to calculating the characteristic low frequency room modes of a simple rectangular room. For a full model of a sound source in space the FEM is less appropriate due to the very high mesh density in the area around the source required to represent the large pressure gradient leading to prohibitively long processing times. Again, this is particularly relevant due to the length of typical RIRs and the requirement to work over the full audio bandwidth.

The finite difference method has been used successfully in room acoustics problems where it has provided a realisable and accurate method for modelling low frequency regions in small rooms where the density of the sampling grid used is not too high and so computation times remain comparatively low. However it is perhaps the related modelling method using the digital waveguide approach that has proved to be most successful. The simplicity of the model makes it particularly favourable, yet the wave propagation that results, due to the simple scattering equations, when observed is as natural and detailed as one would expect if a stone were dropped into a pond. In a non-trivial sense this method closely approximates the real world behaviour of actual objects. Wave phenomena can be clearly demonstrated and observed and acoustic resonances peculiar to the body being modelled are successfully identified. The waveguide mesh technique has also been used successfully to model a range of different bodies and objects, with acoustic spaces being one pertinent example. For a small mesh at a low sampling rate real time behaviour is possible making this method relatively economical. Again

this is related to the simplicity of the scattering equations. For a 2-D rectilinear mesh the scattering junction equations can be implemented efficiently using fixed point arithmetic with only seven add operations and a binary shift to divide by two.

The main limiting factor with waveguide mesh models, as with finite difference and finite element techniques, is related to the size of the discretizing mesh required to allow the propagation of a full audio bandwidth signal. A large dense mesh has severe implications on both the processing time required to extract a RIR of any useful length and the memory size needed to store the junction variables. This is clearly evident in the comparative study presented in [Campos, 1999] and is particularly the case if a full 3-D implementation of an acoustically interesting room is required. However it can be argued that this is purely a problem related to the potential computing power available on the hardware platform on which the model is currently implemented. What might take days to process using current technology could take hours or even minutes given a year or two of progress in processor architecture. Even within the scope of the research period on which this thesis is based, there have been speed-up factors in model execution time of several orders of magnitude due to new hardware becoming available with system upgrades. Other possible solutions involve implementing the model algorithm directly for specific hardware or using a number of similar host processors or workstation nodes to distribute the computation load using parallel processing techniques. These methods are facilitated further by the fact that the scattering equations on which these models are based are actually very simple.

The dispersion error problem is perhaps more difficult to address although this too is not insurmountable. The advantage of the rectilinear mesh is mainly in the simplicity of its topology, particularly if a mesh is to be constructed to fit over a non-trivial, irregularly shaped room. It could also be easily implemented in hardware due to the scattering equations effectively reducing to seven additions and a binary shift. However the rectilinear mesh exhibits frequency dependent and direction dependent dispersion. This dependence on the direction of wave propagation can be effectively eliminated using a triangular mesh topology consisting of 6-port scattering junctions. As shown in Figure 4.13(c) the speed of propagation in this case is consistent across all directions. This does not however eliminate the frequency dependent nature of the dispersion error although it has been argued that in some cases this may not be pertinent in terms of the resultant audio effect. Theoretically dispersion places a limit on the highest frequency that can be propagated accurately through the mesh, lower than that given by f_{update} . Note that for a particular mesh f_{update} is dependent only on the distance between scattering junctions. This limit due to dispersion is in general taken as being $0.25 \times f_{update}$ [Savioja and Välimäki, 1999] and [Van Duyne and Smith, 1993]. The easiest solution to this problem would therefore seem to involve oversampling the mesh to increase the effective

bandwidth and low-pass filtering the output to obtain the valid frequency band. The implications of this then relate to being one of computation time as the mesh will have to be considerably denser. A denser mesh will place further demands on the memory requirements of the model implementation and the number of actual operations that have to be carried out per iterative time step due to the increased number of junctions. The triangular mesh also has a number of further overheads when compared with a similar rectilinear based model that will influence the overall computation time:

A larger number of scattering junctions are required per unit area/unit volume.

Each scattering junction is linked to six others rather than four increasing the memory requirements per junction.

The scattering equations no longer involve a divide by 2, rather a divide by 3. The model is thus not as easily realised in hardware.

The increased complexity of the required grid and the associated housekeeping involved in its management when modelling an arbitrary, non-trivial space.

However, as discussed above, a problem with the implementation of the model based solely on computation time can be solved - or potentially solved - using other methods.

Therefore, it would appear that waveguide mesh models offer an applicable and suitable solution to the problem of modelling the acoustics of a room. This is due to their simplicity, flexibility, and success in similar areas including the field of room acoustics where the rectilinear mesh has already been used. They are also suitable for producing a visualisation of the wave propagation in a room and this has already been demonstrated [Savioja et al, 1994]. If the issue of computation time is not considered as being of paramount importance then the triangular waveguide mesh offers the most appropriate topological arrangement of scattering junctions in the 2-D plane for such a model. This is due to the minimisation of the directionally dependent component of the dispersion error, leaving it a function of frequency only, a problem that could easily be solved by over-sampling the mesh and low-pass filtering the output. It is this reasoning, therefore, that leads to the hypothesis that for modelling the acoustics of a room the triangular mesh offers a considerable improvement in terms of accuracy over a corresponding rectilinear model. For a successful and realisable investigation into this hypothesis a number of basic compromises have to be considered.

Dimensionality

It is clear that the triangular waveguide mesh does not as readily tessellate to three dimensions as the rectilinear mesh does. Obviously this would be required for a complete and accurate model. However it should be possible to produce a model that closely approximates the behaviour of sound in a room based on the 2-D plane only. Both the rectilinear and triangular mesh models have been shown to work successfully for modelling 2-D plates and membranes.

It should be possible to extend the physical size of these synthesis models to the order of a typical room with an appropriately high mesh sampling rate to give a bandwidth applicable for the propagation of an arbitrary audio signal. Working only in the 2-D plane will facilitate model development as it will keep computation times within reasonable limits whilst allowing high mesh sampling rates to be used suitable for full audio bandwidth processing. Further, if the model shows promising results in two dimensions then it is a relatively trivial matter - given appreciable computing power - to extend the model to the full 3-D case. This is due to the lack of inherent dimensionality in the basic scattering equations and the premises they are based upon. If it is proved that the triangular mesh is a suitable model in two dimensions then it may be sufficient to construct a 3-D case by stacking up and linking together parallel triangular mesh sheets using 8-port scattering junctions - effectively giving a rectilinear mesh in the vertical plane. However a detailed analysis of the dispersion error present in such a structure would be required as it would clearly differ in the vertical plane from that in the horizontal plane although it would also remain to be seen if this was a subjectively pertinent error¹.

If the mesh is limited to two dimensions the question remains as to whether this is a suitable equivalent system appropriate for modelling the behaviour of sound within a room.

Mesh Sampling Rate

If a waveguide mesh is to be used to process an arbitrary audio signal then an appropriate mesh sampling rate must be chosen corresponding to the sampling rate of this audio input. Using Equation (4.27) for a 2-D mesh with $c = 343\text{m/s}$ and $d = 0.011\text{m}$ results in $f_{update} = 44097.75\text{Hz}$, sufficiently close enough to 44.1kHz, the standard audio CD sampling rate. This would theoretically allow wave frequencies up to approximately 22050 Hz to be propagated. Note that according to [Van Duyne and Smith, 1993] and [Savioja et al, 1996b], the upper limit for valid frequencies on the rectilinear mesh is actually $0.25 \times f_{update}$, reducing this highest frequency value to approximately 11025Hz. This should still be a useful bandwidth for processing most audio signals. Over-sampling the mesh by setting $d = 0.0055$ and low-pass filtering the output would in theory allow full CD sample rate processing, but would be prohibitively slow. Conversely it should be possible to set $d = 0.022\text{m}$ for some instances. In this case $f_{update} = 22048.88\text{Hz}$, allowing frequencies up to approximately 11025Hz to be propagated, valid up to 5512.5Hz if dispersion error is considered.

¹ The 3-D tetrahedral waveguide mesh or the 3-D deinterpolated rectilinear mesh could prove to be more suitable alternatives. See [Van Duyne and Smith, 1996] and [Savioja and Välimäki, 1996] respectively.

Development Platform

The waveguide mesh model is to be implemented in software using the C programming language on a generic Silicon Graphics UNIX workstation running the IRIX operating system. This should allow the model to be portable across a range of IRIX workstations of varying capabilities, with instant improvements in run time if a more powerful generation of machines is made available². The other advantage offered by the Silicon Graphics platform is the advanced hardware accelerated graphics routines that can be accessed in C via the OpenGL programming library [Woo et al, 1997]. This allows the resulting wave propagation in the model to be rendered to the screen and visualised in a number of different ways. The flexible approach of a software-based model utilising the fast floating-point capabilities of the Silicon Graphics machines also negates one of the main advantages the rectilinear mesh has over the triangular mesh. This is that the rectilinear mesh can be implemented efficiently in hardware using only addition operations and a binary shift. A software implementation may sacrifice the speed and efficiency of a model designed to run on specific hardware but will in turn allow greater flexibility in development. Further, as the triangular mesh is the model to be primarily developed and investigated, and requires a floating-point multiplication in the scattering equations, a hardware-based implementation may not actually offer any particular advantage as it would with the rectilinear mesh.

Computation time

It has been conjectured that, theoretically, given enough computing power, a complete and accurate waveguide model of the acoustics of a room should be possible. However from the perspective of developing and implementing a test case that would involve modelling a typically sized room it is clearly not appropriate to presume that an infinite amount of processing power is available. To this end compromises have been imposed upon the waveguide model as discussed above, with the most significant being the two dimensional limitation, so that results can be obtained and analysed with relative ease and without putting too much demand on available computing resources. It is evident however that if audio bandwidth processing is required any such model working at one of the suggested sampling rates will result in a mesh consisting of many thousands of junctions. Such a model would still be some way away from running in real time. If it is accepted that this model must run as an offline process then it is clear that it would not be possible to process an arbitrary sound source, especially if it is real time or of significant duration. The waveguide mesh model of an acoustic space is potentially being considered as an equivalent system to an actual room as discussed in Chapter 2.2.

² This has already been the case with model development starting on an R3000 based Indigo workstation and being completed on an 8xR10000 node Origin server.

As in other similar equivalent systems, the RIR is the key, both to revealing the properties of the model and, when used in a convolution routine, the manner in which an arbitrary sound source of indefinite duration can effectively be placed in, and processed by, the virtual room. Therefore part of the development of this waveguide model will require an investigation into how a suitable excitation signal can be input to the system and correspondingly measured at a suitable output.

Chapter 5

Mesh Construction and Implementation

5.1 Introduction

The previous chapter highlighted the methods appropriate for modelling the soundfield within an enclosed space, and concluded that a digital waveguide mesh is potentially the most accurate, flexible and easy to implement whilst still remaining reasonably efficient in terms of computation time. Waveguide mesh models also lend themselves readily to providing a visualisation of the wave propagation behaviour within the space, a desirable consideration for any such model as highlighted in Chapters 2 and 4. Previous studies have shown that the rectilinear mesh is indeed applicable to modelling a room and generating a RIR [Savioja et al, 1994], [Savioja et al, 1995] and [Savioja et al, 1996b]. However, it was shown that dispersion error limits the effective usefulness of this mesh topology (Chapter 4.5.4). It has been hypothesised that the triangular waveguide mesh is a more accurate solution to this problem as it minimises the dispersion error, making it a function of frequency only. The rectilinear mesh by comparison exhibits dispersion error that is dependent on both frequency and the direction of wave propagation. The chapter concluded with a specification of how this hypothesis should be tested in terms of model implementation with a number of factors that have to be considered:

The model is to be implemented in two dimensions only.

This will facilitate development as computation times will be within reasonable limits whilst allowing high mesh sampling rates to be used suitable for full audio bandwidth processing. However, if the mesh is limited to two dimensions the question remains as to whether this is a suitable equivalent system appropriate for modelling the behaviour of sound within a room.

Mesh sampling rates must correspond to industry standard audio sampling rates.

This will allow a (theoretically) full audio bandwidth RIR to be extracted from the mesh. Dispersion error works to effectively lower this ideal value.

The mesh models are to be implemented in software using the C programming language on a generic Silicon Graphics UNIX workstation running the IRIX operating system and supporting the OpenGL graphics library.

The high mesh sampling rates imply that the model will not run in real time.

It will therefore be considered only as an offline process with results being based on both visual feedback of the resulting wave propagation and analysis of the measured RIRs and associated processed audio samples.

Based on these specifications this chapter will explore the issues involved in implementing a 2-D rectilinear and triangular waveguide mesh. This will include definition of the appropriate scattering junctions, how the mesh is to be constructed including the boundaries, signal input and output, and the theoretical properties of the model including a detailed analysis of the dispersion error. The practical issues of how the model is to be structured, coded and tested for the Silicon Graphics platform as well as how the wave propagation is to be visualised will also be discussed.

5.2 Unit Scattering Junctions

The general scattering equations for an N -port scattering junction that determine the behaviour of the waveguide model have been introduced in Chapter 4.5. The scattering equations for the 4-port rectilinear mesh have also been introduced but are re-included here for completion and comparison. This 4-port junction is the general constituent component of the rectilinear mesh. The 6-port junction is the similar general constituent component of the triangular mesh. These are arranged as shown in Figure 5.1.

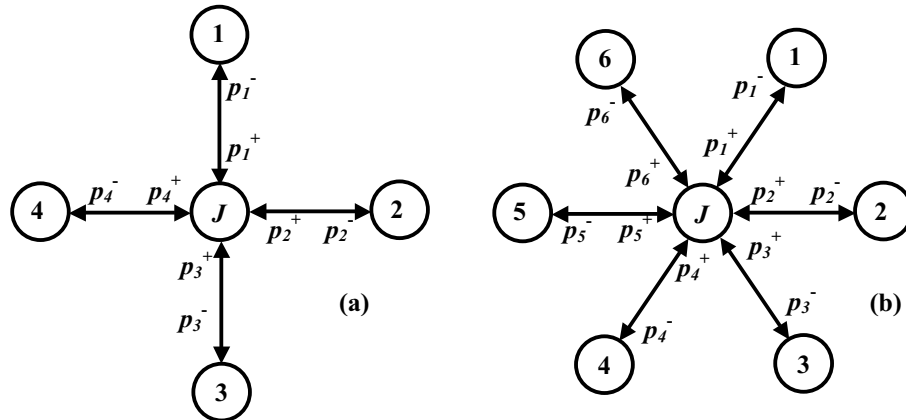


Figure 5.1 General Scattering Junctions. (a) The 4-port scattering junction used in the rectilinear mesh; (b) the 6-port junction used in the triangular mesh.

In the rectilinear mesh, the signal pressure p_J at the general 4-port scattering junction J based on the incoming signals to the junction is:

$$p_J = \frac{1}{2} [p_1^+ + p_2^+ + p_3^+ + p_4^+] \quad (5.1a)$$

Similarly, the expression for the signal pressure p_J in the triangular mesh at the general 6-port scattering junction J based on the signals input to the junction is:

$$p_J = \frac{1}{3} [p_1^+ + p_2^+ + p_3^+ + p_4^+ + p_5^+ + p_6^+] \quad (5.1b)$$

Common to both topologies is the equation for signals emerging from the scattering junction J based on the input signal along the same waveguide and the junction pressure itself:

$$p_i^\square = p_j \square p_i^+ \quad (5.2)$$

As the waveguides are equivalent to bi-directional unit-delay lines, the input to a scattering junction is equal to the output from a neighbouring junction into the connecting waveguide at the previous time step. This is expressed as:

$$p_{J,i}^+ = z^{\square 1} p_{i,J}^\square \quad (5.3)$$

These three expressions [(5.1a), (5.2) and (5.3) or (5.1b) (5.2) and (5.3)] are the basic equations of motion of the waveguide mesh for the topology being considered and form the foundation of the algorithm that is to be implemented. Note again that there exists an equivalent finite difference relation for these equations for both the rectilinear mesh (see Chapter 4.7.3 and Appendix A) and the triangular mesh [Fontana and Rocchesso, 1995].

5.3 Mesh Construction

Given a 2-D room geometry with an overall maximum width and length, and a mesh sampling rate that will imply a definite distance between scattering junctions, a specific mesh has to be constructed to fit over and within the enclosed 2-D space. This mesh will, for the most part, consist of general 6-port or 4-port scattering junctions as defined above. However, these junctions cannot be used for the whole mesh structure as they cannot deal with what happens at a boundary such as a wall or at certain room features, for example when an acoustically large object is placed in the centre of the room. This leads to a number of special case junction types as described below.

5.3.1 Boundary Conditions – The General Case

The most convenient and straightforward way to consider what happens at the boundary of a mesh structure is to set a boundary junction as having only one other neighbour. The effect of a boundary in a real room is to produce a reflection of a sound wave, usually with some frequency dependent absorption of the wave energy at the boundary itself. In a digital waveguide structure a reflection is caused by a change in the impedance of the waveguide. This can be conceptualised by connecting a dummy junction on the other side of the boundary junction, essentially within the boundary itself [Savioja et al, 1996b] and [Savioja, 1997]. The connecting waveguides on either side of the boundary junction will therefore have different characteristic impedances, Z_1 and Z_2 respectively. Consider such a boundary junction as would be found in a typical 2-D rectilinear mesh, as shown in Figure 5.2. If at a boundary the impedance changes from Z_1 to Z_2 the reflection coefficient r is defined as:

$$r = \frac{Z_2 \square Z_1}{Z_2 + Z_1} \quad (5.4)$$

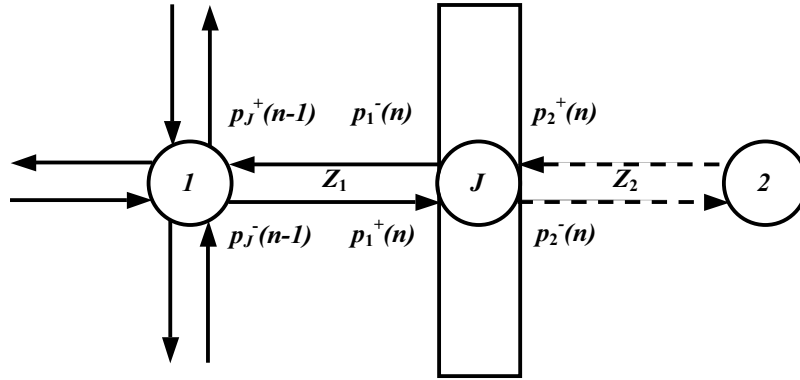


Figure 5.2 Termination of a waveguide mesh due to a boundary resulting in a reflection. A dummy junction "within" the boundary is used in the derivation of the scattering equations for this case.

It can be seen from Equation (5.4) that it is the ratio of the impedances that is pertinent and so it is possible to express impedance Z_2 in terms of impedance Z_1 :

$$Z_2 = \square \cdot Z_1 \quad (5.5)$$

Where \square is the ratio between the two impedances. Substituting Equation (5.5) in Equation (5.4) allows the ratio between the two impedances to be expressed in terms of the reflection coefficient r :

$$\square = \frac{1+r}{1-\square r} \quad (5.6)$$

Considering Figure 5.2, clearly there is no contribution into the boundary junction, J , from the dummy junction, 2. Therefore:

$$p_2^+(n) = 0 \quad (5.7)$$

Similarly, the output from the boundary junction back into the mesh is the input from junction 1 multiplied by the change in impedance, the reflection factor r :

$$p_1^\square(n) = r \cdot p_1^+(n) \quad (5.8)$$

Using Equation (4.18), the sound pressure for the boundary junction can be calculated as a function of the sound pressures of the incident travelling waves, p_i^+ :

$$p_J(n) = \frac{2 \cdot \frac{1}{Z_1} \cdot p_1^+(n)}{\frac{1}{Z_1} + \frac{1}{\square \cdot Z_1}} \quad (5.9)$$

Cancelling out the impedance factor $1/Z_1$, substituting (5.6) for \square and re-arranging gives:

$$p_j(n) = (1 + r) \cdot p_1^+(n) \quad (5.10)$$

Alternatively, if a finite difference formulation is required in accordance with Chapter 4.5.3 and Equation (4.25), Equation (5.10) can be expressed as a difference equation:

$$p_j(n) = (1 + r) \cdot p_1(n-1) - r \cdot p_j(n-2) \quad (5.11)$$

Similarly, it follows that a DSP formulation is also possible as expressed in Equation (5.12). Note that Equation (5.11) is derived in more detail in Appendix A.

$$P_j = \frac{(1 + r) \cdot z^{-1} p_1}{1 + rz^{-2}} \quad (5.12)$$

Given the pressure signal value at the junction on a boundary it is possible to calculate the proportion of the signal reflected back from the boundary into the mesh using Equation (5.2) as normal. However in this simple case for the rectilinear mesh where a boundary junction only has one neighbour, substituting Equation (5.10) in Equation (5.2) gives:

$$p_1^-(n) = r \cdot p_1^+(n) \quad (5.13)$$

This equation demonstrates that the reflected wave signal from the boundary, p_1^- , is clearly some proportion of the incident wave, p_1^+ , determined according to the value of the reflection factor, r . The proportion of the wave's energy that is not absorbed at the boundary effectively passes through to the dummy junction on the other side of the wall. Similarly from this equation it can be seen that the valid range of values for r will range from +1 to -1. Total reflection with a reversal in the phase of the incident wave is the result if $r = -1$. Total reflection with a preservation in the phase of the incident wave is the result if $r = +1$. For a value between these bounds partial absorption of the incident wave is the result, with phase reversal/preservation determined by either a negative or positive value. It follows that setting $r = 0$ should result in a total absorption of the incident wave, modelling anechoic conditions. However, it will be seen that this is not actually the case (see Chapter 6.2.5).

Note that when an actual sound wave hits a solid wall, only a reflection of the pressure signal with preservation of phase is possible. At the boundary between the air and the wall the velocity component of the wave must be zero, as the wall does not move, implying that all of the wave's energy is stored in the pressure component. Clearly the energy stored in the pressure component cannot move forwards in the direction of the propagating wave so it bounces back in the reverse direction, resulting in a change of phase in the velocity component of the wave, but

not the pressure component. Also the incident pressure wave superimposes constructively with the reflected wave at the boundary, so while the velocity component at the wall is zero, the pressure component is twice as large.

Reflection with an associated change in phase of the pressure component of the sound wave is only possible when travelling from a bounded region (for example, an enclosed tube open at one end) to an unbounded region (for example, free space). In this case the pressure component is zero at the boundary and the velocity component is twice as large.

These two cases arise due to the difference in acoustic impedance at the boundary [Howard and Angus, 1996]. At a solid boundary the impedance of the boundary is greater than the propagating medium and in the second case it is smaller. Therefore to model what approaches real world conditions, only values of r between 0 and +1 are valid, as this will give a reflection of the incident wave with a preservation of phase.

These boundary conditions are still a considerable simplification of what happens at a real boundary. Note that there is no direct correlation between the value of the reflection factor, r , and standard measured absorption coefficients for actual physical materials. Further r is not defined as being frequency dependent, whereas the amount of absorption/reflection at a boundary varies with the frequency. However, this mesh termination method is the most commonly used for waveguide mesh modelling of room acoustics [Savioja et al, 1994], [Savioja et al, 1995], [Savioja et al, 1996b], and has also been used in waveguide mesh synthesis techniques [Laird et al, 1998]. The reasons for this are mainly due to the simplicity of the methodology and the fact that similar scattering equations to those used for a standard junction can be constructed and used for the boundary junctions. This helps in the design and implementation of the model and reduces computation time, whilst still allowing r to be varied in a more general manner so as to investigate the resulting acoustic effect. It should be possible to correlate r more exactly with actual physical quantities, based on measurements of acoustic impedance, with complex values used for the waveguide impedance Z_i in order to account for frequency dependence. Alternatively r in Equations (5.11)-(5.12) can be replaced with any digital filter [Savioja et al, 1996b], and [Huopaniemi et al, 1997] describes how filters suitable for modelling glass panels, plasterboard on a frame, and plasterboard on fibreboard with holes have been designed using analytically measured data and implemented as part of a simple rectilinear waveguide mesh model.

These boundary conditions are also similar in concept and implementation to the standard Kelly-Lochbaum scattering junction between two lossless tubes as commonly used in modelling

the vocal tract [Rabiner and Schafer, 1978]. Considering the k th tube with a cross-sectional area A_k , the pressure and volume velocity within the tube have the form:

$$p_k(x,t) = \frac{\rho c}{A_k} \left[u_k^+ \left(t - \frac{x}{c} \right) + u_k^- \left(t + \frac{x}{c} \right) \right] \quad (5.14)$$

$$u_k(x,t) = u_k^+ \left(t - \frac{x}{c} \right) - u_k^- \left(t + \frac{x}{c} \right) \quad (5.15)$$

where x is the distance measured from the left hand end of the k th tube ($0 \leq x \leq l_k$) and u_k^+ and u_k^- are positive and negative-going travelling waves in the k th tube, respectively. At the junction between the tube k and tube $(k+1)$ it can be shown that:

$$u_{k+1}^+(n) = (1 + r_k)u_k^+(n-1) + r_k u_{k+1}^-(n) \quad (5.16)$$

$$u_k^-(n+1) = -r_k u_k^+(n-1) + (1 - r_k)u_{k+1}^-(n) \quad (5.17)$$

where $r_k = (A_{k+1} - A_k)/(A_{k+1} + A_k)$ and $-1 \leq r_k \leq +1$. It is possible to represent such a system as shown in Figure 5.3.

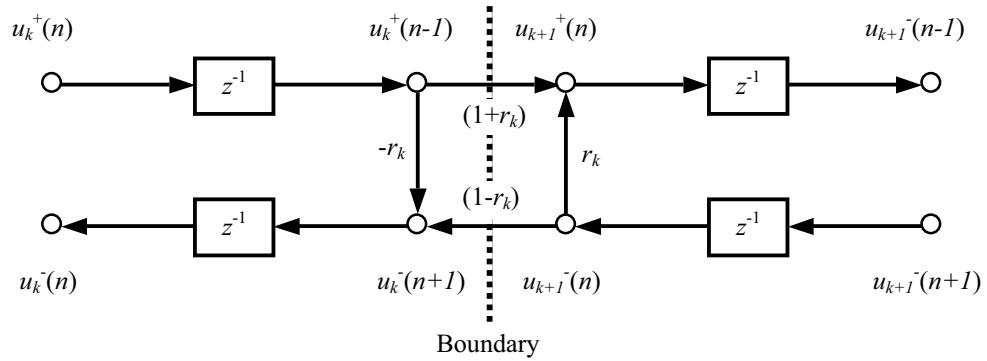


Figure 5.3 Signal-flow representation of the junction between two lossless tubes, from [Rabiner and Schafer, 1978].

If the scattering junction on the boundary is considered to be junction J in Figure 5.2, then the left- and right-hand junctions can be similarly considered as junctions 1 and 2 respectively. As with the latter case, clearly there will be no contribution back into the mesh from the right-hand junction, as this is effectively within the solid boundary. This implies that $u_{k+1}^-(t) = 0$ and so Equations (5.16)-(5.17) reduce to:

$$u_{k+1}^+(n) = (1 + r_k)u_k^+(n-1) \quad (5.18)$$

$$u_k^-(n+1) = -r_k u_k^+(n-1) \quad (5.19)$$

Note that from examining Figure 5.3 and Equation (5.19), it can be seen that the reflected wave signal from the boundary is clearly some proportion of the incident wave determined according

to the value of the reflection factor r and hence shows an equivalence with Equation (5.13). Note that as these equations are considering volume velocity rather than pressure, Equation (5.19) additionally shows that there is an associated reversal in the phase of the reflected wave.

5.3.2 Boundary Conditions – Exceptional Cases

In the rectilinear mesh the scattering equations for most boundary junctions can be taken care of using the method above and Equations (5.10) and (5.13) with the only variation being which waveguide element is actually connected to the junction on the boundary. However this does not take into account every type of boundary junction. Consider the junction that is conceivably present at the corner of a rectangular room model as shown in Figure 5.4.

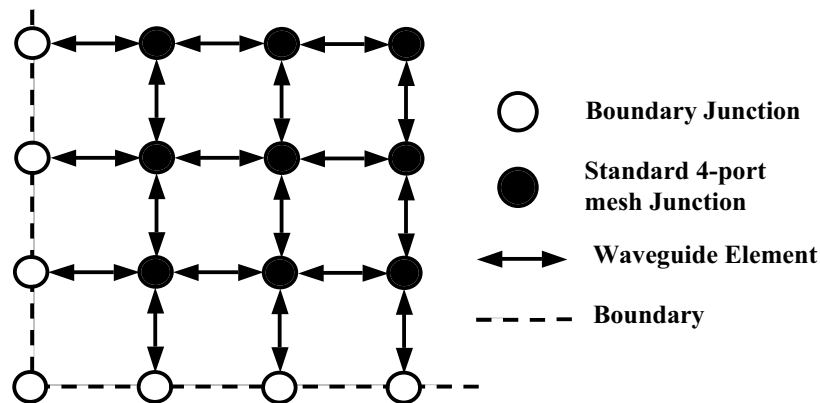


Figure 5.4 A corner of the rectilinear mesh. Note that the left corner junction on the boundary is not actually connected by a waveguide element to any other junction.

Note that the bottom left junction, although being part of the boundary is not actually a physical part of the rectilinear mesh and as such is not connected to any other junction by a waveguide element. From an implementation perspective this junction does not exist as it is not part of the mesh itself. A further complication is added if a room is more complex than the simplest rectangle. Consider a rectangular room with a small simple projection in the left side wall as shown in Figure 5.5:

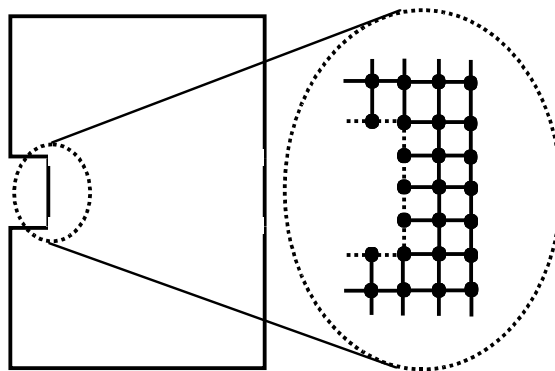


Figure 5.5 A more complex room where the presence of an alcove results in scattering junctions at the inner corners connected to the rest of the mesh via two waveguide elements rather than one which is the more general case.

In this case a boundary junction exists on a corner of the mesh which is physically connected to the rest of the mesh by two waveguide elements. Note that this junction is different from the more typical boundary junction as previously discussed. The general boundary junction is connected to the rest of the mesh using only one waveguide element rather than two. This in turn leads to a different set of scattering equations. Note further that in Figure 5.5 the two corner junctions shown will differ slightly in the actual scattering junctions used due to the different connections present. The upper corner junction has a waveguide element connecting it to the junction in the row above it, and to the junction to the right of it on the same row. The lower corner junction has waveguide elements connecting it to the junction to the right of it again and to the junction in the row below it, rather than above it. The scattering equations for both of these cases will actually be the same but will involve different inputs to the boundary junctions and outputs from it. These scattering equations are derived in a similar manner to the example given above with the boundary junction under consideration being connected to one single dummy junction on the other side of the boundary. The corner junctions in Figure 5.5 are therefore considered for derivation purposes as 3-port scattering junctions with two connections to actual junctions and one connection to the dummy junction on the other side of the boundary. For convenience, terminology based on compass directions will be used to refer to the validity and existence of junctions connected with associated waveguide elements. Therefore the upper corner junction in Figure 5.5 has North (N) and East (E) connections valid only. Referring to Figure 5.1(a) if a junction J has N and E connections valid, then the only junctions required for the scattering equations will be junctions 1 and 2 respectively. Similarly the lower corner junction has South (S) and East (E) connections valid to junctions 2 and 3 respectively. The ten distinct junction types that could arise in the rectilinear mesh, with associated valid connections and scattering equations are summarised in Table 5.1.

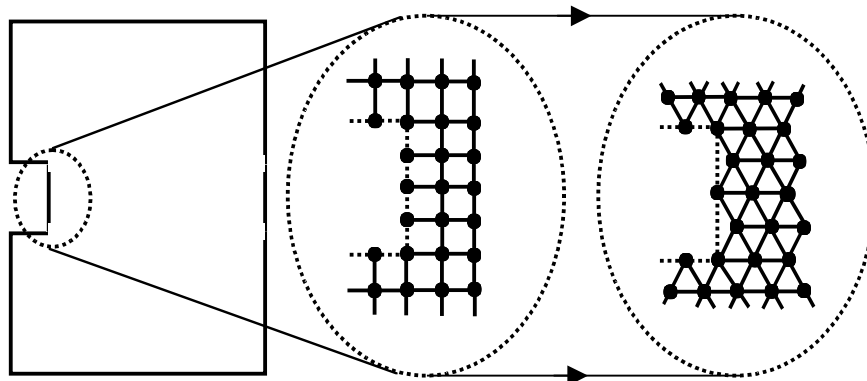


Figure 5.6 The same room as shown in Figure 5.4 with rectilinear and triangular waveguide representations. The triangular representation highlights more junction types deviating from the general 6-port junction than in the case of the rectilinear mesh.

TYPE	JUNCTION STRUCTURE	VALID CONNECTION	SCATTERING EQUATION	JUNCTION OUTPUT
0		N Connection E Connection S Connection W Connection	$p_J(n) = \frac{1}{2} \prod_{i=1}^4 p_i^+$	$P_i^{\square} = p_J(n) \square p_i^+(n)$ For $i = 1,2,3,4$.
1		N Connection	$p_J(n) = (1+r) \cdot p_1^+(n)$	$P_1^{\square} = r \cdot p_1^+(n)$
2		E Connection	$p_J(n) = (1+r) \cdot p_2^+(n)$	$P_2^{\square} = r \cdot p_2^+(n)$
3		S Connection	$p_J(n) = (1+r) \cdot p_3^+(n)$	$P_3^{\square} = r \cdot p_3^+(n)$
4		W Connection	$p_J(n) = (1+r) \cdot p_4^+(n)$	$P_4^{\square} = r \cdot p_4^+(n)$
5		N Connection E Connection	$p_J(n) = \frac{2(1+r)}{3+r} \cdot (p_1^+(n) + p_2^+(n))$	$P_1^{\square} = p_J(n) \square p_1^+(n)$ $P_2^{\square} = p_J(n) \square p_2^+(n)$
6		E Connection S Connection	$p_J(n) = \frac{2(1+r)}{3+r} \cdot (p_2^+(n) + p_3^+(n))$	$P_2^{\square} = p_J(n) \square p_2^+(n)$ $P_3^{\square} = p_J(n) \square p_3^+(n)$
7		S Connection W Connection	$p_J(n) = \frac{2(1+r)}{3+r} \cdot (p_3^+(n) + p_4^+(n))$	$P_3^{\square} = p_J(n) \square p_3^+(n)$ $P_4^{\square} = p_J(n) \square p_4^+(n)$
8		N Connection W Connection	$p_J(n) = \frac{2(1+r)}{3+r} \cdot (p_1^+(n) + p_4^+(n))$	$P_1^{\square} = p_J(n) \square p_1^+(n)$ $P_4^{\square} = p_J(n) \square p_4^+(n)$
9		No Connections		

Table 5.1 The ten distinct junction types that could arise in the rectilinear mesh, with associated valid connections and scattering equations.

Boundaries and boundary junctions in the triangular mesh are dealt with in exactly the same way as the examples presented here for the rectilinear mesh. However, as a general junction in the triangular mesh is connected to six others rather than four as in the rectilinear mesh, boundary conditions have to be handled with considerably more care as the number of possible junction types is much greater. For instance consider again the room displayed in Figure 5.5, but this time modelled using the triangular mesh, as shown in Figure 5.6.

Using the triangular mesh results in a number of boundary junctions differing both from each other and from those cases arising in the rectilinear mesh. Referring to Figure 5.6 the simple boundary junctions consisting of only one actual connection (and one connection to a dummy junction on the other side of the boundary) in the rectilinear mesh, due to the horizontal walls in the alcove as drawn, now have two actual connections (plus one dummy connection) in the triangular mesh. Boundary junctions occurring due to vertical walls (as drawn) are more complex as only alternate rows will actually have a junction placed on the boundary. The “indented” rows between these rows do not therefore have a set of scattering equations as would usually be found at a boundary where a reflection factor has to be considered, and are simply dealt with as standard 5-port scattering junctions. This implies that there is essentially a reduction in the mesh density and hence the spatial sampling interval along such vertically positioned boundaries. The actual extent of this effect on the physical results obtained has as yet to be ascertained. A possible solution exists by adding a junction to the end of such a row using fractional delay lines in the waveguide element so that this additional junction is actually placed on the defined boundary, restoring the spatial sampling interval. This has been used successfully in other general waveguide models of complex structures including waveguide mesh modelling of drum skins [Laird et al, 1998] and [Fontana and Rocchesso, 1995].

The corners of the alcove give rise to other junction types, as do other possible physical arrangements that could be found in a simple 2-D enclosed room. The twenty distinct junction types that could arise in the triangular mesh, with associated valid connections and scattering equations are summarised in Table 5.2. Again compass directions will be used to refer to the validity and existence of junctions connected with associated waveguide elements. In this case the six compass points, NE, E, SE, SW, W and NW will refer to the connections to junctions 1, 2, 3, 4, 5 and 6 respectively as shown in Figure 5.1(b).

5.4 Mesh Excitation

Given that a mesh has been constructed to model the required enclosed space and that each junction in the mesh behaves according to its well defined scattering equations as listed in Tables 5.1 and 5.2, a method must be found that allows an excitation signal to be input into the mesh at a discrete point or set of points. Clearly this excitation must be applied such that none of the equations governing the behaviour of the mesh are violated. There are two possible methods for achieving this:

1. Apply an excitation directly at a specific general scattering junction according to the equations governing that junction and those surrounding it.

TYPE	JUNCTION STRUCTURE	VALID CONNECTION	SCATTERING EQUATION	JUNCTION OUTPUT
0		NE, E, SE Connections; NW, W, SW Connections	$p_J(n) = \frac{1}{3} \prod_{i=1}^6 p_i^+(n)$	$p_i^\square = p_J(n) \prod p_i^+(n)$ For $i = 1, 2, \dots, 6$.
1		SE Connection SW Connection	$p_J(n) = \frac{2(1+r)}{3+r} \cdot (p_3^+(n) + p_4^+(n))$	$p_3^\square = p_J(n) \prod p_3^+(n)$ $p_4^\square = p_J(n) \prod p_4^+(n)$
2		NE Connection NW Connection	$p_J(n) = \frac{2(1+r)}{3+r} \cdot (p_1^+(n) + p_6^+(n))$	$p_1^\square = p_J(n) \prod p_1^+(n)$ $p_6^\square = p_J(n) \prod p_6^+(n)$
3		NE Connection E Connection SE Connection	$p_J(n) = \frac{1+r}{2+r} \cdot (p_1^+(n) + p_2^+(n) + p_3^+(n))$	$p_i^\square = p_J(n) \prod p_i^+(n)$ For $i = 1, 2, 3$.
4		NW Connection W Connection SW Connection	$p_J(n) = \frac{1+r}{2+r} \cdot (p_4^+(n) + p_5^+(n) + p_6^+(n))$	$p_i^\square = p_J(n) \prod p_i^+(n)$ For $i = 4, 5, 6$.
5		SE Connection	$p_J(n) = (1+r) \cdot p_3^+(n)$	$p_3^\square = r \cdot p_3^+(n)$
6		SW Connection	$p_J(n) = (1+r) \cdot p_4^+(n)$	$p_4^\square = r \cdot p_4^+(n)$
7		NE Connection	$p_J(n) = (1+r) \cdot p_1^+(n)$	$p_1^\square = r \cdot p_1^+(n)$
8		NW Connection	$p_J(n) = (1+r) \cdot p_6^+(n)$	$p_6^\square = r \cdot p_6^+(n)$
9		NE, E, SE Connections; NW, SW Connections	$p_J(n) = \frac{2}{5} \prod_{i=1}^6 p_i^+(n); i = 5$	$p_i^\square = p_J(n) \prod p_i^+(n)$ For $i = 1, 2, \dots, 6; i = 5$.
10		NE, SE Connections; NW, W, SW Connections;	$p_J(n) = \frac{2}{5} \prod_{i=1}^6 p_i^+(n); i = 2$	$p_i^\square = p_J(n) \prod p_i^+(n)$ For $i = 1, 2, \dots, 6; i = 2$.
11		NE Connection E Connection SE Connection NW Connection	$p_J(n) = \frac{2(1+r)}{5+3r} \cdot (p_1^+(n) + p_2^+(n) + p_3^+(n) + p_6^+(n))$	$p_i^\square = p_J(n) \prod p_i^+(n)$ For $i = 1, 2, 3, 6$;

TYPE	JUNCTION STRUCTURE	VALID CONNECTION	SCATTERING EQUATION	JUNCTION OUTPUT
12		NE Connection NW Connection W Connection SW Connection	$p_j(n) = \frac{2(1+r)}{5+3r} \cdot (p_1^+(n) + p_4^+(n) + p_5^+(n) + p_6^+(n))$	$p_i^\square = p_j(n) \square p_i^+(n)$ For $i = 1,4,5,6$.
13		NE Connection E Connection SE Connection SW Connection	$p_j(n) = \frac{2(1+r)}{5+3r} \cdot (p_1^+(n) + p_2^+(n) + p_3^+(n) + p_4^+(n))$	$p_i^\square = p_j(n) \square p_i^+(n)$ For $i = 1,2,\dots,4$.
14		SE Connection NW Connection W Connection SW Connection	$p_j(n) = \frac{2(1+r)}{5+3r} \cdot (p_3^+(n) + p_4^+(n) + p_5^+(n) + p_6^+(n))$	$p_i^\square = p_j(n) \square p_i^+(n)$ For $i = 3,4,\dots,6$.
15		E Connection SE Connection	$p_j(n) = \frac{2(1+r)}{3+r} \cdot (p_2^+(n) + p_3^+(n))$	$p_2^\square = p_j(n) \square p_2^+(n)$ $p_3^\square = p_j(n) \square p_3^+(n)$
16		W Connection SW Connection	$p_j(n) = \frac{2(1+r)}{3+r} \cdot (p_4^+(n) + p_5^+(n))$	$p_4^\square = p_j(n) \square p_4^+(n)$ $p_5^\square = p_j(n) \square p_5^+(n)$
17		NE Connection E Connection	$p_j(n) = \frac{2(1+r)}{3+r} \cdot (p_1^+(n) + p_2^+(n))$	$p_1^\square = p_j(n) \square p_1^+(n)$ $p_2^\square = p_j(n) \square p_2^+(n)$
18		NW Connection W Connection	$p_j(n) = \frac{2(1+r)}{3+r} \cdot (p_5^+(n) + p_6^+(n))$	$p_5^\square = p_j(n) \square p_5^+(n)$ $p_6^\square = p_j(n) \square p_6^+(n)$
19		No Connections		

Table 5.2 The twenty distinct junction types that could arise in the triangular mesh, with associated valid connections and scattering equations.

- Replace the junction where a signal is required to be applied with a specific junction that has an additional waveguide element attached that allows an external signal to be applied to the mesh.

Method 2 is similar to the Wave Digital Hammer Method used for exciting strings and plates as described in [Van Duyne et al, 1994]. However with this method, as is found in real percussive instruments, the input junction is designed so that as the excitation is applied to the model, the model acts back upon the excitation load as well. Clearly when applying an excitation signal to a real room this is generally not the case – or at least the effect of the air pressure back upon the

excitation source is certainly negligible enough that it can be disregarded. Therefore an input junction has to be constructed such that energy can be applied *to* the system without it drawing any energy *from* the system. What is required is a one-way input waveguide element, as shown in Figure 5.7. In this example a 5-port junction has been constructed with all impedances equal consisting of a general 4-port junction with an additional one-way input waveguide element attached to it. The scattering equations are somewhat more involved due to the one-way nature of the input element. The signal at the junction J , similar to the 5-port scattering junctions, types 9 and 10 in Table 5.2, is given by:

$$p_J = \frac{2}{5} [p_1^+ + p_2^+ + p_3^+ + p_4^+ + p_5^+ + p_{IN}^+] \quad (5.20)$$

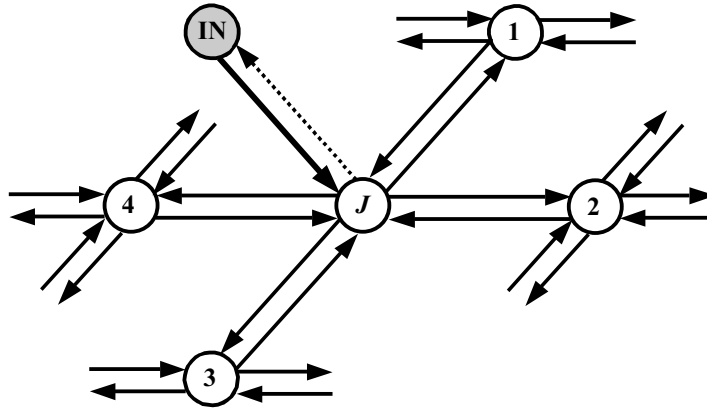


Figure 5.7 Mesh Excitation using a one way waveguide element to input a signal from a specific input junction to the main mesh. No amount of signal is allowed to return back to the input junction.

However as it is a requirement at a junction that the sum of the input volume velocities equals the sum of the output volume velocities (see Equation (4.14)), and there is no output back along the input waveguide element, the outputs from the junction are defined as:

$$p_i^- = p_J(n) - \frac{3}{5}p_i^+(n) - \frac{3}{20}p_{IN}^+(n) \quad (5.21)$$

This method is useful in that any scattering junction can be replaced with an input junction, and any appropriate signal can then be applied into the mesh in such a way that the mesh conditions are adhered to. However, this method does add a further degree of complexity to the model due to the increased number of junction types that potentially have to be catered for.

Method 1 is much simpler to apply and implement in the model. In this case a junction is loaded with an initial value while all other junction values are set to zero. Again this must be executed so that none of the mesh equations or conditions are violated and this is discussed in

[Savioja et al, 1996b] for the DSP formulation of the 3-D rectilinear mesh. If an excitation of value y is required at a specific scattering junction in a uniform mesh than the incoming pressures for all the waveguides connected to it have to be set also. Using Equation (4.18):

$$y = \frac{2 \prod_{i=1}^N \frac{p_i^+}{Z_i}}{\prod_{i=1}^N \frac{1}{Z_i}} \quad (5.22)$$

Note however that all the impedances will be equal as the mesh is uniform and homogeneous. Therefore:

$$y = \frac{2}{N} \prod_{i=1}^N p_i^+ \quad (5.23)$$

This in turn implies:

$$\frac{y}{2} = \frac{1}{N} \prod_{i=1}^N p_i^+ \quad (5.24)$$

Therefore the incoming sound pressures along each waveguide element for an excitation signal of value y at the junction in question are given by:

$$p_i^+ = \frac{y}{2} \quad \square \quad i = 1, 2, \dots, N \quad (5.25)$$

Therefore, to apply an excitation signal y to the mesh at a specific junction will involve injecting a signal of value $y/2$ into each of the delay lines incident to the junction in question. Note that Equation (5.25) is valid for both rectilinear and triangular mesh structures.

In practice it turns out that Method 1 is the simplest and most flexible to implement as part of the mesh model. It does not involve new junction types or more complex scattering equations for the set input junctions yet still allows flexibility in the type of signal that can be applied and its associated duration. Initial implementations of these models indicated that when compared this method seemed to give the most “natural” results in terms of the observed visual behaviour of the mesh to the applied input. The resulting wave motion is smoother, more stable, of higher amplitude, with more energy being transferred into the mesh, and with less high frequency distortion.

As with real rooms the problem remains of finding an input signal of sufficient energy suitable for exciting the whole audible frequency spectrum. Applying a Dirac impulse by loading a junction with an initial sound pressure value and setting all others to zero actually results in an unnaturally sharp impulse at the input point, resulting in spurious high frequencies propagating through the mesh. This can be dealt with by applying a smoother Gaussian pulse as the input signal as shown in Figure 5.8(b). However in this case if the duration of the Gaussian pulse is too long then the input signal will not excite the whole range of frequencies that it is possible for the mesh to propagate successfully resulting in an inaccurate RIR measurement.

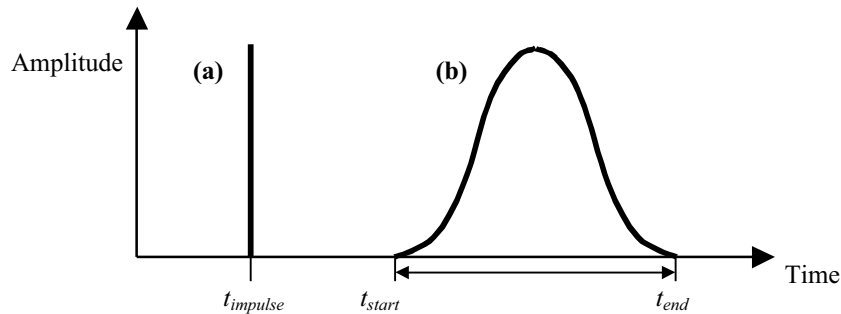


Figure 5.8 Mesh excitation signals. (a) Dirac single sample impulse. (b) Smoothed Gaussian Impulse applied over a number of time steps.

5.5 Mesh Output

Obtaining an output signal from the mesh - the RIR for the modelled room if the input signal is a suitable impulse - is a simple matter of recording the value calculated at every time step for a specific scattering junction on the mesh. This method would seem to offer a significant improvement over the measurement methods used in real rooms. Firstly, the measurement is being made at a discrete single point on the mesh and shows no direction dependent characteristics - although these are both subject to the inherent limitations of the mesh model being used. Both of these properties are more difficult to achieve with a microphone-based recording set-up in a real room. Secondly the RIR is not subject to the particular frequency response peculiarities of the recording and measurement chain. Although real RIRs can be post-processed to remove the influence of the playback, recording and measurement equipment used, this is obviously not required with these types of model.

A RIR recorded at a single point in this manner will obviously contain most of the auditory cues required to impart information to the listener about the characteristics of the modelled room. This will include source distance, room size, early reflection information and reverberation time – the general environmental context of the acoustic space. This single RIR measurement is generally sufficient for both analysis purposes and basic room acoustic/reverberation processing for musical applications. Most of the results presented as part of this thesis in the following

chapter are based on single point, and therefore single channel or mono, RIR measurements. Obviously for binaural listening or stereo processing and playback, and for successful listener location of the sound source within the room, one single measurement is insufficient. There are a number of possible extensions to this basic single point measurement technique, the simplest of which is to take two measurements at points either side of the actually selected output point giving a slightly de-correlated pair of RIRs. The next step in complexity would be to make the distance between this pair of measurement points approximately equal to the average interaural distance between the ears on the human head. The significant interaural time and intensity difference cues that would arise as a result of this could further be improved upon by placing a spherical object between the two points giving rise to shadowing and diffraction effects as would occur with a real human head. The ultimate level of complexity would be to construct a mesh with a fine enough resolution to model the actual shape of the human head, and more importantly, the ridges and contours of the pinna resulting in a BRIR suitable for auralization purposes. In this implementation, if a stereo RIR is required, for simplicity and immediacy, the simple close spaced pair method has been used.

It is also possible to encode a soundfield by decomposing it into spherical harmonic components [Bamford and Vanderkooy, 1995]. The zero order pressure component is termed W and is omni-directional, picking up all sounds from all directions equally. The first order velocity components are figure-of-eight responses pointing forward, left and up, and are termed X , Y and Z respectively. These four spherical harmonic components are represented visually in Figure 5.9.

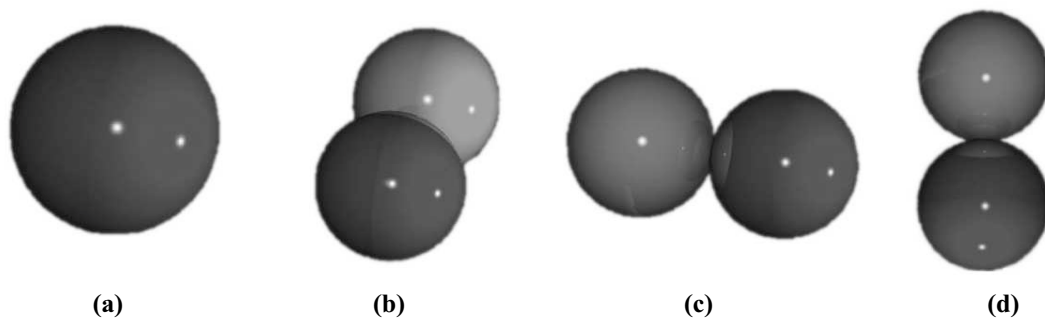


Figure 5.9 A soundfield can be decomposed into four spherical harmonic components known as Ambisonic B-format. (a) W , the zero order pressure component; and X , Y and Z first order velocity components pointing, (b) forwards; (c) to the left; (d) and upwards respectively.

The four signals, W , X , Y and Z are known as B-format. Reproducing a soundfield using this four channel B-format signal is possible using an appropriate Ambisonic decoding scheme and a multi-speaker array [Gerzon, 1992]. It is possible to derive horizontal only B-format signals - W , X and Y only - from the mesh at any point resulting in a B-format multi-channel RIR.

Using this encoding method it is possible to recreate the soundfield in the modelled room complete with acoustic cues associated with the location of a sound source in relation to the listener. This surround sound format is more natural and immersive than standard stereo whilst avoiding the level of complexity and detail required of the model in order to obtain a BRIR.

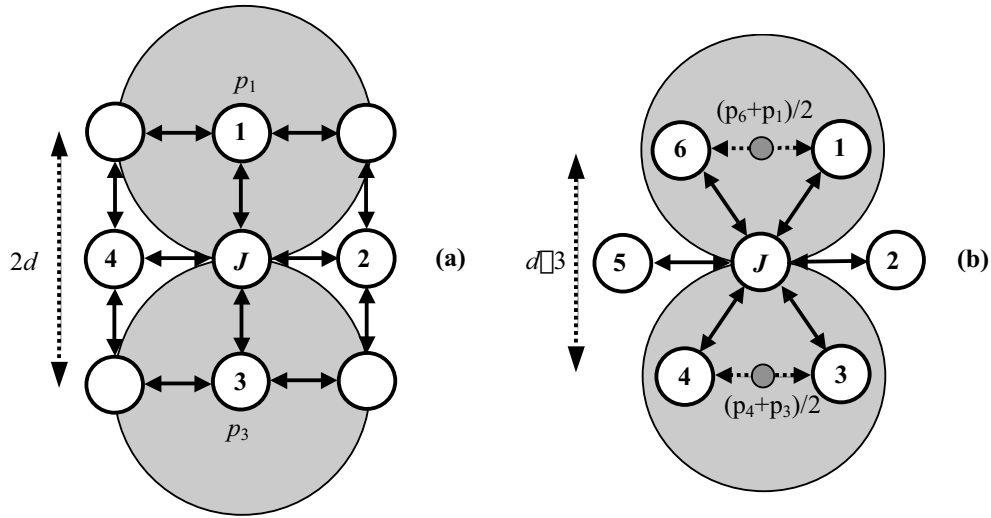


Figure 5.10 Measuring the B-format X component from the mesh. (a) Rectilinear mesh measurements are taken either side of a central point to arrive at an approximation to the derivation of the pressure component. (b) Triangular mesh two measurements are taken at either side and the mean value of each pair is used.

Deriving an approximate 3-channel B-format RIR from the mesh is straightforward. Clearly measuring the sound pressure signal value at a single junction point will give an omnidirectional zero order pressure component, as already used in the simple mono RIR measurement. The first order velocity responses can be thought of as the differential of the pressure plot, which can be approximated by taking two further measurements, either side of a central junction, for each component and dividing by the spatial difference. Figure 5.10(a) shows how it would be possible to arrive at the B-format X component in this way for the rectilinear mesh. The Y component would be derived in a similar fashion but along the other coordinate axis. The triangular mesh is slightly more complex in that adjacent rows do not line up with each other. A possible solution is shown in Figure 5.10(b) where a single value in line with the central junction is derived by averaging the two measurements on either side of it.

Therefore from Figure 5.10(a) the X B-format RIR component for the rectilinear mesh can be calculated from:

$$RIR_X = \frac{p_1(n) - p_3(n)}{2d} \quad (5.26)$$

Similarly, from Figure 5.10(b) the X B-format component for the triangular mesh can be calculated from:

$$RIR_X = \frac{p_1(n) + p_6(n) - p_3(n) - p_4(n)}{2d\sqrt{3}} \quad (5.27)$$

5.6 Dispersion Error

Chapter 4.5.4 introduced the concept of dispersion error in waveguide mesh structures and Figure 4.13 displayed contour plots of normalised wave speed against plane wave speed and direction for a number of mesh topologies. From these results it becomes apparent that the triangular waveguide mesh all but eliminates the directional dependent component of this dispersion error, making it a function of frequency only. An analysis of the dispersion error present in both the rectilinear and triangular waveguide mesh structures is presented here, following [Van Duyne and Smith, 1996], [Laird, 1999] and [Aird, 1999]. Consider again Equation (4.26) the DSP finite difference formulation of the scattering equations for the 2-D rectilinear mesh:

$$p_J = \frac{z^{\square 1} \cdot \frac{1}{2} \sum_{i=1}^4 p_i}{1 + z^{\square 2}} \quad (5.28)$$

Note that a similar expression exists for the 2-D triangular mesh:

$$p_J = \frac{z^{\square 1} \cdot \frac{1}{3} \sum_{i=1}^6 p_i}{1 + z^{\square 2}} \quad (5.29)$$

Dealing with the rectilinear mesh first of all and taking the spatial Fourier transform of equation (5.28) gives the following quadratic expression in terms of z^{-1} :

$$1 + bz^{\square 1} + z^{\square 2} = 0 \quad (5.30)$$

where:

$$b = \square \frac{1}{2} \sum_{i=1}^4 e^{jP_i^t(\square)} \quad (5.31)$$

Where \square is the two-dimensional spatial frequency vector and the spatial positions of the four neighbouring scattering junctions have been replaced by their linear phase terms according to:

$$p_i \square p(\square) e^{jP_i^t(\square)} \quad (5.32)$$

Note further that:

$$\begin{aligned} \square &= [\square_x \square_y] \\ P_1^t &= [0, 1] \\ P_2^t &= [1, 0] \\ P_3^t &= [0, \square 1] \\ P_4^t &= [\square 1, 0] \end{aligned} \quad (5.33)$$

Substituting Equation (5.33) into (5.31) and simplifying gives:

$$b = \cos(\Delta_x) \cos(\Delta_y) \quad (5.34)$$

Note that $b^2 \leq 4 \Delta^2$ and so from the solution to the standard form of the quadratic equation:

$$ax^2 + bx + c = 0 \quad (5.35)$$

Define $G(\Delta)$, the spectral amplification factor of the spatial spectrum after one time step as:

$$G(\Delta) = \frac{b}{2} \pm j \frac{\sqrt{4 \Delta^2 - b^2}}{2} \quad (5.36)$$

Equation (5.36) shows that plane waves propagate without loss ($|G| = 1$). The phase of G corresponds to the spatial phase shift of a plane wave in the direction of travel in one time sample, where:

$$\angle G(\Delta) = \angle(\Delta) = \tan^{-1} \left[\frac{\sqrt{4 \Delta^2 - b^2}}{b} \right] \quad (5.37)$$

Therefore the phase distance travelled in one time sample by a spatial plane wave of frequency $|\Delta|$ and direction Δ is:

$$c(\Delta) = \frac{\angle(\Delta)}{|\Delta|} \quad (5.38)$$

where $c(\Delta)$ is the frequency dependent speed of plane wave travel measured in spatial samples per time sample. Note that [Van Duyn and Smith, 1996] state that *phase distance* corresponds to a *phase advance* in time domain language. It is therefore Equation (5.38) that can be used to calculate the dispersion error plots introduced in Figure 4.13. Note that it is more convenient to plot Equation (5.38) with Equation (5.37) rearranged as:

$$\angle(\Delta) = \frac{1}{\sqrt{\Delta_x^2 + \Delta_y^2}} \cos^{-1} \left[\frac{b}{2} \right] \quad (5.39)$$

where, for the rectilinear mesh:

$$b = \cos(\Delta_x) + \cos(\Delta_y) \quad (5.40)$$

Equations (5.38) and (5.39) can also be used for plotting the dispersion error for the triangular mesh, but in this case Equation (5.33) becomes:

$$\begin{aligned}
 \underline{\omega} &= [\omega_x, \omega_y] \\
 P'_1 &= \left[\cos \frac{\omega}{3}, \sin \frac{\omega}{3} \right] \\
 P'_2 &= [1, 0] \\
 P'_3 &= \left[\cos \frac{\omega}{3}, \sin \frac{\omega}{3} \right] \\
 P'_4 &= \left[\cos \frac{\omega}{3}, \sin \frac{\omega}{3} \right] \\
 P'_5 &= [1, 0] \\
 P'_6 &= \left[\cos \frac{\omega}{3}, \sin \frac{\omega}{3} \right]
 \end{aligned} \tag{5.41}$$

And so Equation (5.40) becomes:

$$b = \frac{2}{3} \left(\cos(\omega_x) + \cos\left(\frac{1}{2}\omega_x + \frac{\sqrt{3}}{2}\omega_y\right) + \cos\left(\frac{1}{2}\omega_x - \frac{\sqrt{3}}{2}\omega_y\right) \right) \tag{5.42}$$

The dispersion error plots for the rectilinear mesh are presented in Figure 5.11 and for the triangular mesh in Figure 5.12.

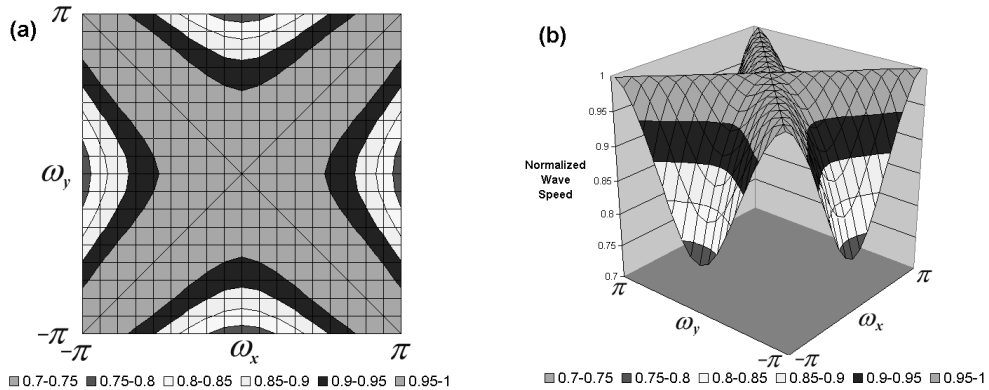


Figure 5.11 Dispersion error as measured on the rectilinear mesh. (a) Contour plot; (b) 3-D plot.

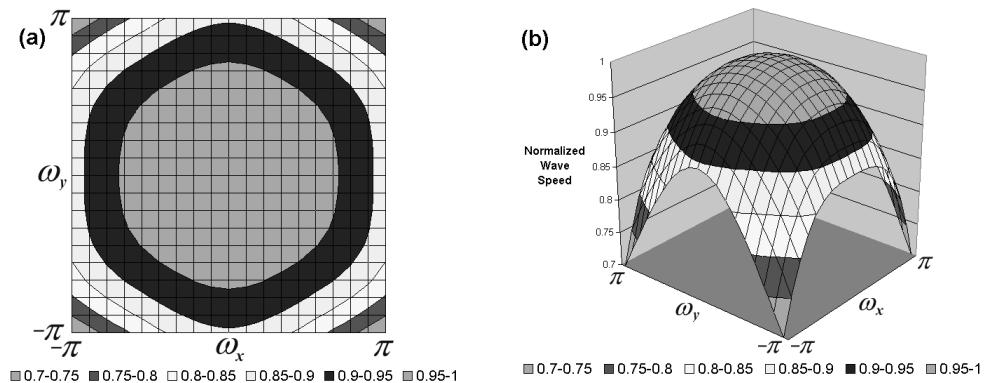


Figure 5.12 Dispersion error as measured on the triangular mesh. (a) Contour plot; (b) 3-D plot.

It can now be clearly seen in more detail what was previously stated in Chapter 4.5.4. The centre region of the plot corresponds to low plane wave frequencies and the outer regions correspond to high frequencies. The angular position on the plot relative to the centre, being the frequency plane origin, corresponds to the direction of plane wave travel on the mesh. On the rectilinear mesh, as previously stated, Figure 5.11 shows that there is no dispersion when travelling diagonally relative to the mesh coordinate system but that there is a considerable drop in wave speed for high frequencies when travelling along the coordinate axes themselves. Figure 5.12 shows that with the triangular waveguide mesh, the dispersion error is minimised such that it is almost totally independent of the direction of propagation. Further, in the rectilinear mesh for $\varphi_x = \varphi/2$, $\varphi_y = 0$ - by symmetry this corresponds to a wave travelling along the direction of the waveguides themselves - there is an approximate 6% reduction in wave speed. For the hexagonal mesh there is only an approximate 3% reduction in wave speed for the same direction of travel for a wave of the same frequency.

5.7 Software Design and Implementation

The waveguide mesh models have been implemented in software using the C programming language on a generic Silicon Graphics UNIX workstation running the IRIX operating system. These models have been collectively titled the *WaveVerb* System. This is short for Waveguide Mesh Reverberation System. The following chapter section discusses some of the more pertinent points that have been raised in the development of the *WaveVerb* models, including some coding design considerations.

The high mesh sampling rates required imply that the model will not run in real time so this is not a software design consideration. A number of working versions exist for demonstrating and testing both the rectilinear and triangular waveguide meshes, either with or without graphical feedback. Graphical feedback and visual analysis have already been identified as important features for such models in Chapters 2 and 4. However, visually rendering the mesh and the resultant wave propagation through it is a non-trivial task in terms of the computation time. As discovered in Chapter 4.5.4, although the scattering equations themselves that drive the mesh are simple to implement and execute, a mesh capable of propagating an audio bandwidth signal requires many junctions. For example more than 120,000 junctions are required for a 4.66m x 3.2m room at 44.1kHz, with an execution run in the order of 90,000 iterations for a 2s RIR. The added overhead of rendering the position of each junction at each iteration is an added load to the total length of time taken for the RIR to be generated. Therefore versions exist for both model topologies that run without graphical feedback or user interaction, considerably speeding up the total execution time.

5.7.1 Memory Usage

Although the waveguide scattering equations are simple to implement and execute, when they operate on the large data structure that is the result of a typical mesh consisting of tens of thousands of junctions these simple addition, subtraction and multiplication operations become a serious processing constraint as they have to be carried out so many times. Therefore care must be applied when defining the mesh variables and structures used within the code. The work of [Campos, 1999] highlights an associated problem in the benchmarking of various hardware platforms in the processing of a simple 3-D rectilinear mesh. The platforms investigated include Silicon Graphics Workstations (based on R3000, R4000 and R5000 RISC processors), a Pentium Pro PC based system and a Silicon Graphics 8 node Origin 2000. In this work the entire mesh is declared as a single, large, indexed 3-D matrix, implying that the whole data structure must be held in the computer's memory for it to be operated upon. The benchmarking results that are displayed in this work show that, with the exception of the Origin that has 4Gb of main system memory and fast fibre channel disk accessing, every other machine reaches a severe performance cut-off point. This point is related directly to the mesh size used such that the data structure created cannot be accommodated in the hardware's main memory and so has to be temporarily stored on the computer hard-disk, severely curtailing the model's performance and increasing computation time.

These results are further supported by [Scott, 1998] where, amongst other methods discussed for implementing efficient signal processing algorithms on Silicon Graphics platforms, memory optimisation is encouraged. This is because although the host processor is very fast, the memory system is relatively slow. If it is not possible to get good cache performance then the application itself can be seriously crippled. The following example is cited that has a direct bearing on the implementation and organisation of the waveguide mesh structure:

“For example, in image-processing, “tiling” is a common practice. Suppose a number of consecutive operations are to be performed on an image. The “obvious” way would be to perform each operation on the entire image, then proceed to the next operation. However, assuming the image doesn't fit in the cache, this gets the worst possible cache performance, since the image has to be reloaded from main memory every time it is touched. A far superior approach is to operate on small “tiles” which fit in the cache: perform all the operations on one tile, then proceed to the next.”

[Scott, 1998]

Also recommended is the use of single precision floating point arithmetic rather than double. Double precision arithmetic can be costly both in terms of execution time and the amount of

memory used in a large data structure. These performance suggestions give further credence to the use of non-graphical versions of the waveguide models. The requirements for a similar sized data structure to the mesh model for the positional information for each junction to enable rendering to the screen together with the general additional program elements used to handle a windows type interface and user interaction seriously increases the memory requirements of such an application with the associated performance based limitations as discussed above.

5.7.2 Description of Program Structures

The 2-D mesh - and hence room - size is set by defining its overall length and width, even if the room deviates from a basic rectangular shape. If alcoves or sloping walls are desired as part of the room's features then the maximum width and length values are still used as reference values. These measurements are either supplied at the coding stage before compilation in terms of the number of scattering junctions required or, if the graphical version of the software is being used, in terms of physical measurements, in metres, as defined by the user. At each time step in the model execution, the main mesh data structure containing all the variables associated with each junction has to be traversed completely from element to element, where the scattering equations according to the junction type are applied as appropriate. Taking into account the comments made regarding the division of the mesh structure into smaller more manageable sub-structures, this has led to the development of the model using `row` elements and `junction` elements. These are defined as follows for the triangular mesh (note similar structures exist for the rectilinear mesh):

Row Element:

```
typedef struct {
    int flag;
    int indent;
    int offset;
    int index;
    junction *j;
} row;
```

Junction Element:

```
struct junction {
    short int type;
    float yval;
    float coeff;
    float abs_coeff;
    float inNE;
```

```

float outNE;
float inE;
float outE;
float inSE;
float outSE;
float inSW;
float outSW;
float inW;
float outW;
float inNW;
float outNW;
junction *NE, *E, *SE, *SW, *W, *NW;
};

```

The Row Element consists of four integer variables and a pointer to an array of Junction Elements. The four integer variables are used to define the properties of the row in question as follows:

flag:	A Boolean integer used to denote whether a row is “odd” (= 0) or “even” (= 1). Note this is only used in the triangular mesh.
indent:	A row shorter than the defined maximum value is described as being indented and can have one of four possible #define’d values: <ul style="list-style-type: none"> 0 - Row is maximum width as given. LEFT - Row is indented from the left side (West) wall. RIGHT - Row is indented from the right side (East) wall. BOTH - Row is indented from both side walls.
offset:	If a row is indented from the left side (West) wall or from both walls then the junctions in the row in question are offset from those in a row of maximum width by this value.
index:	The number of junction elements (scattering junctions) in a row.

Using these four integer variables it is possible to describe a great many possible geometrical features, as shown in Figure 5.13. Figure 5.13(a) shows the data structure used to describe the small triangular waveguide mesh shown in Figure 5.13(b).

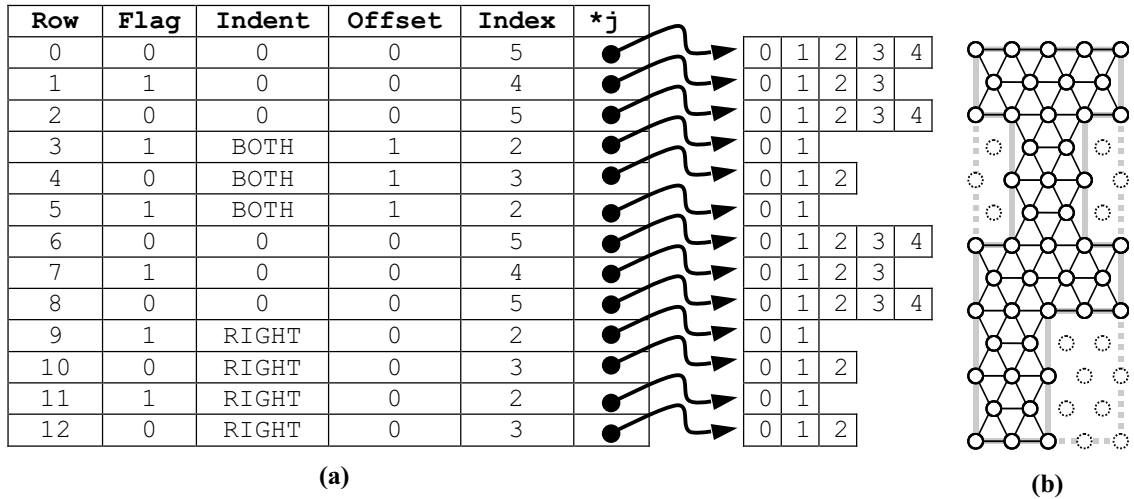


Figure 5.13 A typical data structure used to define the triangular mesh and how it is interpreted by the program. (a) Data structure consisting of row elements that contain general set-up parameters and a pointer to an array of junction elements. (b) The resulting triangular waveguide mesh.

The junction element structures are those that correspond to the scattering junctions themselves and an array of them, according to the number of scattering junctions required, is declared for each row in the mesh structure, as shown in Figure 5.13. A junction element, in the case of the triangular mesh, consists of an integer variable, 15 float variables and 6 pointers to other junction elements as follows:

type	:	Junction type as defined in Tables 5.1 and 5.2.
yval	:	Signal pressure value, $p(n)$ at scattering junction.
abs_coeff	:	Absorption coefficient, $ 1 \geq r$, used for boundary junctions.
coeff	:	Actual coefficient used in scattering equations according to Tables 5.1 and 5.2 and the value of <code>abs_coeff</code> .
inNE	:	Equivalent to $p_1^+(n)$.
outNE	:	Equivalent to $p_1^-(n)$.
inE	:	Equivalent to $p_2^+(n)$.
outE	:	Equivalent to $p_2^-(n)$.
inSE	:	Equivalent to $p_3^+(n)$.
outSE	:	Equivalent to $p_3^-(n)$.
inSW	:	Equivalent to $p_4^+(n)$.
outSW	:	Equivalent to $p_4^-(n)$.
inW	:	Equivalent to $p_5^+(n)$.
outW	:	Equivalent to $p_5^-(n)$.
inNW	:	Equivalent to $p_6^+(n)$.
outNW	:	Equivalent to $p_6^-(n)$.

```

*NE, *E,
*SE, *SW,
*W, *NW : Pointers to other connected junction elements.

```

The six additional pointers to junction elements that are part of each junction element structure are used to set the connections between the various junction types throughout the mesh. Initially at startup all of these junction pointers for each element are set to point to the `NULL` element giving a mesh consisting of junction points only. The mesh is then traversed establishing connections between the junction points according to the junction type, effectively inserting all of the waveguide elements between the junction points that are deemed to be valid. The connection is made, assuming that it is valid, by setting each pointer according to its compass direction to the address of the appropriate junction element it has to be connected to. This is shown in Figure 5.14 for the simpler case of the rectilinear mesh.

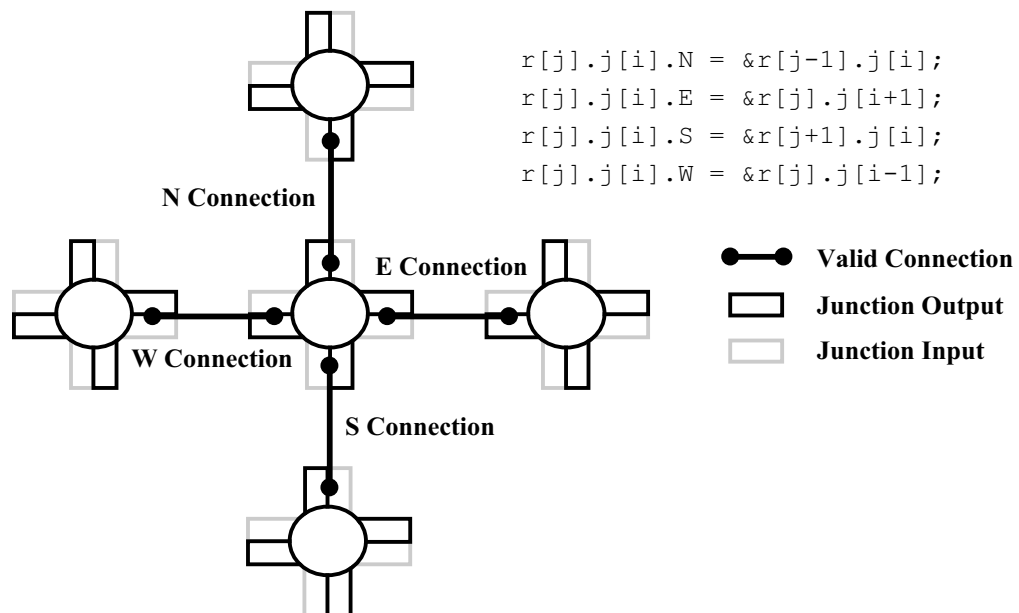


Figure 5.14 Valid connections are made between junctions using pointers to their neighbours on the mesh according to the corresponding junction types.

When it is required to pass a signal between junctions according to Equation (5.3) it becomes a simple matter of checking to ensure that each of these pointers does not return a `NULL` value, this implying that there is no actual connection. If the pointer is not the `NULL` value the current junction `out` value for the connection in question is set to the appropriate `in` value of the junction it is pointing to as shown in Figure 5.15.

Two further structures exist analogous to the row and junction element structures described above. These structures are defined as `row_pos` and `junction_pos` as follows:

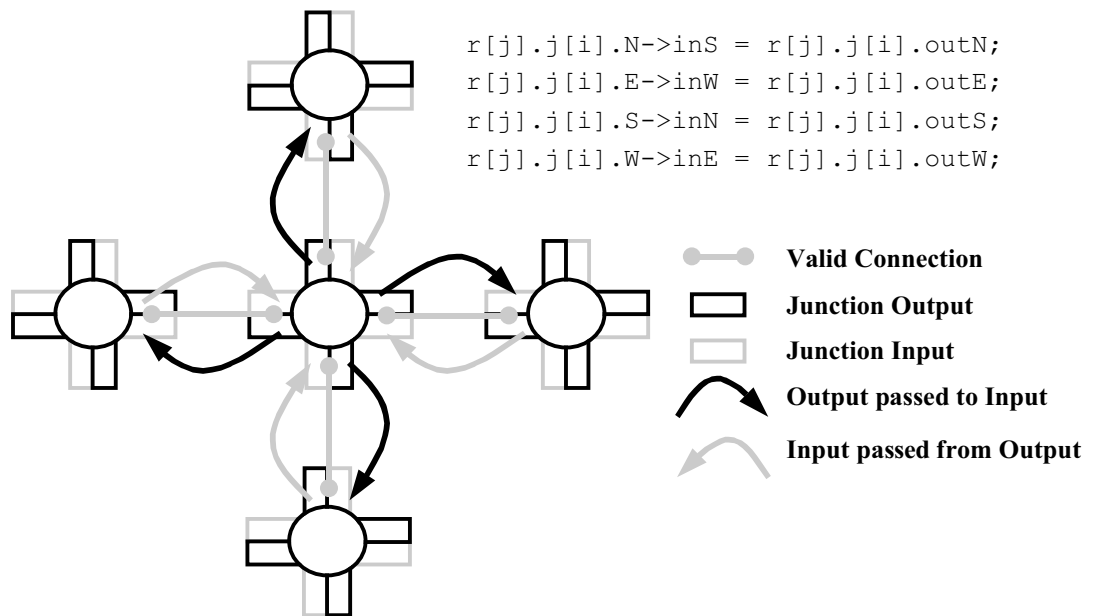


Figure 5.15 Passing a signal from junction to junction involves setting the output value equal to the input value of neighbouring junctions (and vice versa) according to the connections that are valid.

Structure for Screen z-Coordinates of rows of junctions

```

typedef struct {
    float zcoord;
    junction_pos *jpos;
}row_pos;
  
```

Structure for Screen x-Coordinates of junctions in a row

```

typedef struct {
    float xcoord;
}junction_pos;
  
```

These two structures are organised in the same manner as the row and junction elements and are used to store information about the on-screen positions of each junction for rendering purposes. Therefore a `row_pos` structure contains the single coordinate position for the row (labelled as the z coordinate), and a pointer to an array of single junction position values (labelled as the x coordinate) each corresponding to a junction element in the main mesh data structure. In this way much of the information for rendering purposes is dealt with separately from the main mesh data structure speeding up both execution time when graphics are used, and making rendering to the screen more efficient. The coordinate information contained with these structures, once defined for a mesh, is static and never altered so doesn't have to be recalculated during mesh animation, again speeding up the rendering process.

In the full graphical implementation of the triangular mesh, three further structure types exist. These form the constituent elements of three separate linked lists that are used to handle multiple input points, the addition and placement of simple objects in the mesh, and the placement and properties of boundaries for the whole room and for the objects placed within it. They are defined as follows:

Structure for a boundary – handled using a linked list

```
struct boundary{
    int x_coord;
    int z_coord;
    float *point1[2];
    float *point2[2];
    float coeff;
    boundary *next;
};
```

Structure for an input point – handled using a linked list

```
struct inputs{
    int x_coord;
    int z_coord;
    int delay;
    int length;
    float *data;
    inputs *next;
};
```

Structure for an object – handled using a linked list

```
struct objects {
    int x_coord;
    int z_coord;
    int width;
    int length;
    objects *next;
};
```

The linked list of boundary objects (of which there will always be at least four elements, corresponding to each of the four walls in a simple enclosed rectangular room) consists of the following variables:

<code>x_coord</code>	:	Anchor point of boundary section, given in terms of the index of the junction element on the row it starts at.
<code>z_coord</code>	:	Second anchor point of boundary section, given in terms of the index of the row element it starts at.
<code>point1[2]</code>	:	On-screen coordinates of the start point of the boundary section.
<code>point2[2]</code>	:	On-screen coordinates of the end point of the boundary section.
<code>coeff</code>	:	Absorption coefficient associated with boundary section.
<code>*next</code>	:	Pointer to next element in the <code>boundary</code> linked list.

The linked list of input points (of which there will always be at least one) consists of the following variables:

<code>x_coord</code>	:	Coordinate of input point given in terms of the x index of the selected junction element.
<code>z_coord</code>	:	Second coordinate of input point given in terms of the z index of the row element the input junction is on.
<code>delay</code>	:	A number of time steps allowing the input to be delayed and applied some time after $t = 0$.
<code>length</code>	:	Length in time steps of the applied input.
<code>*data</code>	:	Pointer to an array defined by the value of <code>length</code> containing the values of the input signal to be applied.
<code>*next</code>	:	Pointer to next element in the <code>inputs</code> linked list.

Note that at the moment the only type of signal that can be applied is a smooth Gaussian impulse. The linked list of objects consists of the following variables:

<code>x_coord</code>	:	Anchor point of the object, given in terms of the x index of the junction element the top left corner of the object is placed on.
<code>z_coord</code>	:	Second anchor point of object, given in terms of the z index of the row element the top left corner junction is placed on.
<code>width</code>	:	Width of object given in number of junctions.
<code>length</code>	:	Length of object given in number of rows.

*next : Pointer to next element in the objects linked list.

Further structures exist, but these are related to the features and properties of the graphical interface and user interaction. The reader is directed to Appendix F, CD-2 for the fully commented code listing where further details can be found if required.

5.8 Program flow

Although the different versions of *WaveVerb* - graphical and command line, rectilinear and triangular - are implemented quite differently, they all have in common the same basic iterative two-pass computation algorithm describing program flow and the way in which the model is executed. This is shown graphically in Figure 5.16. The graphical implementations of the model in addition to following this basic algorithm also have to take care of the rendering of the mesh animation and allow user interaction. However, this is carried out as a background process as an inherent part of the event handling functions of the window manager and graphical user interface toolkit used in the construction of the front end. In this way, although these features reduce the overall performance, they do not significantly interrupt the functionality of the main model computation algorithm.

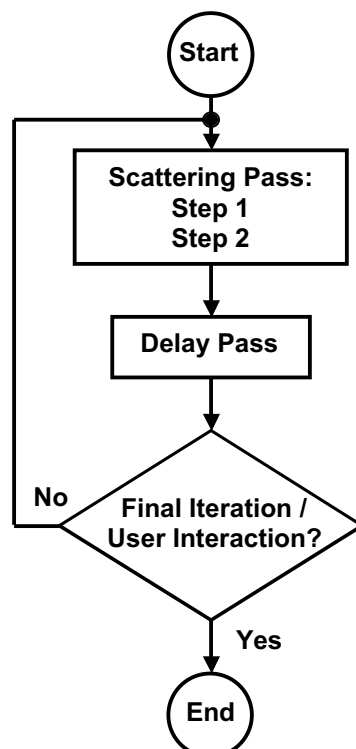


Figure 5.16 Basic iterative two-pass computation algorithm describing program flow and model execution common to all software implementations of the waveguide models.

5.8.1 Initialisation

The Initialisation of the mesh is the most involved part of the execution process. Given a minimum set of easily understandable parameters supplied by the user/programmer relating to the room that is to be modelled, the program sets about automatically defining and constructing a valid mesh suitable for the task. The set of parameters required for initialisation are as follows:

Length	- Number of junctions or size in metres
Width	- Number of junctions or size in metres
Density	- Physical distance between scattering junctions, in metres.
Output Point	- Junction coordinates of single point where mesh output is measured.
Boundaries	- Number of walls; default = 4; default absorption coefficient $r = +1.0$
Input Point	- Junction coordinates of default input point; length = 4; delay = 0

If the room is defined to be anything other than a simple rectangle then each row of junction elements has to be declared individually according to the parameters defined in Figure 5.13. This definition will include how each row is indented, the number of junction elements in each row and whether the junctions are offset from the left side (West) wall. Given these few parameters the mesh is constructed and initialised according to the following list of functions, each of which is called and executed in turn. Note that there are additional initialisation functions used for setting up the user interaction and graphical elements of those versions of *WaveVerb*, but they are overlooked at this point as they have no direct bearing on the main model algorithm.

allocate_rows()

Allocate and declare (“length” x “width”) data structure for junction coordinates for rendering purposes. Allocate and declare “length” row element structures each pointing to an array of “`r[i].index`” junction element structures.

allocate_walls()

Allocate a linked list for information regarding the end points of each wall. This is the boundary linked list that also holds information for each boundary associated with an object. Note that this function merely sets up the head of the linked list with appropriate pointers. It then calls up another function to actually setup the walls of the room and add them to the head of the linked list.

init_junctions()

Pass through the 2-D data structure of junction elements initialising scattering junction values and junction input/output values.

init_coeffs()

Pass through the 2-D data structure of junction elements initialising all absorption coefficients to zero.

init_connections()

Pass through the 2-D data structure of junction elements initialising connections to neighbours. Note that no junctions are connected initially.

init_junction_type()

Pass through the 2-D data structure of junction elements, row by row, setting junction types accordingly. Rows are further sorted according to whether they are:

- A row before an indented row
- A row after an indented row
- A full width row that isn't before or after an indented row

set_connections()

Pass through the 2-D data structure of junction elements setting connections to neighbouring junctions according to junction type.

init_mesh()

Pass through the 2-D data structure of junction elements setting the on screen coordinates for graphical rendering. The positions depend upon the relative dimensions of the mesh so that it is drawn with the correct 3-D perspective when viewed.

init_walls()

For each defined wall or object boundary set pointers to the appropriate junction element coordinates for each end point and set the absorption coefficient.

init_wall_coeffs()

For each scattering junction that lies on one of the wall or object boundaries set the appropriate absorption coefficient as part of that junction element's properties.

allocate_inputs()

Allocate the linked list for input point parameters. By default there will be one input so the list must be declared and initialised with this one element.

allocate_objects()

Allocate and initialise the linked list for a default object. This merely sets the head of the list to point to the NULL element until the user actually places an object in the room.

set_coeffs()

Pass through the 2-D data structure of junction elements setting junction coefficients dependent upon boundaries and junction type. These coefficients are used in the wave propagation algorithm.

5.8.2 Scattering Pass

The Scattering Pass is a two step process. Step 1 involves calculating the value for each junction element on the mesh according to the junction inputs (Equations (5.1a) and (5.1b)). Step 2 calculates the outputs from each junction based on the junction value and the associated input value along the same connection (Equation (5.2)).

The junctions elements are traversed across the whole mesh, allowing these two steps to be executed at each, using two nested FOR loops. The outer FOR loop moves in turn from row element to row element. The inner FOR loop acts upon each junction element in the array associated with the row element in question. For each junction element a conditional `switch` statement is then executed with each `case` condition corresponding to a junction type each with its own defined set of 2-step scattering pass equations as listed in Tables 5.1 and 5.2. These scattering pass equations are executed in place within the `switch` statement, using pre-defined pre-compiled macros wherever possible. The `switch` statement is in turn within the nested FOR loops, themselves within a function called `scatter()`. The purpose of this code design is twofold. Firstly, by working on a row structure at a time, each with its own set of junction element structures, the mesh is partitioned into smaller sections or “tiles”, as discussed in 5.7.1, allowing more efficient memory management. Secondly, as all calculations are carried out in place, this avoids further unnecessary conditional branching which can reduce automatic code optimisation during compilation and generally proves to be inefficient in any case [Scott, 1998].

5.8.3 Delay Pass

In the delay pass the junction output values calculated as Step 2 of the scattering pass are effectively passed along valid junction connections to become the inputs to the junctions

immediately neighbouring each element as in Equation (5.3). This process can be seen in Figure 5.15. As with the scattering pass, this takes place within two nested FOR loops, traversing the mesh element by element a single row structure at a time. Each junction has six possible connections in the triangular mesh and four in the rectilinear mesh. A check is done on each connection for each element, and if this test returns `NULL` then there is no connection and a signal is not passed. If the connection does exist the signal is passed along to the neighbouring elements that have been connected together using pointers and memory addressing in the initialisation stage of the algorithm. Again this is shown more clearly in Figures 5.14 and 5.15.

5.9 Output Formats

All model implementations allow a number of different output formats so that the RIR measurements, whether mono, stereo or horizontal B-format as introduced in 5.5, can be imported into other software packages. A RIR can be saved as one of three main file types:

ASCII text data (.dat) file

ASCII text *WaveVerb* Room Impulse Response (.wvr) file.

Matlab ASCII (.m) file.

The .wvr file is preceded with a header describing the most pertinent features of the room model from which it has been generated. It is defined as follows:

```
#WaveVerbRIR           : File identifier
#Number of audio channels : 1, 2, or 4, for mono, stereo or B-format.
#Length, Width          : Mesh dimensions, in number of junctions.
#Input_z, Input_x       : Junction coordinates of default Input point.
#Output_z, Output_x     : Junction coordinates of Output point.
#Density                 : Distance between junctions in metres.
```

These *WaveVerbRIR* files can be converted into other file types using the additional *WaveVerb* Analysis Module. This separate executable program allows these .wvr files to be loaded and viewed in both the time and frequency domains. The room dimensions supplied in the file header also enables the Analysis Module to plot the theoretical axial and tangential modes that would be present in a 2-D “room” of that particular size, against the low frequency response of the RIR file. Examples of this analysis will be presented in the next chapter. Using the Analysis Module .wvr files can be converted to binary data files and more universal AIFF soundfiles, allowing them to be imported into a wide range of audio editing software packages.

5.10 Mesh Animation and Visualisation

The mesh is rendered and visualised using the OpenGL (GL stands for Graphics Library) software interface to the accelerated graphics hardware that is part of all Silicon Graphics workstations [Woo et al, 1997]. OpenGL's main purpose is to render two and three dimensional objects into a frame buffer, with these objects being described as sequences of vertices, which define geometric objects, or pixels which define images. OpenGL performs several processing steps on this data to convert it to pixels to form the final desired image in the frame buffer that is displayed on the computer screen. OpenGL and the Silicon Graphics hardware have a number of benefits that are suitable for visualising the waveguide mesh model as an animation.

5.10.1 Double Buffering

This is graphics hardware that supplies two complete colour frame buffers. This allows one to be displayed whilst the other is being rendered. When the frame held in the back buffer has been completely rendered it is swapped with the front buffer currently being displayed. The front buffer is now used for back buffer rendering and the previously rendered back buffer is promoted to front buffer and displayed. A frame is only displayed when the rendering is complete so that a partially rendered mesh is never displayed. Double-buffering allows quick smooth animations to be displayed.

5.10.2 Viewing and Modelling

The rendering of the model is done in three dimensions. Even though the room to be modelled is only two-dimensional, it is still treated as a three-dimensional object, with the third dimension showing the junction values by displacing the junction elements from their graphical rest points on the mesh. In this way the `row_pos` and `junction_pos` coordinate values never change as they determine the z (depth position into screen) and x (horizontal position across screen) coordinate values. It is only the y (vertical position across screen) coordinate that varies and this is determined by the actual signal pressure value at the junction. Therefore `row_pos` and `junction_pos`, once defined at the initialisation stage, consist of constant values that are effectively used as a static look-up table for rendering purposes. However, this three-dimensional graphical object still has to be viewed as a two dimensional representation on a flat screen. This is achieved by treating the viewing process separately from the rendering process. A common analogy is to treat the graphical object as a “real” scene such as a flower in a pot and the computer screen or viewport as a camera taking a picture of the scene as shown in Figure 5.17 from [Woo et al, 1997]. As the rendering of the mesh is handled separately from the viewing and visual perception of the model, it therefore becomes a relatively easy matter to allow the user to interact with and control it. Examples that have been implemented include placing simple objects into the mesh, zooming in or out from it or representing the signal

pressure and resulting wave propagation in different ways - for instance mapping junction values to colour intensity rather than displacement.

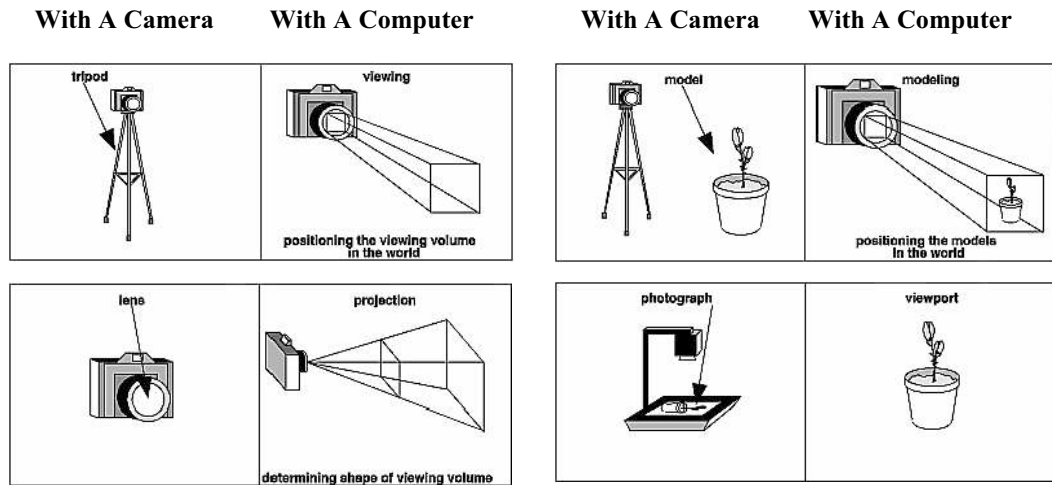


Figure 5.17 The camera analogy showing how a computer deals with the rendering and viewing of an object as two separate entities, a feature used by OpenGL [Woo et al, 1997].

The mesh animation is a very simple process, with a single frame being rendered after each iteration of the computational algorithm (after the delay pass). At this point the y coordinates of each scattering junction position are updated (according to the scaled pressure value of each junction), and mapped to either the junction's 3-D vertical position, or an appropriate colour value. The mesh is then created using these y values and the pre-defined x and z coordinates for each junction using simple OpenGL geometric object primitives.

5.10.3 Testing and Verification

The waveguide mesh models have been tested and had their behaviour verified using methods such as visual feedback, mesh construction analysis, numerical analysis, and RIR analysis.

Visual Feedback

The importance of visual feedback and analysis as a tool to aid both the user and developer of an acoustic modelling system was highlighted in Chapter 2.9. Further, waveguide mesh structures are well suited to both visualisation and animation [Savioja et al, 1994]. This visual feedback has proved invaluable in the testing and verification of the waveguide mesh models. The resulting wave propagation after an input signal has been applied is natural and uniform and irregularities due to errors in either the mesh construction or model implementation are easily spotted. This is facilitated by the number of mesh rendering options that are available to the user and the ability to view the mesh construction over a wide range of angles and perspectives.

Mesh Construction Plots

As has been highlighted in Chapter 5.8.1, the initialisation of the mesh is the most involved part of the execution process, with there being significant possibility for error at either the coding or definition stages. Therefore an additional option was added to automatically generate an ASCII text file after the initialisation stage and before actual wave propagation. This allowed any number of the `row` or `junction` elements to be displayed in a text-based representation of the mesh geometry. This would help to identify, for instance, if a junction type had been set incorrectly, or whether or not the junctions along a boundary had the appropriate reflection/absorption conditions.

Numerical Analysis

Smaller rectangular meshes were also defined and tested over a limited number of iterations. This allowed numerical data at each scattering junction to be plotted, analysed and compared with results generated directly, by calculating the output from each junction given the input according to the scattering equations, using more traditional mathematical tools such as calculator, pen and paper.

RIR Analysis

The data values output from specific scattering junctions within the mesh were also analysed for potential errors, either directly by examining the numerical values against what might be expected, or by representing the output as an audio soundfile that could be further manipulated and analysed using an appropriate PC software audio editing package.

5.11 Summary

This chapter has examined a number of pertinent issues in the design and implementation of the *WaveVerb* Digital Waveguide Mesh Reverberation System. The *WaveVerb* system encompasses a number of different implementations as follows:

- rectilinear Mesh with graphical visualisation and basic user interaction

- pre-defined and compiled Rectilinear Mesh running from a command line with no visualisation or user interaction

- triangular Mesh with graphical visualisation and user interaction including the definition and placement of objects within the modelled room

- pre-defined and compiled Triangular Mesh running from a command line with no visualisation or user interaction

- additional Analysis Module allowing RIR measurements to be examined and exported to other file formats.

The scattering junctions that will be used to define wave propagation through the mesh have been defined for the general case building on their original derivation in Chapter section 4.5.2. The situations arriving when constructing a real, finite and bounded mesh have also been examined leading to the derivation of the sets of scattering equations that are used to cater for junctions placed on boundaries within and around the mesh. This has further led to the introduction of junction types being used for convenience of implementation with 10 distinct junction types having been defined for the rectilinear mesh and 20 for the triangular mesh.

Methods of inputting a signal to the mesh and measuring a RIR output have been examined. Output format possibilities include RIR measurements in mono, stereo and horizontal-only Ambisonic B-format surround sound.

Dispersion error is present in both model topologies and measures have been derived and results examined graphically using 2-D and 3-D contour plots. These measures have established that:

dispersion error is reduced on the triangular mesh when compared to the rectilinear mesh

dispersion error is virtually independent of the direction of propagation on the triangular mesh unlike the rectilinear mesh that displays very different errors for diagonal and axial propagation. Therefore on the triangular mesh the dispersion error is further reduced to being a function of frequency only.

These results confirm those of [Van Duyne and Smith, 1996] and [Laird et al, 1998], that the triangular mesh is a more accurate model than the rectilinear mesh for 2-D wave propagation.

Some of the software design considerations for the various constituent *WaveVerb* elements have also been explored given that the models have been implemented in software using the C programming language on a generic Silicon Graphics UNIX workstation running the IRIX operating system. Given that the mesh generated for anything but the most trivial room results in a significantly large data structure, some memory optimisation techniques have been investigated according to [Scott, 1998], including the decomposition of the mesh into smaller, more manageable “tiles”. These smaller elements, together with the other main model specific structures and data types, have been introduced and their properties investigated. This has included how they can be defined and arranged to give a mesh structure for a required room size and shape, and how they have been coded to implement the waveguide mesh scattering equations.

The general model computational algorithm has been shown to be a three stage process. The first is the initialisation stage which sets about automatically defining and constructing a valid

mesh suitable for the task, given a minimum set of easily understandable parameters relating to the room that is to be modelled. An overview of the function calls used in this initialisation procedure has been included. The second stage implements the first part of the scattering equations, known as the *scattering pass*, where all the junction pressure values are calculated according to the signals incident upon each junction and the junction type, as defined in Tables 5.1 and 5.2. The scattering pass also calculates the associated output values from each junction. The third stage implements the second part of the scattering equations, known as the *delay pass*, where the outputs from each junction are passed along the waveguide element connections to become the inputs to the adjacent junctions.

The *WaveVerb* system records and outputs a RIR measurement in a number of different possible file formats, including standard ASCII text, as a .dat file, as a Matlab .m file or in *WaveVerb*'s own particular .wvr format. The *WaveVerb* Analysis Module allows these measurements to be converted and exported as other formats including AIFF soundfiles. This module also allows these RIR measurements to be examined in both the time and frequency domains, and plots the modal characteristics of the 2-D modelled room for comparison purposes.

Finally some of the mesh animation and visualisation concepts have been considered including how this is to be achieved and implemented using OpenGL on the Silicon graphics platform, and how the models have been tested and verified.

To summarise, this chapter has investigated how the waveguide models are to be implemented, both theoretically and practically, and has therefore prepared the groundwork for the results that follow in the next chapter. These results will test and compare both models in order to prove or disprove the hypothesis on which this thesis is based.

Chapter 6

Results

6.1 Introduction

The previous chapter examined how a waveguide mesh model could be implemented in software, with a number of important factors being considered. The general mesh scattering junction - either 4-port or 6-port depending on mesh topology - gives rise to a number of different junction types that are used in the mesh model of a room to take care of the different and varied boundary conditions that may occur. Given a simple set of easy to understand room measurements and associated properties the *WaveVerb* System sets about automatically defining and constructing a valid mesh suitable for the task using row element and junction element structures. This mesh is initialised and all connections between junctions are set according to the previously defined junction types. After initialisation the model is executed using a two step algorithmic process, the first step being the *scattering pass*, the second the *delay pass*.

Output from the model includes RIR measurements in mono, stereo and horizontal only Ambisonic B-format surround sound. These RIRs can be saved in a variety of proprietary and common file formats.

A detailed analysis of the dispersion error on both mesh topologies has revealed, as was already suggested in Chapter 5.5.4 and stated in [Van Duyne and Smith, 1996] and [Laird et al, 1998], that the triangular waveguide mesh offers a considerable improvement over the rectilinear mesh, minimising dispersion and reducing it to being a function of frequency only. The *WaveVerb* system will be used to examine and compare the relative performance based properties of the rectilinear and triangular waveguide mesh models in order to support this theoretical claim, and to prove, or otherwise, the hypothesis on which this thesis is based. This chapter therefore presents a series of results based on the current implementation of the *WaveVerb* System. A number of 2-D “rooms” have been modelled with varying geometries and absorption characteristics and RIR measurements have been measured accordingly. The majority of these measurements are single point mono RIRs although some multi-channel RIRs have also been measured for demonstration purposes. These RIRs are analysed and presented using the following:

- low frequency response and modal analysis
- time averaged spectral analysis

spectral analysis using a sonogram
 comparison of room acoustics parameters
 convolution processing of anechoic audio.

In addition to these methods, and in accordance with Chapters 2.9 and 5.10, results will also be presented using visually rendered representations of the model, using both static snapshots and short animated MPEG movies. Note that unless otherwise stated these visual representations are direct screen captures of the wave motion as shown on the graphical interface of the *WaveVerb* System.

6.2 Observation of Standard Wave Phenomena

Waveguide mesh structures are essentially a discretized physical analogue of a continuous medium supporting wave propagation. The structures examined in this thesis being analogous to air in an enclosed space - the 2-D room system as introduced in Chapter 2.2. As such, when visualised, these mesh models should exhibit standard typical wave phenomena, such as reflection, diffraction and interference. Therefore the first step in establishing whether these waveguide models are a suitable equivalent system to an enclosed space is to examine the resulting wave motion on the mesh for evidence of these phenomena.

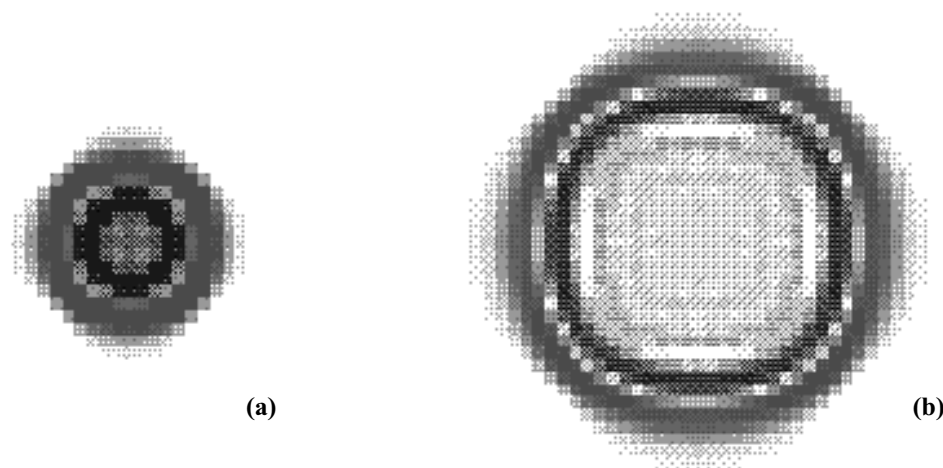


Figure 6.1 The rectilinear mesh is excited with a Gaussian impulse applied over 6 time steps: (a) immediately after the impulse has been applied; (b) a further 18 time steps after (a).

6.2.1 Mesh Excitation and Observation of Wavefront

Figure 6.1 shows the resultant wave motion on the rectilinear mesh at two points in time after a Gaussian impulse has been applied over 6 time steps. As with a stone dropped into a pond the excitation results in the spreading out of a circular wavefront in all directions. Figure 6.1(a) shows this wavefront just after the excitation signal has finished and Figure 6.1(b) shows this

same wavefront again 18 time steps later. Note however that the circular wavefront is not quite uniform. Figure 6.1(a) is almost diamond shaped and Figure 6.1(b) has clearly evident “fuzzy” edges on the top, bottom and sides of the wavefront. This is actually evidence of the effect of the direction dependent dispersion error present on the rectilinear mesh. Note that the edges of the wavefront along the diagonals to the mesh structure (if it were to be super-imposed on top of this image) are actually still quite sharp and defined. According to Figure 5.11 there is no dispersion on the rectilinear mesh along the diagonals to the mesh coordinate system. However the top, bottom and sides of the wavefront are not so well defined due to the dispersion error being at a maximum in these directions according to Figure 5.11.

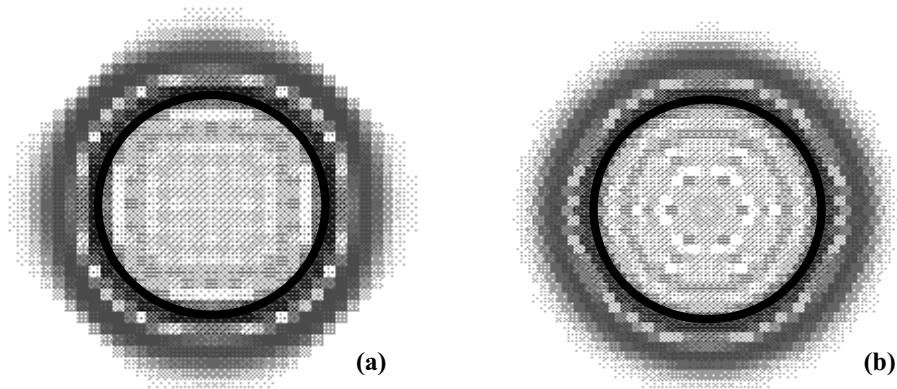


Figure 6.2 Two wavefronts at the 14th time step after the same input signal has been applied. (a) On the rectilinear mesh; (b) on the triangular mesh. A black circle has been added to both wavefronts to aid comparison.

Figure 6.2 shows two wavefronts at the 14th time step after the same input has been applied for the same length of time. Figure 6.2(a) shows the wavefront on the rectilinear mesh and Figure 6.2(b) shows the wavefront on the triangular mesh. A black circle has been drawn on both of these figures to aid comparison. Although still not totally uniform, the wavefront on the triangular mesh is much closer to being circular than that shown on the rectilinear mesh.

6.2.2 Reflection

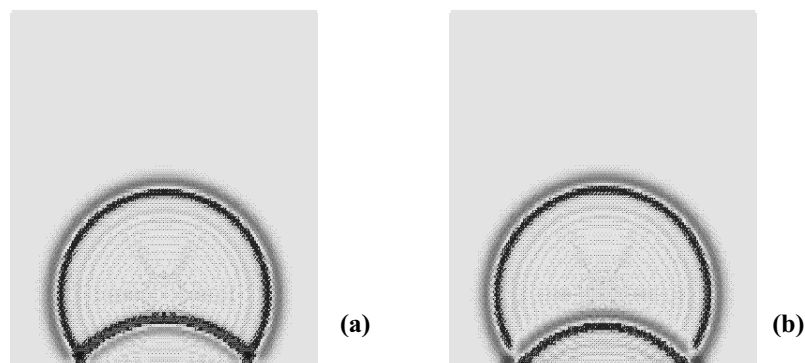


Figure 6.3 Reflection at a wall on the triangular waveguide mesh, with a simple rectangular room being modelled. (a) With a reversal in phase of the incident wave; (b) the phase of the incident wave is preserved.

Reflection is clearly evident in the resulting wave propagation on both mesh topologies. Figure 6.3 shows two examples taken from the same room as modelled using the triangular mesh. Note that the light grey wavefront represents a wave of positive displacement (a compression as the propagating signal being considered is pressure), and the darker wavefront represents a wave of negative displacement (a rarefaction). Figure 6.3(a) shows a clear reflection at the lower wall with the phase of the incident wave being reversed. Figure 6.3(b) shows the same reflection with the phase of the incident wave being preserved. Phase reversal at a wall is determined by the absorption coefficient r with negative values resulting in phase reversal and positive values resulting in phase preservation. Setting all the boundaries in the room to give phase reversing reflections effectively sets all the values at these scattering junctions to zero resulting in the axial modes being absent from the low frequency response analysis of the RIR. These modes are the result of a pressure maximum at the boundary of a room [Everest, 1994] and this cannot happen if the pressure value at the boundary is always zero. Phase preserving reflections at a boundary allow a pressure maximum and hence axial modes can be observed.

Setting the absorption coefficient $r = 0$ should model an anechoic room. That is, all the wave energy is absorbed at the walls with no reflections. The actual effect of this is shown in Figure 6.4. This figure also shows the graphical interface that allows the user to define and interact with the model as part of the *WaveVerb* System.

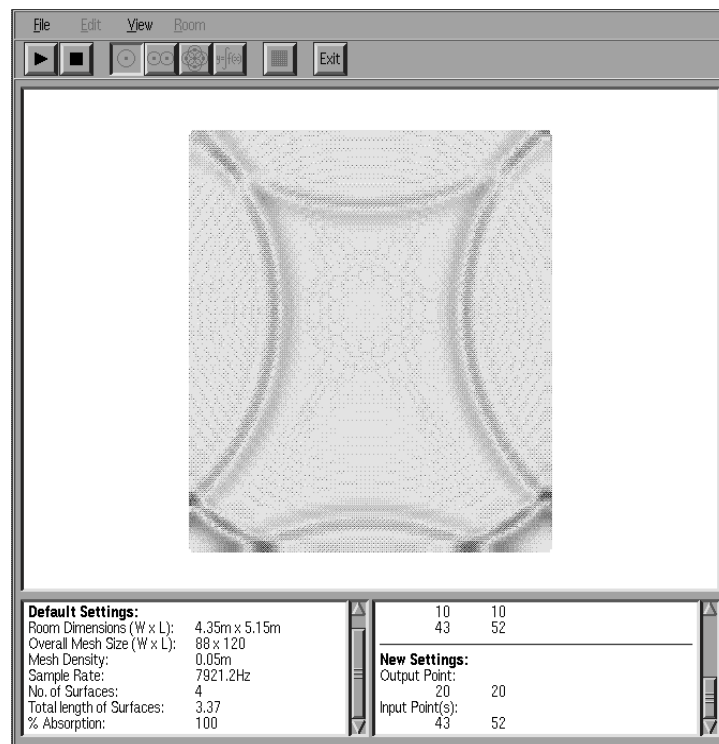


Figure 6.4 The graphical interface for the *WaveVerb* system allowing visualisation of the resulting wave propagation and user interaction. The example shown has all wall absorption coefficients set to $r = 0$, modelling anechoic conditions.

Notice that in Figure 6.4, despite the boundary conditions being set for total absorption, a proportion of the wave energy has been reflected, as suggested in Chapter 5.3.1. This is again due to the discrete and frequency dependent nature of the waveguide mesh and the associated mesh boundary conditions. Although most of the energy is “absorbed” at the boundary, the simulated anechoic conditions actually generate minor reflections at higher frequencies [Savioja et al, 1994]. This will be discussed further in Section 6.2.5

6.2.3 Diffraction and Interference

One of the most significant benefits in using a waveguide mesh in modelling the acoustics of a room is that diffraction and interference effects are a natural consequence of the resulting wave propagation. An example is shown in Figure 6.5 where a rectilinear mesh models a rectangular room with a dividing wall partitioning it into two coupled spaces. This dividing wall has gaps placed in it and when an impulse is applied in one half of the room, the wave propagates through the gaps in the wall and proceeds to spread out into the other half of the room. The curved edge of the resulting re-constructed wavefront gives a clear example of diffraction and constructive interference as the three individual waves unite in a single wavefront.

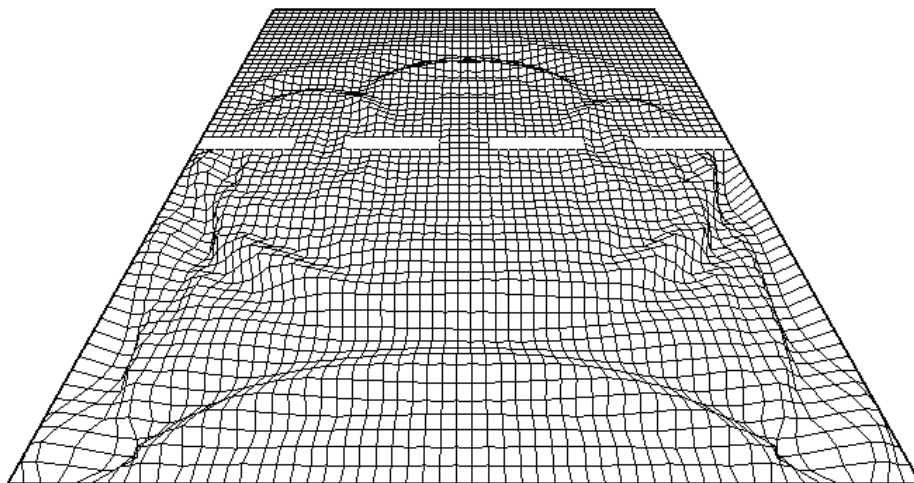


Figure 6.5 Diffraction and interference effects on the rectilinear mesh due to the gaps in the dividing wall placed into this model of a rectangular room.

Figure 6.6 shows a typical example of what would happen if standard ray tracing (see Chapter 4.2.2) were used to model the RIR for the example in Figure 6.5. As there is no clear path between the sound source and the listening position the direct sound passing through the gaps in the walls will not be detected until it has been reflected from walls and surfaces in the other half of the room. Therefore as the waveguide mesh inherently models the natural diffraction properties of wave propagation it can be seen to offer an improvement over methods based simply on the geometry of the room. Note that the presence of the dividing wall in this otherwise simple room would cause added geometrical complexity and hence a non-trivial problem for the associated Image-Source model.

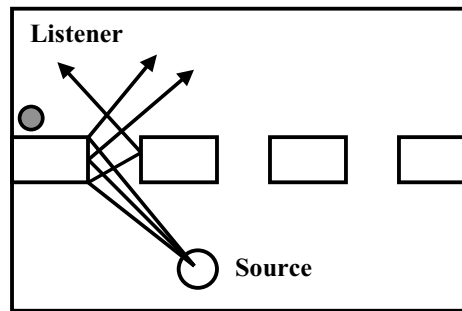


Figure 6.6 A ray-tracing example of the situation shown in Figure 6.5. As diffraction is not accounted for there is no direct path between source and listener leading to errors in the RIR.

Examples of diffraction on the triangular mesh for a similarly defined room can be found in Appendix F, CD-2, the data CD that is supplied as part of this thesis. Two examples are supplied and can be found in the *Animations* folder under the names of *mesh.mpg* and *colour.mpg*. Note that a freeware MPEG player is included on the data CD to allow playback of these animations. Details of how to do this are supplied in Appendix D. Both of the animations show the same room with the same applied impulse, and demonstrate diffraction effects due to the partitioning wall. *mesh.mpg* shows the room rendered as a 3-D mesh with pressure at a junction displayed as displacement along the vertical axis. It also demonstrates how the user can change their viewing perspective relative to the rendered object as the user effectively zooms in to the room from above and then the room is tilted backwards so that the wave displacement on the mesh can be clearly observed. The interference pattern that is created due to the two gaps in the wall can be clearly seen in the upper half of the room. *colour.mpg* shows the room rendered as a 2-D colour temperature plot, with pressure at a junction displayed as a colour scale relating to temperature, from cold to hot. This scale ranges from blue (rarefaction) passing through yellow (at rest point) to red (compression). Most of the examples of wave propagation presented in this chapter are greyscale representations of this *WaveVerb* viewing option.

Diffraction of sound due to an object being placed in the room can also be observed and is shown in Figure 6.7.

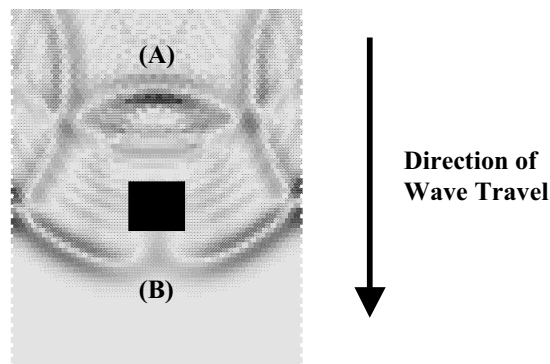


Figure 6.7 Diffraction and reflection due to an object being placed in the room. (A) Shows the reflected wave and (B) shows the diffracted wave.

The object in this example has all of its boundaries set with an absorption coefficient of $r = +1.0$. Both the reflected wave, labelled **(A)**, and the diffracted wave, labelled **(B)**, are clearly apparent, with the latter about to re-form as a single unified wavefront.

6.2.4 Further Interference Effects

Other examples of interference, not directly related to diffraction can also be observed on the mesh. For instance the principle of “speaker delay towers” can be demonstrated. It is common practice at large concert venues, where the audience stretches back for some distance from the main stage, to support the main speaker stacks located on or near the stage, with additional, smaller arrays of speakers. These speakers are placed at distinct points in and around the audience to give a consistent sound level across the whole auditorium. This becomes even more critical at outdoor venues where sound is essentially travelling in a free field. However, if a direct feed were to be taken from the main front of house mixing console or power amps to these additional speakers, the audience close to them would hear sound from these speakers *before* the sound from the main on-stage system, due to the finite speed of sound, resulting in a slight echo effect. Therefore the audio feeds to these additional speaker towers have to be delayed slightly according to their distance from the stage and the speed of sound. If calculated correctly this results in a coherent and uniform, reinforced sound for the whole audience.

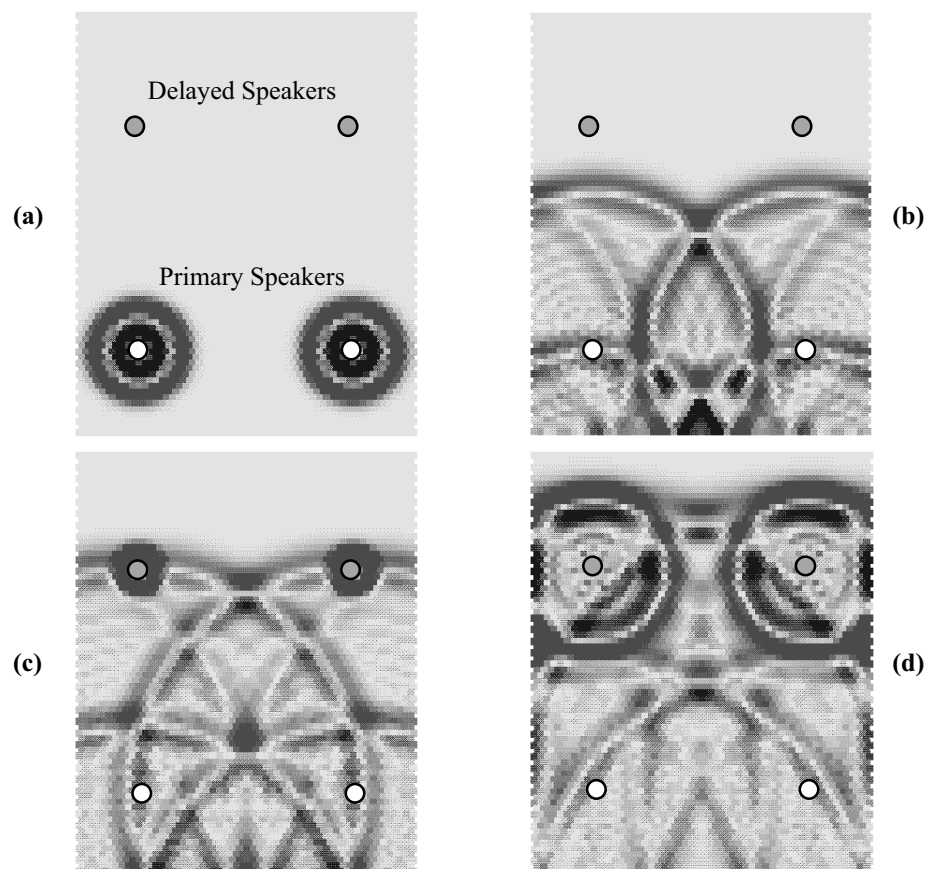


Figure 6.8 Demonstrating the principle of speaker delay towers. (a) initial impulses; (b) wavefront travelling along the length of the room; (c) delayed impulses are applied; (d) reinforced wavefront continues through room.

This principle is demonstrated using a rectangular room model as shown in Figure 6.8, although on a much smaller scale. Figure 6.8(a) shows two impulses being applied to the mesh with the first principle wavefront being shown travelling along the length of room in Figure 6.8(b). As this wavefront reaches the “speaker delay towers” in Figure 6.8(c) they similarly apply two further impulses to the mesh. The result is the reinforced uniform wavefront that can be seen in Figure 6.8(d) and hence an example of constructive interference. Note that real speakers would have a more hemispherical (semi-circular for a 2-D representation) directional dependent output and hence the wavefronts travelling in the reverse direction to that of the outgoing principle wavefront, that can be seen in Figure 6.8(d), would not be so much of a problem.

A final example of interference can be demonstrated using a geometrical room design similar to that found in some concert halls or churches where one end of the space is approximately semi-circular or concave. This can result in an uneven distribution of modes and sound pressure level due to the focusing properties of the shape of the room as demonstrated in Figure 6.9.

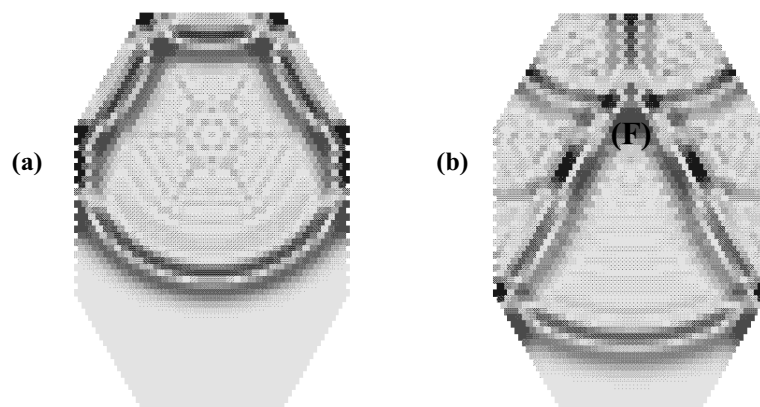


Figure 6.9 A room with slightly concave ends. (a) The reflections from the three angled walls at the upper end of the room start to converge; (b) the result is a focal point marked (F) giving an uneven distribution of sound pressure level.

The three reflections from the angled walls at the upper concave end of the room converge constructively at the focal point (F), with the result that the sound energy concentrated at this point will lead to the undesirable acoustic properties mentioned above. Increased absorption at these walls would help to alleviate this problem as would diffusers on the walls as they would help to scatter the sound waves over a wider area avoiding the convergence at (F).

6.2.5 Discussion

It is evident that standard wave phenomena such as propagation, reflection, diffraction and interference can be clearly observed on the waveguide mesh models. It should be re-iterated that these properties have not been explicitly simulated or implemented as part of the model, rather they are an inherent part of the resulting wave propagation that occurs due to the

waveguide mesh's underlying structure and equations of motion. The complex wave motion that can be observed is a natural consequence of these simple scattering equations. As such waveguide mesh models can be seen to offer an improvement over traditional geometric methods of modelling a RIR as these methods cannot take into account the diffraction and interference effects that are a natural consequence of sound travelling in a real enclosed space. Furthermore the triangular mesh would already appear to be the more accurate model of the two topologies, with the wavefront present after an applied impulse being closer to that of a uniform circle than that on the rectilinear mesh. The deformed shape of the wavefront on the rectilinear mesh is a direct result of the direction dependent dispersion error inherent in this mesh topology.

Note further that in both cases there are “ripples” evident behind the primary circular wavefront. There are two possible causes for this effect, the first being the termination or truncation of the finite input signal effectively resulting in a discontinuity and the addition of high frequency components [Lynn and Fuerst, 1996]. The second possible cause is due to numerical error, as once displaced from rest the pressure value at a junction will never return to an exact value of zero, but will rather oscillate about this rest point until the error becomes so small that it is beyond the limits of precision of the system.

However, although visually the mesh structures appear to closely parallel natural wave propagation, the anechoic results reveal that this is not always the case due to the mesh essentially being a discrete approximation. The boundary conditions appear to be an oversimplification of reality even though they are consistent with the mesh construction, and offer a satisfactory solution enabling reflection and absorption to be modelled without significant detriment to the overall behaviour of the mesh. By contrast, real acoustic boundaries are both frequency and direction dependent and this has not been considered in the derivation of the boundary conditions as presented in Chapter 5.3. High frequency reflections at anechoic boundaries have been noted in previous waveguide mesh studies [Savioja et al, 1994]. A further insight to the properties of such boundaries can be gained from examining another wave propagation model analogous to the waveguide mesh structure.

The Transmission Line Matrix (TLM) method [Johns and Beurle, 1971] is a discretized time domain model generally used for investigating electromagnetic wave propagation [Akhtarzad and Johns, 1975]. It has however been applied to other disciplines such as general acoustics [Pomeroy and Jaycocks, 1996], and is similar in implementation to the rectilinear waveguide mesh model. In TLM, in order to model airborne acoustics, the space is required to be effectively unbounded. In practical terms, the boundary of the actual mesh used has to approximate a free space boundary - or in room acoustics terms, an anechoic wall. A wave

crossing such a boundary should effectively disappear from the model as if it had continued to propagate, without any reflection or other modification to the bounded mesh. TLM uses a resistive matched termination to the transmission line segments at the edge of the mesh giving a first order approximation to this situation [Pomeroy and Jaycocks, 1996], effectively the same method as used in the waveguide mesh model. However, TLM results show that waves striking the boundary at non-normal angles of incidence will not see a matched termination, resulting in some reflection. The problem is complicated further by discretized or “stepped” boundaries that are not parallel to the mesh structure yet are attempting to model an ideally continuous and smooth boundary. The ends of each “step”, no matter how high a mesh sampling rate is used, will act to scatter and reflect high frequency waves [Pomeroy and Jaycocks, 1996]. This effect would be even worse in a triangular mesh topology, as a rectangular boundary is only parallel with the waveguide elements along a single pair of walls (North and South). These comments seem to be in agreement with the results observed in Figure 6.4 and in [Savioja et al, 1994].

There are a number of possible improvements that can be implemented to model the boundary of a waveguide mesh more accurately. For anechoic conditions, TLM modelling techniques suggest recalculating the required impedance every few time steps for each point on the boundary in order to take account of the angle of arrival for the incident waves [Pomeroy and Jaycocks, 1996]. More generally, the impedance based boundary conditions can be replaced using a digital filter to model the frequency dependent absorption characteristics of real materials. This has been attempted on a 2-D rectilinear mesh [Huopaniemi et al, 1997], although with limited success due to the directionally dependent nature of wave propagation on this mesh topology being equally applicable to the boundary reflection characteristics. It is also possible to model more diffuse reflections at the boundaries, scattering wave energy in every direction regardless of the angle of incidence. This has been attempted by pre-varying the angle of incidence of a wave in a random fashion over time at the boundary junctions on the mesh using circulant matrices. This may prove to be an even more accurate model, particularly as the amount of diffusion can be varied and frequency dependence can also be implemented as an extension to this technique. This method has been applied to 2-D drum membranes based on a triangular mesh topology [Laird et al, 1999].

6.3 Case Study

The results presented in the following sections are the outcome from a particular study using the *WaveVerb* system. This involved making RIR measurements for both mesh topologies across a range of room sizes, with varying source-listener combinations and boundary absorption coefficients. Four different-sized rooms were used, with the same four source-listener combinations in each, although the input point is always anchored relative to the top left corner

of the room as drawn. The four rooms with the four different listener positions marked in each are shown in Figure 6.10. The direct source-to-listener distances, which will be the same for all rooms are summarised in Table 6.1.

LISTENER POSITION:	DIRECT LINE DISTANCE:
1	3.96
2	1.0
3	2.8
4	4.47

Table 6.1 The direct source to listener distances for the four variable listener positions used in each room with the same source location.

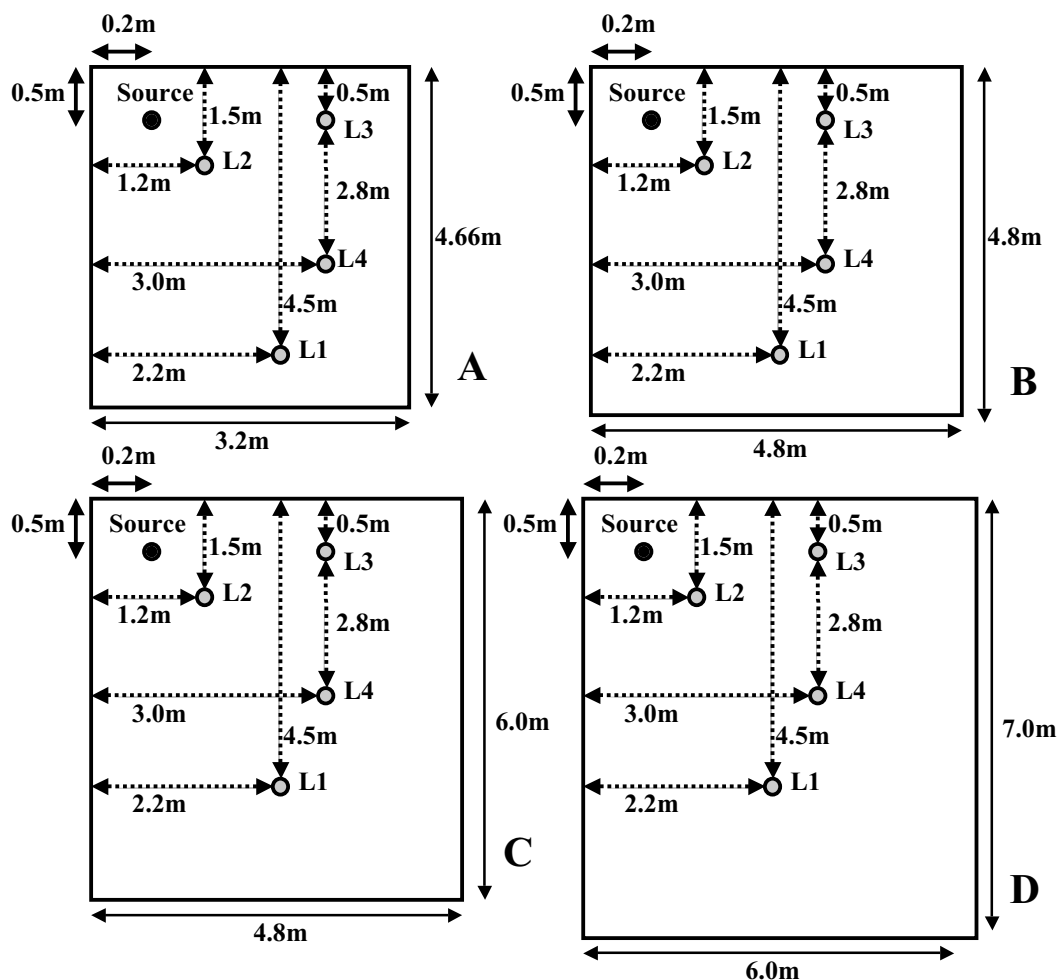


Figure 6.10 The four different sized rooms used as part of the case study with the same four source-listener combinations in each. Note the sound source input point is always anchored relative to the top left corner of the room as drawn.

Note that Room A corresponds to one of the Sempeyer room dimension ratios as given in Table 2.1, providing that this theoretical 2-D room has a height of 2.0m. These room dimensions are

chosen to give a favourable distribution of the room modes. Note further that given Room A has a desirable rectangular geometry, Room B has been defined to be a “worst case” scenario as it is square, which should result in “stacking” or close coincidence of these resonant frequencies.

The junction spacing is set at 0.011m giving a mesh sampling rate of approximately 44.1kHz according to Equation (4.27). A smooth Gaussian impulse will be applied as the excitation signal over four mesh iterations. Each room is modelled for each source-listener pair for three different scenarios that vary the absorption conditions in the room by varying the reflection coefficients at the walls according to Table 6.2. These absorption conditions are applied to both mesh topologies. This table also states the length of the desired RIR in seconds and number of iterations in order to record the total reverberant decay. Notice that the room model with the least absorption, and so the highest reflection coefficients, has the longest RIR measurement.

ABSORPTION CONDITION:	NORTH WALL, r :	EAST WALL, r :	SOUTH WALL, r :	WEST WALL, r :	RIR LENGTH, ITERATIONS:	RIR LENGTH, SECONDS:
Abs0.9	0.9	0.9	0.9	0.9	132300	3.0
Abs0.4	0.4	0.4	0.4	0.4	88200	2.0
AbsComplex	0.9	0.2	0.3	0.4	88200	2.0

Table 6.2 Each of the four rooms is modelled for each of the four source-listener combinations for three different scenarios that vary the absorption conditions in the room by varying the reflection coefficients at the walls. The total absorption in the room will determine the length of the RIR that has to be measured.

Finally, Table 6.3 gives the dimensions of each of the four rooms for each mesh in number of junctions together with the total number of junctions required to model the whole room.

ROOM:	ROOM LENGTH (RECT):	ROOM WIDTH (RECT):	TOTAL JUNCTIONS (RECT):	ROOM LENGTH (TRI):	ROOM WIDTH (TRI):	TOTAL JUNCTIONS (TRI):
A	425	292	124100	491	292	143372
B	437	437	190969	505	437	220685
C	546	437	238602	631	437	275747
D	637	546	347802	735	546	401310

Table 6.3 The dimensions of each of the four rooms for each mesh given in number of junctions together with the total number of junctions required to model the whole room.

6.4 Modal Analysis

In addition to the three absorption scenarios carried out as part of this case study, as described in Table 6.2, another scenario was simulated with all walls in all rooms for both mesh topologies being totally reflective and phase preserving. That is, all walls were set with a reflection coefficient of $r = +1.0$. The smooth impulse as described in Chapter 6.4 was used as the excitation signal and a 2.0s RIR was measured at each of the four listener output points. These RIR measurements were then loaded into the *WaveVerb* Analysis module. The RIR has the first 0.2s removed to eliminate any transient response, and the remaining 1.8s has an FFT applied to it using a Kaiser-Bessel window. The low frequency region of the resulting frequency response, up to the approximate critical frequency of the room in question (see Chapter 2.5 and Equation (2.8)), is then examined with the analytical room modes as calculated using Equation (2.6) being plotted on the same graph for comparison. Note that as the room is a 2-D simulation only the axial (reflections between two surfaces) and tangential (reflections between four surfaces) modes are valid.

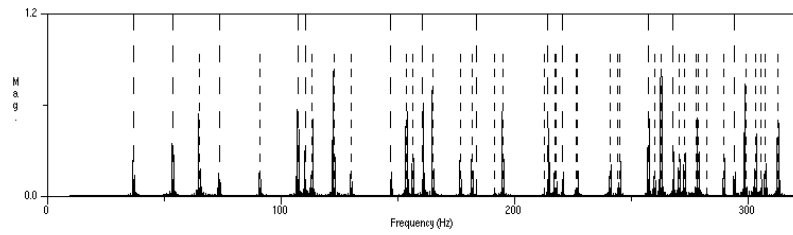
The results that follow over the next four pages show these low frequency response/modal analysis plots for each of the four rooms. The graphs are presented in pairs, each pair being the response for the rectilinear and triangular meshes for each of the four source-listener combinations within each room. The vertical scale in each graph shows the magnitude value relative to the whole plot in each case, and is therefore not consistently identical across the whole range of results. However the purpose of this analysis is to establish the validity of the model at low frequencies, so it is the distribution and existence of these resonant peaks that is the salient feature in these graphs, not their magnitudes relative to each RIR measurement.

In all cases the analytical axial modes are drawn as the long dashed vertical lines and the analytical tangential modes are drawn as the short dashed lines.

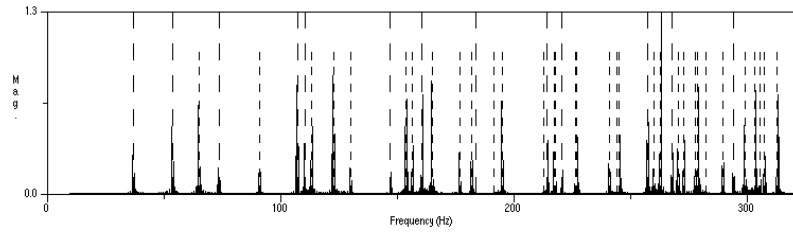
6.4.1 Room A

(Predicted Axial Modes: — — — · Predicted Tangential Modes: - - - - -)
 Output Point 1:

Rectilinear

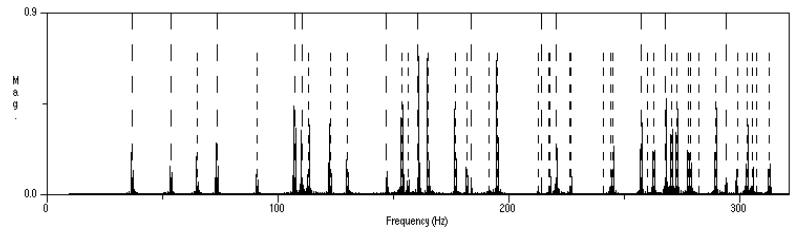


Triangular

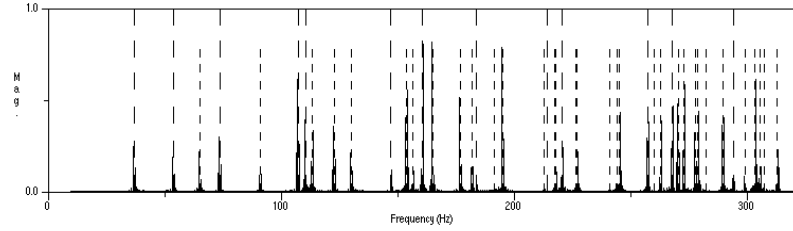


Output Point 2:

Rectilinear

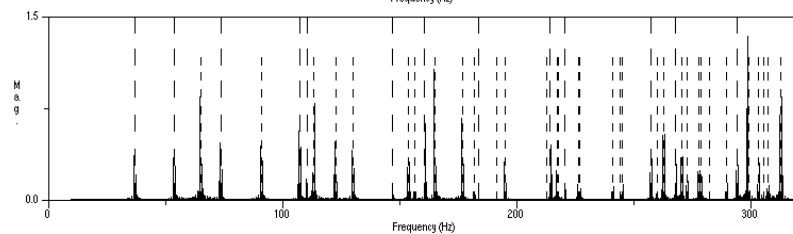


Triangular

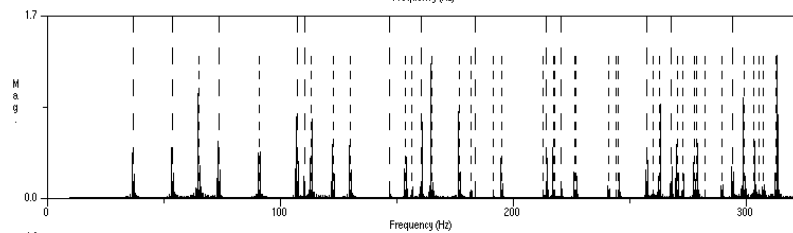


Output Point 3:

Rectilinear

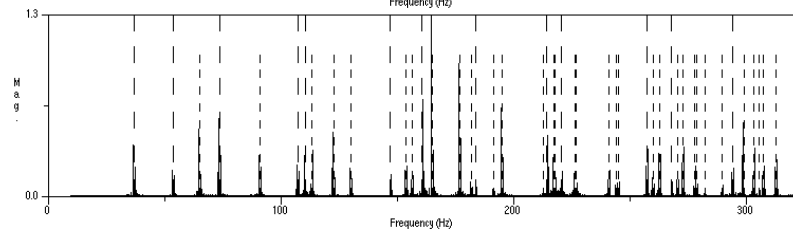


Triangular

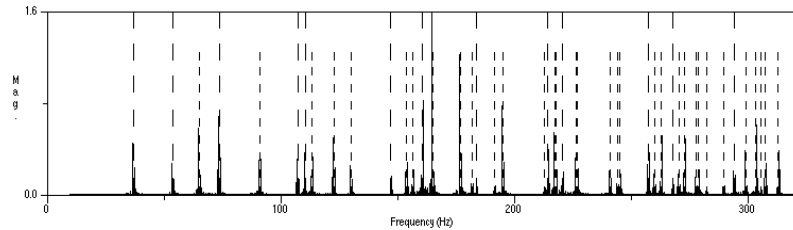


Output Point 4:

Rectilinear



Triangular

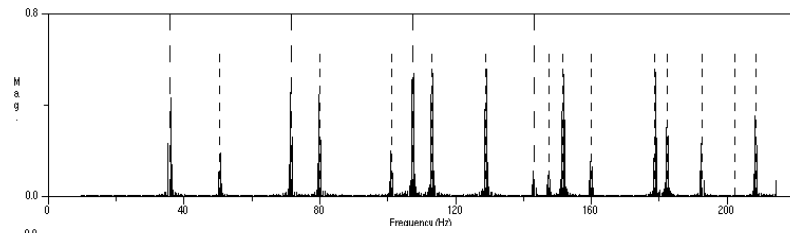


6.4.2 Room B

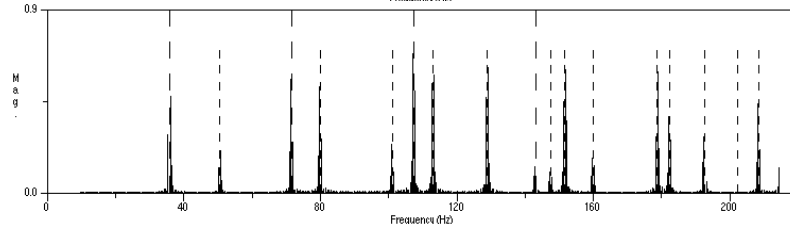
(Predicted Axial Modes: — — — · Predicted Tangential Modes: - - - - -)

Output Point 1:

Rectilinear

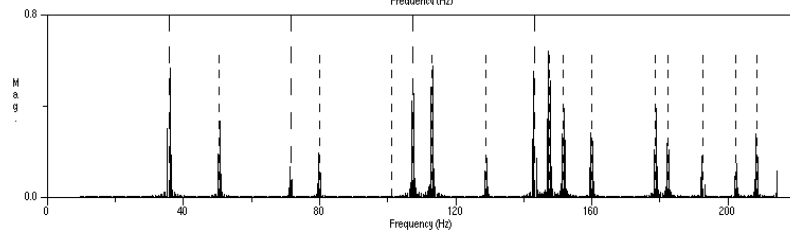


Triangular

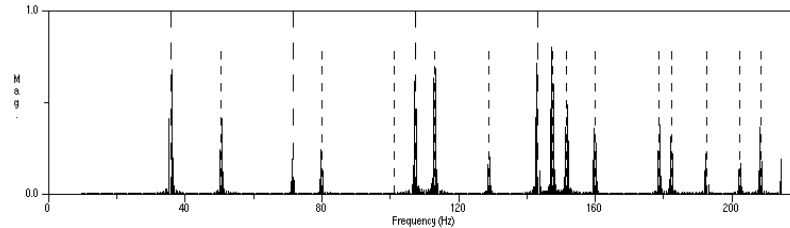


Output Point 2:

Rectilinear

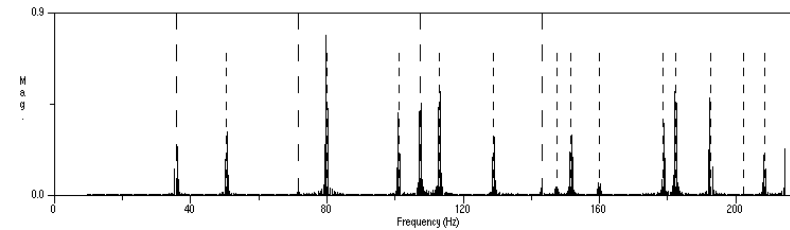


Triangular

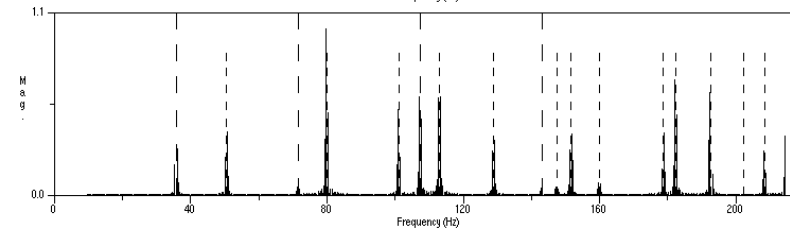


Output Point 3:

Rectilinear

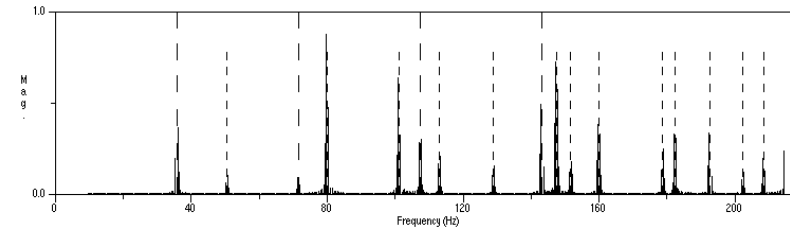


Triangular

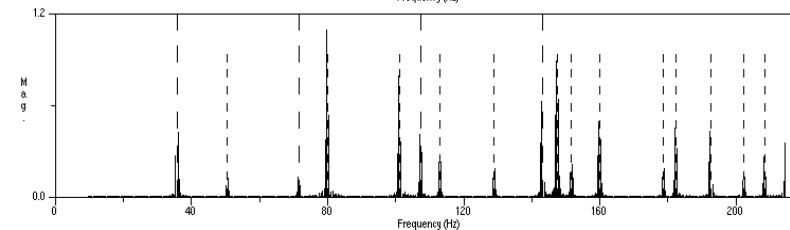


Output Point 4:

Rectilinear



Triangular

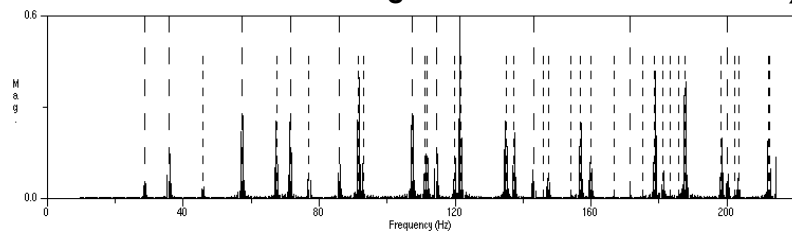


6.4.3 Room C

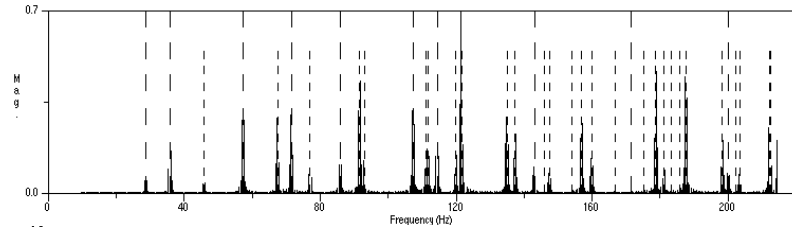
(Predicted Axial Modes: — — — · Predicted Tangential Modes: - - - - -)

Output Point 1:

Rectilinear

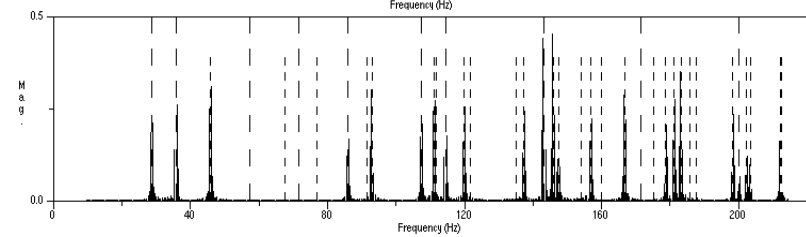


Triangular

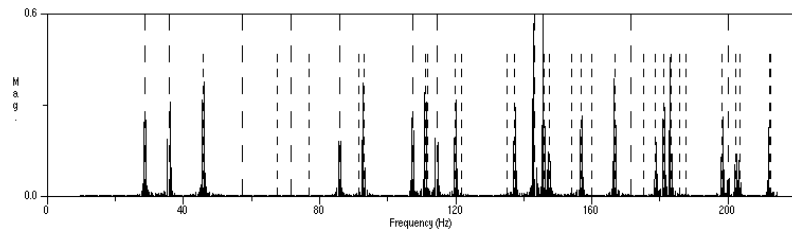


Output Point 2:

Rectilinear

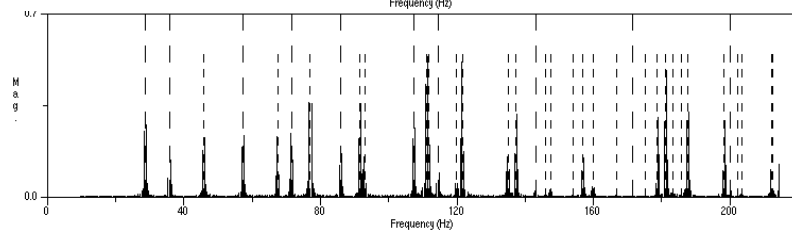


Triangular

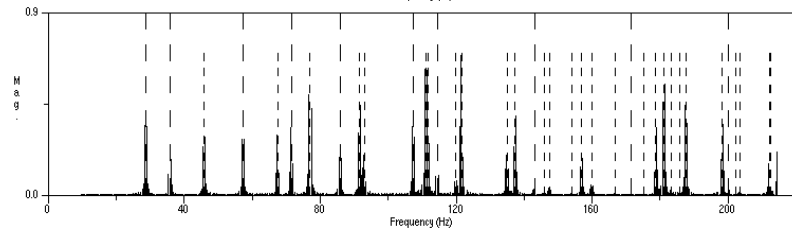


Output Point 3:

Rectilinear

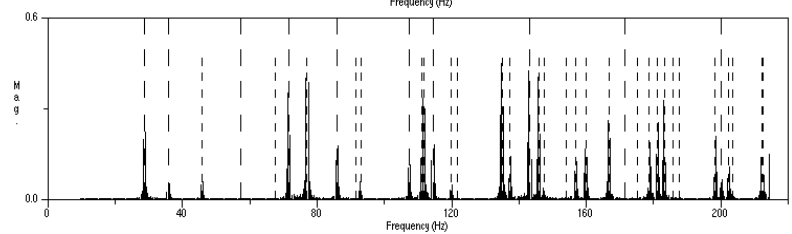


Triangular

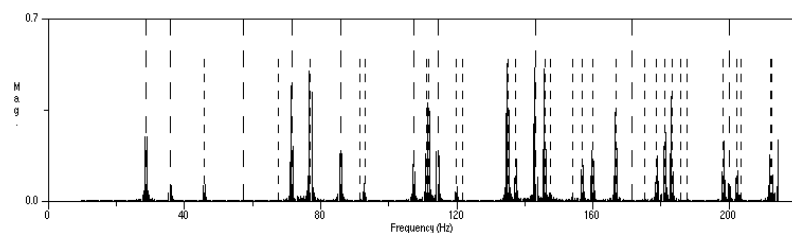


Output Point 4:

Rectilinear



Triangular

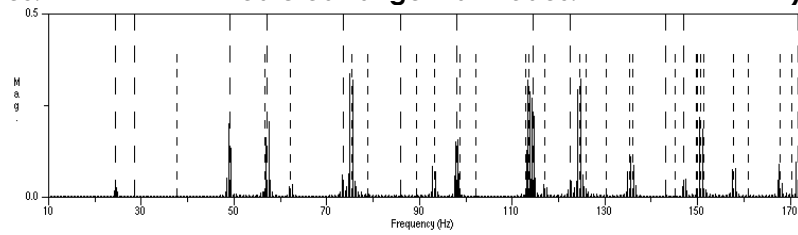


6.4.4 Room D

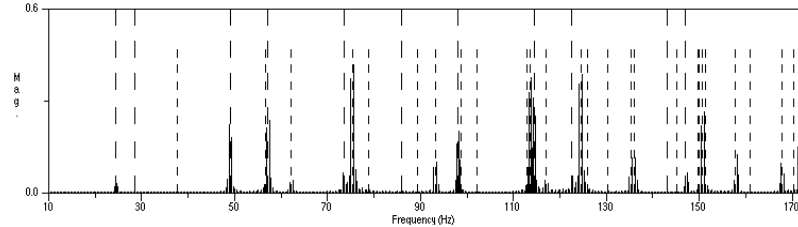
(Predicted Axial Modes: — — — · Predicted Tangential Modes: - - - - -)

Output Point 1:

Rectilinear

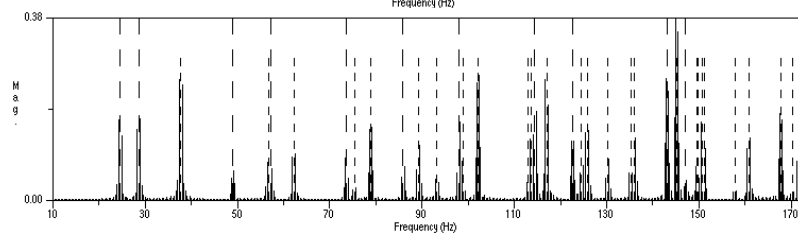


Triangular

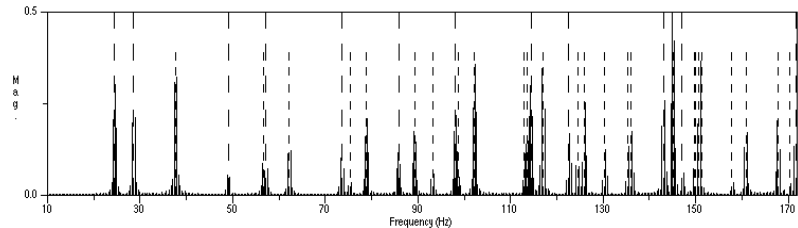


Output Point 2:

Rectilinear

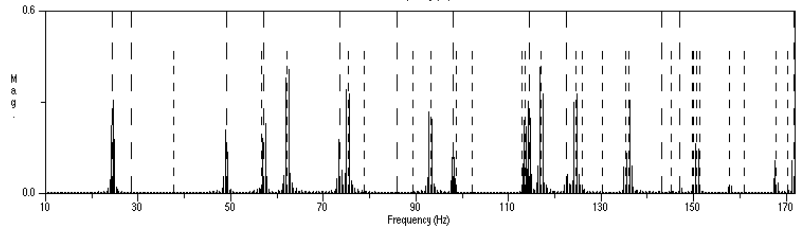


Triangular

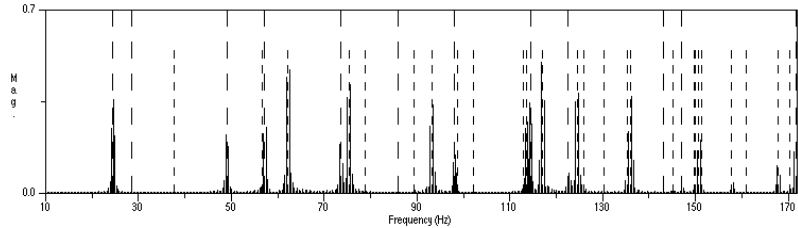


Output Point 3:

Rectilinear

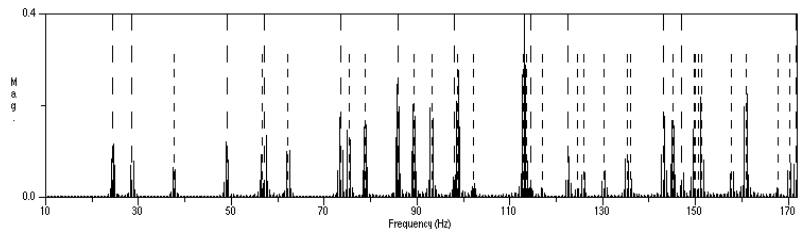


Triangular

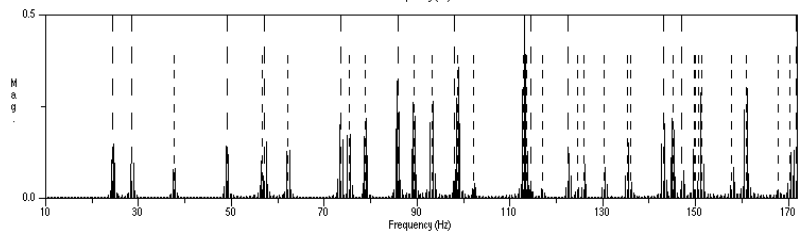


Output Point 4:

Rectilinear



Triangular



6.4.5 Discussion

There are a number of pertinent points about the properties of the waveguide meshes being studied that can be gleaned from these low frequency response/modal analysis plots. Clearly the RIR measurements correspond accurately to the low frequency acoustic characteristics of the theoretical rooms being modelled. This is true across all four room sizes and all source-listener output combinations. The relative magnitudes of the modal frequencies in a real room vary with position, and again this can be observed in these results with the relative magnitudes of the resonant peaks varying across each of the four output points. This can be clearly seen for Room B, Output Points 3 and 4. Examining the positions of these two points in Figure 6.10 reveals that they vary only in their position along the length of the room. Their positions relative to the width of the room and the west (left) and east (right) side walls remains the same. This implies that given all other conditions equal, the magnitude of any axial modes on the east-west axis would be constant for both positions. However the relative magnitudes of the axial modes along the axis between the north and south walls could be expected to vary. In the plots for Room B, Outputs 3 and 4, the magnitudes of the first and third axial modes (denoted by the long vertical dashed lines) are approximately constant. The second and fourth axial modes are virtually non-existent in the frequency response for Output Point 3 but are clearly evident in the frequency response for output Point 4 – particularly in the case of the fourth axial mode.

The results of Room B clearly show the effects a square room will have on the distribution of the room modes. Note first of all there are fewer analytical axial and tangential modes and the resonances as measured are clearer and suggest a higher relative magnitude than many of the results from the other rooms, agreeing with what was stated in Chapter 2.4. By contrast the Sepmeyer Room (Room A) proves inconclusive as to whether the distribution of modes is any more favourable than Room C or Room D as all exhibit some pairs of coincident frequencies, although these are all lower magnitude tangential modes. What would be more revealing is a plot of all three sets of axial modes (floor to ceiling included) as the length of Room C (6.0m) and the width of Room D (6.0m) are both low order multiples of the assumed height (2.0m). This is not the case for Room A. However this obviously cannot as yet be catered for by the 2-D only *WaveVerb* System.

Perhaps what is most interesting from these results at first glance is the fact that there is an almost exact correlation between the relative magnitudes for each pair of results for both mesh topologies. Previous results, eg. [Laird et al, 1998], examining the theoretical resonant frequencies of waveguide mesh structures show that as frequency increases the correspondence between the measured results and those expected becomes worse due to dispersion error. As it has already been established that the triangular mesh is theoretically the better model of the two

due to a minimisation of this dispersion error (see Chapter 5.6) it might have been natural to assume that the rectilinear mesh would not prove to be as accurate at picking out the modal frequencies. These results show that the models are equal in this respect and this is due to the high mesh density used. Previous studies have only measured small objects (drum membranes or plates for instance) using a relatively coarse mesh and have not considered the larger dimensions and high mesh sampling rates required to successfully model an enclosed room, even if it has been constrained to two dimensions. The reason for this apparent anomaly – the fact that at this point both mesh topologies appear to give equivalent results - can be found by examining the dispersion error plots of Figures 5.11 and 5.12. It is clear that for both topologies the low absolute frequencies, corresponding to the region in the centre of these plots, exhibit minimal dispersion error, of the order of 0.05%. Due to the high mesh sampling rate used, it is only as the frequency becomes much greater that the dispersion error becomes a significant problem. The density of the modal distribution increases significantly with frequency in the case of a room and so this dispersion error effect is more difficult to detect. It has also been suggested that due to this increased density of distribution at higher frequencies for a large bandwidth, this dispersion error may not be an important factor in an audio context [Van Duyne and Smith, 1993]. It has also been noted that the rectilinear mesh is actually only valid for up to one tenth of the sampling rate of the mesh [Huopaniemi et al, 1997]³. The triangular mesh should improve on this value given the dispersion error calculations - and the modal regions of the rooms modelled as part of this thesis are well below this limit. Hence the equivalence between the two models in the low frequency response analysis presented above.

6.5 Frequency Response Analysis

The section that follows examines the overall frequency response of the measured RIRs for each absorption scenario, room, and output point combination. In each case a pair of RIR estimates corresponding to the two mesh topologies have been loaded into *Cool Edit Pro*, a PC software audio editor [Syntrillium, 1999]. A time averaged spectral analysis is performed over the whole length of each RIR and the results plotted using the software's built in features. The results that follow show these plots as the Room Frequency Responses (RFRs) from the triangular and rectilinear meshes drawn on the same axes, with the darker of the two lines representing the RFR from the triangular mesh. A sonogram for each pair of results is also plotted using this software, allowing a time varying frequency analysis to be displayed. In these cases the sonogram for rectilinear mesh is displayed above that of the triangular mesh.

³ Note this value is less than that given by $0.25 \times f_{update}$ this being the theoretical upper limit of validity on the rectilinear mesh. See Chapter 4.6, [Van Duyne and Smith, 1993] and [Savioja et al, 1996b].

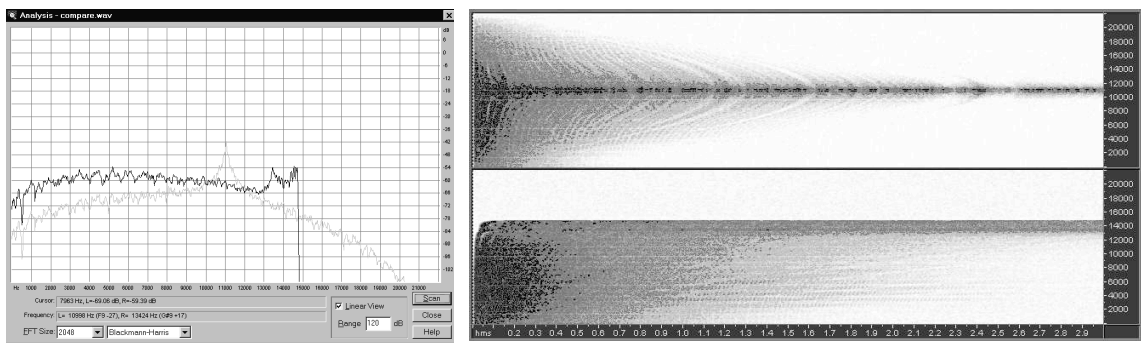
Key To Graphs:

Each RFR is plotted with frequency, f , on the x -axis varying from 0Hz to 22050Hz and amplitude on the y axis ranging from -106dB to 0dB . Note again that the triangular mesh is plotted with the darker of the two lines displayed. The sonograms are plotted with time, t , on the x axis ranging from 0s to 3.0s for Examples 6.5.1, 6.5.4, 6.5.7 and 6.5.10 (these example rooms having the least absorption hence the longest RIRs - see Table 6.2) and 0s to 2.0s for the remaining examples. In all cases the y axes range from 0Hz to 22050Hz. Note again that the sonogram for the rectilinear mesh is displayed above that of the triangular mesh.

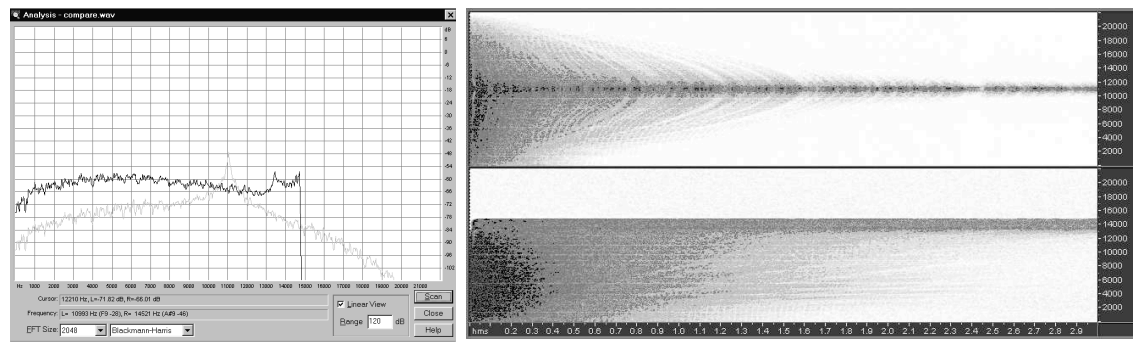
6.5.1 Room A – Abs0.9

(Note that a detailed key to these graphs can be found on page 134)

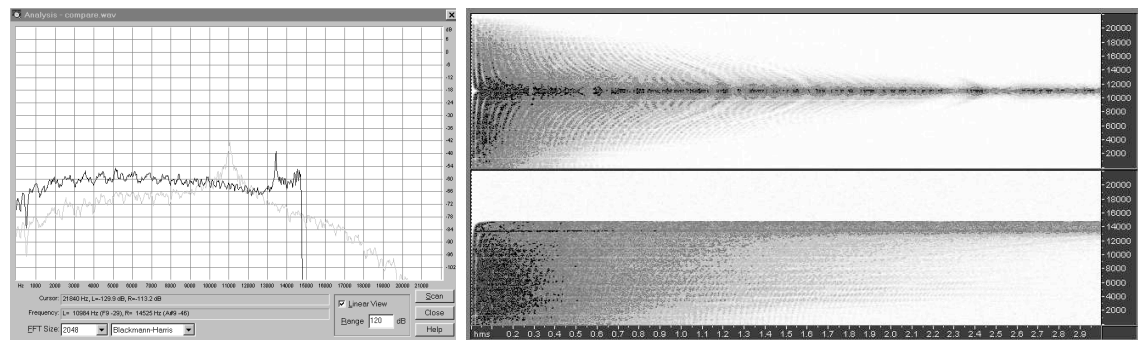
Output Point 1:



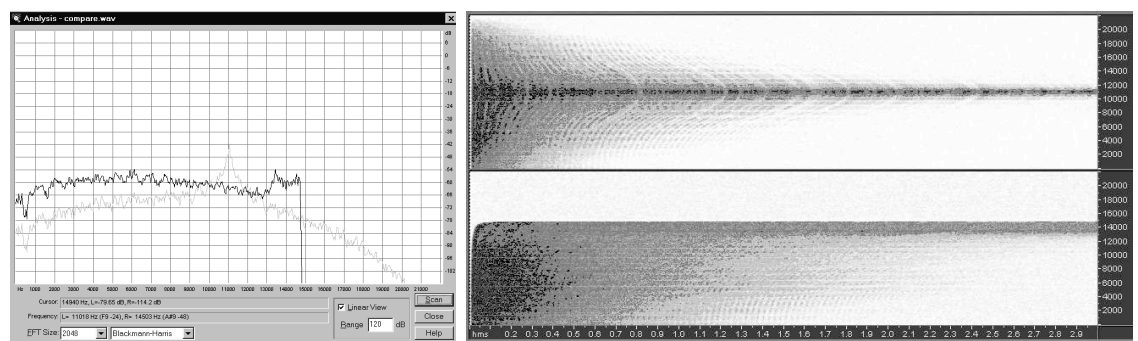
Output Point 2:



Output Point 3:



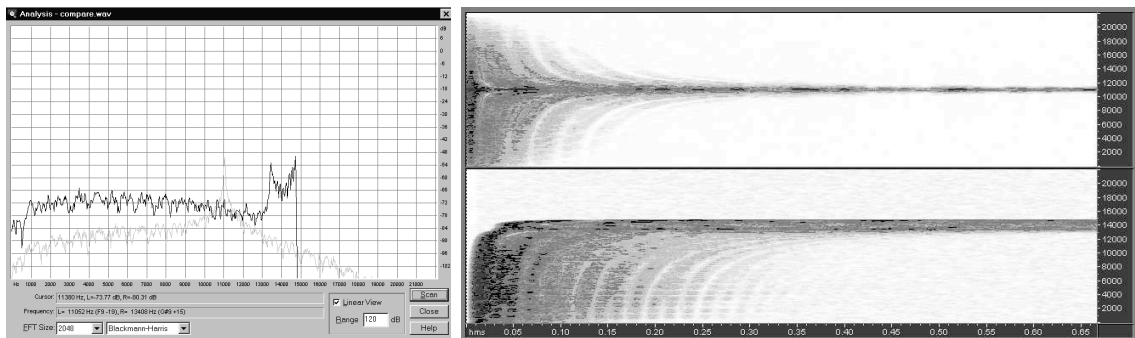
Output Point 4:



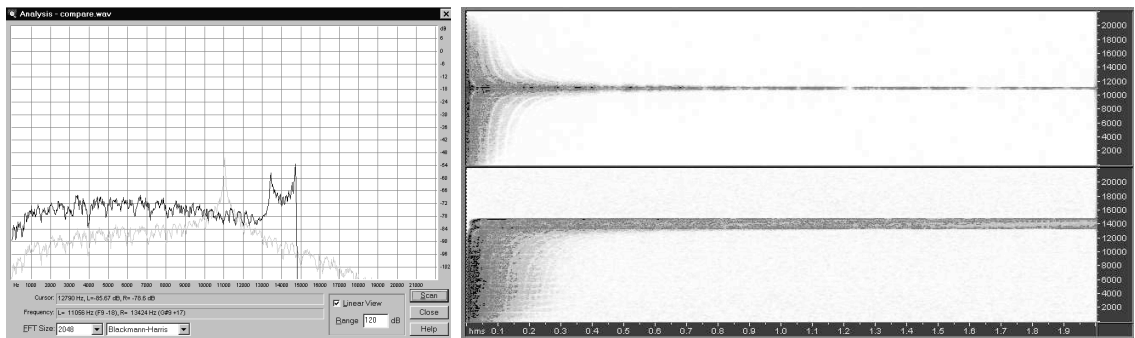
6.5.2 Room A – Abs0.4

(Note that a detailed key to these graphs can be found on page 134)

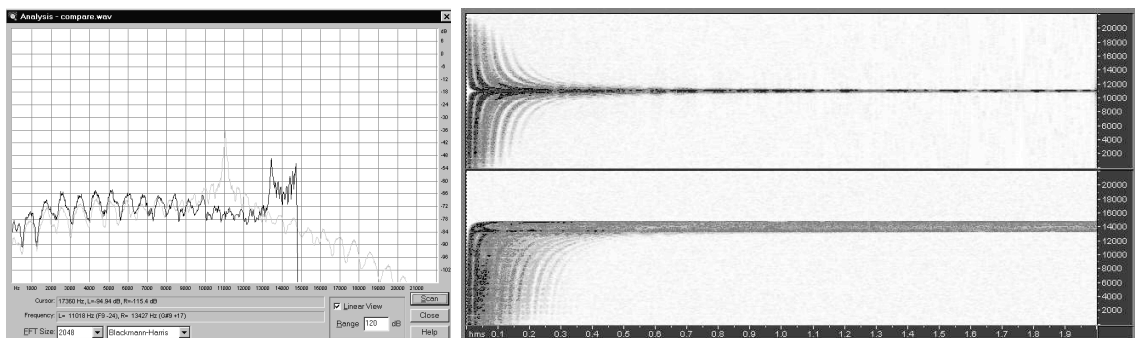
Output Point 1:



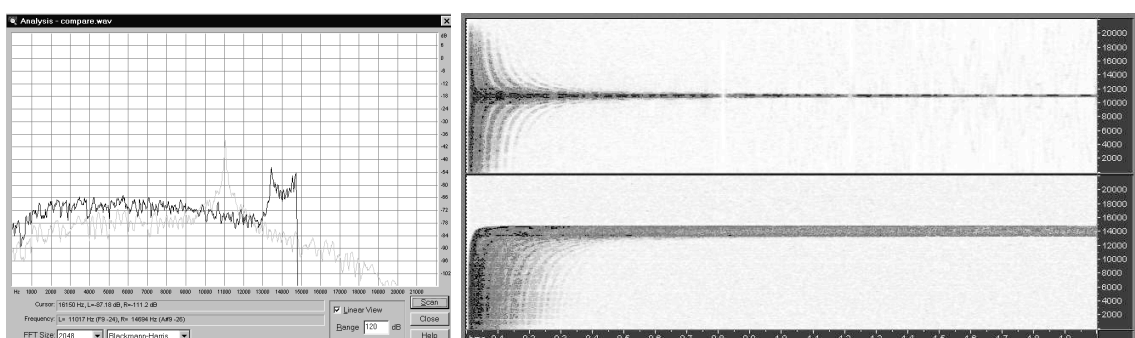
Output Point 2:



Output Point 3:



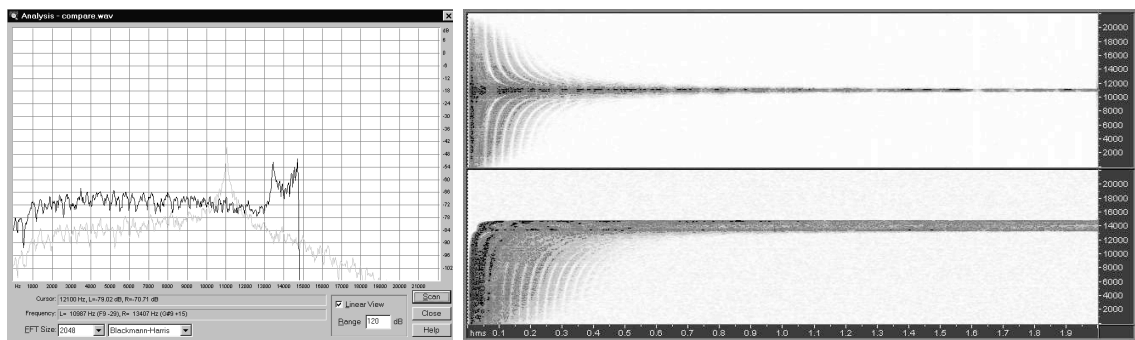
Output Point 4:



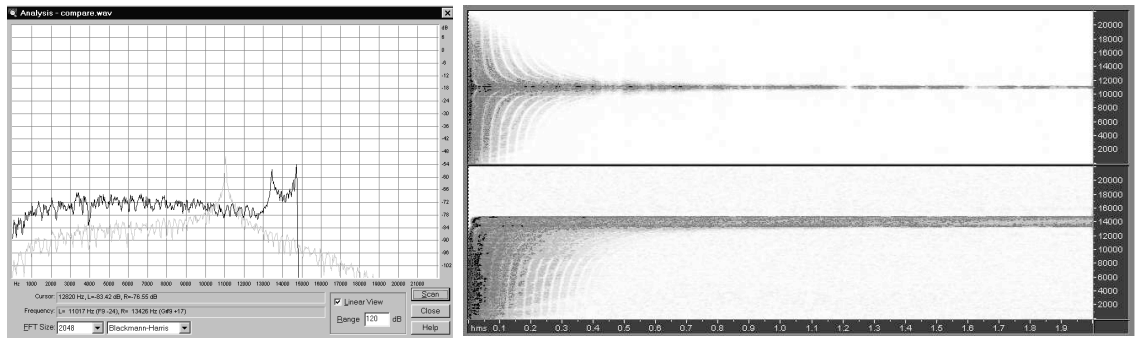
6.5.3 Room A – AbsComplex

(Note that a detailed key to these graphs can be found on page 134)

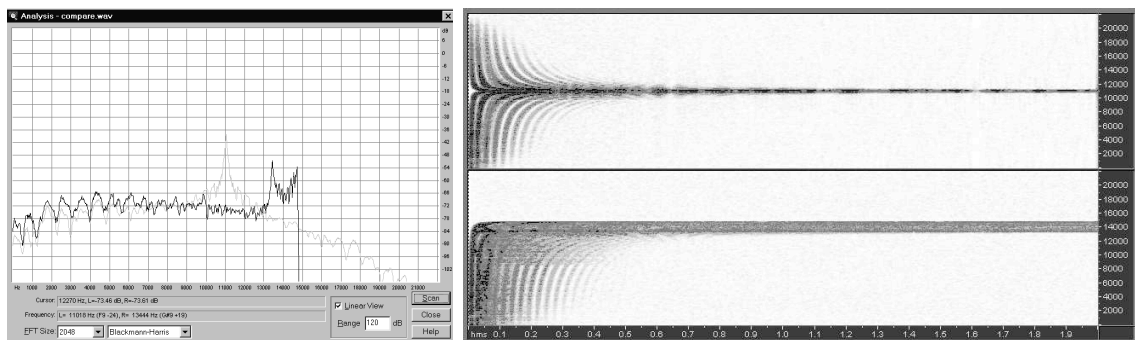
Output Point 1:



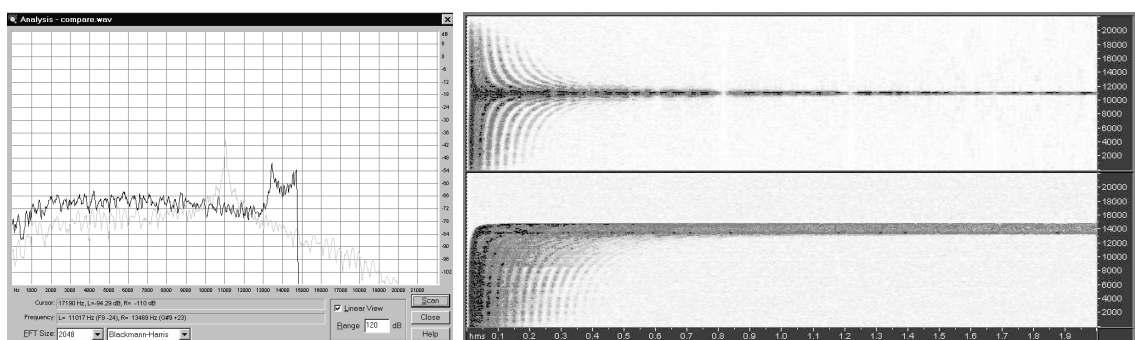
Output Point 2:



Output Point 3:



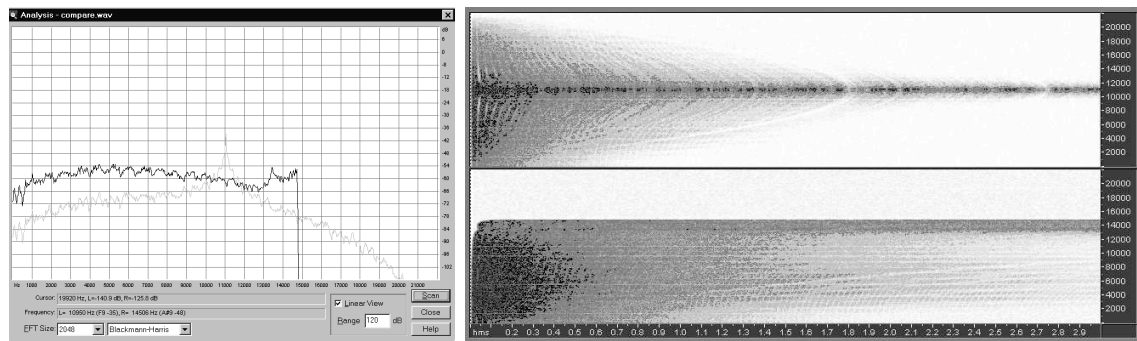
Output Point 4:



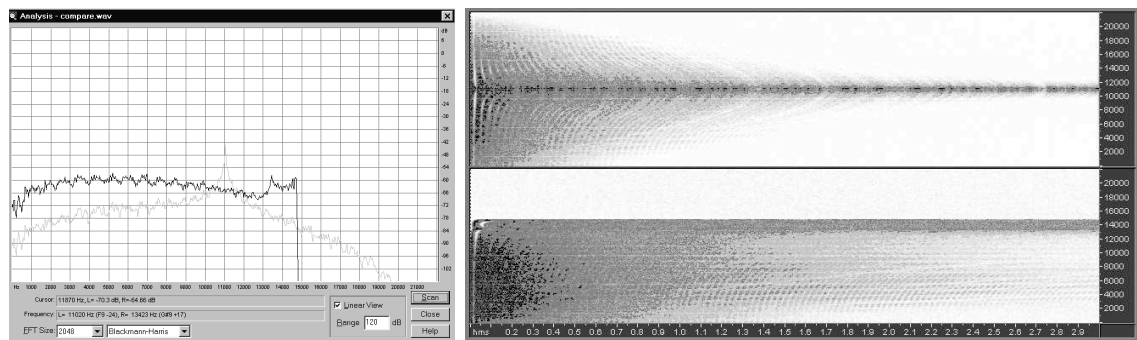
6.5.4 Room B – Abs0.9

(Note that a detailed key to these graphs can be found on page 134)

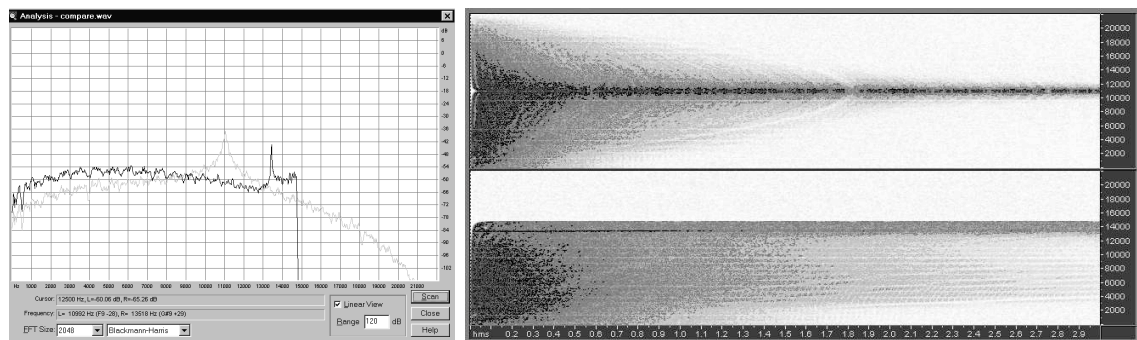
Output Point 1:



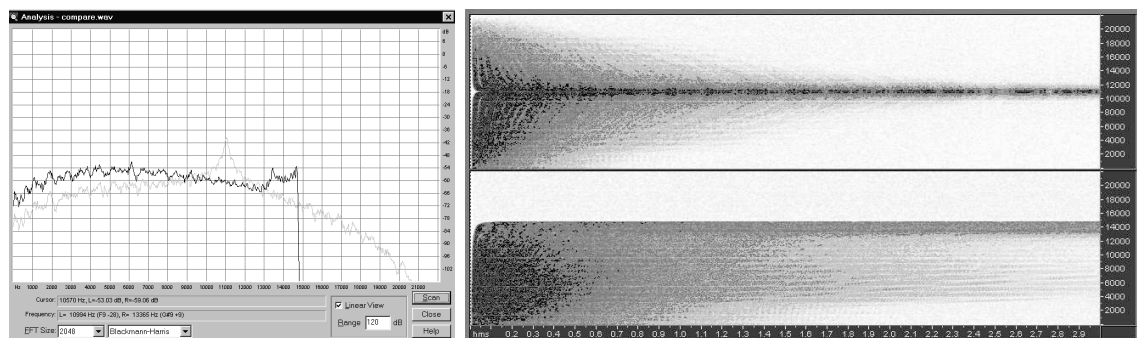
Output Point 2:



Output Point 3:



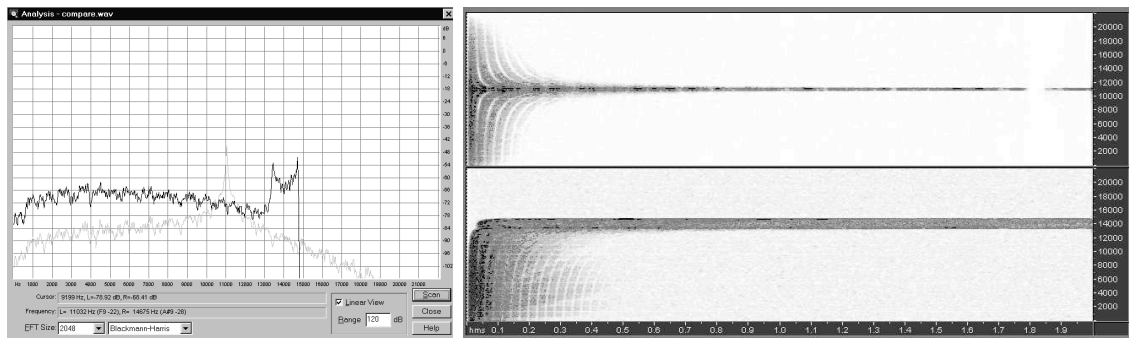
Output Point 4:



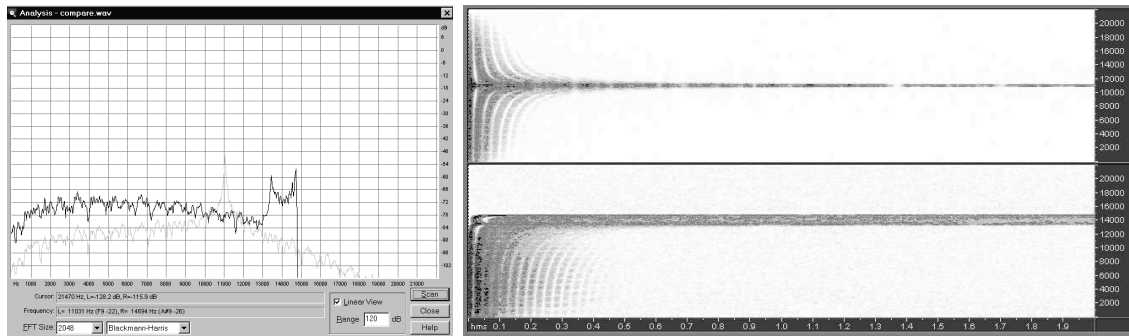
6.5.5 Room B – Abs0.4:

(Note that a detailed key to these graphs can be found on page 134)

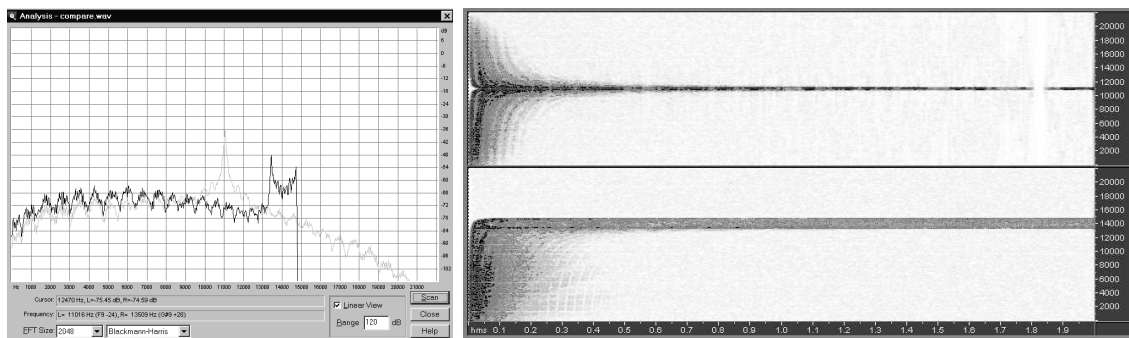
Output Point 1:



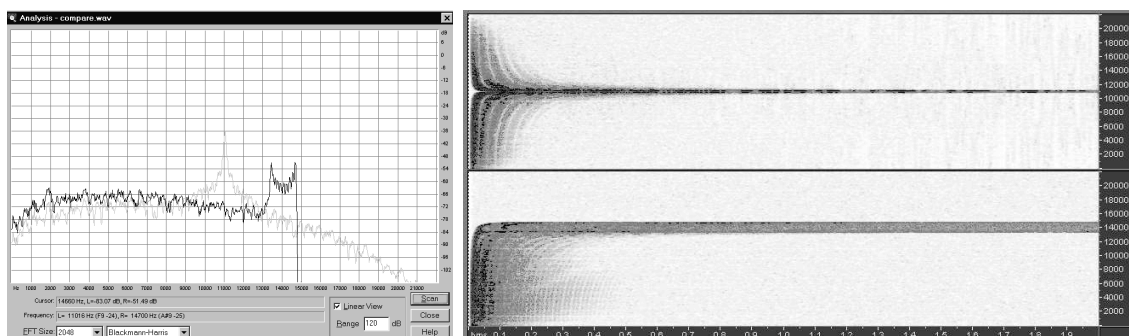
Output Point 2:



Output Point 3:



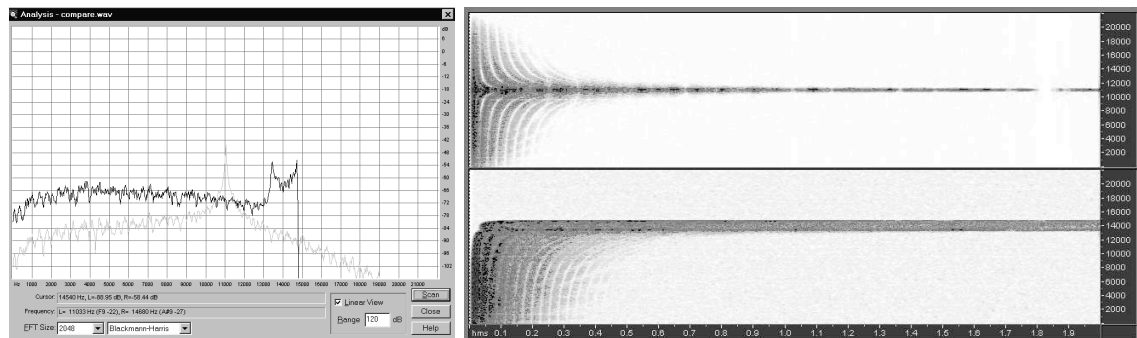
Output Point 4:



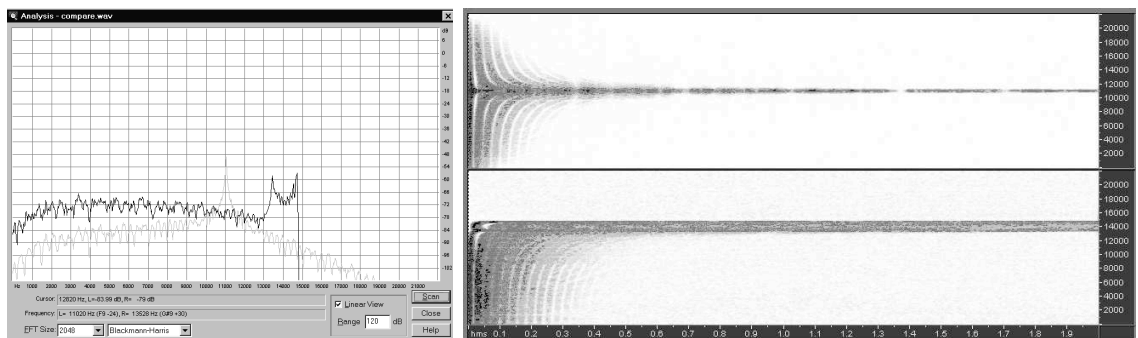
6.5.6 Room B – AbsComplex

(Note that a detailed key to these graphs can be found on page 134)

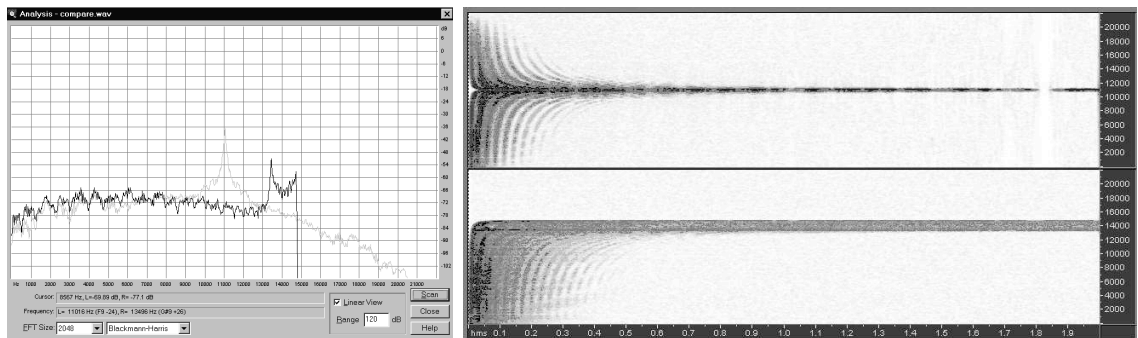
Output Point 1:



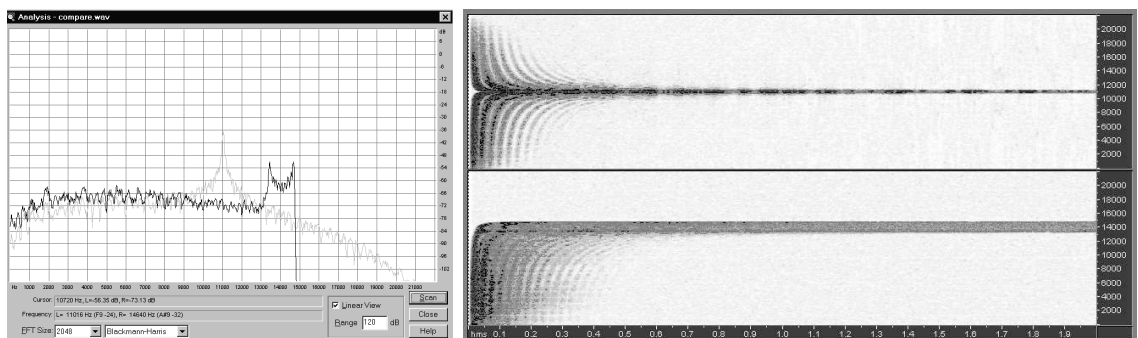
Output Point 2:



Output Point 3:



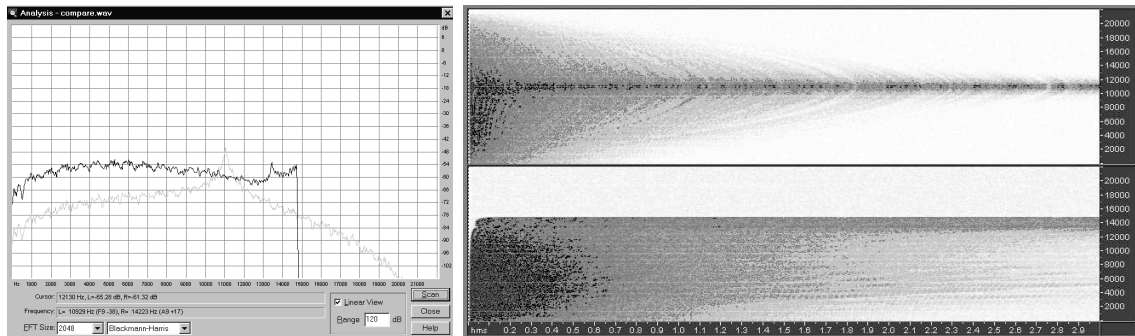
Output Point 4:



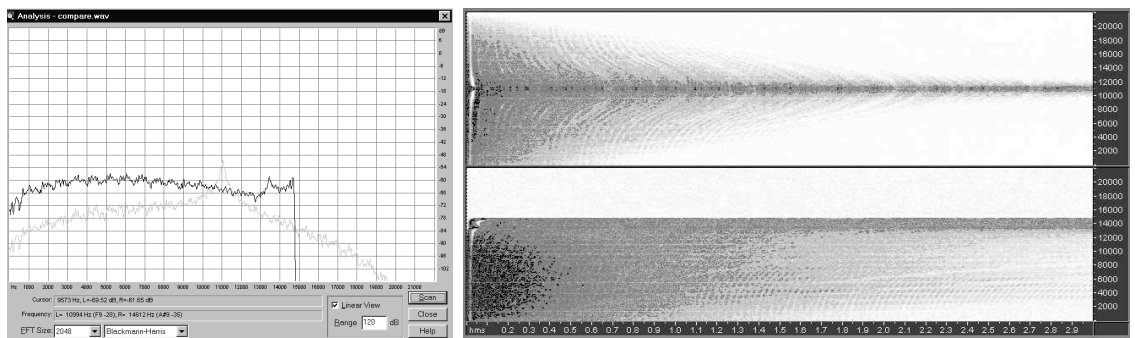
6.5.7 Room C – Abs0.9

(Note that a detailed key to these graphs can be found on page 134)

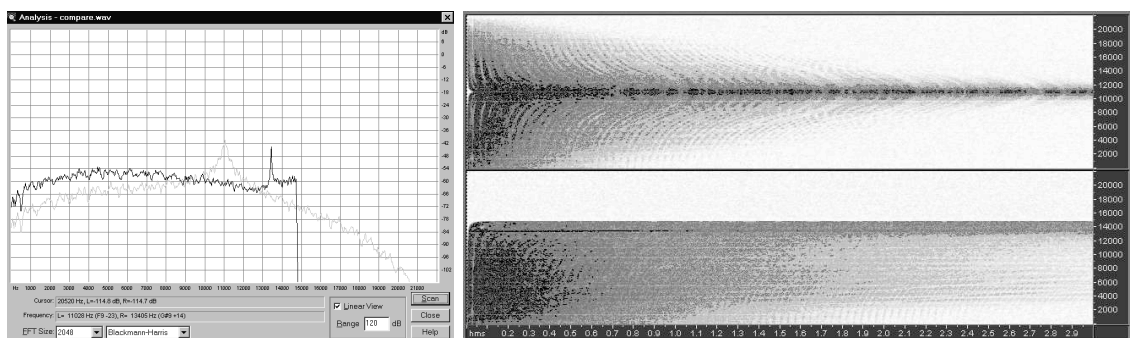
Output Point 1:



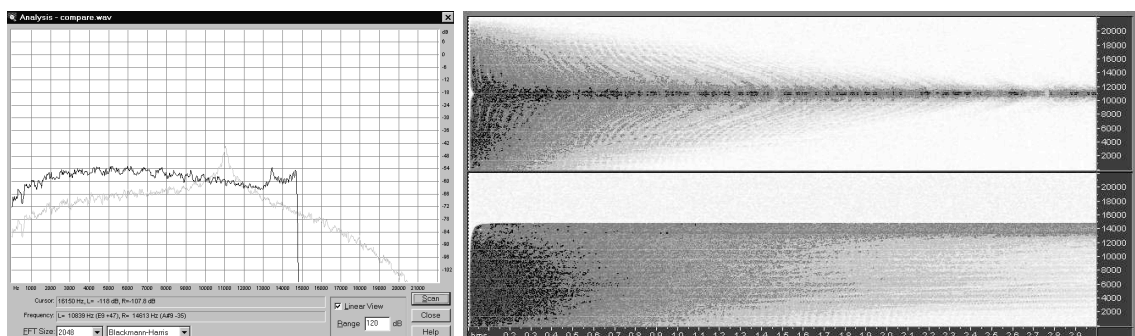
Output Point 2:



Output Point 3:



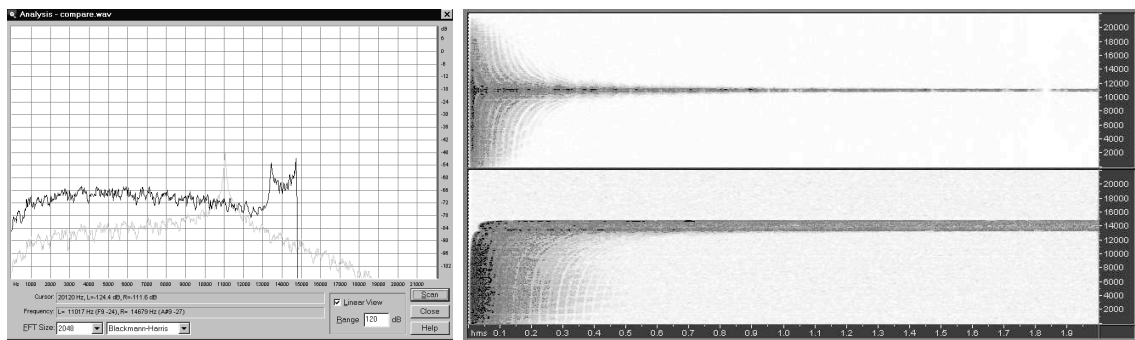
Output Point 4:



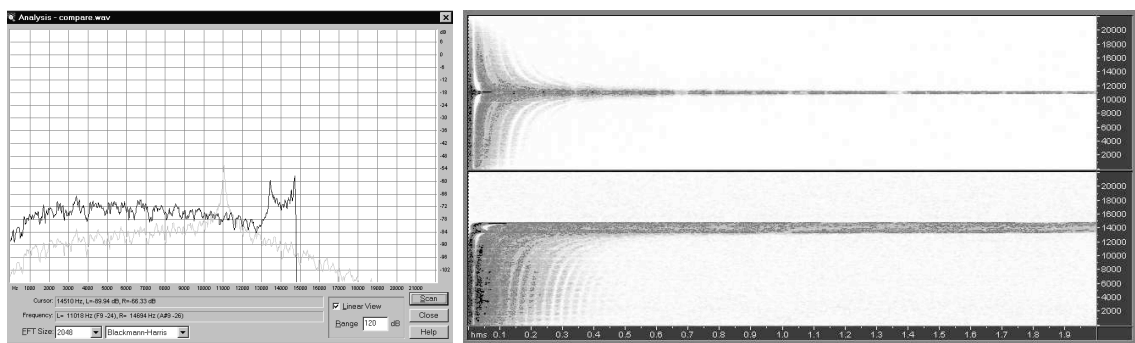
6.5.8 Room C – Abs0.4

(Note that a detailed key to these graphs can be found on page 134)

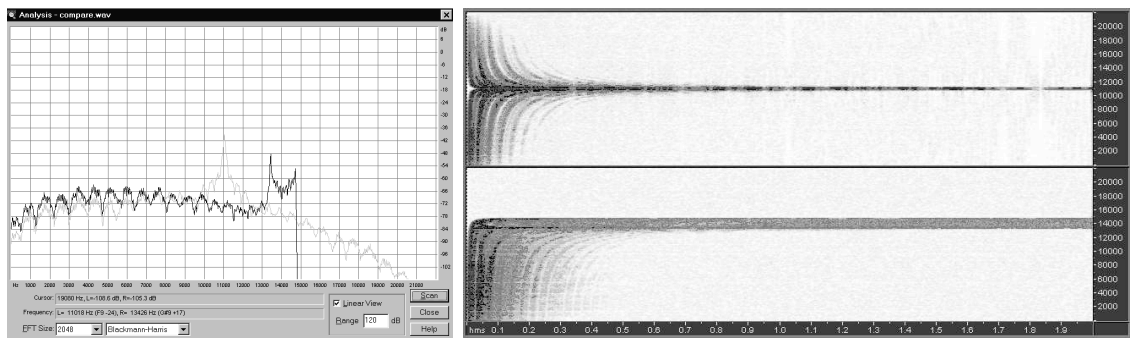
Output Point 1:



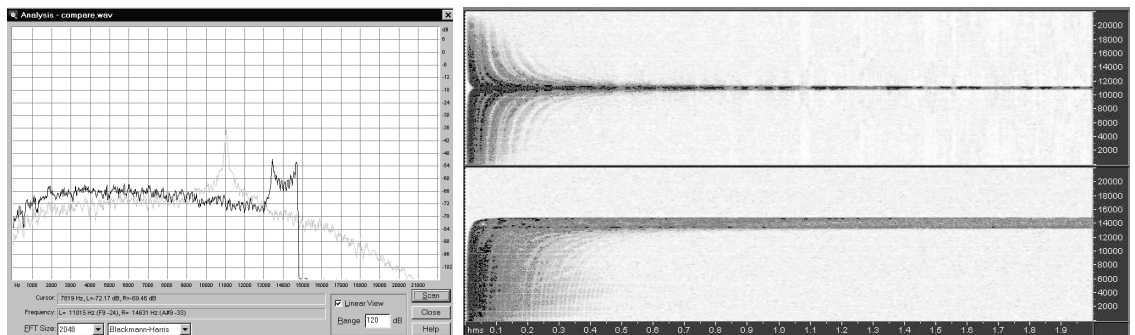
Output Point 2:



Output Point 3:



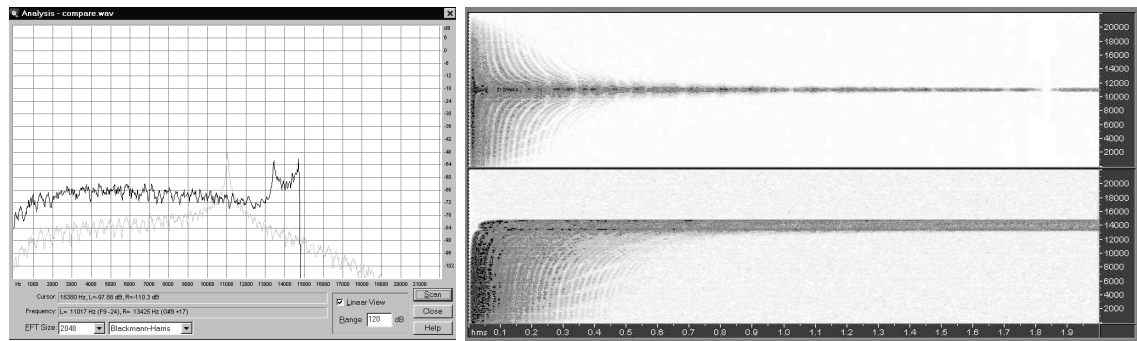
Output Point 4:



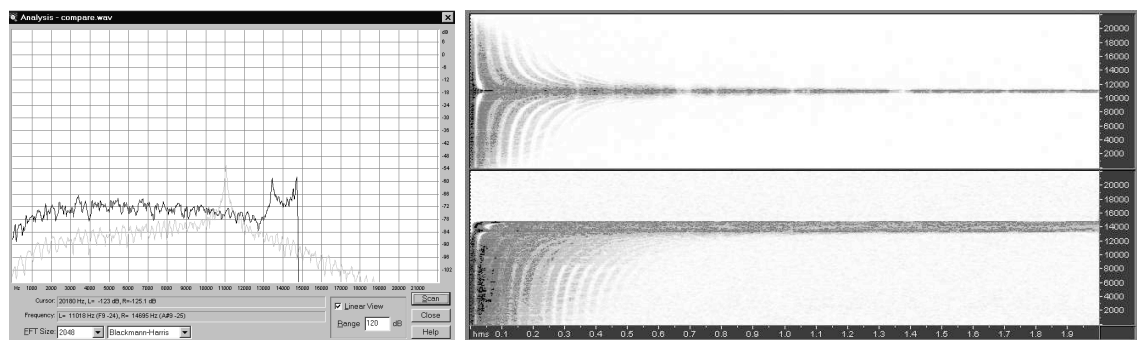
6.5.9 Room C – AbsComplex

(Note that a detailed key to these graphs can be found on page 134)

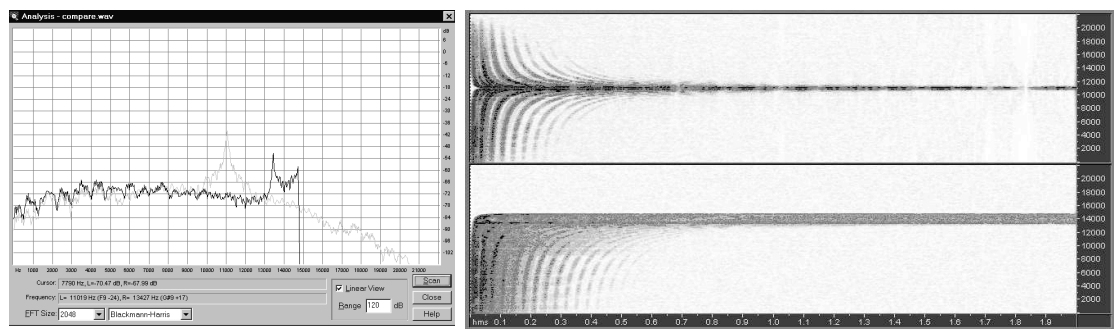
Output Point 1:



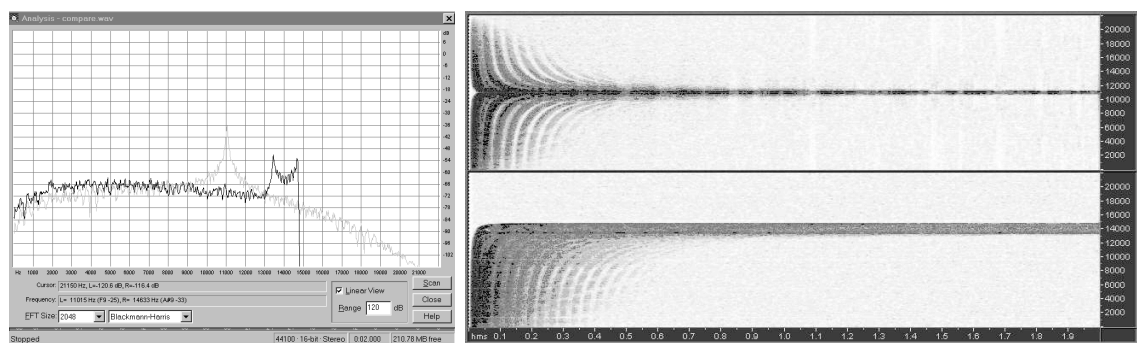
Output Point 2:



Output Point 3:



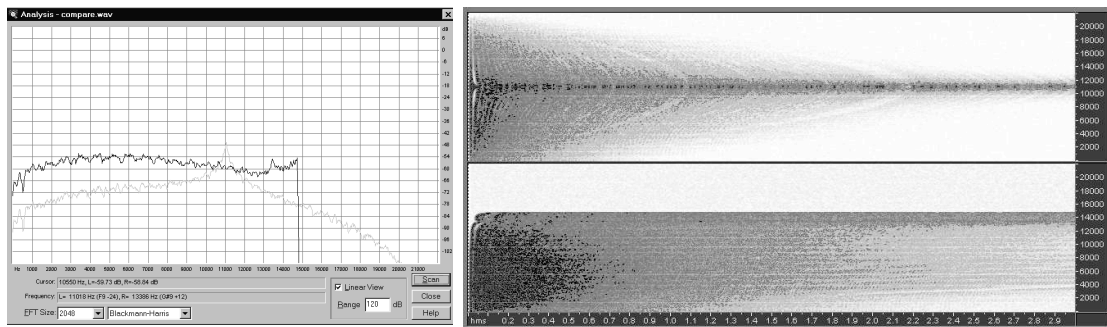
Output Point 4:



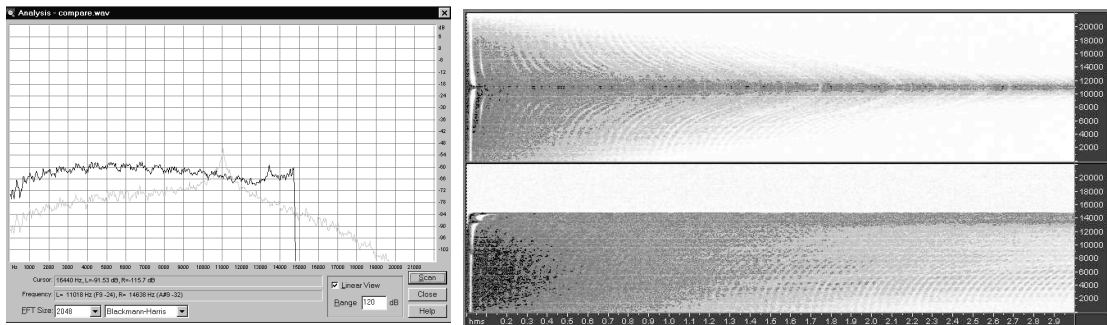
6.5.10 Room D – Abs0.9

(Note that a detailed key to these graphs can be found on page 134)

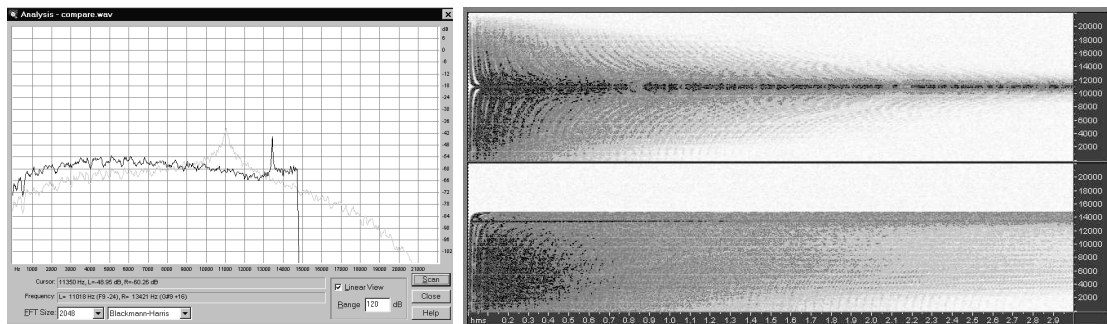
Output Point 1:



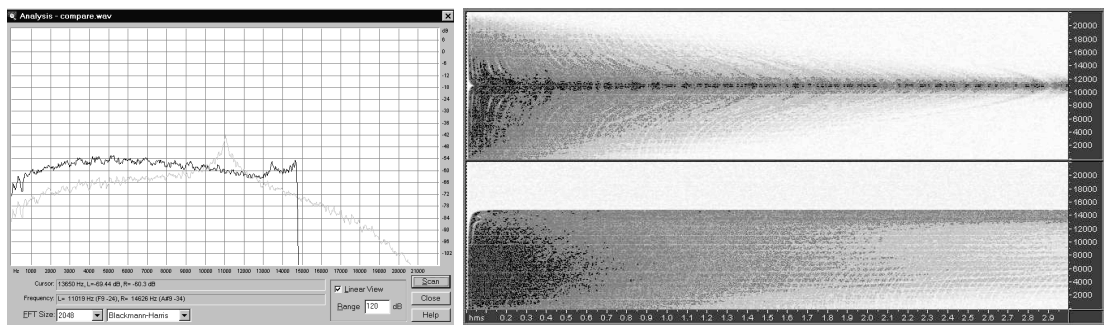
Output Point 2:



Output Point 3:



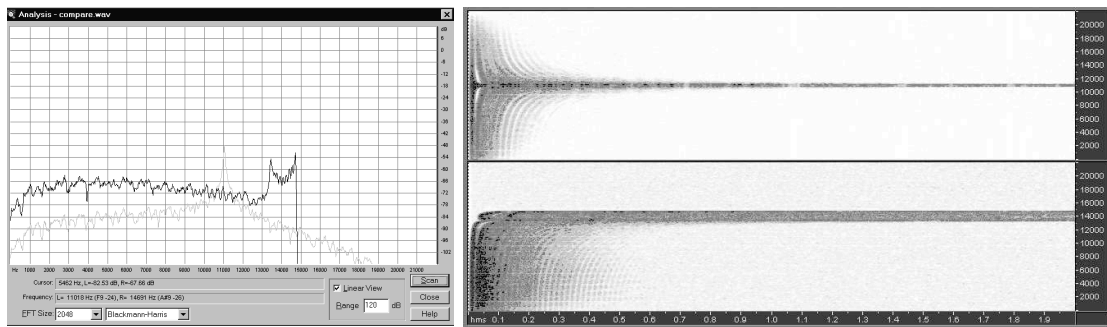
Output Point 4:



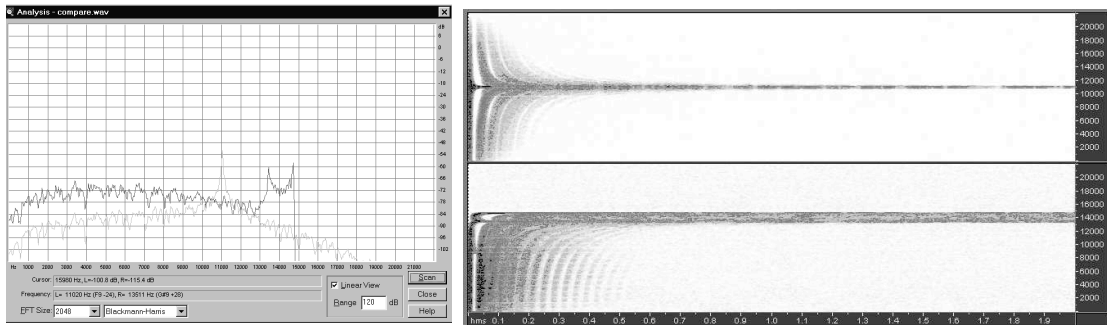
6.5.11 Room D – Abs0.4

(Note that a detailed key to these graphs can be found on page 134)

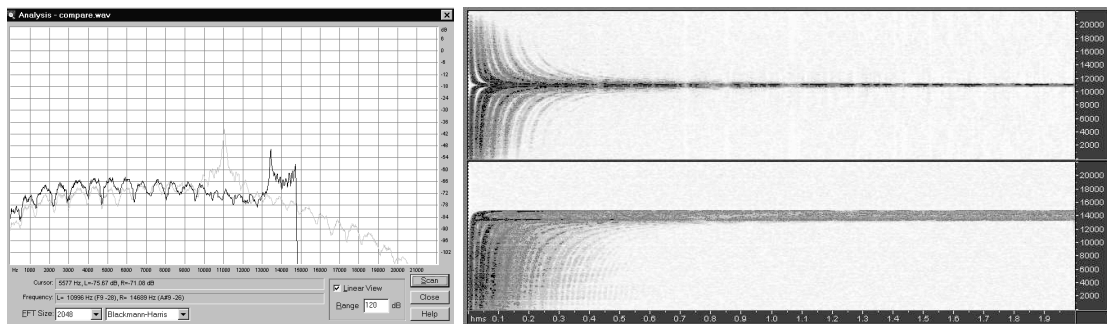
Output Point 1:



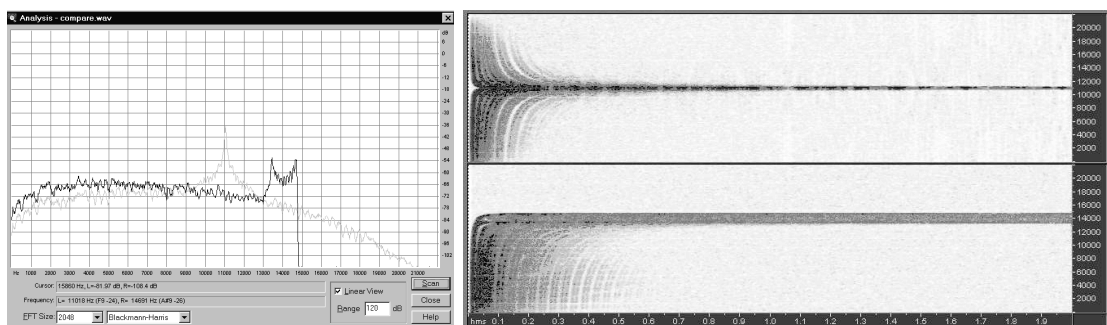
Output Point 2:



Output Point 3:



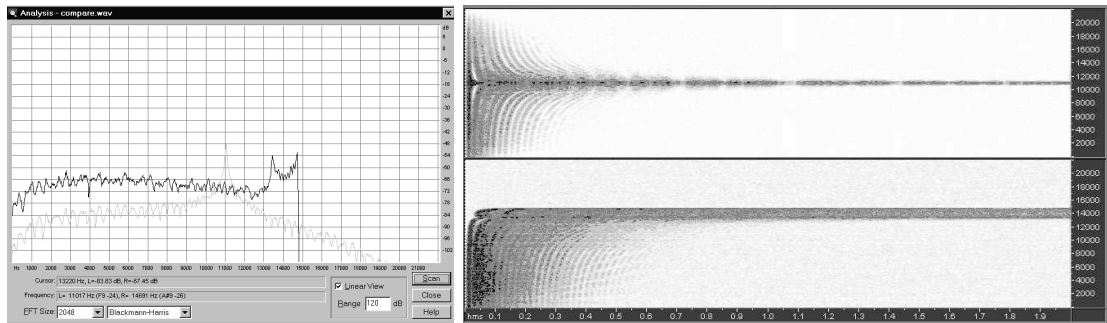
Output Point 4:



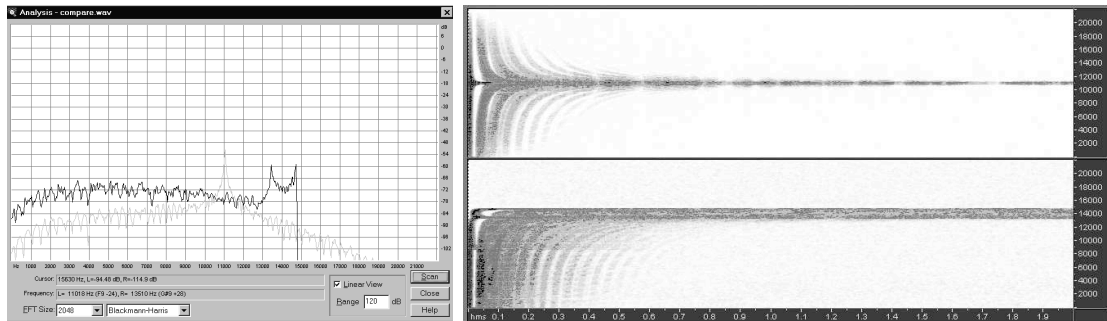
6.5.12 Room D – AbsComplex

(Note that a detailed key to these graphs can be found on page 134)

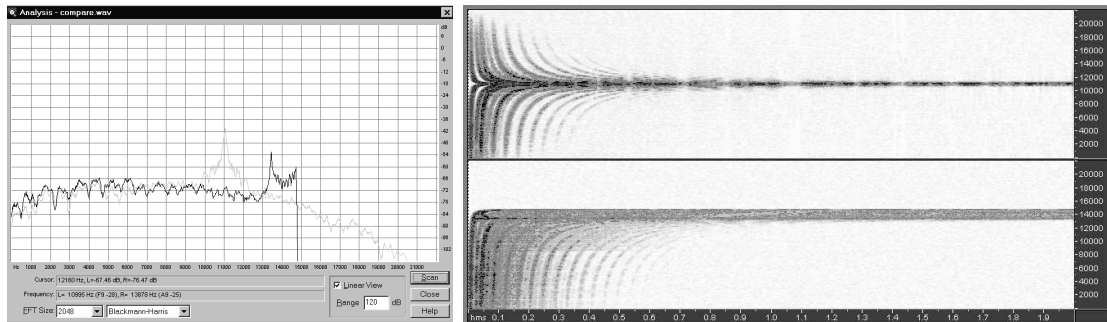
Output Point 1:



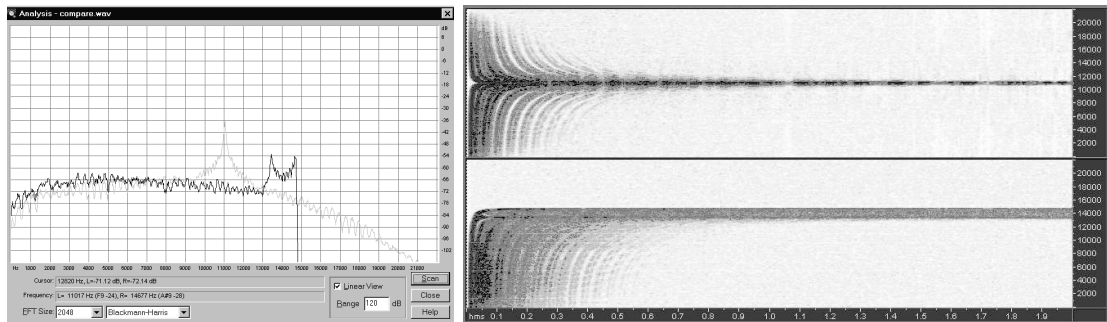
Output Point 2:



Output Point 3:



Output Point 4:



6.5.13 Discussion

According to these frequency response graphs there is a clear difference between the RIR measurements from the triangular mesh and the rectilinear mesh and this is consistent across all room sizes, absorption coefficients and output points. The main feature in the triangular mesh frequency response plots is the well defined cut-off point. This can be clearly seen in both the time averaged spectral plot and in the sonogram. In the latter this cut-off can be identified by the thick gray line running through the entire plot, above which is an area of white area showing that any frequencies present have been attenuated to such an extent that they are negligible. This sharp and well defined cut-off point is the natural upper limit of the mesh above which no frequency can be successfully propagated. This is a common property of all lattice type structures that support wave propagation:

“All problems discussed deal with periodic structures of various kinds, and they all lead to similar results: these structures, be they electric lines or crystal lattices, behave like band-pass filters. If energy dissipation is omitted, there is a sharp distinction between frequency bands exhibiting wave propagation without attenuation (passing bands) and those showing attenuation and no propagation (stopping bands).”

[Brillouin, 1953]

The cut-off point is related to the mesh sampling rate and hence the distance between scattering junctions. In this case study it is at approximately 14.7kHz for all measurements and this can be seen to equal $f_{update}/3$, with $f_{update} = 44.1\text{kHz}$ as defined for this particular triangular mesh. This result is constant for all triangular mesh structures examined so far:

$$f_{cut-off} = \frac{1}{3} \cdot f_{update} \quad (6.1)$$

where $f_{cut-off}$ is the natural cut-off point for a waveguide mesh with a triangular topology and f_{update} is defined by Equation (4.27).

Conversely for the rectilinear mesh there is no evident value for $f_{cut-off}$. Rather a well defined resonant peak is present in all frequency response measurements and this can be clearly observed in both the time averaged frequency plots and sonograms. Further, the sonogram shows that the frequency response above this peak is actually a reflection of the frequency response below it. This “mirroring” of the frequency response in measurements taken from the rectilinear mesh has been observed in previous studies, for instance [Van Duyne and Smith, 1993] and [Savioja et al, 1996b] although it hasn’t been explained in any great detail. The explanation with reference to [Savioja, 1999] is presented as follows. Figure 6.11 shows a typical section of the rectilinear mesh with a single input point and two output points.

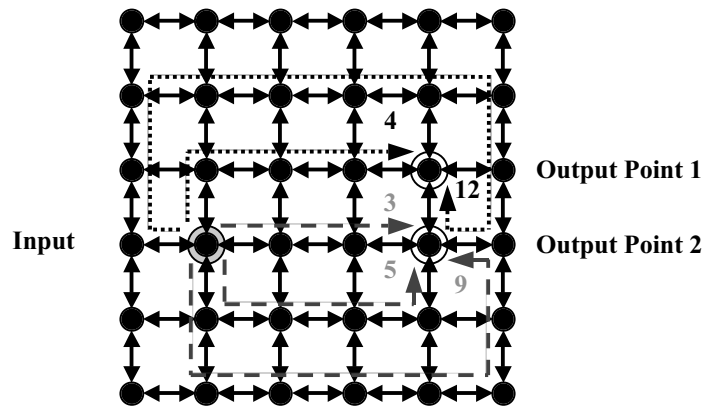


Figure 6.11 A typical section from a rectilinear mesh with an input point and two output points labelled. Some potential paths between the input and each output have been marked and the number of constituent waveguide elements that make up each path length have been noted.

Note that from Figure 6.11, any path from the Input to Output Point 1 involves traversing an even number of waveguide elements. In contrast, any path from the Input to Output Point 2 involves traversing an odd number of waveguide elements. In fact it is true for any two points on the rectilinear waveguide mesh that the length of *every* route between them involves either an exclusively even number of waveguide elements or an exclusively odd number of waveguide elements. It is not possible to find a pair of points where there exists two routes between them, one consisting of an odd number of waveguide elements and the other consisting of an even number. This property has a significant implication for any RIR measurement made from the rectilinear mesh that is not immediately apparent. This is due to a smooth Gaussian pulse being used as the excitation signal, applied over a number of iterations, masking the resultant effect in the time domain - although not in the frequency domain as is evident from the frequency response plots presented in this chapter. The reason a smooth impulse is used is to apply sufficient energy to the mesh in order to generate a propagating wave of a significant amplitude whilst minimising possible high frequency distortion. If a single Dirac impulse is applied as the excitation signal, the resulting RIR has a higher noise floor but the time domain implications of this odd/even path length property are clearly evident as shown in Figure 6.12:

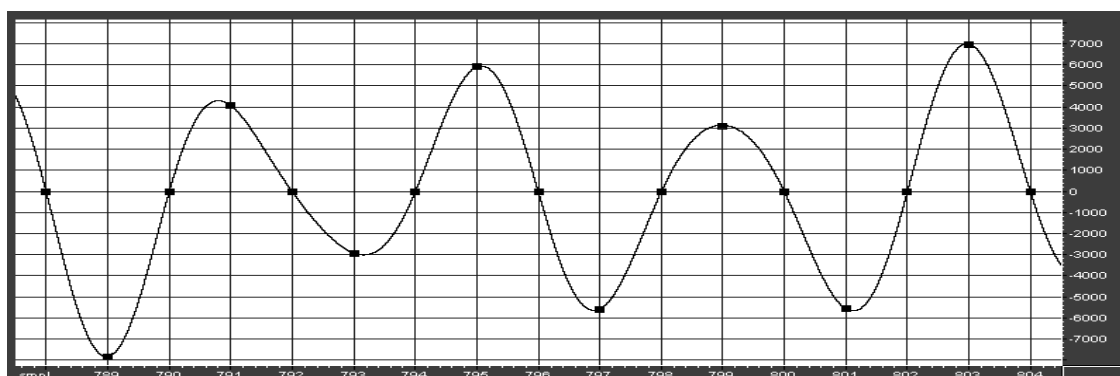


Figure 6.12 A close up view of a RIR measurement taken from the rectilinear mesh with the Dirac impulse used as the excitation signal. Note that every other sample value is equal to zero.

The close-up view of the RIR measurement shown in Figure 6.12 reveals that every other sample value is exactly zero. Considering Figure 6.11 it can be seen why this is the case. The shortest path length between the Input and Output Point 2 is 3 waveguide elements. Therefore it will take a single impulse 3 time steps to travel this distance after time $t = 0$, giving the first non-zero sample value in the RIR at time $t = 3$. The two next longest paths are both 5 waveguide elements long taking 5 time steps, giving a non-zero value at time $t = 5$. Similarly the next longest paths will be 7 waveguide elements long, take 7 time steps and arrive at time $t = 7$. However as there are no even path lengths between the Input and Output Point 2, the RIR sample values at $t = 4, t = 6, t = 8, \dots$ will always be zero. Therefore any RIR measured from a rectilinear mesh is effectively under-sampled, and has a bandwidth - ignoring any additional detrimental effects due to dispersion - that is only valid up to $0.25 \times f_{update}$ rather than $0.5 \times f_{update}$ as would be expected normally according to the Sampling Law [Lynn and Fuerst, 1996]. The resonant peak that is clearly evident in the frequency response plots for the measured RIRs, and about which this “mirroring” of the frequency response actually occurs, can be seen to equal this expected value of $0.25 \times f_{update}$. Further, due to this aliasing of the frequency response the natural pass-band cut-off point of the rectilinear mesh, clearly evident in the triangular mesh results, cannot be clearly identified from these graphs. This aliasing effect does not occur on the triangular mesh as between any two junctions there can be seen to be at least two paths, with one taking an even number of time steps and the other taking an odd number. This implies that every sample in the RIR will have a non-zero value and so the signal will not be under-sampled.

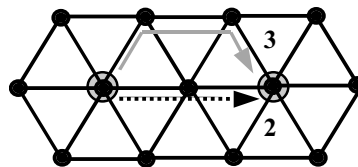


Figure 6.13 Path lengths on the triangular mesh: There always exists an odd length and an even length path between any two points and so the output signal is not under-sampled.

This property of the periodicity of the transfer function about $0.25 \times f_{update}$ has been previously noted for the case of an arbitrary number of elementary, connected tubes - essentially a series of 1-D waveguides - as used to model the human vocal tract [Rabiner and Schafer, 1978]. The minimum time before a signal partially reflected at a scattering junction can influence the conditions at any tube junction is equal to the time taken for the reflected component to return to the previous junction and then be reflected back to the point under consideration, hence always resulting in an even number of tube lengths being traversed.

It would therefore seem that from these results the triangular waveguide mesh gives a more “accurate” RIR frequency response than the rectilinear mesh. The term “accurate” implying

that given that the two meshes are of equal density, and ignoring additional detrimental dispersion error effects, the triangular mesh is valid for up to one-third of the value of f_{update} whereas the rectilinear mesh is only valid for up to one-quarter of the value of f_{update} .

There are further points that can be noted from these results. In all cases the low frequencies present in the frequency response, including the room modes, become more heavily damped with time in the rectilinear mesh than in the triangular mesh. Due to the relatively small size and associated resonant properties of these modelled structures when considering low frequency sound waves, it would be expected to notice the room modes being a dominant acoustic feature. Clearly the heavy attenuation in the low frequency region that is present in the case of the rectilinear mesh prevents this from being the case. Associated with this is the fact that in general the frequency response results from the triangular mesh are more consistently flat across all measurements, including this low frequency region, this being a more desirable property for most rooms. In fact for some rooms and halls designed for musical performance an increase in the level of the low frequency region is the desired effect [Howard and Angus, 1996].

Note that in nearly all cases for Output Point 3 there is a much improved correlation between the two mesh topologies in the low frequency region. This correlation is most noticeable when the absorption in the room is high (Abs0.4 and AbsComplex). It is suggested that this could be related to what is known as the *boundary effect* [White, 1995b]. When listening to a sound source in a room close to a large, hard reflective surface, there is an associated rise in the low frequency response due to these waves being reflected from the surface in phase with the incident waves. This property in effect doubles the amount of perceived bass that is heard. Output Point 3 is close to the North (top) wall and in the case of Room A, the East (right) wall, suggesting that this could be the case. However Output Point 4 is also close to the South (bottom) wall in Room A and Room B yet no such correlation exists. Further there is no associated lift in the bass response of the triangular mesh, although the generally linear frequency response properties of this topology could mean that the effect is less noticeable. Given that this correlation is quite prominent and consistent over the results presented here, yet is *only* a function of position and mesh topology suggests that it is most likely due to the directionally dependent nature of the rectilinear mesh, perhaps working in tandem with the boundary effect. Currently the exact reason for this effect still eludes us and more RIR measurements in the locale of Output Point 3 are required to investigate this position dependent effect.

Finally it can be seen from these frequency response plots that both mesh topologies have a substantial and consistent noise floor, manifesting itself as a resonant peak at the cut-off point on the triangular mesh and at $0.25 \times f_{update}$ on the rectilinear mesh. In most cases the triangular

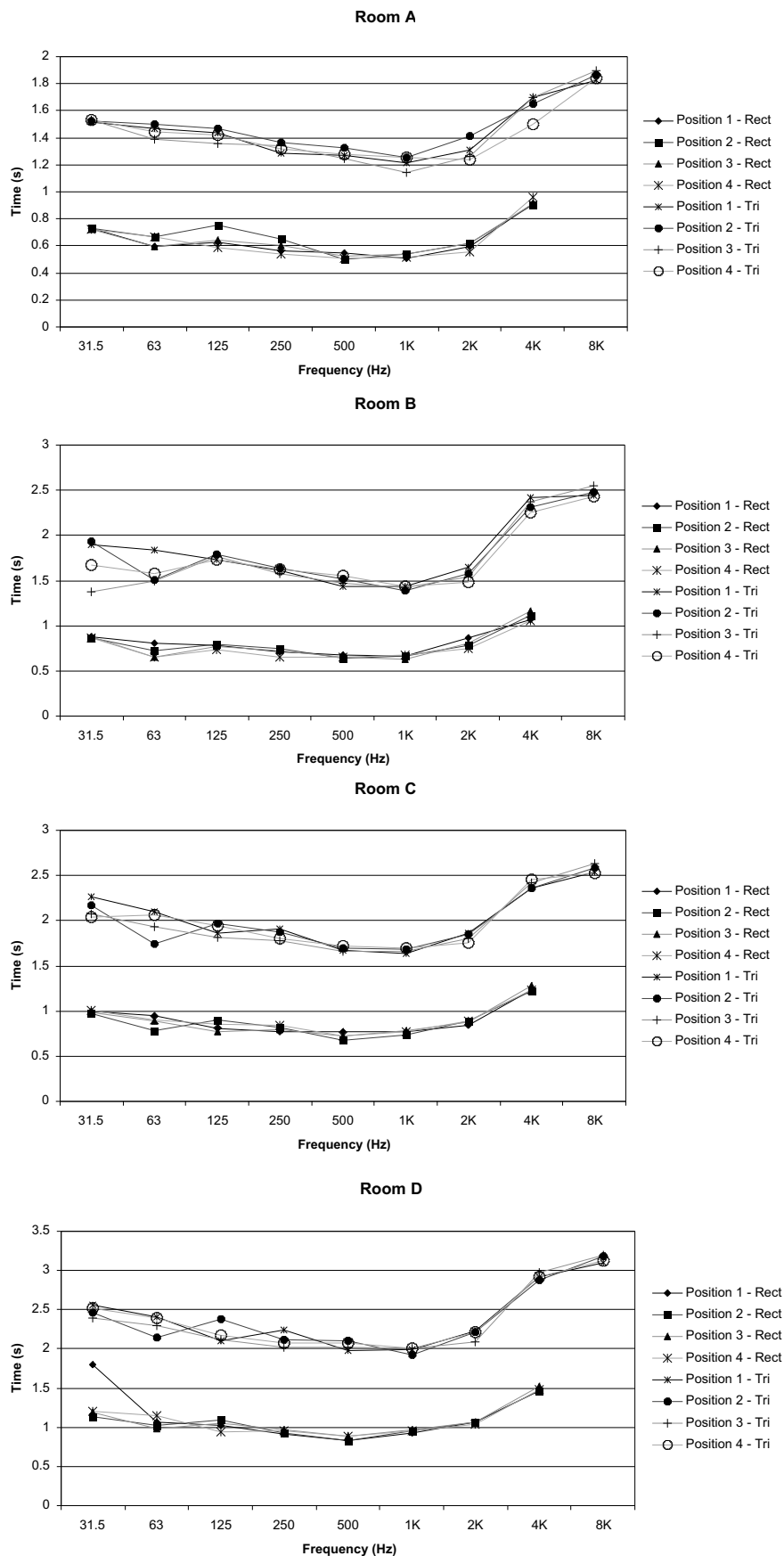
mesh exhibits a double peak, with the second being approximately 1000Hz below $f_{cut-off}$. This resonance remains even after the main body of the RIR containing the majority of its energy has decayed and can be clearly heard in the actual impulse responses presented in Appendix F, CD-2, as a high pitched ring. Note further these resonances can be evidenced for even small mesh models where cumulative errors propagating through the mesh might not be so noticeable. This is mainly due to the discrete nature of the model and truncation and rounding errors in the calculations. As discussed in Chapter 6.2.5, a scattering junction, once disturbed from its initial rest value of $p(n) = 0$, will never actually return to rest, but will rather oscillate by a small yet discrete value either side of zero. The relatively low RIR output signal values have to be normalised when converted into soundfiles resulting in a considerable noise floor as a side effect.

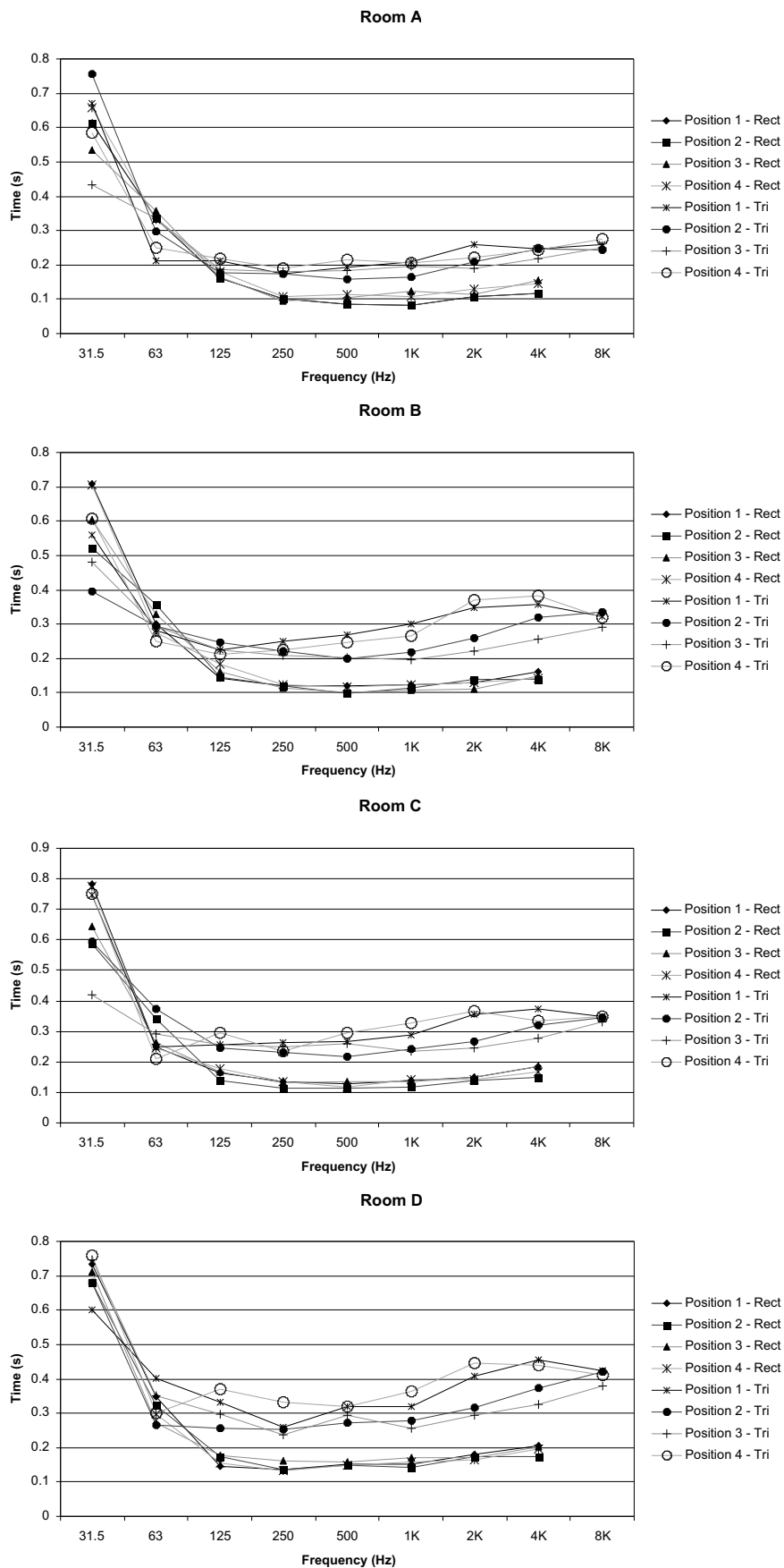
These noise peaks have also been evidenced in [Savioja and Välimäki, 1996], with the rectilinear mesh exhibiting a clear peak at $0.25 \times f_{update}$. However, the triangular mesh is not discussed in this paper, rather the properties of the bilinearly deinterpolated waveguide mesh are described (see also Chapter 4.5.4), which *has* later been shown to have similar properties to the triangular mesh [Savioja and Välimäki, 1999a]. The frequency response of the deinterpolated mesh is very similar to that of the triangular mesh, complete with a double peak and a sharp cut-off at $1/3 \times f_{update}$. However, no explanation for this property is given and more research is clearly required in this area.

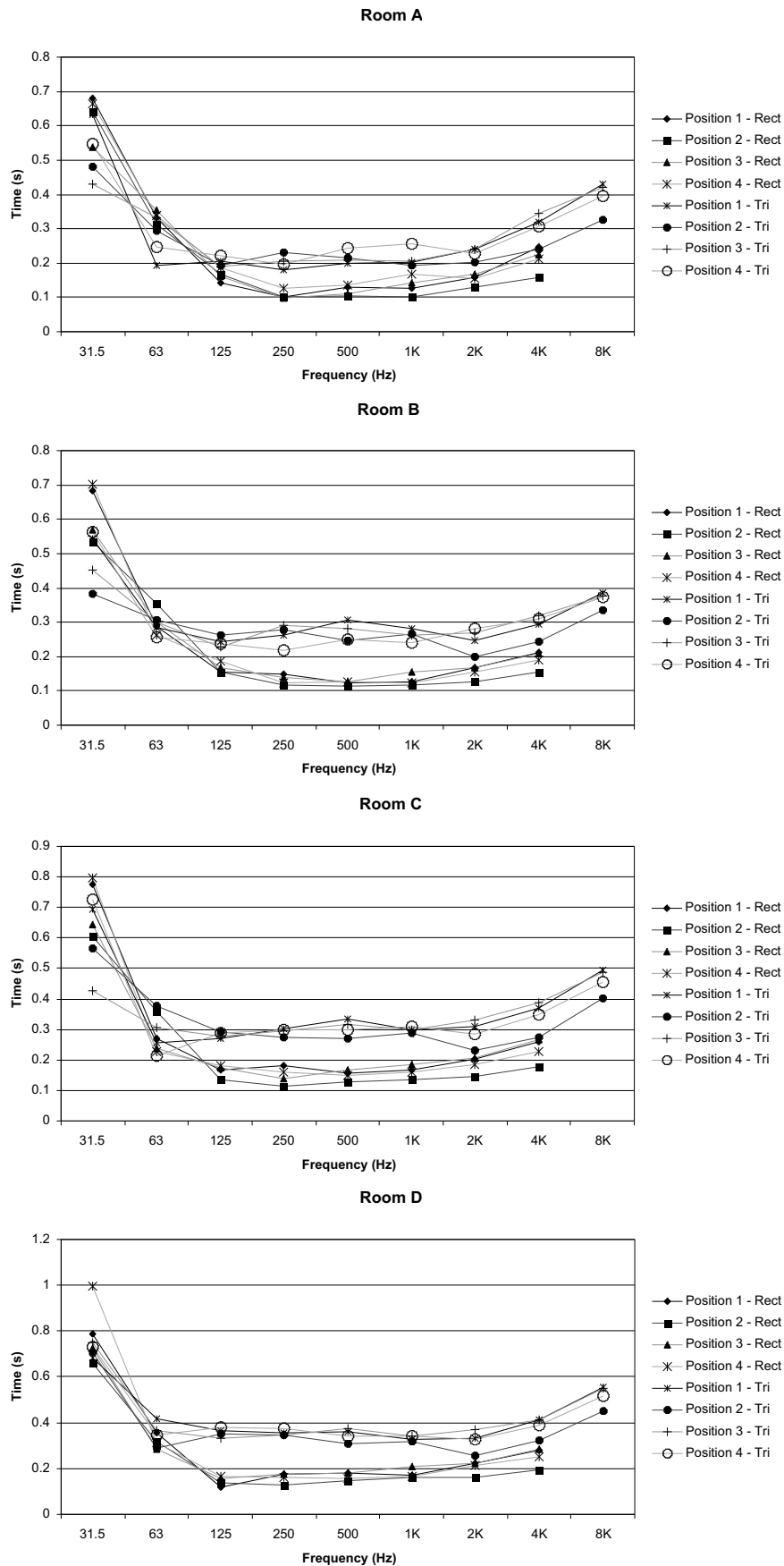
6.6 Acoustic Parameter Analysis

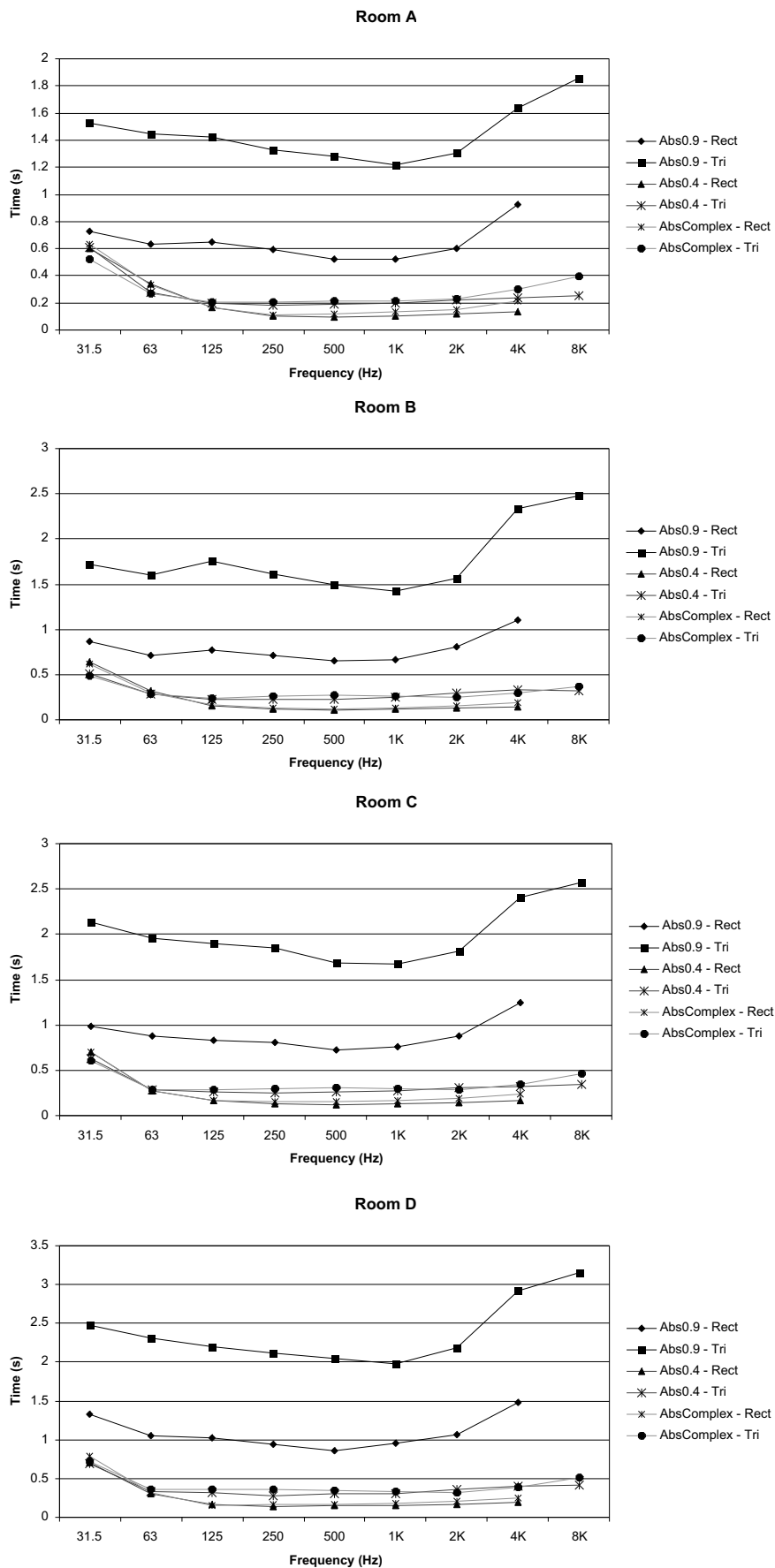
What follows is an analysis of the measured RIRs according to ISO3382 [ISO3382, 1997] and a presentation of appropriate acoustic parameters. These parameters have been extracted from the RIRs using the *Aurora* Acoustic Parameters plug-in extension [Farina and Righini, 1999] for *Cool Edit Pro* [Syntrillium, 1999]. This software tool extracts acoustic parameters from a RIR based on the procedure described in ISO3382 across (in this case) nine octave bandwidths and includes automated noise reduction to improve the signal-to-noise ratio. Note that in the results that follow, the measurement at the bandwidth centred at 8kHz is not always included. It is not always possible for the analysis software to extract a valid value for a particular parameter and this bandwidth correlates with the cut-off points of the mesh topologies in question. The parameters presented here include reverberation time (RT_{60}) based on T_{30} , the early to late sound index or Clarity (C_{80}), and Early Decay Time (EDT) - (see Chapter 2.7 and [ISO3382, 1997]). The RT_{60} measurements include those for each Output Point for each room and for all absorption conditions. It is often applicable to take the arithmetic mean of the reverberation time measurements to give a spatial average for the whole space [ISO3382, 1997] and so these measurements are also included for comparison purposes. Clarity measures will usually vary

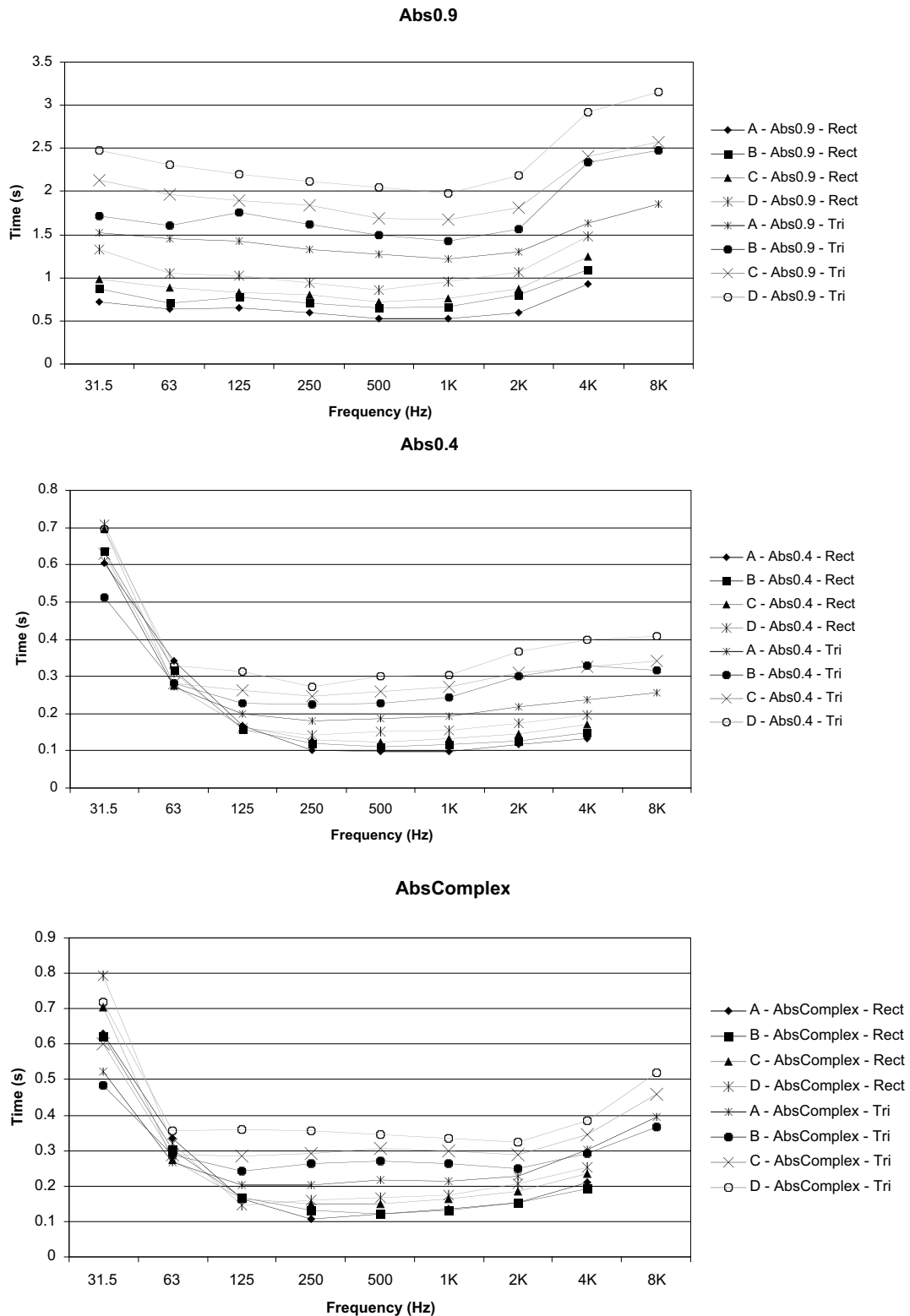
spatially according to source-listener distance and the effect of early reflections and so it is not applicable to take an average measure. Instead the results presented compare the value of C_{80} for Output Point 2 (the closest to the input point) and Output Point 4 (the furthest from the input point) across each room and for all absorption conditions. EDT measures are also included, but inconsistent results mean that they are only shown for each Room under Abs0.9 absorption conditions. Finally a comparison is made between the mean EDT values for each room and the corresponding mean RT_{60} values. All of the results for each RIR, as extracted using *Aurora*, are presented as raw data in Appendix B.

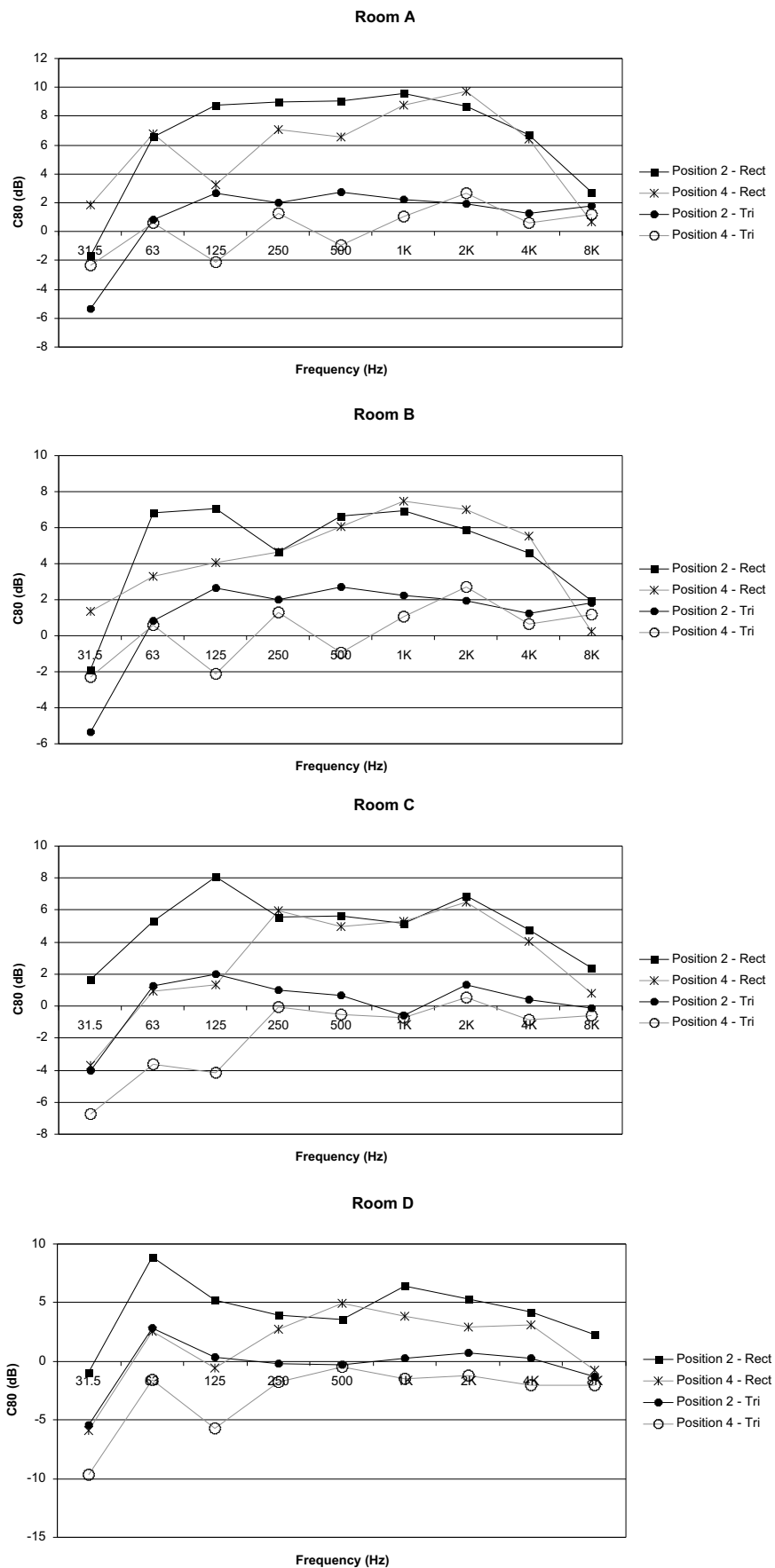
6.6.1 RT_{60} - Abs0.9

6.6.2 RT_{60} – Abs0.4

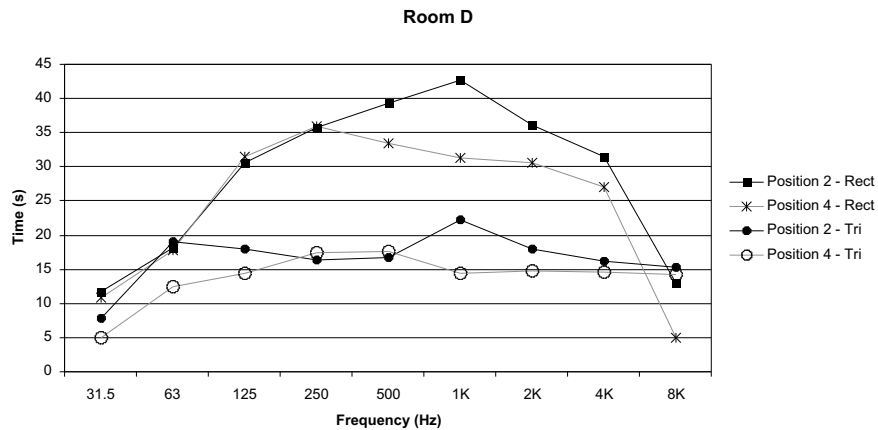
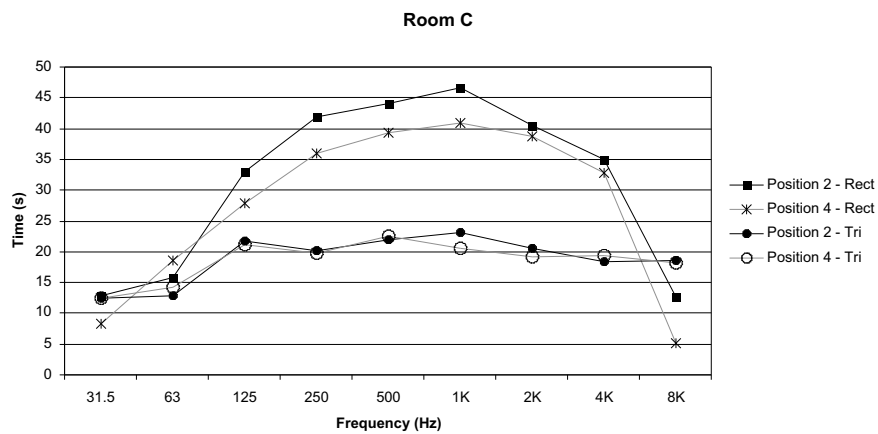
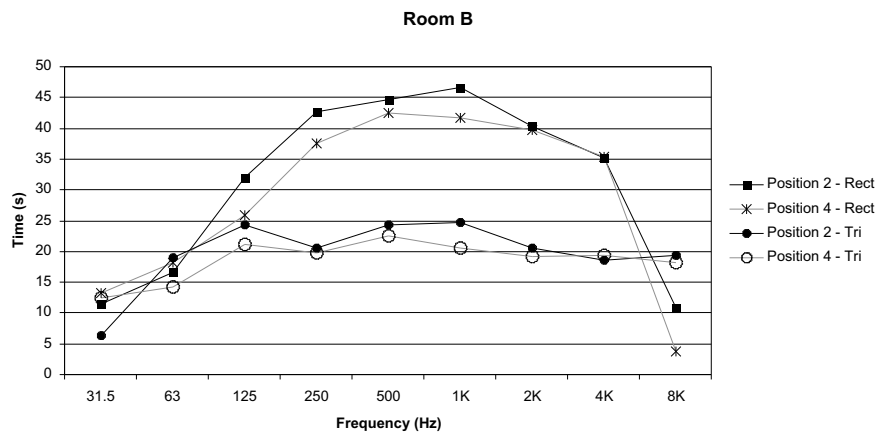
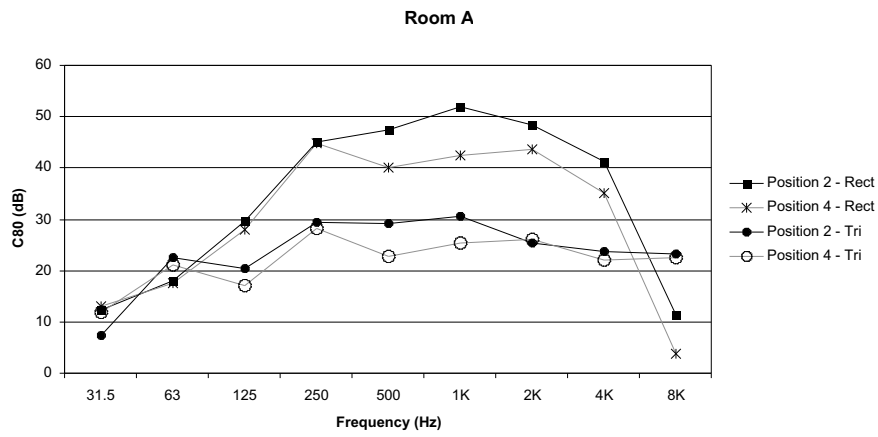
6.6.3 RT_{60} - AbsComplex

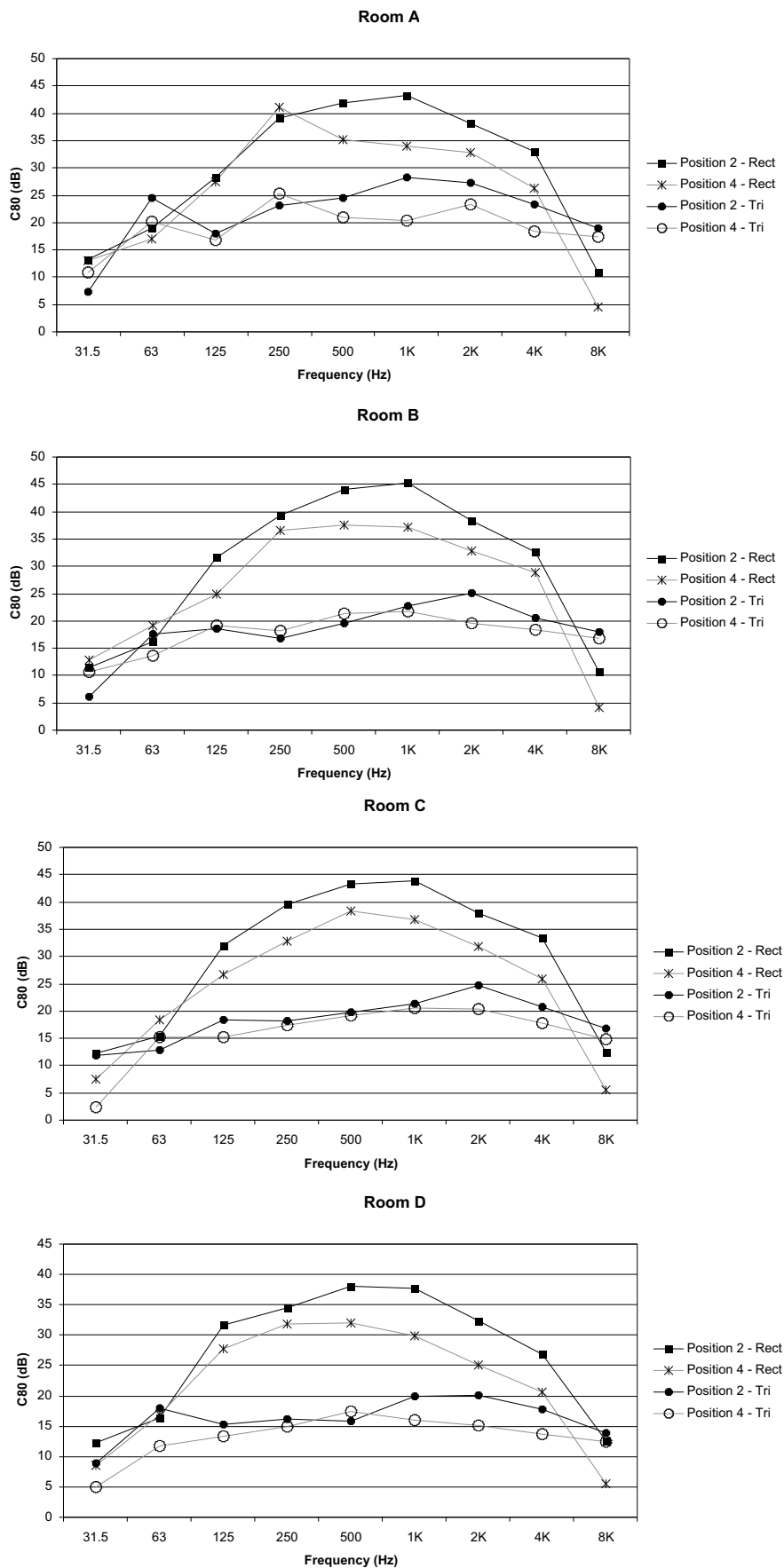
6.6.4 Spatial Average RT_{60} – For Each Room

6.6.5 Spatial Average RT_{60} – For Each Absorption Condition

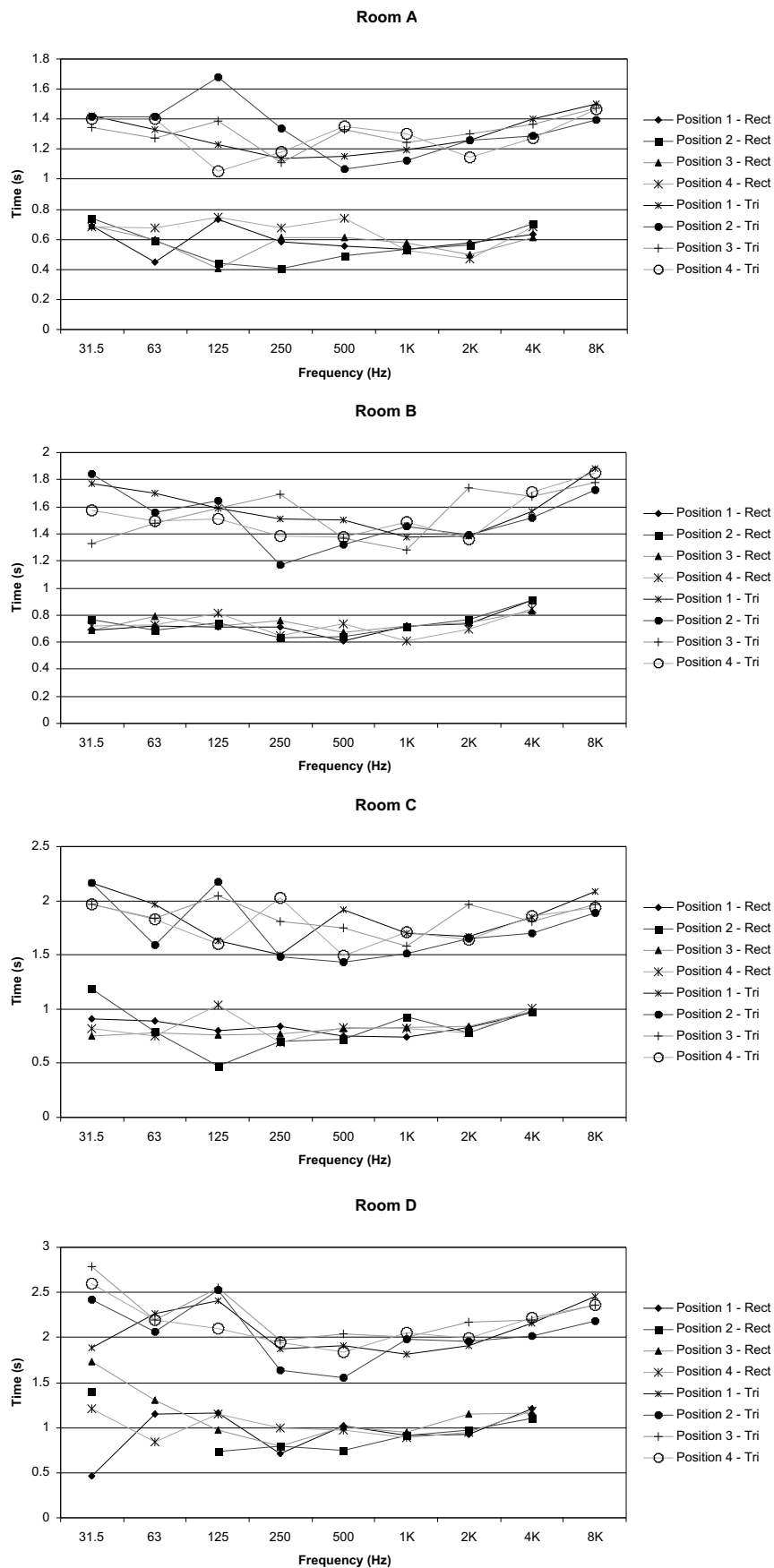
6.6.6 C_{80} – Abs0.9

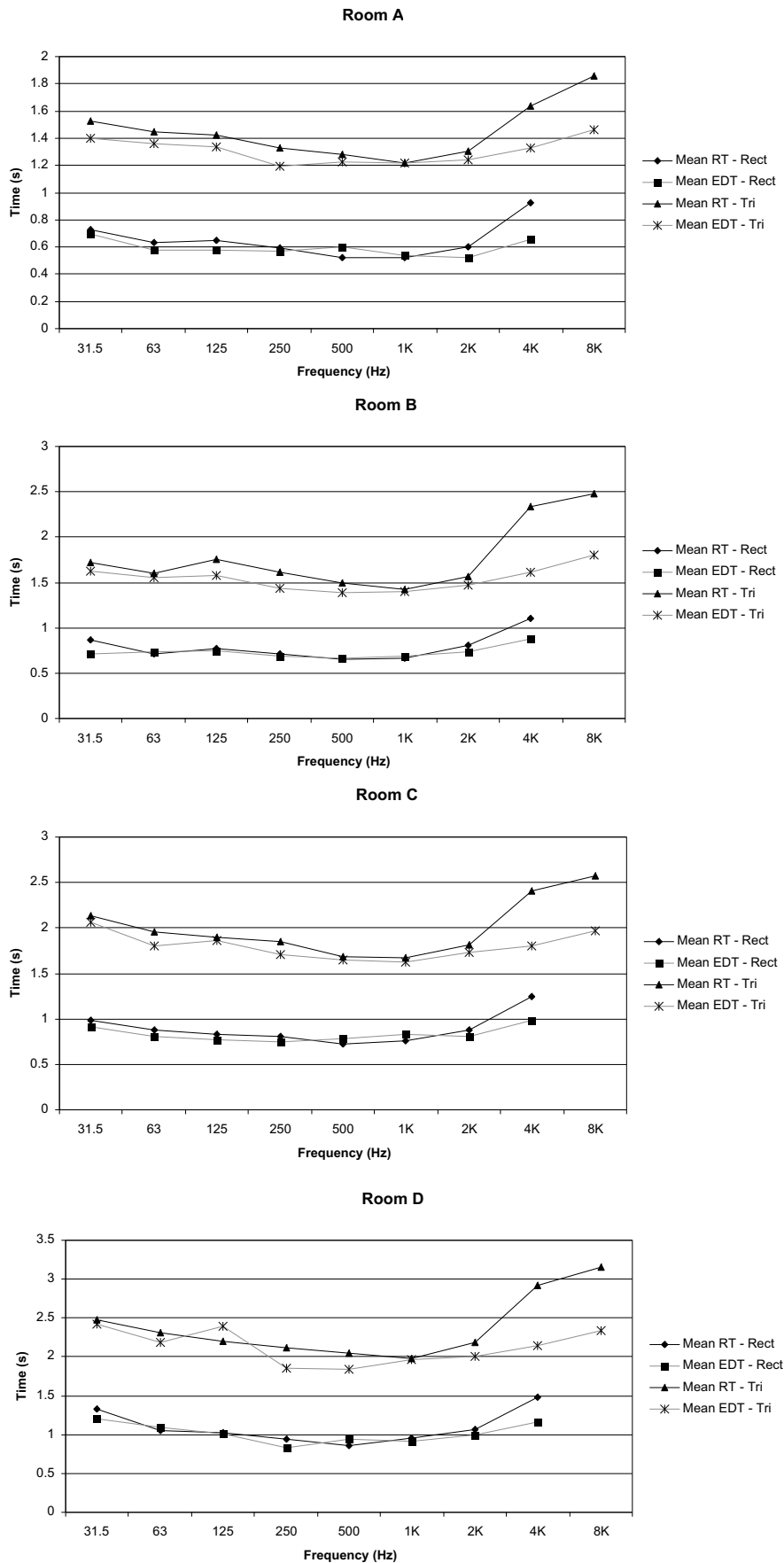
6.6.7 C₈₀ – Abs0.4



6.6.8 C_{80} – AbsComplex

6.6.9 EDT – Abs0.9



6.6.10 EDT and RT_{60} - Spatially Averaged - Abs0.9

6.6.11 Discussion

Reverberation Time Measurements

Notice first that the RT_{60} measurements for both topologies are generally consistent across all four output points for each room and for each set of absorption coefficients agreeing with the principle that the reverberant sound in a room is diffuse, visiting all parts of the room with equal probability (see Chapter 2.3). This also establishes the spatially averaged graphs shown in 6.6.4 and 6.6.5 as valid measurements. These spatially averaged RT_{60} values reveal more clearly the overall reverberant properties of the rooms modelled and the mesh used. If both mesh topologies are compared, then for every room, and for each set of absorption conditions the triangular mesh results in a longer reverberation time. This difference in the RT_{60} values between mesh topologies can also be observed in the sonogram frequency response plots. It can be seen consistently across every pair of results that the RIR measured from the rectilinear mesh decays quicker than that from the triangular mesh. This is particularly noticeable in the low frequency region.

The clearest difference in RT_{60} values can be observed in the Abs0.9 cases. Considering the physical properties of the modelled rooms for these examples, setting the absorption coefficients at each wall to only $r = 0.9$ implies that there will be relatively little energy absorbed at each reflection, in turn implying a long RT_{60} value even though the rooms in question are quite small. This would suggest that the longer RT_{60} value produced via the triangular mesh topology is actually closer to the what would be expected if this 2-D room were a physical reality.

Attempts were made to arrive at an independent RT_{60} value for the Abs0.9 case for Room D using the Sabine Equation (see Chapter 2.7.1). Two approaches were used, the first assumed that Equation (2.9) could be simply reduced in dimensionality to consider areas rather than volumes, and one-dimensional lengths rather than areas. The second extended the modelled room to a third dimension with total absorption at both the ceiling and floor and used the standard Sabine Equation. Both methods assumed that the reflection coefficients paralleled real-world absorption coefficient values, with a reflection coefficient of 0.9 giving a corresponding absorption coefficient of 0.1. Both methods estimated RT_{60} values in the order of 4.0 - 4.5s. This would indicate that the longer RT_{60} values in the region of 2.5 – 3.0s produced using the triangular mesh topology *are* actually closer to what might be expected in the real world than those produced using the rectilinear mesh (1.0 - 1.5s). However, it was felt that the assumptions made in arriving at this result were too great to give a reliable metric against which the mesh results could be compared.

Although this apparently large difference in RT_{60} does not seem to be as common for the other absorption conditions there is actually a common trend. In general it would seem that, apart from in the lowest bandwidths, the RT_{60} value for the triangular mesh is approximately twice that of the rectilinear mesh. The lowest two bandwidths do not agree with this as they yield similar values. This is probably due to difficulties in calculating an accurate value for RT_{60} . The low level of absorption present in the Abs0.9 case will give a relatively long decay across all frequencies. This even takes into account the fact that there is increased damping in the low frequency region for the rectilinear mesh, a fact that is highlighted by examining the frequency response results in the previous section. This low level of absorption implies that an accurate calculation of RT_{60} based on the linear least squares regression of the measured decay curve is relatively easy, particularly as it is based on the value T_{30} , the rate of decay from 5dB below the initial level to only 35dB below. The greater levels of absorption in the Abs0.4 and AbsComplex cases will result in a significantly shorter decay curve, with the noise floor inherent in these mesh models becoming more problematic for an accurate calculation. The increased damping that is evident in the low frequency region will further hinder an accurate measurement. This problem is confirmed by examining the values for RT_{60} based on T_{30} and T_{20} in Appendix B, for the Abs0.9 cases when compared against the other absorption conditions. Note that T_{20} refers to the value of RT_{60} based on a decay rate measured from 5dB below the initial level to 25dB below. There is some variation in the values of T_{30} and T_{20} across all rooms for the Abs0.4 and AbsComplex cases, particularly in the lower bandwidths, whereas they are in much closer agreement for the Abs0.9 absorption conditions across all frequencies. If the RIR has been measured carefully with a low noise floor compared with the initial level, the RT_{60} values as calculated using T_{20} and T_{30} should be close to being equal, given a monotonic decay. Note that non-monotonic decay can be the result of particularly problematic room modes or acoustically coupled spaces [Everest, 1994].

As the room size increases so do the RT_{60} values, and as the absorption increases the RT_{60} values decrease. Both of these properties are in agreement with what would be expected for a real 3-D space. There is also a general trend in that the RT_{60} values for the upper and lower bandwidths are slightly higher than for the middle range. The rise in the lowest bandwidth can be attributed to room modes due to the highly regular geometries of the rooms studied. It is also highly likely that the rise in the highest bandwidth is due to the effect of resonant peaks at $0.25 \times f_{update}$ for the rectilinear mesh and $f_{cut-off}$ for the triangular mesh.

Clarity Measurements

Perhaps surprisingly the C_{80} measures are generally higher for the rectilinear mesh indicating that the early sound is more prominent than the diffuse reverberant field. However this result follows on naturally from the RT_{60} measurements as a high level of reverberant sound will give

poor clarity for both speech and music and hence a low value for C_{80} . It can be seen that out of the two measurements shown in each case, Position 2 - being the shorter of the two direct line distances between input and output - gives a higher value for C_{80} than Position 4. This is another property in agreement with experience of real acoustic spaces as the intelligibility of a source in a highly reverberant space can be improved upon by moving closer to it so increasing the ratio of early to late arriving sound. Similarly C_{80} generally increases as the absorption in the modelled rooms increases and decreases as the room size increases, again agreeing (inversely) with the RT_{60} properties discussed above.

Early Decay Time Measurements

The properties of the EDT measurements generally agree with those of the RT_{60} measurements, as would be expected although there is greater variation in values across positions for each mesh topology. This variation could be due to the decay of position dependent room modes. When the spatially averaged EDT and RT_{60} values are compared they are in close agreement, again as expected as the two parameters are essentially equivalent. However, the EDT values for the triangular mesh are slightly higher than the corresponding RT_{60} values. This would indicate that the first part of the RIR decay carries slightly more energy than the late part, giving a fast initial decay followed by a slowly decaying tail [Tronchin and Farina, 1997]. In the case of these simplified rectangular rooms this is probably due to modal decay, although it is generally a desirable property of multi-purpose spaces as it gives good clarity and intelligibility for speech and singing, whilst music will benefit from the liveness present due to the high reverberation time.

6.7 Audio Examples

Some of the measured RIRs presented have been used to process audio samples in order to analyse the resultant effect and to see if the samples have the environmental context of the modelled room imposed upon them. All of the processing briefly described below has been carried out within the *Cool Edit Pro* software package.

Before these RIRs are used creatively in this manner, frequency domain noise reduction is applied to improve the overall signal-to-noise ratio using tools within *Cool Edit Pro*. This involves performing a frequency analysis of the last 0.5s of the required RIR using a 4096 point FFT. This process assumes that by this point in time the actual required RIR information has decayed below the noise floor and that the remaining noise present in the signal is consistent across the whole length of the soundfile. Upon selecting the whole of the RIR and applying the noise reduction process again, the original noise profile based on the last 0.5s of the RIR is removed from the whole file by inverse filtering in the frequency domain. This helps to reduce

the effect of the large resonant peaks around $f_{cut-off}$ and f_{update} for the triangular and rectilinear mesh topologies respectively. The RIR is then truncated after it has decayed, using visual and aural cues to dictate the actual truncation point. This is because the length of the measured RIR is invariably longer than the actual useful RIR measurement. Finally the RIRs measured from the rectilinear mesh are low-pass filtered at $f_{cut-off}$ to remove the aliased part of the signal.

A number of different sampled sound sources have been used as follows:

- anechoic recorded speech (female)
- anechoic recorded acoustic guitar
- close-miked drum kit
- close-miked singing (female)
- sampled acoustic piano

Each sample has been convolved with RIRs measured from Room D, being the largest of the four rooms modelled. The samples are presented on the accompanying audio CD (see Appendix E, CD-1) alternately in pairs for the rectilinear RIR and the triangular RIR varying according to the actual RIR measured and used. The first two sets of examples are based around the anechoic speech (Tracks 1-26) and guitar samples (Tracks 27-52) convolved with each RIR measured from Room D as follows:

- Original Sample
- Rectilinear Mesh, Abs0.9, Position 1
- Triangular Mesh, Abs0.9, Position 1
- Rectilinear Mesh, Abs0.9, Position 2
- Triangular Mesh, Abs0.9, Position 2
- Rectilinear Mesh, Abs0.9, Position 3
- Triangular Mesh, Abs0.9, Position 3
- Rectilinear Mesh, Abs0.9, Position 4
- Triangular Mesh, Abs0.9, Position 4
- Rectilinear Mesh, Abs0.4, Position 1
- Triangular Mesh, Abs0.4, Position 1
- Rectilinear Mesh, Abs0.4, Position 2
- Triangular Mesh, Abs0.4, Position 2
- Rectilinear Mesh, Abs0.4, Position 3
- Triangular Mesh, Abs0.4, Position 3
- Rectilinear Mesh, Abs0.4, Position 4
- Triangular Mesh, Abs0.4, Position 4
- Rectilinear Mesh, AbsComplex, Position 1

Triangular Mesh, AbsComplex, Position 1
Rectilinear Mesh, AbsComplex, Position 2
Triangular Mesh, AbsComplex, Position 2
Rectilinear Mesh, AbsComplex, Position 3
Triangular Mesh, AbsComplex, Position 3
Rectilinear Mesh, AbsComplex, Position 4
Triangular Mesh, AbsComplex, Position 4
Triangular Mesh, AbsComplex, Position 4 – Stereo RIR.

The following three sets of examples are based around the drum (Tracks 53-60), singing (Tracks 61-68) and piano (Tracks 69-76) samples. Each sample is convolved with the RIR measured at Position 4 from Room D for each set of absorption conditions as follows:

Original Sample
Rectilinear Mesh, Abs0.9, Position 4
Triangular Mesh, Abs0.9, Position 4
Rectilinear Mesh, Abs0.4, Position 4
Triangular Mesh, Abs0.4, Position 4
Rectilinear Mesh, AbsComplex, Position 4
Triangular Mesh, AbsComplex, Position 4
Triangular Mesh, AbsComplex, Position 4 – Stereo RIR.

Note that all samples are in mono apart from the last in each series. This example has been convolved with a stereo RIR measurement in order to demonstrate this output format from the triangular mesh. A full track listing to the accompanying audio CD is supplied in Appendix C.

6.7.1 Discussion

A number of features are apparent in the processed audio samples. The most obvious is the fact that the noise floor is considerably lower on the results from triangular mesh despite noise reduction treatment being applied to both types of RIR. Therefore, even if the listener decides that the rectilinear mesh gives a more natural acoustic effect over the triangular mesh, any benefit is at the detriment of the quality of the overall signal.

It is possible to notice a slight difference in the quality of the acoustic effect as it varies according to listener/output position around the room. This appears to be most noticeable on the samples processed using the AbsComplex absorption conditions. The Abs0.4 and Abs0.9 conditions, as the absorption values are constant over all boundaries, are more likely to produce an acoustic field that is invariable to reverberation, modal distribution and early reflection

patterns across spatial positioning. The AbsComplex absorption conditions vary for each boundary giving a less regular acoustic field and so a more variable response at each of the four output points. However, it should still be noted that this variation is only slight given the regular geometry of the room and its relatively small size.

The drum and guitar samples are particularly interesting as they contain a clearly obvious percussive transient attack at the start of each note/sound. When processed these transients result in a slight, yet noticeable, high frequency resonance. This is in agreement with the observed physical behaviour of both mesh structures in that they do not respond well to high amplitude impulsive signals as this introduces high frequency distortion. Hence the need to use a smooth Gaussian pulse as the mesh excitation signal.

The results from the Abs0.9 absorption conditions are highly reverberant, and this sounds “unrealistic” and “unnatural”. There are two reasons for this. Firstly the room is highly reflective given its relatively small size and this amount of reverberation would usually be associated with a space considerably larger. Therefore the resultant processed audio sounds unrealistic. However this is perhaps an interesting creative effect, and the concept parallels that of reverberation chambers, the first artificial reverberation devices (see Chapter 3.2.1). Secondly this unrealistic sound is further enhanced by the regular geometry of the room and the regular distribution of absorption around the walls. This gives an associated regular quality to the reverberant, similar manner to the way in which the loop time in a comb filter causes this unit reverberator to ring at a specific pitch. This is particularly noticeable in the decay at the end of the singing sample and in the decay of some of the notes of the anechoic recorded guitar. It is in these quieter, decaying passages of sound that the poorer qualities of any reverberation algorithm become apparent.

By far the best results are demonstrated using the RIR measurements taken from the triangular mesh with the AbsComplex absorption conditions. The resulting sounds are full and natural, and do not conflict with the way the space should be perceived in terms of its geometrical features. There is a low noise floor and no evidence of the regularity associated with some of the examples from the other sets of absorption conditions. These results are further enhanced when a stereo RIR is used as can be heard in the additional processed samples for AbsComplex, Position 4. However there is still evidence of high frequency distortion on percussive sounds and on some of the sibilant elements of the spoken female voice.

6.8 Summary

This chapter has presented a series of results based on the current implementation of the *WaveVerb* System where four 2-D “rooms” have been modelled with varying absorption characteristics and RIR measurements. These RIRs have been analysed and presented in different ways revealing a number of important properties about waveguide mesh structures when used for modelling room acoustics.

Standard wave phenomena such as propagation, reflection, diffraction and interference can be clearly observed on the waveguide mesh structures for both mesh topologies, offering an improvement over traditional geometric methods of modelling a RIR. The triangular mesh offers an improvement over the rectilinear mesh as the wavefront present after an impulse has been applied is closer to that of a uniform circle. The deformed shape of the wavefront on the rectilinear mesh is a direct result of the direction dependent dispersion error inherent in this mesh topology. Simulating an anechoic room has revealed that the boundary conditions, although consistent with the mesh construction, and offering a satisfactory solution in that they enable reflection and absorption to be modelled, act to scatter and reflect high frequency waves. Possible alternative solutions to this problem have been presented drawing on some of the ideas used in TLM and waveguide sound synthesis. These solutions involve replacing the currently implemented impedance-based boundary conditions with frequency-dependent, digital filter transfer functions.

The RIR measurements correspond accurately to the low frequency acoustic characteristics of the theoretical rooms being modelled. This is true across all four room sizes and all source-listener output combinations. The relative magnitudes of the modal frequencies in a real room vary with position, and again this can be observed in these results with the relative magnitudes of the resonant peaks varying across each of the four output points. There is also an almost exact correlation between the relative magnitudes for each pair of results for both mesh topologies showing that they are both equally valid for modelling low frequency wave propagation. This is due to the high mesh density used in these models with the effect that dispersion error only becomes apparent at higher frequencies across the valid bandwidth.

Spectral analysis of the RIRs reveals that the triangular mesh frequency response exhibits a well defined cut-off point being the natural upper limit of the mesh above which no frequency can be successfully propagated. This is a common property of all lattice type structures that support wave propagation. The cut-off point is related to the mesh sampling rate and hence the distance between scattering junctions and can be seen to equal $f_{update}/3$, with $f_{update} = 44.1\text{kHz}$ as defined for this particular triangular mesh.

In the case of the rectilinear mesh there is a well defined resonant peak present in all frequency response measurements. Further, the frequency response above this peak is actually a reflection of the frequency response below it. This is due to the fact that for any two points on the rectilinear waveguide mesh the length of *every* route between them involves either an exclusively even number of waveguide elements or an exclusively odd number of waveguide elements. It is not possible to find a pair of points where there exists two routes between them, one consisting of an odd number of waveguide elements and the other consisting of an even number. This results in an RIR measurement where every other sample value is exactly zero, if a Dirac impulse is used as the excitation signal. Therefore any RIR measured from a rectilinear mesh is effectively an under-sampled signal, and has a bandwidth - ignoring any additional detrimental effects due to dispersion - that is only valid up to $0.25 \times f_{update}$ rather than $0.5 \times f_{update}$ as would be expected normally according to the Sampling Law. The resonant peak that is clearly evident in the frequency response plots for the measured RIRs, and about which this “mirroring” of the frequency response actually occurs, can be seen to equal this expected value of $0.25 \times f_{update}$. This aliasing effect does not occur on the triangular mesh, as between any two junctions at least two paths exist, with one consisting of an even number of waveguide elements and the other consisting of an odd number. This implies that every sample in the RIR will have a non-zero value and so the signal will not be under-sampled. This property has already been identified in the similar case of the 1-D waveguide model of the human vocal tract.

In all cases the low frequencies present in the frequency response, including the room modes, become more heavily damped with time in the rectilinear mesh than in the triangular mesh. Associated with this is the fact that in general the frequency response results from the triangular mesh are consistently flatter across all measurements, including this low frequency region.

Both mesh topologies also have a substantial and consistent noise floor, manifesting itself as a resonant peak at the cut-off point on the triangular mesh and at $0.25 \times f_{update}$ on the rectilinear mesh. This is mainly due to the discrete nature of the model and truncation and rounding errors in the calculations.

A number of standard acoustic parameters have been examined in relation to each RIR measurement. RT_{60} values for both topologies are generally consistent across all four output points for each room and for each set of absorption coefficients agreeing with the principle that the reverberant sound in a room is diffuse, visiting all parts of the room with equal probability. If both mesh topologies are compared then for every room, and for each set of absorption conditions the triangular mesh results in a longer reverberation time, approximately twice that of the rectilinear mesh. However this is not consistent across the lower bandwidths of rooms

with higher levels of absorption due to the difficulties in making an accurate measurement. As the room size increases so do the RT_{60} values, and as the absorption increases the RT_{60} values decrease. Both of these properties are in agreement with what would be expected for a real 3-D space.

C_{80} measures are generally higher for the rectilinear mesh indicating that the early sound is more prominent than the diffuse reverberant field. However this result follows on naturally from the RT_{60} measurements as a high level of reverberant sound will give poor clarity for both speech and music and hence a low value for C_{80} . It can be seen that out of the two measurements shown in each case, Position 2 - being the shorter of the two direct line distances between input and output - gives a higher value for C_{80} than Position 4. This is another property in agreement with experience of real acoustic spaces. C_{80} generally increases as the absorption in the modelled rooms increases and decreases as the room size increases, again agreeing (inversely) with the RT_{60} measurements.

The properties of the EDT measurements generally agree with those of the RT_{60} measurements, as would be expected. When the spatially averaged EDT and RT_{60} values are compared they are also in close agreement, again as expected as the two parameters are essentially equivalent.

Finally some of the RIR measurements have been convolved with a number of varied audio samples to investigate the resultant audio effect. The noise floor is considerably lower on the results from triangular mesh despite noise reduction treatment being applied to both types of RIR. It is possible to notice a slight difference in the quality of the acoustic effect as it varies according to listener/output position around the room. This appears to be most noticeable on the samples processed using the AbsComplex absorption conditions. The Abs0.4 and Abs0.9 conditions, as the absorption values are constant over all boundaries, are more likely to produce an acoustic field that is invariant with respect to reverberation, modal distribution and early reflection patterns across spatial positioning.

Sounds or notes with a percussive transient attack, when processed, result in a slight, yet noticeable, high frequency resonance. This is in agreement with the observed physical behaviour of both mesh structures in that they do not respond well to high amplitude impulsive signals as this introduces high frequency distortion.

The best acoustic effect is demonstrated using the RIR measurements taken from the triangular mesh with the AbsComplex absorption conditions. The resulting sounds are full and natural, and do not conflict with how the space should be perceived in terms of its geometrical features. There is a low noise floor and no evidence of the regularity associated with some of the

examples from the other sets of absorption conditions. These results are further enhanced when a stereo RIR is used. However there is still evidence of high frequency distortion on percussive sounds and on some of the sibilant elements of the spoken female voice.

Chapter 7

Conclusions

7.1 Summary and Conclusions

The goal of this thesis was to investigate the use of digital waveguide mesh structures as a modelling paradigm applicable to the problem of room acoustics, with an emphasis on their use as applicable to computer based musical composition. In particular this thesis has attempted to demonstrate that this novel implementation of the triangular waveguide mesh offers a significant improvement in terms of quality and accuracy over the more commonly implemented rectilinear topology. This chapter begins with a re-statement of the hypothesis on which this thesis is based, summarises the methods by which these research goals have been achieved, and draws conclusions from the results obtained. This chapter then identifies directions in which the work may usefully be extended in the future, and finally outlines the publications that have resulted from the novel aspects of this work.

7.1.1 Hypothesis

The triangular digital waveguide mesh is a paradigm applicable to the problem of successfully modelling the acoustics of an enclosed space, offering a significant improvement in quality and accuracy over that of the more commonly used rectilinear digital waveguide mesh.

This hypothesis has been supported in three ways:

1. Theoretically, by examining the underlying principles and properties of the triangular and rectilinear waveguide mesh topologies, with particular emphasis on their dispersion error characteristics.
2. Practically, using a wide variety of both visual and audio examples showing how the waveguide mesh structures behave, and how measured RIRs can be used successfully or otherwise to impart an environmental context on the source material.
3. Analytically, by comparing the measured RIRs from both mesh topologies against theoretical expectation and standardised acoustical parameters.

This thesis started by examining the general acoustic properties of a room, identifying the characteristic growth of sound and introducing the concepts of direct sound, early reflections,

reverberation and room modes. The Room Impulse Response was introduced as a unique measurement of the source/listener/ room system combination, from which it should be possible to determine the characteristic features of sound propagation in an enclosed space. It was concluded that:

The RIR is fundamental to the successful musical use of any such wave propagation/room acoustic model because when used in a convolution signal processing operation it becomes the digital realisation of the virtual space.

The RIR can also be used for qualitative analysis of the space being modelled, and hence the model itself, via the use of frequency domain analysis, and comparison of acoustical parameters according to ISO3382.

Visual feedback is also important, for both analysing purposes and for enabling high level control and definition of model parameters.

Investigating a number of generic, explicit and exact room acoustic simulation methods lead to the introduction of digital waveguide mesh models. Their potential use as a tool for modelling physical objects was discussed. The benefits they offered over other comparable models were highlighted as follows:

simplicity of the basic model

complexity of the resulting wave propagation, closely simulating natural wave phenomena

flexibility in terms of the two and three-dimensional structures they are capable of simulating

potential for visualisation and user interaction with the physical model

their partial success to date in modelling the acoustics of a room.

A survey of previous analytical studies highlighted the potential of the hypothesis as stated above. Out of all the potential 2-D mesh topologies, the triangular mesh can be shown to minimise the dispersion error that is inherent in all lattice based models, reducing it to being a function of frequency only, rather than frequency and direction of wave propagation. A number of conclusions were also reached as to how the hypothesis should be tested in terms of the model implementation:

The model would be implemented in two dimensions only.

Mesh sampling rates must be selected so that they correspond to industry standard audio sampling rates.

The mesh models were implemented in software using the C programming language on a generic Silicon Graphics UNIX workstation running the IRIX operating system and supporting the OpenGL graphics library.

The high mesh sampling rates imply that the model will be considered as an offline process only.

Based on this specification the detailed theory behind the rectilinear and triangular waveguide mesh structures was covered. This included how the mesh is terminated at a boundary and introduced the concept of scattering junction types, with ten junction types being identified for the rectilinear mesh and twenty for the triangular mesh. Mesh input and output was examined and a detailed analysis and comparison of the dispersion error present in both concluded that:

Dispersion error is reduced on the triangular mesh when compared to the rectilinear mesh.

Dispersion error is virtually independent of the direction of propagation on the triangular mesh unlike the rectilinear mesh that displays very different errors for diagonal and axial propagation. Therefore on the triangular mesh the dispersion error is further reduced to being a function of frequency only.

The waveguide mesh models were introduced as being implemented as part of the *WaveVerb* Digital Waveguide Mesh Reverberation System. A number of software design considerations for the various constituent *WaveVerb* elements were explored. This included:

Memory optimisation techniques, required due to the significantly large data structure that is the result of defining a large audio bandwidth waveguide mesh.

Definition and arrangement of the mesh structure given a limited set of high level instructions based on room size and absorption conditions.

The basic three stage waveguide mesh algorithm, consisting of an initialisation stage, the scattering pass and the delay pass.

An overview of visualisation and rendering techniques within OpenGL.

Part of the software design process specified that the model should be capable of storing an output as a number of file formats allowing compatibility with other software and the potential for further development. The actual RIR output formats from the mesh were specified as:

single channel mono

two channel stereo

horizontal-only three-channel Ambisonic B format.

A number of tests and simulations were performed on the *WaveVerb* models, for both the rectilinear and triangular mesh topologies on a number of 2-D “rooms” with varying absorption characteristics and source/listener combinations.

Standard wave phenomena can be clearly observed on the waveguide mesh structures for both mesh topologies, offering an improvement over traditional geometric methods of modelling a RIR. The triangular mesh offers an improvement over the rectilinear mesh as the wavefront present after an impulse has been applied is closer to that of a uniform circle. The deformed shape of the wavefront on the rectilinear mesh is a direct result of the direction dependent dispersion error inherent in this mesh topology. However, simulating an anechoic room has revealed that the boundary conditions, although consistent with the mesh construction, and offering a satisfactory solution in that they enable reflection and absorption to be modelled, act to scatter and reflect high frequency waves. A number of possible solutions to this problem drawing on some of the ideas used in the Transmission Line Matrix Method and waveguide sound synthesis have been presented.

The RIR measurements accurately predicted the low frequency acoustic characteristics of the theoretical rooms being modelled. There is also an almost exact correlation between the relative magnitudes of the highlighted room modes for both mesh topologies showing that they are both equally valid for modelling low frequency wave propagation. This is due to the high mesh density used in these models with the effect that dispersion error only becomes apparent at high frequencies.

Spectral analysis of the RIRs revealed that the triangular mesh frequency response exhibits a well defined cut-off point equal to $f_{update}/3$, being the natural upper limit of the mesh above which no frequency can be successfully propagated. In the case of the rectilinear mesh, spectral analysis revealed that there is a well defined resonant peak present in all frequency response measurements. Further, the frequency response above this peak is actually a reflection of the frequency response below it. This is due to the fact that for any two points on the rectilinear waveguide mesh the length of *every* route between them involves either an exclusively even number of waveguide elements or an exclusively odd number of waveguide elements. The implication is that any RIR measured from a rectilinear mesh is effectively an under-sampled signal, and has a bandwidth that is only valid up to $0.25 \times f_{update}$. The resonant peak that is clearly evident in the frequency response plots for the measured RIRs, and about which this “mirroring” of the frequency response actually occurs, can be seen to equal this expected value of $0.25 \times f_{update}$. This aliasing effect does not occur on the triangular mesh as between any two junctions at least two paths exist, with one consisting of an even number of waveguide elements and the other consisting of an odd number.

The spectral analysis also revealed that in general the frequency response results from the triangular mesh are consistently flatter across all measurements. Both mesh topologies also

have a substantial and consistent noise floor, manifesting itself as a resonant peak at the cut-off point on the triangular mesh and at $0.25 \times f_{update}$ on the rectilinear mesh.

A number of standard acoustic parameters have been examined in relation to each RIR measurement. RT_{60} values for both topologies are generally consistent across all four output points for each room and for each set of absorption coefficients agreeing with the principle that the reverberant sound in a room is diffuse, visiting all parts of the room with equal probability. If both mesh topologies are compared then for every room, and for each set of absorption conditions the triangular mesh results in a longer reverberation time, approximately twice that of the rectilinear mesh. However this is not consistent across the lower bandwidths of rooms with higher levels of absorption due to the difficulties in making an accurate measurement. As the room size increases so do the RT_{60} values, and as the absorption increases the RT_{60} values decrease. Both of these properties are in agreement with what would be expected for a real 3-D space. Further, the EDT measurements generally agree with those of the RT_{60} measurements, again as expected as the two parameters are essentially equivalent.

C_{80} measures were generally higher for the rectilinear mesh indicating that the early sound is more prominent than the diffuse reverberant field. However this result follows on naturally from the RT_{60} measurements as a high level of reverberant sound will give poor clarity for both speech and music and hence a low value for C_{80} . Measurement points closer to the input point result in higher values for C_{80} . Similarly, C_{80} generally increases as the absorption in the modelled rooms increases and decreases as the room size increases, again agreeing (inversely) with the RT_{60} measurements.

Finally some of the RIR measurements were convolved with a variety of audio samples to investigate the resultant environmental context. The noise floor is considerably lower on the results from the triangular mesh despite noise reduction treatment being applied to both types of RIR. It is possible to notice a slight difference in the quality of the acoustic effect as it varies according to listener/output position around the room. This appears to be most noticeable on the samples processed using the AbsComplex absorption conditions. The Abs0.4 and Abs0.9 conditions, as the absorption values are constant over all boundaries, are more likely to produce an acoustic field that is invariable to reverberation, modal distribution and early reflection patterns across spatial positioning. Sounds or notes with a percussive transient attack, when processed, result in a slight yet noticeable high frequency resonance due to both mesh structures responding poorly to sharp, impulsive signals at a high amplitude.

The best acoustic effect was demonstrated using the RIR measurements taken from triangular mesh with the AbsComplex absorption conditions. The resulting sounds are full and natural,

and do not conflict with the how the space should be perceived in terms of its geometrical features. There is a low noise floor and no evidence of the regularity associated with some of the examples from the other sets of absorption conditions. These results are further enhanced when a stereo RIR is used. However there is still evidence of high frequency distortion on percussive sounds and on some of the sibilant elements of the spoken female voice. In general this demonstrates that even though these models are limited to being only two-dimensional, careful choice of absorption conditions can lead to a suitably natural environmental context being added to the original sampled audio. In this way the waveguide mesh parallels early electro-mechanical reverberation devices such as the plate reverb.

This evaluation has revealed that:

In general, waveguide mesh structures are applicable to modelling acoustic wave propagation with both model topologies being valid in the low frequency region.

Waveguide mesh structures offer a significant advantage over traditional explicit geometrical modelling techniques as they demonstrate natural wave phenomena such as diffraction and interference as a natural consequence of their implementation.

Theoretically, the triangular waveguide mesh offers a significant improvement over the rectilinear mesh in terms of measured dispersion error.

This result has been confirmed practically, with the effect of this dispersion error having been demonstrated by observing the wavefront of an applied impulse, using a visualisation of the wave propagation on the mesh.

RIRs measured from the rectilinear mesh are under-sampled due to the mesh topology, limiting the effective bandwidth of the result to $0.25 \times f_{update}$. RIRs measured from the triangular mesh are not under-sampled and have been shown to be valid up to $1/3 \times f_{update}$ for the same given sampling rate.

Analysis of acoustical parameters are consistent with real world parallels, with RT_{60} values for the triangular mesh being approximately twice that of the rectilinear mesh, and hence closer to what might be expected of the modelled rooms were they real, given their geometrical shape and relative absorption characteristics.

Both mesh topologies suffer from a significant noise floor although the audio examples show that, after noise reduction has been applied to both measured RIRs, this is perceptually less significant for the triangular mesh.

Careful choice of non-regular absorption values, together with a stereo RIR measurement results in an effective and natural environmental context being added to sampled audio.

Therefore the goals set out in the introduction to this thesis, and re-stated at the start of this chapter have been achieved. The triangular waveguide mesh topology is indeed a model applicable to the problem of successfully modelling the acoustics of an enclosed space, offering

a significant improvement in quality and accuracy over that of the more commonly used rectilinear waveguide mesh topology.

7.2 The Future

It is perhaps appropriate that as this program of research comes to its conclusion, a new generation of room modelling technology, in the form of the Sony DRE 777 Sampling Reverb [Robjohns, 1999], becomes commercially available. This is based on real-time convolution, a process that - working in non-real-time - has been fundamental to this research process. With this technology reaching its maturity the question is raised as to whether there is still a need for “traditional” modelling methods, when a CD-ROM can supply a significant number of accurately captured audio landscapes. However it will no doubt always be the case that the musician, composer or audio engineer will want to alter and edit these virtual realities to suit their own myriad ends. The RIR is only a static snapshot of the measured acoustic space, so how should these additional virtual realities be created given the limited set one is given to work with? Perhaps a near infinite library of RIR snapshots would be required, or a portable, personal RIR capture kit. Or perhaps the reverse engineering of a given RIR to its constituent acoustic environmental elements - enabling high level editing of physical and geometrical parameters - in order to re-synthesize a new virtual RIR could provide the answer (a technique already used in sound synthesis).

It would seem therefore, that even though the technology and methodology may change, the same basic problem that has ultimately driven this thesis will remain: How do we capture the audio landscape we see/hear in our mind’s eye/ear, and auralize it as a virtual or physical reality? As yet there is no way of measuring the impulse response of this unique, complex and esoteric system...

Specific suggestions for further work are detailed in the following section.

7.3 Further Work

7.3.1 Boundary Conditions and Air Absorption

As discussed in Chapter 6.2.5 the boundary conditions as currently implemented are still a crude approximation to reality, giving significant high frequency reflections when simulating anechoic conditions. Associated with this is the fact that the absorption conditions as currently implemented, using the reflection coefficient r , bear a minimal relation to the real world materials that would be found covering the surface of a room, and neither are they frequency dependent. Replacing the impedance relation with a digital filter implementation, designed to

model a real material in a frequency dependent manner, has proven to closely approximate real world conditions for the 2-D rectilinear mesh [Huopaniemi et al, 1997]. However, the directional dependent nature of this topology, as already discussed, results in a directional variance to the accuracy of the results. It is suggested that as the triangular mesh minimises this directional variation, terminating the mesh at a boundary with a digital filter will give a significantly more accurate model. A further improvement would be the ability to model variable diffusion, currently successful in the accurate modelling of a 2-D drum membrane [Laird et al, 1999].

The effect of air absorption is an important factor in larger acoustical spaces, having a low pass filtering effect on sound wave propagation, and being dependent on temperature, humidity and distance. It is possible to describe this effect as a first order Infinite Impulse Response (IIR) filter [Huopaniemi et al, 1997]. This could be included as part of the scattering equations for each junction type, or in order to save complexity and computation time at each junction, “lumped” at the end of each row of junctions as part of the boundary junction equations.

7.3.2 Three Dimensions and Parallel Implementation

Although it has been shown that this 2-D mesh is capable of generating an effective and natural environmental context, for a truly realistic model the current implementation has to be extended to three dimensions. Although this is relatively easy to implement in terms of the scattering equations used, there are other more difficult issues to resolve: for instance, the topology used, how the wave propagation is visualised and how the user is allowed to define and interact with the model. Currently the only application of a 3-D waveguide mesh has been the rectilinear implementation for low frequency modelling of room acoustics [Savioja et al, 1994] and [Savioja et al, 1995]. Other mesh topologies have been suggested, for instance, the bilinearly deinterpolated variation on the rectilinear waveguide mesh [Savioja and Välimäki, 1996], and the tetrahedral waveguide mesh [Van Duyne and Smith, 1995]. It should also be possible to construct a 3-D topology based on the triangular waveguide mesh [Fontana and Rocchesso, 1999]. However, there is the additional implication that the directional dependent dispersion error on such 3-D mesh structures can prove to be even more variable and inconsistent than on a similar 2-D model, making them even more difficult to use successfully [Van Duyne and Smith, 1995].

In order to implement any 3-D mesh at the high mesh sampling rates suggested and used within this thesis, a significant re-design of the model is required in order to make it more efficient in terms of computation time. Alternatively, an implementation for specific hardware or for a parallel array of processor nodes or workstations would be required. Associated with this is the

author's desire to re-design the model to work on a standard PC processor, perhaps as part of a larger audio processing environment or software package. This would allow the *WaveVerb* system to take advantage of recent improvements in PC CPU performance and provide access to a much wider potential user base.

7.3.3 Surround Sound

Although Ambisonic B-format output is currently implemented as part of the *WaveVerb* system, this thesis has not concentrated on its use or assessed its ability. Clearly this is a further novel aspect of this research as there are few if any multi-channel, surround-sound, room acoustics simulation packages currently available. It would also be desirable to allow 5.1 surround-sound output as this is a more commonly used format (although it is possible to derive 5.1 surround sound from Ambisonic B-format). It is further suggested that, rather than using the method currently implemented, a more accurate B-format signal could be derived by integrating a range of values over a more complete surface area according to the shapes of the spherical harmonic components as shown in Figure 5.9.

7.3.4 User Interface

Finally, there is great potential in improving the currently implemented user interface, the most immediate being the incorporation of an external text file for initial room definition and initialisation, rather than having to re-compile a particular module of the executable code. A further enhancement would be to design a specific Computer Aided Design (CAD) package running a low sampling rate version of the mesh model to allow room definition, manipulation and testing. This module would then generate its own definition file that could be used to initialise an efficient high sampling rate implementation of the model, that would then in turn generate the required RIR.

The visualisation and rendering aspects of this work also have implications in the use of the *WaveVerb* System as a tool for teaching the fundamental aspects of wave propagation as an interactive “ripple-tank” demonstration.

7.4 Publications

The novel aspects of the work presented in this thesis have resulted in original contributions to knowledge in the fields of waveguide mesh techniques, and the musical application of room acoustics modelling, and these have been presented in a number of publications:

the potential use of the *WaveVerb* System as a multi-channel spatial simulation system for computer music applications was discussed in [Murphy and Howard, 1998a], and [Murphy et al, 1998]

a verification of the waveguide mesh as applicable to the problem of room acoustics modelling was documented in [Murphy and Howard, 1998b]

a comparison of the triangular and rectilinear waveguide mesh topologies was dealt with in [Murphy and Howard, 1999a]

a general overview of the *WaveVerb* system as a triangular waveguide mesh model was presented and detailed in [Murphy and Howard, 1999b].

Additionally, the *WaveVerb* system has been featured in [Malham, 1998], as a visual medium for demonstrating wave propagation in an enclosed space.

Appendix A Mathematical Derivations

7.5 The General Scattering Equation

The sound pressure in a waveguide when considered as a column of air is represented by p_i , the volume velocity by v_i and the impedance of the waveguide by Z_i . The input to a waveguide is termed p_i^+ and the output p_i^- . The signal $p_{i,J}^+$ therefore represents the incoming signal to junction i along the waveguide from the opposite junction J . Similarly, the signal $p_{i,J}^-$ represents the outgoing signal from junction i along the waveguide to the opposite junction J . Note that in this case the volume velocity is equal to pressure divided by the characteristic impedance:

$$v_i = p_i / Z_i \quad (\text{A.1})$$

The delay elements are bi-directional and so the sound pressure in one waveguide element is defined as the sum of its input and output:

$$p_i = p_i^+ + p_i^- \quad (\text{A.2})$$

As the waveguides are equivalent to bi-directional unit-delay lines, the input to a scattering junction is equal to the output from a neighbouring junction into the connecting waveguide at the previous time step. This can be expressed as:

$$p_{J,i}^+ = z^{-1} p_{i,J}^- \quad (\text{A.3})$$

If a number of strings intersect at a junction without loss of energy it is required that all the velocities of all the strings are equal so that they move together at that single point, and that all the forces exerted by all the strings must sum to zero so that they balance each other [Van Duyne and Smith, 1993]. These conditions can be expressed explicitly for an air column waveguide element using wave variables based on volume velocity and pressure as follows:

3. The sum of the input volume velocities, v_i^+ , equals the sum of the output volume velocities, v_i^- – the flows add to zero:

$$\sum_{i=1}^N v_i^+ = \sum_{i=1}^N v_i^- \quad (\text{A.4})$$

4. The sound pressures in all crossing waveguides are equal at the junction:

$$p_1 = p_2 = \dots = p_i = \dots = p_N \quad (\text{A.5})$$

Given (A.1) and (A.2), the volume velocity in a waveguide can be expressed as:

$$v_i = v_i^+ + v_i^- \quad (\text{A.6})$$

where, as volume velocity is a vector quantity:

$$v_i^+ = \frac{p_i^+}{Z_i} \quad (\text{A.7})$$

and:

$$v_i^- = - \frac{p_i^-}{Z_i} \quad (\text{A.8})$$

Substituting (A.7) and (A.8) in (A.6):

$$v_i = \frac{1}{Z_i} (p_i^+ - p_i^-) \quad (\text{A.9})$$

Rearranging (A.2) and substituting in (A.9):

$$\begin{aligned} v_i &= \frac{1}{Z_i} (p_i^+ - (p_i - p_i^+)) \\ &= \frac{1}{Z_i} (2p_i^+ - p_i) \end{aligned} \quad (\text{A.10})$$

Now, from (A.4):

$$\sum_i v_i = 0 \quad (\text{A.11})$$

Therefore, substituting (A.10) in (A.11):

$$\sum_i \left(\frac{2p_i^+}{Z_i} - \frac{p_i}{Z_i} \right) = 0 \quad (\text{A.12})$$

$$\sum_i \left(\frac{2p_i^+}{Z_i} - \frac{p_i}{Z_i} \right) = 0$$

$$\sum_i \frac{2p_i^+}{Z_i} = \sum_i \frac{p_i}{Z_i} \quad (\text{A.13})$$

Given (A.5), let $p_1 = p_2 = p_3, \dots, = p_J$, and so (A.12) becomes:

$$2 \sum_i \frac{p_i^+}{Z_i} = \sum_i \frac{p_i}{Z_i}$$

$$\begin{aligned} \square \quad 2 \square_i \frac{p_i^+}{Z_i} &= p_J \square_i \frac{1}{Z_i} \\ \square \quad p_J &= \frac{2 \square_i \frac{p_i^+}{Z_i}}{\square_i \frac{1}{Z_i}} \end{aligned} \quad (\text{A.14})$$

And from (A.2):

$$p_i^\square = p_J \square p_i^+ \quad (\text{A.15})$$

And so Equations (A.14) and (A.15) give the general scattering equations for the interconnection of several waveguides at a point. #

7.6 Finite Difference Formulation of Scattering Equations

Substituting Equation (A.15) in (A.3) gives:

$$\begin{aligned} p_{J,i}^+ &= z^{\square 1} (p_i \square p_{i,J}^+) \quad (\text{A.16}) \\ \square \quad p_{J,i}^+ &= z^{\square 1} (p_i \square z^{\square 1} (p_J \square p_{J,i}^+)) \\ \square \quad p_{J,i}^+ &= z^{\square 1} (p_i \square z^{\square 1} p_J + z^{\square 1} p_{J,i}^+) \\ \square \quad p_{J,i}^+ &= z^{\square 1} p_i \square z^{\square 2} p_J + z^{\square 2} p_{J,i}^+ \\ \square \quad p_{J,i}^+ (1 \square z^{\square 2}) &= z^{\square 1} p_i \square z^{\square 2} p_J \\ \square \quad p_{J,i}^+ (1 \square z^{\square 2}) &= z^{\square 1} (p_i \square z^{\square 1} p_J) \\ \square \quad p_{J,i}^+ &= \frac{z^{\square 1}}{(1 \square z^{\square 2})} (p_i \square z^{\square 1} p_J) \end{aligned} \quad (\text{A.16})$$

Equation (A.14) for the 4-port lossless scattering junction reduces to:

$$p_J = \frac{1}{2} \cdot \square_{i=1}^4 p_i^+ \quad (\text{A.17})$$

Substituting (A.16) in (A.17), noting that $p_{J,i}^+$ is equivalent to p_i^+ :

$$p_J = \frac{1}{2} \cdot \square_{i=1}^4 \frac{z^{\square 1}}{(1 \square z^{\square 2})} (p_i \square z^{\square 1} p_J) \quad (\text{A.18})$$

$$\begin{aligned}
 \square p_J &= \frac{1}{2} \frac{z^{\square 1}}{(1 \square z^{\square 2})} \cdot \prod_{i=1}^4 (p_i \square z^{\square 1} p_J) \\
 \square p_J &= \frac{1}{2} \frac{z^{\square 1}}{(1 \square z^{\square 2})} \cdot \prod_{i=1}^4 p_i \square 4z^{\square 1} p_J \square \\
 \square p_J &= \frac{1}{2} \frac{z^{\square 1}}{(1 \square z^{\square 2})} \cdot \prod_{i=1}^4 p_i \square \frac{2z^{\square 2}}{(1 \square z^{\square 2})} p_J \\
 \square p_J \square + \frac{2z^{\square 2}}{(1 \square z^{\square 2})} \square &= \frac{1}{2} \frac{z^{\square 1}}{(1 \square z^{\square 2})} \cdot \prod_{i=1}^4 p_i \\
 \square p_J \square \frac{1+z^{\square 2}}{1 \square z^{\square 2}} \square &= \frac{1}{2} \frac{z^{\square 1}}{(1 \square z^{\square 2})} \cdot \prod_{i=1}^4 p_i \\
 \square p_J &= \frac{1}{2} \frac{z^{\square 1}}{(1+z^{\square 2})} \cdot \prod_{i=1}^4 p_i \tag{A.19}
 \end{aligned}$$

Rewriting and rearranging (A.19) in terms of the time index n , and the scattering junctions p_1, \dots, p_4 , immediately adjacent to p_J :

$$p_J(n) \square p_J(n \square 2) = \frac{1}{2} (p_1(n \square 1) + p_2(n \square 1) + p_3(n \square 1) + p_4(n \square 1)) \tag{A.20}$$

Adding $(-2p_J(n-1))$ to both sides of (A.20):

$$\begin{aligned}
 \square p_J(n) \square 2p_J(n \square 1) \square p_J(n \square 2) &= \frac{1}{2} (p_1(n \square 1) + p_2(n \square 1) + p_3(n \square 1) + p_4(n \square 1)) \\
 &\quad \square 2p_J(n \square 1) \\
 \square p_J(n) \square 2p_J(n \square 1) + p_J(n \square 2) &= \frac{1}{2} [p_1(n \square 1) \square 2p_J(n \square 1) + p_3(n \square 1)] \tag{A.21} \\
 &\quad + \frac{1}{2} [p_2(n \square 1) \square 2p_J(n \square 1) + p_4(n \square 1)]
 \end{aligned}$$

Equation (A.21) being the standard second-order difference scheme for the 2-dimensional hyperbolic partial differential wave equation. #

7.7 Finite Difference Formulation of Boundary Conditions

The connecting waveguides on either side of the boundary junction will have different characteristic impedances, Z_1 and Z_2 respectively. Consider such a boundary junction as would be found in a typical 2-D rectilinear mesh, as shown in Figure A.1.

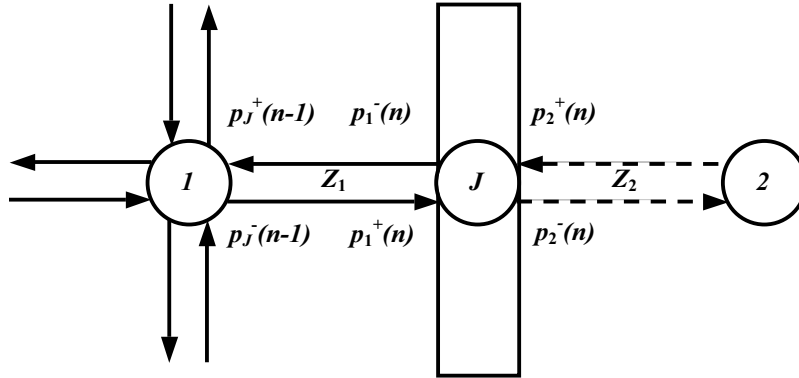


Figure A.1 Termination of a waveguide mesh due to a boundary resulting in a reflection. A dummy junction "within" the boundary is used in the derivation of the scattering equations for this case.

If at a boundary the impedance changes from Z_1 to Z_2 the reflection coefficient r is defined as:

$$r = \frac{Z_2 - Z_1}{Z_2 + Z_1} \quad (\text{A.22})$$

It is possible to express impedance Z_2 as a multiple \square , of Z_1 :

$$Z_2 = \square \cdot Z_1 \quad (\text{A.23})$$

Substituting Equation (A.23) in Equation (A.22) allows the ratio between the two impedances to be expressed in terms of the reflection coefficient r :

$$\square = \frac{1 + r}{1 - r} \quad (\text{A.24})$$

Considering Figure A.1, clearly there is no contribution into the boundary junction, J , from the dummy junction, 2. Therefore:

$$p_2^+(n) = 0 \quad (\text{A.25})$$

The output from the boundary junction back into the mesh is the input from junction 1 multiplied by the change in impedance, the reflection coefficient r :

$$p_1^{\square}(n) = r \cdot p_1^+(n) \quad (\text{A.26})$$

Using Equation (A.14), the sound pressure for the boundary junction can be calculated as a function of the sound pressures of the incident travelling waves, p_i^+ :

$$p_j(n) = \frac{2 \cdot \frac{1}{Z_1} \cdot p_1^+(n)}{\frac{1}{Z_1} + \frac{1}{\square Z_1}} \quad (\text{A.27})$$

$$\square p_j(n) = \frac{2 \cdot p_1^+(n)}{1 + \frac{1}{\square}}$$

$$\square p_1^+(n) = \frac{1}{2} p_j(n) \cdot \frac{\square}{\square} + \frac{1}{\square} \frac{\square}{\square} \quad (\text{A.28})$$

Equations (A.3) and (A.15) can be rewritten as:

$$p_1^+(n) = p_j^{\square}(n \square 1) \quad (\text{A.29})$$

$$p_j^{\square}(n \square 1) = p_1(n \square 1) \square p_j^+(n \square 1) \quad (\text{A.30})$$

respectively. Using (A.29) and (A.26):

$$\begin{aligned} p_j^+(n \square 1) &= p_1^{\square}(n \square 2) \\ &= r \cdot p_1^+(n \square 2) \end{aligned} \quad (\text{A.31})$$

Substituting (A.28) in (A.31):

$$p_j^+(n \square 1) = \frac{r}{2} \cdot \frac{\square}{\square} p_j(n \square 2) \cdot \frac{\square}{\square} + \frac{1}{\square} \frac{\square}{\square} \quad (\text{A.32})$$

Equating (A.29) and (A.30) and substituting (A.32) in (A.30):

$$p_1^+(n) = p_1(n \square 1) \square \frac{r}{2} \cdot \frac{\square}{\square} p_j(n \square 2) \cdot \frac{\square}{\square} + \frac{1}{\square} \frac{\square}{\square} \quad (\text{A.33})$$

Substituting (A.31) in (A.27):

$$p_J(n) = \frac{2 \cdot p_1(n-1) + \frac{r}{2} \cdot p_J(n-2)}{1 + \frac{1}{r}}$$

$$\Rightarrow p_J(n) = \frac{2 \cdot p_1(n-1)}{1 + \frac{1}{r}} + r \cdot p_J(n-2) \quad (\text{A.34})$$

And finally substituting Equation (A.24) in (A.34) gives an expression in terms of the arbitrary reflection coefficient, r :

$$p_J(n) = \frac{2 \cdot p_1(n-1)}{1 + \frac{1}{r}} + r \cdot p_J(n-2) \quad (\text{A.35})$$

This (A.35) can be rearranged to give:

$$p_J(n) = (1+r) \cdot p_1(n-1) + r \cdot p_J(n-2) \quad (\text{A.36})$$

The finite difference formulation of the boundary conditions in accordance with the expressions (A.20) and (A.21). #

Appendix B

Octave Band Acoustical Parameters

This Appendix contains the original octave bandwidth acoustic parameters as taken from the RIR measurements presented in the four-room case study in Chapter 6. All parameters were measured using the *Aurora* Acoustical Parameters software [Farina and Righini, 1999], according to ISO3382 [ISO3382, 1997].

7.8 Room A – Abs0.9

ROOM A - Abs0.9 - Position 1

Rectilinear Mesh

Band	Lin	31.5	63	125	250	500	1K	2K	4K	8K	16K
C50 [dB]	-1.483	-3.931	-1.375	1.851	3.059	1.149	6.048	4.459	2.879	-0.2285	-2.568
C80 [dB]	-0.05258	2.795	8.299	4.196	6.663	7.015	8.665	8.697	7.119	1.498	-1.444
D50 [%]	41.55	28.8	42.15	60.5	66.92	56.58	80.1	73.63	65.99	48.68	35.63
TS [ms]	319.8	79.78	60.29	50.33	46.46	52.17	32.22	34.71	45.43	177.1	358.7
EDT [s]	9.528	0.6879	0.4509	0.7296	0.5804	0.5568	0.5306	0.5743	0.6303	2.776	9.3
RT20 [s]	--	0.7073	0.6134	0.5367	0.5002	0.5453	0.5124	0.5499	0.8836	--	--
r RT20	--	0.9944	0.9786	0.9583	0.9872	0.9874	0.9929	0.994	0.9974	--	--
RT30 [s]	--	0.7285	0.5983	0.6249	0.5611	0.5492	0.5071	0.5977	0.9115	--	--
r RT30	--	0.9976	0.9891	0.9783	0.9893	0.9914	0.9972	0.9951	0.9977	--	--

Triangular Mesh

Band	Lin	31.5	63	125	250	500	1K	2K	4K	8K	16K
C50 [dB]	-1.194	-7.299	-4.838	-3.468	-1.65	-3.388	-0.5941	-0.8554	-0.505	-1.159	-5.385
C80 [dB]	1.147	-1.623	1.528	-1.393	1.048	1.244	1.125	1.918	1.393	1.486	-2.728
D50 [%]	43.17	15.7	24.71	31.04	40.62	31.43	46.59	45.09	47.1	43.37	22.44
TS [ms]	113.7	133.3	111.5	103.1	91.57	96.53	84.65	84.87	93.92	99.7	300.2
EDT [s]	1.566	1.426	1.33	1.229	1.141	1.154	1.195	1.258	1.401	1.502	4.689
RT20 [s]	5.681	1.526	1.437	1.432	1.256	1.272	1.141	1.264	1.515	1.682	--
r RT20	0.8561	0.9997	0.995	0.9867	0.9968	0.9933	0.9981	0.9983	0.9921	0.9984	--
RT30 [s]	--	1.519	1.47	1.433	1.282	1.269	1.213	1.313	1.702	1.824	--
r RT30	--	0.9999	0.9978	0.9946	0.9982	0.9941	0.9975	0.9988	0.9924	0.9968	--

ROOM A - Abs0.9 - Position 2

Rectilinear Mesh

Band	Lin	31.5	63	125	250	500	1K	2K	4K	8K	16K
C50 [dB]	-0.2752	-7.31	5.055	3.34	6.257	3.165	5.845	4.137	3.243	0.5839	-1.285
C80 [dB]	1.587	-1.681	6.538	8.737	9.019	9.026	9.586	8.707	6.685	2.714	0.4444
D50 [%]	48.42	15.67	76.2	68.33	80.86	67.45	79.35	72.16	67.84	53.36	42.66
TS [ms]	280.4	94.24	44.14	43.99	40.09	39.2	30.28	36.45	43.76	164.8	315.2

EDT [s]	8.286	0.7392	0.5909	0.4376	0.4088	0.4936	0.5325	0.559	0.7032	2.416	8.457
RT20 [s]	--	0.7083	0.6464	--	0.6479	0.5013	0.5191	0.5863	0.8142	--	--
r RT20	--	0.9903	0.9769	--	0.9939	0.9972	0.9982	0.9927	0.994	--	--
RT30 [s]	--	0.7287	0.6666	0.7507	0.6476	0.5028	0.5375	0.6193	0.9072	--	--
r RT30	--	0.9968	0.9902	0.9466	0.9977	0.994	0.9985	0.9963	0.9937	--	--

Triangular Mesh

Band	Lin	31.5	63	125	250	500	1K	2K	4K	8K	16K
C50 [dB]	-1.206	-10.86	-0.4171	-0.891	0.3812	-1.411	-0.7352	-0.4965	-1.448	-0.9152	-3.543
C80 [dB]	1.426	-5.34	0.82	2.638	2.013	2.709	2.24	1.96	1.238	1.803	-1.398
D50 [%]	43.1	7.586	47.6	44.89	52.19	41.95	45.78	47.15	41.74	44.75	30.67
TS [ms]	105.1	148.3	95.5	94.73	90.54	80.43	79.04	84.17	92.21	92.98	255.9
EDT [s]	1.438	1.416	1.418	1.678	1.336	1.07	1.125	1.257	1.29	1.395	4.133
RT20 [s]	4.492	1.522	1.476	1.471	1.366	1.282	1.249	1.278	1.522	1.68	8.795
r RT20	0.8875	0.9998	0.9944	0.985	0.9968	0.9946	0.9967	0.9972	0.9987	0.9966	0.9855
RT30 [s]	6.884	1.523	1.498	1.468	1.366	1.326	1.254	1.411	1.647	1.863	--
r RT30	0.9215	0.9999	0.9978	0.994	0.9982	0.9972	0.9988	0.995	0.9967	0.9949	--

ROOM A - Abs0.9 - Position 3

Rectilinear Mesh

Band	Lin	31.5	63	125	250	500	1K	2K	4K	8K	16K
C50 [dB]	-2.701	-5.988	1.489	5.363	2.265	2.769	-0.6968	5.629	3.259	-1.529	-4.044
C80 [dB]	-0.885	0.2534	4.022	12.31	7.532	7.003	6.501	10.34	7.345	0.6116	-2.314
D50 [%]	34.94	20.12	58.49	77.47	62.75	65.42	46.	78.52	67.93	41.29	28.27
TS [ms]	376.6	86.29	57.98	38.06	44.42	50.22	60.	32.1	46.73	216.7	419.
EDT [s]	10.46	0.6896	0.5988	0.4074	0.6095	0.6103	0.5753	0.4973	0.613	3.308	10.54
RT20 [s]	--	0.6971	0.5967	0.6519	0.4735	0.5579	0.5232	0.5998	0.8271	--	--
r RT20	--	0.983	0.9462	0.9722	0.9798	0.9897	0.995	0.9921	0.9956	--	--
RT30 [s]	--	0.7195	0.597	0.6392	0.6048	0.5253	0.5373	0.6157	0.9149	--	--
r RT30	--	0.9938	0.9794	0.9897	0.9719	0.9934	0.998	0.9963	0.9951	--	--

Triangular Mesh

Band	Lin	31.5	63	125	250	500	1K	2K	4K	8K	16K
C50 [dB]	-1.961	-9.277	-3.421	0.1188	-2.458	-3.156	-5.413	-1.142	-0.7152	-2.11	-4.797
C80 [dB]	0.6951	-3.564	-1.264	4.019	1.613	0.2537	0.3646	1.234	1.445	0.9691	-2.568
D50 [%]	38.9	10.56	31.27	50.68	36.22	32.59	22.33	43.46	45.89	38.09	24.89
TS [ms]	118.6	137.	111.2	86.31	91.05	104.1	112.4	91.01	94.2	101.8	276.2
EDT [s]	1.559	1.348	1.272	1.387	1.113	1.33	1.246	1.302	1.363	1.472	3.921
RT20 [s]	5.655	1.531	1.36	1.333	1.338	1.188	1.105	1.238	1.592	1.712	--
r RT20	0.8658	0.9997	0.9925	0.99	0.9943	0.9924	0.991	0.9984	0.9951	0.9947	--
RT30 [s]	--	1.53	1.388	1.36	1.339	1.246	1.144	1.264	1.701	1.895	--
r RT30	--	0.9999	0.9968	0.9958	0.9979	0.9959	0.9963	0.9992	0.9968	0.9947	--

ROOM A - Abs0.9 - Position 4

Rectilinear Mesh

Band	Lin	31.5	63	125	250	500	1K	2K	4K	8K	16K
C50 [dB]	-2.347	-4.731	5.384	-0.8396	3.01	2.811	5.449	6.486	2.999	-1.017	-4.127
C80 [dB]	-0.9323	1.843	6.754	3.266	7.061	6.535	8.798	9.73	6.442	0.7044	-2.769
D50 [%]	36.81	25.18	77.55	45.18	66.67	65.64	77.81	81.66	66.61	44.17	27.88
TS [ms]	325.	82.68	47.39	66.79	40.49	42.8	33.28	29.96	44.25	191.4	371.1

EDT [s]	8.069	0.6809	0.6757	0.7479	0.6727	0.7385	0.5238	0.4712	0.6851	3.04	8.045
RT20 [s]	--	0.6998	0.6558	0.4523	0.5005	0.5072	0.4937	0.554	0.8543	--	--
r RT20	--	0.9926	0.9567	0.9834	0.9956	0.9877	0.9957	0.9975	0.994	--	--
RT30 [s]	--	0.7232	0.663	0.5864	0.5434	0.5055	0.5195	0.5557	0.9568	--	--
r RT30	--	0.997	0.9853	0.9676	0.9938	0.9956	0.9957	0.999	0.9924	--	--

Triangular Mesh

Band	Lin	31.5	63	125	250	500	1K	2K	4K	8K	16K
C50 [dB]	-1.449	-8.1	-0.3998	-5.626	-2.349	-3.475	-1.094	-0.1566	-2.643	-0.8297	-4.556
C80 [dB]	1.016	-2.304	0.5931	-2.11	1.279	-0.958	1.074	2.693	0.6324	1.204	-2.501
D50 [%]	41.74	13.41	47.7	21.49	36.8	31.	43.74	49.1	35.24	45.24	25.94
TS [ms]	108.7	135.8	99.95	116.4	90.2	110.3	92.29	74.72	95.78	98.86	292.8
EDT [s]	1.487	1.399	1.405	1.054	1.178	1.35	1.302	1.144	1.272	1.466	4.395
RT20 [s]	4.408	1.531	1.426	1.442	1.236	1.333	1.111	1.269	1.446	1.721	--
r RT20	0.8835	0.9999	0.9906	0.9819	0.9945	0.9934	0.998	0.9985	0.998	0.9968	--
RT30 [s]	--	1.529	1.441	1.419	1.32	1.276	1.251	1.238	1.499	1.842	--
r RT30	--	0.9999	0.9965	0.9914	0.996	0.9971	0.9924	0.9992	0.9988	0.9972	--

7.9 Room A – Abs0.4

ROOM A - Abs0.4 - Position 1

Rectilinear Mesh

Band	Lin	31.5	63	125	250	500	1K	2K	4K	8K	16K
C50 [dB]	6.636	3.131	14.26	19.25	28.38	33.17	38.92	32.96	28.8	9.042	6.253
C80 [dB]	8.596	12.35	18.13	29.6	43.96	46.47	51.71	48.37	41.22	11.33	8.405
D50 [%]	82.17	67.28	96.38	98.83	99.85	99.95	99.99	99.95	99.87	88.91	80.84
TS [ms]	70.2	47.5	24.87	16.12	8.241	6.264	3.456	3.09	4.031	40.18	71.71
EDT [s]	--	0.3064	0.1543	0.1531	--	0.1119	--	--	--	0.6838	--
RT20 [s]	6.15	0.5534	0.3208	0.1415	0.1137	0.08449	0.09084	0.113	0.1153	6.07	6.013
r RT20	0.9684	0.9641	0.9448	0.9509	0.9497	0.9605	0.9695	0.9486	0.9472	0.9563	0.9675
RT30 [s]	--	0.6129	0.3357	0.1609	0.1001	0.08518	0.08377	0.1087	0.1161	--	--
r RT30	--	0.9849	0.9838	0.9762	0.9755	0.9714	0.985	0.9808	0.9709	--	--

Triangular Mesh

Band	Lin	31.5	63	125	250	500	1K	2K	4K	8K	16K
C50 [dB]	9.738	2.03	6.193	16.44	17.43	11.81	17.58	16.95	18.19	15.97	-0.683
C80 [dB]	11.28	13.83	27.25	21.96	26.54	22.96	27.07	24.26	25.19	24.49	0.9771
D50 [%]	90.4	61.48	80.63	97.78	98.22	93.81	98.28	98.02	98.51	97.53	46.07
TS [ms]	47.23	49.69	33.76	17.42	16.54	20.84	8.686	8.278	8.915	10.27	261.8
EDT [s]	0.3487	0.3276	0.2928	0.1297	0.1782	0.2949	--	0.1546	0.2065	0.1922	6.732
RT20 [s]	6.597	0.5954	0.1051	0.2319	0.1705	0.1811	0.1928	0.2527	0.2041	0.2222	--
r RT20	0.9744	0.9005	0.9561	0.9797	0.9864	0.9762	0.9768	0.9768	0.9618	0.9923	--
RT30 [s]	--	0.6716	0.211	0.2105	0.1743	0.1923	0.2096	0.2594	0.2453	0.258	--
r RT30	--	0.9739	0.8643	0.9906	0.9863	0.9854	0.9851	0.987	0.9773	0.9869	--

ROOM A - Abs0.4 - Position 2

Rectilinear Mesh

Band	Lin	31.5	63	125	250	500	1K	2K	4K	8K	16K
C50 [dB]	6.635	3.131	14.26	19.25	28.41	33.23	38.95	32.96	28.81	9.042	6.252
C80 [dB]	8.596	12.35	18.13	29.61	45.16	47.5	51.96	48.37	41.27	11.33	8.404

D50 [%]	82.17	67.28	96.38	98.83	99.86	99.95	99.99	99.95	99.87	88.91	80.84
TS [ms]	70.22	47.5	24.87	16.12	8.236	6.274	3.459	3.093	4.031	40.19	71.73
EDT [s]	--	0.3064	0.1543	0.1531	--	0.1119	--	--	--	0.6839	--
RT20 [s]	6.15	0.5534	0.3207	0.1414	0.1138	0.08446	0.09083	0.113	0.1153	6.071	6.014
r RT20	0.9684	0.9641	0.9448	0.9509	0.9497	0.9605	0.9695	0.9486	0.9472	0.9563	0.9675
RT30 [s]	--	0.6129	0.3356	0.1608	0.1001	0.08502	0.08373	0.1087	0.1161	--	--
r RT30	--	0.9849	0.9838	0.9762	0.9753	0.9715	0.985	0.9808	0.9709	--	--

Triangular Mesh

Band	Lin	31.5	63	125	250	500	1K	2K	4K	8K	16K
C50 [dB]	12.55	0.3295	19.95	12.33	19.24	15.32	19.67	15.72	16.67	15.69	3.288
C80 [dB]	15.05	7.407	22.53	20.44	29.42	29.14	30.59	25.4	23.63	23.18	4.68
D50 [%]	94.73	51.9	99.	94.47	98.82	97.15	98.93	97.39	97.89	97.37	68.07
TS [ms]	20.51	54.53	24.49	23.65	17.61	14.46	8.553	9.06	8.712	9.942	117.8
EDT [s]	0.2434	0.4224	0.1615	0.1949	0.2492	0.1918	0.198	0.2302	0.2009	0.2126	2.284
RT20 [s]	--	0.3917	--	0.2097	0.1023	0.1589	0.1603	0.2189	0.2464	0.2295	--
r RT20	--	0.9767	--	0.9915	0.9641	0.9755	0.9892	0.9892	0.9863	0.9886	--
RT30 [s]	--	0.7547	0.2972	0.1784	0.1746	0.1589	0.1655	0.2082	0.2457	0.2437	--
r RT30	--	0.8727	0.9246	0.988	0.9171	0.9905	0.9952	0.9953	0.9952	0.9948	--

ROOM A - Abs0.4 - Position 3

Rectilinear Mesh

Band	Lin	31.5	63	125	250	500	1K	2K	4K	8K	16K
C50 [dB]	0.481	2.28	11.26	21.08	28.54	28.62	38.56	33.99	25.12	4.189	-0.015
C80 [dB]	1.033	11.02	15.79	31.08	43.71	44.53	52.42	50.21	35.16	4.837	0.6966
D50 [%]	52.77	62.83	93.04	99.23	99.86	99.86	99.99	99.96	99.69	72.4	49.91
TS [ms]	230.	49.52	28.05	14.53	9.4	6.623	3.178	5.198	5.861	124.1	230.5
EDT [s]	7.784	0.3238	0.19	0.113	--	--	0.01759	--	--	2.875	7.407
RT20 [s]	--	0.498	0.3467	0.1491	0.08673	0.1051	0.1049	--	--	--	--
r RT20	--	0.9695	0.9798	0.9781	0.9182	0.9281	0.856	--	--	--	--
RT30 [s]	--	0.5344	0.3587	0.1642	0.09417	0.103	0.1222	0.1146	0.1552	--	--
r RT30	--	0.988	0.9943	0.9897	0.9652	0.9498	0.9257	0.864	0.9261	--	--

Triangular Mesh

Band	Lin	31.5	63	125	250	500	1K	2K	4K	8K	16K
C50 [dB]	10.15	-0.6308	9.78	14.57	13.62	14.13	15.7	20.02	17.25	13.95	2.457
C80 [dB]	12.81	6.606	13.51	24.71	28.06	27.74	27.28	30.66	26.19	22.53	4.734
D50 [%]	91.19	46.38	90.48	96.62	95.84	96.28	97.38	99.01	98.15	96.13	63.78
TS [ms]	38.71	57.04	33.43	20.65	18.32	17.77	11.03	10.45	11.52	10.87	158.4
EDT [s]	0.3209	0.4424	0.2467	0.2044	--	--	--	--	--	--	3.315
RT20 [s]	9.859	0.4076	0.2807	0.1744	0.1688	0.1826	0.2234	0.1793	0.2057	0.2246	--
r RT20	0.8882	0.9932	0.9739	0.9825	0.9415	0.9665	0.97	0.9678	0.9748	0.9803	--
RT30 [s]	--	0.4347	0.3355	0.1878	0.18	0.1828	0.1958	0.1897	0.2194	0.2483	--
r RT30	--	0.9947	0.984	0.9924	0.9693	0.9737	0.9745	0.9795	0.9867	0.9883	--

ROOM A - Abs0.4 - Position 4

Rectilinear Mesh

Band	Lin	31.5	63	125	250	500	1K	2K	4K	8K	16K
C50 [dB]	-0.2398	2.236	13.48	18.25	33.53	29.14	32.66	27.73	24.68	3.045	-0.918

C80 [dB]	0.4568	12.94	17.52	27.95	44.73	40.07	42.56	43.56	35.17	3.808	-0.028
D50 [%]	48.62	62.59	95.7	98.53	99.96	99.88	99.95	99.83	99.66	66.85	44.73
TS [ms]	190.5	50.74	26.83	14.11	7.249	5.205	3.505	3.344	3.885	113.	193.6
EDT [s]	3.817	0.3086	0.1606	0.1477	0.04672	0.06928	0.03247	0.0326	0.03185	2.26	3.6
RT20 [s]	--	0.6282	0.3195	0.1698	0.1075	0.0986	--	--	0.1536	--	--
r RT20	--	0.9569	0.9558	0.9897	0.9415	0.9757	--	--	0.8749	--	--
RT30 [s]	--	0.6578	0.332	0.1818	0.1081	0.1126	0.108	0.1298	0.1454	--	--
r RT30	--	0.9865	0.9869	0.9937	0.9836	0.9643	0.9201	0.9156	0.931	--	--

Triangular Mesh

Band	Lin	31.5	63	125	250	500	1K	2K	4K	8K	16K
C50 [dB]	10.21	0.6516	16.52	8.41	18.83	14.11	17.49	17.15	13.82	17.16	0.8677
C80 [dB]	11.91	11.97	20.99	16.99	28.21	22.72	25.27	26.12	22.09	22.53	2.193
D50 [%]	91.31	53.74	97.82	87.4	98.71	96.26	98.25	98.11	96.01	98.11	54.98
TS [ms]	34.7	53.17	28.26	29.41	10.74	13.06	10.62	7.806	9.316	10.41	179.9
EDT [s]	0.308	0.3641	0.1783	0.2645	0.1193	0.1813	0.2186	0.1582	0.2233	0.2419	4.753
RT20 [s]	5.672	0.5245	0.2293	0.2167	0.1964	0.2364	0.1931	0.2053	0.2587	0.2433	--
r RT20	0.9509	0.9145	0.8909	0.9877	0.9907	0.99	0.9739	0.9895	0.9912	0.9684	--
RT30 [s]	--	0.5834	0.2488	0.2179	0.1913	0.2151	0.2051	0.2209	0.2433	0.2764	--
r RT30	--	0.9758	0.9469	0.9954	0.9964	0.9914	0.9881	0.9926	0.9929	0.9837	--

7.10 Room A – AbsComplex

ROOM A – AbsComplex - Position 1

Rectilinear Mesh

Band	Lin	31.5	63	125	250	500	1K	2K	4K	8K	16K
C50 [dB]	2.284	2.487	12.54	24.24	28.38	26.06	27.49	19.74	15.83	5.184	2.106
C80 [dB]	2.444	12.95	17.63	34.82	39.32	38.52	41.13	31.81	24.2	5.416	2.271
D50 [%]	62.85	63.94	94.72	99.62	99.86	99.75	99.82	98.95	97.45	76.74	61.89
TS [ms]	157.8	50.28	25.31	14.08	10.74	6.268	4.025	5.629	4.639	89.75	153.6
EDT [s]	4.547	0.3063	0.1549	0.08822	0.08956	0.04528	0.02787	--	--	1.738	4.184
RT20 [s]	--	0.6601	0.3176	0.1374	0.09978	0.1438	0.1285	0.1815	0.2895	--	--
r RT20	--	0.9572	0.9677	0.9608	0.8599	0.8655	0.9	0.9335	0.946	--	--
RT30 [s]	--	0.6805	0.3319	0.1428	0.1022	0.1292	0.1273	0.1575	0.2464	--	--
r RT30	--	0.9888	0.9902	0.9872	0.9426	0.9608	0.9507	0.9669	0.967	--	--

Triangular Mesh

Band	Lin	31.5	63	125	250	500	1K	2K	4K	8K	16K
C50 [dB]	8.796	1.514	6.78	14.05	14.72	10.06	18.42	16.46	16.16	13.1	-0.869
C80 [dB]	10.76	13.07	24.55	21.2	24.41	21.6	26.57	23.67	19.84	20.08	1.295
D50 [%]	88.34	58.63	82.65	96.21	96.74	91.02	98.58	97.79	97.64	95.33	45.01
TS [ms]	46.78	50.74	32.35	19.67	19.24	21.77	8.88	8.209	9.529	12.34	228.5
EDT [s]	0.4542	0.3459	0.2785	0.1679	0.208	0.2904	--	0.1456	0.2318	0.237	5.82
RT20 [s]	6.36	0.5467	0.1282	0.2176	0.1747	0.1812	0.1734	0.2512	0.3141	0.3361	--
r RT20	0.9641	0.8906	0.9433	0.9922	0.99	0.9717	0.9729	0.9814	0.9534	0.9761	--
RT30 [s]	--	0.6334	0.1923	0.2069	0.1806	0.2003	0.2035	0.2395	0.3202	0.4312	--
r RT30	--	0.9712	0.9295	0.9955	0.9842	0.9766	0.9827	0.9917	0.9788	0.975	--

ROOM A – AbsComplex - Position 2

Rectilinear Mesh

Band	Lin	31.5	63	125	250	500	1K	2K	4K	8K	16K
C50 [dB]	6.268	2.656	15.11	18.1	27.66	32.94	33.41	27.9	22.35	8.54	5.69
C80 [dB]	8.214	13.19	19.	28.25	39.18	41.87	43.25	38.14	33.02	10.92	7.844
D50 [%]	80.9	64.83	97.01	98.48	99.83	99.95	99.95	99.84	99.42	87.72	78.75
TS [ms]	77.56	48.85	24.4	18.07	9.245	4.984	4.068	4.251	5.31	44.21	81.19
EDT [s]	--	0.3121	0.1487	0.1611	0.1239	0.03555	--	--	--	0.6717	--
RT20 [s]	6.081	0.5819	0.2924	0.1592	0.0975	0.1207	0.08408	0.118	0.1553	6.399	5.963
r RT20	0.9722	0.9527	0.9216	0.948	0.9809	0.9609	0.9664	0.9353	0.945	0.9522	0.9719
RT30 [s]	--	0.6407	0.3125	0.169	0.1017	0.1055	0.1025	0.1296	0.1587	--	--
r RT30	--	0.9838	0.9786	0.9842	0.9875	0.9769	0.9431	0.9697	0.9735	--	--

Triangular Mesh

Band	Lin	31.5	63	125	250	500	1K	2K	4K	8K	16K
C50 [dB]	11.56	0.01092	21.19	10.77	15.5	13.94	18.09	18.23	16.16	13.38	2.999
C80 [dB]	14.28	7.359	24.43	17.93	23.06	24.41	28.17	27.24	23.33	19.	4.692
D50 [%]	93.47	50.01	99.24	92.28	97.26	96.12	98.47	98.52	97.64	95.61	66.61
TS [ms]	21.22	55.47	25.05	26.2	19.19	14.11	8.058	8.091	8.878	10.92	110.2
EDT [s]	0.2603	0.4224	0.1725	0.2154	0.2684	0.2362	0.1642	0.1883	0.1911	0.2186	2.023
RT20 [s]	--	0.3789	--	0.2165	0.1819	0.1937	0.1917	0.1957	0.2434	0.3129	--
r RT20	--	0.9763	--	0.9738	0.9324	0.9806	0.9835	0.9858	0.9893	0.9925	--
RT30 [s]	--	0.4811	0.293	0.1926	0.2293	0.2164	0.1919	0.2014	0.2415	0.3271	--
r RT30	--	0.9703	0.8814	0.9886	0.9585	0.9878	0.9933	0.9917	0.9947	0.9968	--

ROOM A – AbsComplex - Position 3

Rectilinear Mesh

Band	Lin	31.5	63	125	250	500	1K	2K	4K	8K	16K
C50 [dB]	0.143	1.92	11.12	21.4	29.19	24.49	24.06	24.99	18.52	3.479	-0.583
C80 [dB]	0.5864	11.36	16.14	31.32	43.19	40.25	39.82	40.26	26.07	4.002	0.0164
D50 [%]	50.82	60.88	92.83	99.28	99.88	99.65	99.61	99.68	98.61	69.02	46.65
TS [ms]	240.2	49.47	26.84	14.31	8.194	9.409	10.44	4.285	6.035	135.3	244.8
EDT [s]	7.679	0.3282	0.1771	0.1077	0.06834	--	--	--	--	3.078	7.318
RT20 [s]	--	0.5201	0.3356	0.1481	0.09057	0.1112	--	--	0.2444	--	--
r RT20	--	0.9605	0.9833	0.9834	0.9266	0.9037	--	--	0.9189	--	--
RT30 [s]	--	0.5364	0.3534	0.162	0.09881	0.1092	0.1428	0.1671	0.2246	--	--
r RT30	--	0.9865	0.9947	0.9909	0.9709	0.9601	0.8804	0.9242	0.9607	--	--

Triangular Mesh

Band	Lin	31.5	63	125	250	500	1K	2K	4K	8K	16K
C50 [dB]	9.721	-0.7975	9.586	14.43	13.37	12.83	10.51	19.33	17.11	12.23	1.615
C80 [dB]	12.43	6.532	14.93	22.88	26.24	23.86	21.87	27.25	22.04	19.71	3.835
D50 [%]	90.36	45.42	90.09	96.52	95.6	95.05	91.83	98.85	98.09	94.35	59.19
TS [ms]	36.9	57.17	32.49	20.88	16.97	20.14	22.18	6.975	10.61	11.04	171.9
EDT [s]	0.3615	0.4445	0.2572	0.2097	--	0.2092	0.3412	--	--	--	3.829
RT20 [s]	8.798	0.3872	0.2676	0.196	0.1725	0.2079	0.2075	0.2307	0.3544	0.3381	--
r RT20	0.8916	0.9922	0.9737	0.9756	0.9439	0.9709	0.9668	0.962	0.9336	0.9674	--
RT30 [s]	--	0.43	0.331	0.1905	0.2068	0.2082	0.207	0.2411	0.3442	0.4201	--
r RT30	--	0.9921	0.9802	0.9874	0.9688	0.9817	0.9834	0.981	0.9764	0.9711	--

ROOM A – AbsComplex - Position 4*Rectilinear Mesh*

Band	Lin	31.5	63	125	250	500	1K	2K	4K	8K	16K
C50 [dB]	0.05966	1.879	12.81	17.18	29.96	24.66	26.74	20.4	17.81	3.546	-0.92
C80 [dB]	0.9021	12.95	17.07	27.43	41.19	35.24	34.09	32.83	26.32	4.553	0.1697
D50 [%]	50.34	60.65	95.02	98.12	99.9	99.66	99.79	99.1	98.37	69.35	44.72
TS [ms]	192.6	51.47	27.19	15.3	7.64	5.875	4.268	5.335	6.193	104.3	199.8
EDT [s]	4.055	0.3134	0.1607	0.1482	0.05054	0.067	0.02977	--	--	1.916	3.829
RT20 [s]	--	0.6306	0.3238	0.1763	0.1096	0.1378	--	--	0.2279	--	--
r RT20	--	0.9554	0.9644	0.9853	0.9495	0.9331	--	--	0.8723	--	--
RT30 [s]	--	0.664	0.337	0.1851	0.1251	0.1357	0.1678	0.1537	0.2117	--	--
r RT30	--	0.986	0.9902	0.9939	0.95	0.9596	0.9164	0.9217	0.9642	--	--

Triangular Mesh

Band	Lin	31.5	63	125	250	500	1K	2K	4K	8K	16K
C50 [dB]	9.207	0.04147	16.06	8.418	16.49	14.15	14.62	15.45	12.34	14.17	0.4976
C80 [dB]	10.96	10.82	20.12	16.82	25.36	20.95	20.29	23.41	18.38	17.48	1.995
D50 [%]	89.28	50.24	97.58	87.42	97.8	96.3	96.66	97.23	94.49	96.31	52.86
TS [ms]	37.97	54.79	28.55	28.86	12.23	12.85	13.26	8.505	10.52	12.99	178.6
EDT [s]	0.3974	0.3841	0.1804	0.2593	0.1409	0.1924	0.2535	0.1678	0.2489	0.2992	4.321
RT20 [s]	5.637	0.4699	0.24	0.2233	0.213	0.2487	0.2309	0.2332	0.3082	0.3605	--
r RT20	0.9507	0.9345	0.8897	0.9854	0.9843	0.9583	0.9587	0.983	0.9804	0.9662	--
RT30 [s]	--	0.5486	0.2471	0.2221	0.1962	0.2431	0.2555	0.2274	0.3075	0.3951	--
r RT30	--	0.972	0.9497	0.9943	0.9852	0.9819	0.9766	0.9887	0.9886	0.9868	--

7.11 Room B – Abs0.9**ROOM B - Abs0.9 - Position 1***Rectilinear Mesh*

Band	Lin	31.5	63	125	250	500	1K	2K	4K	8K	16K
C50 [dB]	-3.268	-6.907	-2.309	-0.2768	3.466	0.8687	2.236	2.806	0.9539	-2.135	-4.292
C80 [dB]	-1.787	0.917	3.467	6.04	6.783	6.025	6.128	5.688	4.511	-0.4285	-2.955
D50 [%]	32.03	16.93	37.01	48.41	68.96	54.98	62.59	65.61	55.47	37.95	27.12
TS [ms]	382.4	92.43	76.98	57.86	51.1	53.56	46.51	48.74	61.82	239.4	417.6
EDT [s]	9.827	0.6905	0.7208	0.7081	0.7132	0.606	0.7161	0.7331	0.9125	4.277	9.744
RT20 [s]	--	0.8707	0.8164	0.7741	0.7167	0.6396	0.6529	0.7646	1.013	--	--
r RT20	--	0.9967	0.9737	0.9868	0.9891	0.9943	0.997	0.9921	0.998	--	--
RT30 [s]	--	0.8769	0.8027	0.7833	0.7083	0.6805	0.662	0.8655	1.066	--	--
r RT30	--	0.9989	0.9899	0.9933	0.9966	0.9966	0.9978	0.9893	0.9965	--	--

Triangular Mesh

Band	Lin	31.5	63	125	250	500	1K	2K	4K	8K	16K
C50 [dB]	-2.278	-9.861	-5.766	-4.57	-1.448	-3.244	-2.93	-2.488	-1.422	-2.433	-5.815
C80 [dB]	0.1114	-3.101	-0.9983	0.6357	0.591	0.851	0.2078	0.7188	0.6216	0.07424	-3.155
D50 [%]	37.18	9.358	20.95	25.88	41.74	32.15	33.75	36.05	41.89	36.35	20.77
TS [ms]	130.1	158.6	139.1	117.5	110.3	110.3	103.8	101.8	109.	127.9	300.4
EDT [s]	1.799	1.767	1.697	1.591	1.508	1.505	1.376	1.386	1.563	1.882	4.464
RT20 [s]	4.165	1.887	1.797	1.666	1.57	1.468	1.449	1.525	2.09	2.194	--
r RT20	0.9313	0.9999	0.9952	0.9963	0.9971	0.9982	0.9966	0.9984	0.989	0.9988	--

RT30 [s]	--	1.898	1.833	1.73	1.611	1.44	1.439	1.654	2.419	2.448	--
r RT30	--	0.9999	0.998	0.9978	0.9986	0.999	0.9988	0.9971	0.989	0.9943	--

ROOM B - Abs0.9 - Position 2

Rectilinear Mesh

Band	Lin	31.5	63	125	250	500	1K	2K	4K	8K	16K
C50 [dB]	-1.389	-8.321	5.755	4.759	0.7138	2.3	3.161	1.992	1.762	-0.3292	-2.032
C80 [dB]	0.5832	-1.895	6.85	7.06	4.658	6.636	6.953	5.892	4.605	1.963	-0.248
D50 [%]	42.07	12.83	79.	74.95	54.1	62.94	67.43	61.27	60.	48.11	38.51
TS [ms]	307.5	100.5	46.53	52.89	52.27	47.37	41.11	47.34	55.5	185.5	337.9
EDT [s]	8.771	0.7644	0.6911	0.741	0.6298	0.6415	0.71	0.7668	0.9056	2.901	8.598
RT20 [s]	--	0.8626	0.7411	0.8032	0.5862	0.6191	0.6747	0.7703	0.9612	9.722	--
r RT20	--	0.998	0.9863	0.9791	0.9833	0.9838	0.9984	0.9976	0.9962	0.9724	--
RT30 [s]	--	0.8635	0.7238	0.7988	0.7524	0.6383	0.6651	0.7784	1.112	--	--
r RT30	--	0.9993	0.9938	0.9936	0.9751	0.9949	0.999	0.9981	0.9909	--	--

Triangular Mesh

Band	Lin	31.5	63	125	250	500	1K	2K	4K	8K	16K
C50 [dB]	-2.112	-11.83	0.4128	-0.6763	-2.883	-1.986	-2.151	-1.339	-2.453	-1.899	-4.074
C80 [dB]	0.498	-5.848	1.155	0.6409	0.4368	1.28	0.6745	1.585	0.7996	0.2859	-2.343
D50 [%]	38.08	6.161	52.37	46.11	33.99	38.76	37.86	42.35	36.24	39.24	28.13
TS [ms]	121.1	173.1	99.53	118.5	98.4	96.98	100.8	94.31	107.4	115.5	275.7
EDT [s]	1.705	1.838	1.559	1.641	1.173	1.317	1.451	1.392	1.521	1.72	4.155
RT20 [s]	4.059	1.93	1.486	1.752	1.695	1.445	1.341	1.48	2.109	2.272	--
r RT20	0.9322	0.9999	0.9973	0.9955	0.9854	0.9954	0.9975	0.9993	0.9951	0.9959	--
RT30 [s]	6.415	1.933	1.502	1.791	1.641	1.515	1.386	1.573	2.313	2.482	--
r RT30	0.9305	1.	0.9986	0.9978	0.9901	0.9974	0.9987	0.9982	0.9926	0.9959	--

ROOM B - Abs0.9 - Position 3

Rectilinear Mesh

Band	Lin	31.5	63	125	250	500	1K	2K	4K	8K	16K
C50 [dB]	-4.409	-5.498	-3.087	2.934	1.665	0.6666	-0.1657	2.538	0.9276	-2.932	-6.661
C80 [dB]	-2.103	0.5874	1.516	6.964	6.131	5.107	4.381	5.853	4.537	-0.3686	-4.337
D50 [%]	26.6	22.	32.94	66.28	59.47	53.83	49.05	64.21	55.32	33.73	17.74
TS [ms]	397.7	87.25	78.32	47.91	50.76	55.52	65.34	47.68	59.86	231.6	456.
EDT [s]	9.373	0.684	0.7881	0.7184	0.7585	0.675	0.723	0.74	0.8338	4.045	9.145
RT20 [s]	--	0.8681	0.6418	0.7608	0.787	0.6337	0.616	0.7907	1.058	--	--
r RT20	--	0.9919	0.9983	0.9899	0.9955	0.996	0.9947	0.9981	0.9917	--	--
RT30 [s]	--	0.8763	0.6498	0.7691	0.7201	0.6484	0.6291	0.8122	1.161	--	--
r RT30	--	0.9977	0.999	0.9943	0.9944	0.9982	0.9975	0.9989	0.994	--	--

Triangular Mesh

Band	Lin	31.5	63	125	250	500	1K	2K	4K	8K	16K
C50 [dB]	-3.207	-7.553	-6.794	-1.974	-3.215	-3.353	-4.304	-2.92	-3.083	-2.863	-5.473
C80 [dB]	-0.5742	-1.973	-2.87	0.8631	-0.3012	0.04856	-0.426	-0.6022	-0.8524	0.2747	-3.76
D50 [%]	32.33	14.94	17.3	38.83	32.29	31.6	27.07	33.8	32.96	34.09	22.1
TS [ms]	142.5	125.4	136.5	111.1	119.2	107.5	117.1	121.3	126.6	123.4	301.6
EDT [s]	1.897	1.331	1.476	1.588	1.69	1.37	1.279	1.737	1.672	1.779	4.417
RT20 [s]	4.487	1.429	1.457	1.715	1.53	1.406	1.541	1.461	2.098	2.309	8.289
r RT20	0.9354	0.999	0.9988	0.9948	0.9892	0.9974	0.9895	0.9973	0.9964	0.9943	0.9891

RT30 [s]	6.399	1.37	1.493	1.765	1.582	1.475	1.418	1.547	2.367	2.546	--
r RT30	0.941	0.9987	0.9988	0.9971	0.9957	0.9978	0.9943	0.9977	0.9934	0.9949	--

ROOM B - Abs0.9 - Position 4

Rectilinear Mesh

Band	Lin	31.5	63	125	250	500	1K	2K	4K	8K	16K
C50 [dB]	-3.603	-5.289	-1.781	0.6705	-0.6444	1.963	2.865	3.912	2.066	-2.435	-5.563
C80 [dB]	-1.414	1.326	3.319	4.048	4.638	6.068	7.474	6.983	5.554	0.2087	-3.538
D50 [%]	30.37	22.83	39.89	53.85	46.3	61.11	65.92	71.11	61.67	36.34	21.74
TS [ms]	325.6	89.7	71.17	62.27	62.89	49.43	43.94	38.94	55.52	196.9	382.2
EDT [s]	6.84	0.7213	0.7265	0.8179	0.6463	0.7338	0.6111	0.6971	0.8419	3.161	7.234
RT20 [s]	--	0.8666	0.667	0.743	0.6601	0.5959	0.6929	0.6988	1.017	9.138	--
r RT20	--	0.9972	0.9974	0.9511	0.9962	0.9924	0.9977	0.9977	0.9986	0.98	--
RT30 [s]	--	0.8655	0.6581	0.7405	0.6526	0.6578	0.6797	0.7492	1.053	--	--
r RT30	--	0.9991	0.9983	0.9811	0.9972	0.9886	0.9983	0.9972	0.9977	--	--

Triangular Mesh

Band	Lin	31.5	63	125	250	500	1K	2K	4K	8K	16K
C50 [dB]	-2.559	-8.232	-5.818	-3.778	-4.851	-2.19	-2.34	-1.317	-3.237	-2.	-5.339
C80 [dB]	-0.1507	-2.432	-1.441	-1.023	-0.4828	0.8678	1.006	1.515	-0.4635	-0.1558	-2.82
D50 [%]	35.68	13.06	20.76	29.53	24.66	37.66	36.85	42.48	32.18	38.69	22.63
TS [ms]	132.1	144.3	130.	119.1	117.	101.9	104.5	91.91	120.9	125.2	294.9
EDT [s]	1.835	1.574	1.492	1.509	1.385	1.377	1.486	1.361	1.704	1.847	4.407
RT20 [s]	3.937	1.674	1.517	1.681	1.548	1.576	1.454	1.504	1.957	2.241	--
r RT20	0.9401	0.9999	0.997	0.9907	0.9951	0.9983	0.9964	0.999	0.9912	0.9995	--
RT30 [s]	--	1.673	1.574	1.734	1.624	1.555	1.437	1.487	2.256	2.426	--
r RT30	--	0.9999	0.9973	0.9957	0.9973	0.9992	0.9982	0.9995	0.9904	0.997	--

7.12 Room B – Abs0.4

ROOM B - Abs0.4 - Position 1

Rectilinear Mesh

Band	Lin	31.5	63	125	250	500	1K	2K	4K	8K	16K
C50 [dB]	2.714	0.661	9.725	26.43	23.95	25.33	25.59	24.7	22.15	5.502	2.486
C80 [dB]	3.002	12.14	18.33	36.09	36.72	37.94	38.74	35.52	34.33	5.901	2.838
D50 [%]	65.14	53.8	90.37	99.77	99.6	99.71	99.72	99.66	99.39	78.02	63.93
TS [ms]	180.5	54.	28.33	15.15	10.1	7.724	5.277	5.426	5.006	105.4	178.3
EDT [s]	6.558	0.3291	0.2803	0.1095	0.1803	0.08972	--	--	--	3.06	6.26
RT20 [s]	--	0.6682	0.241	0.09776	0.1214	0.1117	0.122	0.1281	0.1676	--	--
r RT20	--	0.9464	0.9681	0.9721	0.9266	0.9433	0.9297	0.9377	0.932	--	--
RT30 [s]	--	0.7097	0.2994	0.1428	0.1198	0.1191	0.1248	0.1284	0.1602	--	--
r RT30	--	0.9844	0.9777	0.9491	0.9644	0.9741	0.9695	0.9654	0.9754	--	--

Triangular Mesh

Band	Lin	31.5	63	125	250	500	1K	2K	4K	8K	16K
C50 [dB]	9.869	-2.235	4.808	13.	13.81	11.02	12.38	11.51	14.34	13.28	-0.415
C80 [dB]	12.31	9.169	13.75	23.1	22.18	18.35	19.99	16.57	20.4	19.53	1.279
D50 [%]	90.66	37.41	75.16	95.23	96.01	92.68	94.53	93.4	96.45	95.51	47.61
TS [ms]	36.9	59.55	42.51	19.58	21.55	18.82	13.19	14.19	12.92	13.53	236.8
EDT [s]	0.3016	0.3885	0.328	0.1093	--	0.2611	0.2412	0.2537	0.2303	0.2414	5.871

RT20 [s]	5.827	0.4584	0.2298	0.2474	0.2157	0.2482	0.2489	0.3368	0.2788	0.307	--
r RT20	0.9434	0.9152	0.9507	0.9499	0.9717	0.9916	0.9844	0.989	0.9767	0.9908	--
RT30 [s]	--	0.5605	0.2821	0.2253	0.2484	0.2676	0.2998	0.3482	0.3575	0.3227	--
r RT30	--	0.9654	0.9555	0.9822	0.9846	0.993	0.9823	0.994	0.9694	0.9952	--

ROOM B - Abs0.4 - Position 2

Rectilinear Mesh

Band	Lin	31.5	63	125	250	500	1K	2K	4K	8K	16K
C50 [dB]	6.088	0.6454	12.48	23.16	29.03	28.48	29.48	24.22	24.14	8.481	5.62
C80 [dB]	7.965	11.42	16.54	32.01	42.74	44.61	46.71	40.32	35.12	10.78	7.775
D50 [%]	80.25	53.71	94.65	99.52	99.88	99.86	99.89	99.62	99.62	87.58	78.48
TS [ms]	89.86	51.73	26.31	15.85	6.855	6.976	4.073	4.209	5.054	50.54	91.23
EDT [s]	--	0.3597	0.1702	0.1682	0.04604	--	0.03624	--	--	0.6919	--
RT20 [s]	--	0.5253	0.3417	0.09955	0.1271	0.08825	0.1105	0.1468	0.1299	6.096	--
r RT20	--	0.9262	0.9731	0.938	0.9392	0.8974	0.853	0.8997	0.8976	0.9025	--
RT30 [s]	--	0.5209	0.358	0.1469	0.1187	0.09918	0.1153	0.1389	0.1383	--	--
r RT30	--	0.9802	0.9926	0.9323	0.9624	0.9507	0.9464	0.9283	0.9565	--	--

Triangular Mesh

Band	Lin	31.5	63	125	250	500	1K	2K	4K	8K	16K
C50 [dB]	10.74	-2.502	15.04	16.43	12.6	14.25	15.75	11.98	12.19	12.79	3.009
C80 [dB]	13.96	6.281	19.06	24.22	20.56	24.24	24.64	20.58	18.51	19.3	4.058
D50 [%]	92.23	35.99	96.96	97.78	94.79	96.38	97.41	94.04	94.31	95.	66.66
TS [ms]	21.95	59.75	26.41	23.83	15.42	15.37	9.003	13.19	11.77	10.74	120.6
EDT [s]	0.3176	0.4435	0.1835	0.2608	0.2572	0.2175	--	--	--	--	2.552
RT20 [s]	--	0.3187	0.2771	0.1758	0.2302	0.2017	0.2191	0.2428	0.3102	0.2986	--
r RT20	--	0.9311	0.9003	0.8959	0.964	0.9758	0.9826	0.9729	0.9828	0.9854	--
RT30 [s]	--	0.3943	0.2938	0.2452	0.2199	0.1996	0.2196	0.2579	0.3192	0.3353	--
r RT30	--	0.9557	0.9742	0.9414	0.9867	0.9883	0.9903	0.9837	0.9913	0.9887	--

ROOM B - Abs0.4 - Position 3

Rectilinear Mesh

Band	Lin	31.5	63	125	250	500	1K	2K	4K	8K	16K
C50 [dB]	0.4418	3.053	10.47	22.04	22.72	25.31	28.84	28.67	21.38	4.625	-0.68
C80 [dB]	1.357	10.9	16.25	30.35	37.65	42.75	46.61	44.42	33.37	5.721	0.5426
D50 [%]	52.54	66.88	91.76	99.38	99.47	99.71	99.87	99.86	99.28	74.36	46.09
TS [ms]	272.6	48.41	25.67	14.88	9.314	8.345	5.234	6.208	6.587	130.9	291.3
EDT [s]	9.92	0.3154	0.1556	0.1397	0.1272	--	--	--	--	--	9.642
RT20 [s]	--	0.5346	0.3161	0.1254	0.1281	0.09766	0.1175	0.1166	0.1543	--	--
r RT20	--	0.9775	0.9815	0.9797	0.9422	0.9242	0.9546	0.9579	0.9722	--	--
RT30 [s]	--	0.6047	0.3297	0.162	0.1146	0.1007	0.1086	0.1092	0.1482	--	--
r RT30	--	0.9835	0.9932	0.9752	0.9671	0.9526	0.9637	0.9778	0.9835	--	--

Triangular Mesh

Band	Lin	31.5	63	125	250	500	1K	2K	4K	8K	16K
C50 [dB]	9.448	0.7795	4.987	16.53	12.01	11.95	13.2	16.29	13.84	11.15	2.624
C80 [dB]	12.89	7.61	11.23	23.64	23.53	22.63	24.22	24.29	20.86	19.21	4.759
D50 [%]	89.8	54.48	75.92	97.82	94.08	94.01	95.43	97.7	96.03	92.87	64.66
TS [ms]	34.4	53.95	35.04	18.41	15.75	19.94	18.2	11.73	14.9	15.86	131.7
EDT [s]	0.3297	0.4069	0.3406	0.1735	0.1883	--	0.2888	0.2351	0.2626	0.2845	2.305

RT20 [s]	--	0.4423	0.3081	0.1956	0.1989	0.2107	0.1867	0.2064	0.2408	0.2705	--
r RT20	--	0.9884	0.9874	0.9586	0.9601	0.9683	0.9823	0.9913	0.9917	0.9949	--
RT30 [s]	--	0.482	0.2947	0.2238	0.2077	0.2021	0.1961	0.2212	0.2569	0.2908	--
r RT30	--	0.9907	0.9934	0.977	0.9868	0.9866	0.9924	0.9945	0.9954	0.9959	--

ROOM B - Abs0.4 - Position 4

Rectilinear Mesh

Band	Lin	31.5	63	125	250	500	1K	2K	4K	8K	16K
C50 [dB]	-1.083	2.154	11.25	16.2	25.02	28.3	25.6	26.1	23.44	2.825	-2.056
C80 [dB]	-0.02644	13.15	18.09	25.91	37.58	42.48	41.68	39.79	35.46	3.795	0.7501
D50 [%]	43.8	62.15	93.02	97.66	99.69	99.85	99.73	99.75	99.55	65.71	38.38
TS [ms]	238.5	50.78	26.65	17.81	9.629	5.286	5.518	4.198	4.92	135.9	251.3
EDT [s]	5.593	0.3143	0.1672	0.1565	0.1423	0.06199	--	--	--	--	5.504
RT20 [s]	--	0.6568	0.256	0.1721	0.119	0.124	0.1171	0.1284	0.1512	7.733	--
r RT20	--	0.9502	0.9848	0.9875	0.9611	0.9195	0.9626	0.9379	0.9549	0.9805	--
RT30 [s]	--	0.705	0.2757	0.1831	0.122	0.1175	0.1245	0.1309	0.1426	--	--
r RT30	--	0.9843	0.9905	0.995	0.9873	0.9725	0.9844	0.9795	0.9698	--	--

Triangular Mesh

Band	Lin	31.5	63	125	250	500	1K	2K	4K	8K	16K
C50 [dB]	9.591	0.5313	5.775	11.54	10.11	13.71	11.38	12.91	12.98	13.42	1.376
C80 [dB]	11.64	12.39	14.25	21.24	19.83	22.52	20.63	19.16	19.3	18.09	2.351
D50 [%]	90.1	53.05	79.08	93.45	91.12	95.92	93.22	95.13	95.21	95.65	57.86
TS [ms]	39.18	53.12	35.	25.57	23.14	12.65	17.04	11.42	11.28	13.97	195.1
EDT [s]	0.344	0.3654	0.3211	0.243	0.2748	--	0.2207	0.2211	0.2393	0.2886	6.175
RT20 [s]	5.917	0.5435	0.2197	0.2079	0.2034	0.2254	0.2508	0.3597	0.3113	0.3041	--
r RT20	0.955	0.8633	0.9921	0.9752	0.9875	0.9763	0.9931	0.9848	0.9923	0.9874	--
RT30 [s]	--	0.6079	0.2513	0.2126	0.2235	0.2473	0.2645	0.3709	0.383	0.3194	--
r RT30	--	0.9669	0.99	0.9875	0.9906	0.9874	0.9944	0.9934	0.9834	0.9947	--

7.13 Room B – AbsComplex

ROOM B – AbsComplex - Position 1

Rectilinear Mesh

Band	Lin	31.5	63	125	250	500	1K	2K	4K	8K	16K
C50 [dB]	2.529	0.5891	9.682	24.77	20.92	26.6	24.95	19.72	18.37	5.335	2.135
C80 [dB]	2.809	12.25	18.33	34.18	31.54	37.7	35.52	30.02	27.5	5.753	2.468
D50 [%]	64.16	53.39	90.28	99.67	99.2	99.78	99.68	98.94	98.57	77.35	62.05
TS [ms]	181.7	54.09	28.5	16.19	12.28	6.888	6.147	6.598	5.851	104.	182.5
EDT [s]	6.31	0.3317	0.2757	0.1022	0.169	0.08083	0.08884	--	--	2.885	6.01
RT20 [s]	--	0.6367	0.2408	0.1117	0.1426	0.112	0.1236	0.1716	0.2166	--	--
r RT20	--	0.9471	0.9696	0.9612	0.9519	0.9604	0.9317	0.936	0.934	--	--
RT30 [s]	--	0.6818	0.2885	0.1564	0.149	0.1236	0.1258	0.1665	0.2106	--	--
r RT30	--	0.9835	0.9781	0.9637	0.9764	0.9769	0.9607	0.972	0.9765	--	--

Triangular Mesh

Band	Lin	31.5	63	125	250	500	1K	2K	4K	8K	16K
C50 [dB]	9.562	-2.143	4.12	12.14	10.74	9.806	13.35	10.74	14.48	12.47	-0.315
C80 [dB]	12.21	8.86	12.93	20.31	18.53	16.37	20.16	18.34	19.66	18.93	1.685

D50 [%]	90.04	37.91	72.08	94.25	92.23	90.53	95.58	92.22	96.56	94.64	48.19
TS [ms]	35.36	59.86	43.64	21.22	24.42	19.46	12.45	14.71	13.04	14.11	206.2
EDT [s]	0.3311	0.3812	0.3394	0.1386	0.2486	0.2838	0.2439	0.2864	0.2376	0.2615	4.916
RT20 [s]	5.625	0.4068	0.2299	0.2682	0.2385	0.2932	0.2587	0.2556	0.2703	0.3343	--
r RT20	0.9328	0.9352	0.9553	0.9573	0.9909	0.9911	0.9809	0.9786	0.9774	0.9864	--
RT30 [s]	--	0.5442	0.285	0.244	0.2625	0.3054	0.2812	0.2458	0.2929	0.3864	--
r RT30	--	0.9582	0.9589	0.9842	0.9918	0.9949	0.9899	0.991	0.9882	0.9888	--

ROOM B – AbsComplex - Position 2

Rectilinear Mesh

Band	Lin	31.5	63	125	250	500	1K	2K	4K	8K	16K
C50 [dB]	5.815	0.8387	11.86	23.38	23.94	30.62	31.61	24.53	20.96	8.168	5.18
C80 [dB]	7.724	11.46	16.27	31.61	39.36	44.05	45.17	38.3	32.6	10.59	7.399
D50 [%]	79.23	54.81	93.88	99.54	99.6	99.91	99.93	99.65	99.2	86.77	76.72
TS [ms]	94.89	51.44	27.17	18.79	9.678	5.415	3.606	5.271	6.173	52.45	98.08
EDT [s]	--	0.3537	0.1802	0.2037	--	0.03657	0.02591	--	--	0.6523	--
RT20 [s]	--	0.5178	0.3406	0.06913	0.1174	0.1045	0.157	0.1272	0.1559	6.653	--
r RT20	--	0.9363	0.9762	0.9304	0.9409	0.9326	0.8541	0.8976	0.922	0.9336	--
RT30 [s]	--	0.5336	0.3556	0.1565	0.1169	0.1127	0.1177	0.1264	0.154	--	--
r RT30	--	0.9798	0.9933	0.8723	0.9644	0.9781	0.9625	0.9347	0.9666	--	--

Triangular Mesh

Band	Lin	31.5	63	125	250	500	1K	2K	4K	8K	16K
C50 [dB]	10.56	-2.446	13.62	12.4	9.923	11.56	14.5	14.85	12.08	12.24	3.037
C80 [dB]	13.97	6.214	17.51	18.66	16.73	19.64	22.72	25.17	20.47	17.91	4.351
D50 [%]	91.91	36.28	95.84	94.56	90.76	93.47	96.57	96.83	94.17	94.36	66.8
TS [ms]	22.55	59.73	27.08	27.33	21.3	16.28	8.501	12.24	11.66	11.13	118.
EDT [s]	0.317	0.4408	0.1839	--	0.2429	0.2365	--	--	--	--	2.34
RT20 [s]	--	0.2824	0.3214	0.2538	0.2618	0.2402	0.2637	0.1842	0.2637	0.3302	--
r RT20	--	0.9579	0.9483	0.9499	0.9753	0.9853	0.9811	0.9611	0.9715	0.9921	--
RT30 [s]	--	0.3829	0.308	0.2612	0.2784	0.2459	0.2651	0.199	0.2434	0.335	--
r RT30	--	0.953	0.9834	0.9825	0.9886	0.9911	0.9919	0.9818	0.988	0.9971	--

ROOM B – AbsComplex - Position 3

Rectilinear Mesh

Band	Lin	31.5	63	125	250	500	1K	2K	4K	8K	16K
C50 [dB]	0.4036	2.058	10.	21.76	23.32	21.38	19.12	22.65	16.8	4.234	-1.048
C80 [dB]	1.252	11.18	17.	29.95	34.87	36.9	33.53	35.11	25.84	5.247	0.0864
D50 [%]	52.32	61.63	90.91	99.34	99.54	99.28	98.79	99.46	97.96	72.61	44.
TS [ms]	269.8	49.98	26.28	14.62	9.118	9.561	12.1	5.226	6.837	134.7	296.4
EDT [s]	9.482	0.3348	0.1952	0.1324	9.54e-002	0.1922	--	--	--	--	9.172
RT20 [s]	--	0.5139	0.2723	0.1267	0.1315	0.1199	--	0.1751	0.202	--	--
r RT20	--	0.9727	0.9855	0.9858	0.96	0.9039	--	0.8833	0.9485	--	--
RT30 [s]	--	0.569	0.2989	0.1669	0.1381	0.1269	0.1544	0.1672	0.2096	--	--
r RT30	--	0.9862	0.9897	0.9735	0.9705	0.9605	0.9158	0.9403	0.9699	--	--

Triangular Mesh

Band	Lin	31.5	63	125	250	500	1K	2K	4K	8K	16K
C50 [dB]	9.821	-0.3498	4.965	13.81	11.7	9.85	9.444	15.42	14.33	11.19	2.603
C80 [dB]	13.2	7.076	12.83	22.69	19.25	18.34	17.17	22.91	20.1	18.94	4.42

D50 [%]	90.56	47.99	75.83	96.	93.67	90.62	89.79	97.21	96.44	92.93	64.55
TS [ms]	30.96	55.9	35.15	19.18	17.17	22.41	26.25	9.153	12.77	14.53	138.3
EDT [s]	0.3275	0.4123	0.342	0.1842	0.201	0.2242	0.2944	--	0.2528	0.2762	2.705
RT20 [s]	7.513	0.3488	0.3066	0.207	0.2751	0.2728	0.2531	0.2646	0.3065	0.3103	--
r RT20	0.8546	0.9777	0.9819	0.9765	0.9791	0.9873	0.9927	0.9834	0.969	0.9767	--
RT30 [s]	--	0.4506	0.2996	0.2271	0.2895	0.2817	0.2615	0.2689	0.3184	0.3756	--
r RT30	--	0.9714	0.9913	0.9865	0.9912	0.9949	0.9959	0.9878	0.9859	0.9831	--

ROOM B – AbsComplex - Position 4

Rectilinear Mesh

Band	Lin	31.5	63	125	250	500	1K	2K	4K	8K	16K
C50 [dB]	-0.7941	1.409	12.27	15.38	25.53	26.89	26.75	22.34	18.38	3.039	-2.189
C80 [dB]	0.3215	12.93	19.09	24.86	36.65	37.5	37.21	32.88	28.78	4.2	-0.729
D50 [%]	45.44	58.04	94.4	97.18	99.72	99.8	99.79	99.42	98.57	66.81	37.66
TS [ms]	227.5	52.11	26.53	20.18	8.607	6.738	5.677	6.065	7.103	125.1	247.7
EDT [s]	5.548	0.326	0.1646	0.1601	0.1111	0.07852	0.08971	--	--	--	5.437
RT20 [s]	7.516	0.6631	0.2448	0.1792	0.1221	0.1253	0.1156	0.1519	0.2074	7.304	7.442
r RT20	0.9782	0.9394	0.9854	0.9884	0.9606	0.8728	0.9327	0.8938	0.9197	0.9831	0.9759
RT30 [s]	--	0.703	0.2639	0.186	0.1232	0.1276	0.1244	0.1542	0.189	--	--
r RT30	--	0.9833	0.9899	0.9959	0.9817	0.9456	0.9581	0.9471	0.9586	--	--

Triangular Mesh

Band	Lin	31.5	63	125	250	500	1K	2K	4K	8K	16K
C50 [dB]	9.246	-0.17	5.836	10.91	8.979	13.09	12.38	12.47	12.08	12.82	1.232
C80 [dB]	11.43	10.76	13.58	19.19	18.2	21.38	21.72	19.48	18.32	16.7	2.455
D50 [%]	89.37	49.02	79.31	92.5	88.77	95.32	94.54	94.64	94.17	95.04	57.05
TS [ms]	37.64	54.99	35.17	26.81	23.77	14.92	18.44	11.7	12.08	15.33	176.1
EDT [s]	0.3651	0.393	0.3201	0.2471	0.3139	--	0.2248	0.2355	0.2556	0.3139	5.223
RT20 [s]	5.579	0.4301	0.2462	0.239	0.2022	0.2195	0.2051	0.2917	0.3	0.3584	--
r RT20	0.9467	0.9207	0.9953	0.9732	0.979	0.9652	0.9766	0.9931	0.9873	0.9763	--
RT30 [s]	--	0.5636	0.2551	0.2358	0.2188	0.2483	0.2409	0.2803	0.3108	0.3738	--
r RT30	--	0.9556	0.9972	0.989	0.9882	0.9826	0.9825	0.9955	0.9937	0.9926	--

7.14 Room C – Abs0.9

ROOM C - Abs0.9 - Position 1

Rectilinear Mesh

Band	Lin	31.5	63	125	250	500	1K	2K	4K	8K	16K
C50 [dB]	-1.926	-5.467	-4.996	0.7315	0.04861	1.041	2.848	1.386	0.8809	-1.332	-2.966
C80 [dB]	-0.281	2.075	1.503	2.458	6.302	4.649	5.887	5.015	4.132	0.6641	-1.573
D50 [%]	39.09	22.12	24.04	54.2	50.28	55.97	65.83	57.91	55.05	42.39	33.56
TS [ms]	298.9	92.07	85.91	63.28	63.52	56.34	46.75	54.92	64.33	185.5	342.5
EDT [s]	6.554	0.9062	0.8876	0.7991	0.8383	0.7466	0.7369	0.8323	0.9641	2.818	6.781
RT20 [s]	--	0.9284	0.9383	0.7657	0.7524	0.7655	0.7607	0.8052	1.131	9.944	--
r RT20	--	0.9824	0.9814	0.9935	0.9804	0.9973	0.9958	0.9983	0.9976	0.9672	--
RT30 [s]	--	0.9922	0.9449	0.8032	0.7686	0.7717	0.7686	0.8416	1.234	--	--
r RT30	--	0.9895	0.9942	0.9954	0.9903	0.999	0.9978	0.9985	0.9956	--	--

Triangular Mesh

Band	Lin	31.5	63	125	250	500	1K	2K	4K	8K	16K
C50 [dB]	-3.042	-9.318	-9.005	-3.925	-4.181	-3.78	-2.632	-3.381	-2.714	-2.956	-6.128
C80 [dB]	-0.8758	-3.097	-3.026	-2.314	0.08442	-0.8354	-0.4008	-0.9065	-0.6819	-0.7392	-4.258
D50 [%]	33.17	10.47	11.17	28.83	27.63	29.52	35.3	31.46	34.87	33.61	19.61
TS [ms]	150.3	183.6	157.8	129.3	126.9	131.9	119.4	123.8	131.9	142.3	350.4
EDT [s]	2.082	2.163	1.962	1.628	1.505	1.914	1.704	1.673	1.845	2.089	5.223
RT20 [s]	4.362	2.241	2.085	1.802	1.938	1.644	1.669	1.745	2.138	2.335	--
r RT20	0.9368	0.9982	0.9951	0.9967	0.9924	0.998	0.9986	0.9979	0.9971	0.9972	--
RT30 [s]	--	2.265	2.096	1.856	1.915	1.674	1.642	1.856	2.362	2.532	--
r RT30	--	0.9992	0.9981	0.9977	0.9977	0.999	0.9992	0.9979	0.9949	0.9966	--

ROOM C - Abs0.9 - Position 2

Rectilinear Mesh

Band	Lin	31.5	63	125	250	500	1K	2K	4K	8K	16K
C50 [dB]	0.3653	-3.613	2.548	4.09	2.27	1.819	3.409	3.155	2.383	0.8071	-0.651
C80 [dB]	1.868	1.635	5.324	8.084	5.578	5.6	5.17	6.881	4.749	2.402	0.9818
D50 [%]	52.1	30.33	64.26	71.95	62.78	60.32	68.67	67.4	63.38	54.63	46.26
TS [ms]	239.4	99.9	53.53	49.56	54.66	53.55	42.19	43.69	56.05	150.5	272.
EDT [s]	6.096	1.187	0.7865	0.4734	0.7039	0.7246	0.9325	0.7757	0.9776	2.458	6.874
RT20 [s]	--	0.9637	0.7789	1.012	0.7311	0.6889	0.7074	0.8507	1.101	9.932	--
r RT20	--	0.965	0.9976	0.9725	0.9671	0.9968	0.9956	0.9977	0.9957	0.9716	--
RT30 [s]	--	0.9683	0.7827	0.9033	0.8124	0.6759	0.7309	0.8952	1.217	--	--
r RT30	--	0.9863	0.9985	0.9848	0.9857	0.9984	0.9977	0.9976	0.995	--	--

Triangular Mesh

Band	Lin	31.5	63	125	250	500	1K	2K	4K	8K	16K
C50 [dB]	-2.341	-7.732	-0.5846	-0.5202	-1.529	-2.499	-2.308	-0.9756	-2.205	-2.794	-4.372
C80 [dB]	0.08711	-4.026	1.258	1.996	1.02	0.6639	-0.6059	1.32	0.388	-0.1497	-2.418
D50 [%]	36.84	14.42	46.64	47.01	41.29	36.	37.02	44.41	37.57	34.45	26.76
TS [ms]	132.4	194.6	101.4	116.8	108.5	106.7	108.1	105.	116.	128.4	278.
EDT [s]	1.91	2.167	1.589	2.169	1.481	1.43	1.516	1.649	1.696	1.892	4.317
RT20 [s]	4.005	2.155	1.698	1.945	1.888	1.604	1.603	1.77	2.225	2.342	--
r RT20	0.9445	0.9944	0.9992	0.9936	0.9979	0.9959	0.9981	0.9997	0.9982	0.9957	--
RT30 [s]	--	2.165	1.744	1.97	1.877	1.697	1.682	1.848	2.364	2.584	--
r RT30	--	0.9977	0.9992	0.9968	0.9989	0.9971	0.9977	0.999	0.9976	0.9952	--

ROOM C - Abs0.9 - Position 3

Rectilinear Mesh

Band	Lin	31.5	63	125	250	500	1K	2K	4K	8K	16K
C50 [dB]	-4.514	-6.914	0.7318	2.06	4.31	0.8389	-1.179	2.489	0.1021	-3.622	-6.173
C80 [dB]	-2.266	-0.1012	4.937	5.325	6.96	4.079	2.924	5.513	3.783	-1.087	-4.084
D50 [%]	26.13	16.91	54.2	61.64	72.96	54.81	43.26	63.95	50.59	30.28	19.44
TS [ms]	398.7	100.5	66.67	51.61	49.67	62.31	72.61	51.85	69.32	245.5	459.9
EDT [s]	10.2	0.7539	0.7827	0.757	0.7713	0.8189	0.8288	0.8419	0.9809	3.554	10.16
RT20 [s]	--	0.9961	0.8719	0.8747	0.837	0.7313	0.7621	0.8741	1.137	--	--
r RT20	--	0.9895	0.9838	0.9792	0.9959	0.99	0.9981	0.9992	0.9939	--	--
RT30 [s]	--	0.9891	0.8916	0.7759	0.7987	0.7264	0.7769	0.8833	1.281	--	--
r RT30	--	0.9955	0.9937	0.9851	0.9967	0.9955	0.9991	0.9995	0.9931	--	--

Triangular Mesh

Band	Lin	31.5	63	125	250	500	1K	2K	4K	8K	16K
C50 [dB]	-3.717	-9.644	-3.381	-2.903	-0.93	-3.23	-5.131	-3.398	-2.929	-3.572	-6.292
C80 [dB]	-1.031	-3.702	-0.43	-0.6057	0.7115	-0.8602	-1.737	-0.7516	-0.5188	-0.6829	-4.141
D50 [%]	29.82	9.791	31.46	33.89	44.67	32.22	23.48	31.38	33.75	30.53	19.02
TS [ms]	156.4	169.1	138.4	130.4	117.8	126.2	135.1	132.9	134.	141.8	306.6
EDT [s]	2.085	1.964	1.836	2.044	1.808	1.747	1.578	1.969	1.808	1.967	4.147
RT20 [s]	4.448	2.049	1.916	1.843	1.714	1.631	1.72	1.728	2.292	2.404	8.495
r RT20	0.9398	0.9961	0.9922	0.9884	0.9954	0.9949	0.9987	0.9976	0.9959	0.995	0.9828
RT30 [s]	--	2.074	1.932	1.816	1.783	1.664	1.666	1.797	2.424	2.637	--
r RT30	--	0.9982	0.9966	0.9952	0.9977	0.9978	0.9991	0.9984	0.9974	0.9954	--

ROOM C - Abs0.9 - Position 4
Rectilinear Mesh

Band	Lin	31.5	63	125	250	500	1K	2K	4K	8K	16K
C50 [dB]	-2.867	-10.53	-3.88	0.00195	3.612	3.384	2.984	3.458	1.235	-1.394	-4.523
C80 [dB]	-0.8889	-3.703	0.9532	1.302	5.933	4.977	5.287	6.517	4.063	0.8196	-2.544
D50 [%]	34.07	8.136	29.04	49.99	69.67	68.55	66.53	68.92	57.06	42.04	26.08
TS [ms]	352.4	110.9	81.77	72.16	50.47	48.6	52.55	46.03	65.92	201.8	409.9
EDT [s]	8.431	0.8183	0.7528	1.039	0.6918	0.8283	0.8233	0.7835	1.003	3.383	8.338
RT20 [s]	--	1.004	0.8686	0.7486	0.9112	0.6663	0.7536	0.7937	1.2	9.576	--
r RT20	--	0.9963	0.9306	0.9743	0.9901	0.9934	0.9976	0.999	0.9987	0.9714	--
RT30 [s]	--	1.002	0.8994	0.8524	0.8476	0.7227	0.7744	0.8893	1.232	--	--
r RT30	--	0.9983	0.9748	0.9822	0.9931	0.995	0.9983	0.9943	0.9987	--	--

Triangular Mesh

Band	Lin	31.5	63	125	250	500	1K	2K	4K	8K	16K
C50 [dB]	-2.992	-14.14	-7.852	-5.404	-1.516	-1.723	-2.264	-1.914	-3.086	-2.862	-5.997
C80 [dB]	-0.6993	-6.746	-3.63	-4.174	0.04037	-0.5172	-0.7383	0.5254	-0.8388	-0.5757	-3.3
D50 [%]	33.43	3.713	14.09	22.37	41.36	40.21	37.26	39.16	32.94	34.09	20.09
TS [ms]	144.1	180.9	153.1	151.1	124.3	111.6	122.3	112.5	130.3	135.9	318.7
EDT [s]	2.002	1.971	1.826	1.601	2.027	1.49	1.71	1.643	1.857	1.935	4.993
RT20 [s]	3.878	2.034	2.022	1.934	1.592	1.716	1.604	1.763	2.125	2.397	--
r RT20	0.959	0.9988	0.9903	0.993	0.9955	0.996	0.997	0.9995	0.9955	0.9993	--
RT30 [s]	--	2.043	2.06	1.939	1.805	1.714	1.701	1.76	2.456	2.52	--
r RT30	--	0.9994	0.996	0.997	0.9922	0.9987	0.9975	0.9997	0.9909	0.9985	--

7.15 Room C – Abs0.4
ROOM C - Abs0.4 - Position 1
Rectilinear Mesh

Band	Lin	31.5	63	125	250	500	1K	2K	4K	8K	16K
C50 [dB]	4.812	2.917	11.9	21.12	20.38	24.24	26.22	24.55	20.11	7.252	4.468
C80 [dB]	5.135	11.79	20.33	29.68	34.97	36.01	38.5	34.71	31.64	7.767	4.853
D50 [%]	75.18	66.19	93.94	99.23	99.09	99.62	99.76	99.65	99.03	84.15	73.67
TS [ms]	106.8	49.71	25.48	15.31	11.18	7.835	4.615	5.024	5.135	63.21	108.6
EDT [s]	3.824	0.3429	0.1674	0.1031	0.1207	0.1293	--	--	0.1658	1.441	3.64
RT20 [s]	6.296	0.6815	0.2336	0.1507	0.1445	0.124	0.1317	0.146	0.1747	6.314	6.196
r RT20	0.9786	0.9566	0.9682	0.9696	0.965	0.984	0.9758	0.974	0.9745	0.9758	0.9783

RT30 [s]	--	0.7826	0.2474	0.1651	0.1356	0.1265	0.1373	0.1498	0.1835	--	--
r RT30	--	0.9845	0.987	0.9859	0.984	0.9912	0.9858	0.9876	0.9885	--	--

Triangular Mesh

Band	Lin	31.5	63	125	250	500	1K	2K	4K	8K	16K
C50 [dB]	9.559	-0.3389	4.232	13.05	9.068	11.57	12.5	11.92	12.86	12.39	0.1782
C80 [dB]	12.15	10.41	15.53	17.49	23.34	18.91	18.9	16.07	18.6	18.37	1.714
D50 [%]	90.03	48.05	72.6	95.28	88.97	93.48	94.67	93.96	95.08	94.55	51.03
TS [ms]	36.58	54.99	34.69	21.43	26.04	18.75	12.15	14.14	13.57	14.41	217.8
EDT [s]	0.34	0.3874	0.4063	0.2008	0.3098	0.2627	0.2413	0.2546	0.263	0.2734	5.602
RT20 [s]	6.132	0.6156	0.2273	0.2712	0.1495	0.2466	0.2763	0.3597	0.2996	0.3213	--
r RT20	0.9319	0.9546	0.9545	0.9738	0.9513	0.9897	0.9922	0.9911	0.9891	0.9924	--
RT30 [s]	--	0.7483	0.2488	0.256	0.2628	0.2676	0.2867	0.3568	0.3727	0.3482	--
r RT30	--	0.9778	0.96	0.9887	0.9064	0.9912	0.9951	0.9955	0.9812	0.995	--

ROOM C - Abs0.4 - Position 2

Rectilinear Mesh

Band	Lin	31.5	63	125	250	500	1K	2K	4K	8K	16K
C50 [dB]	7.957	0.9235	10.23	23.51	29.81	28.6	30.84	24.78	24.73	9.994	7.272
C80 [dB]	10.16	12.81	15.77	33.03	41.81	44.15	46.58	40.55	34.97	12.71	9.806
D50 [%]	86.2	55.3	91.33	99.56	99.9	99.86	99.92	99.67	99.66	90.9	84.22
TS [ms]	57.42	51.63	26.67	15.1	7.307	5.987	3.762	3.823	5.051	32.93	59.22
EDT [s]	0.7552	0.3439	0.1625	0.1465	0.05671	0.02364	--	--	0.5803	0.8329	
RT20 [s]	8.489	0.5494	0.3244	0.1132	0.1379	0.1324	0.1329	0.1598	0.1367	8.616	8.361
r RT20	0.9433	0.9388	0.9856	0.9709	0.979	0.9171	0.8616	0.9133	0.8691	0.8782	0.9423
RT30 [s]	--	0.5861	0.342	0.1398	0.1143	0.1149	0.1175	0.1404	0.1504	--	--
r RT30	--	0.9825	0.9951	0.9741	0.9794	0.9696	0.9573	0.9647	0.9534	--	--

Triangular Mesh

Band	Lin	31.5	63	125	250	500	1K	2K	4K	8K	16K
C50 [dB]	10.12	0.08687	7.534	14.56	13.26	13.15	16.82	12.33	12.33	11.46	2.34
C80 [dB]	13.44	12.48	12.79	21.67	20.14	21.85	23.17	20.57	18.37	18.53	3.817
D50 [%]	91.13	49.5	85.	96.62	95.5	95.38	97.96	94.48	94.48	93.33	63.16
TS [ms]	24.3	52.44	30.3	23.09	16.97	16.38	8.336	12.27	11.73	11.39	132.2
EDT [s]	0.3903	0.3688	0.2578	0.2495	0.3124	0.2955	--	--	--	--	2.686
RT20 [s]	--	0.3907	0.373	0.1945	0.2566	0.2139	0.244	0.2671	0.3132	0.328	--
r RT20	--	0.9214	0.9919	0.9695	0.9776	0.9868	0.982	0.9848	0.9894	0.9902	--
RT30 [s]	--	0.5943	0.3728	0.2454	0.2322	0.2181	0.2402	0.2664	0.32	0.3437	--
r RT30	--	0.9387	0.9975	0.9713	0.9821	0.9912	0.9917	0.9917	0.9939	0.9953	--

ROOM C - Abs0.4 - Position 3

Rectilinear Mesh

Band	Lin	31.5	63	125	250	500	1K	2K	4K	8K	16K
C50 [dB]	1.267	0.6608	11.95	20.75	23.94	24.41	25.85	23.22	19.49	4.914	-0.202
C80 [dB]	2.237	13.27	18.06	31.12	36.41	37.62	39.15	37.45	32.	6.171	1.148
D50 [%]	57.24	53.8	93.99	99.17	99.6	99.64	99.74	99.53	98.89	75.61	48.84
TS [ms]	211.6	52.84	27.73	13.73	11.05	7.941	5.683	5.844	6.601	104.7	234.8
EDT [s]	6.117	0.3593	0.1979	0.1138	0.2039	--	--	--	--	--	6.705
RT20 [s]	--	0.5712	0.2246	0.1443	0.129	0.1325	0.1194	0.1545	0.2051	9.093	--
r RT20	--	0.8937	0.9735	0.957	0.9222	0.898	0.8539	0.9229	0.9169	0.8901	--

RT30 [s]	--	0.6453	0.2629	0.1683	0.1306	0.1348	0.1344	0.1506	0.1856	--	--
r RT30	--	0.9732	0.9834	0.9758	0.9467	0.9212	0.9232	0.9291	0.9519	--	--

Triangular Mesh

Band	Lin	31.5	63	125	250	500	1K	2K	4K	8K	16K
C50 [dB]	8.87	-2.256	6.594	10.85	16.13	12.62	11.18	13.39	12.51	10.87	2.163
C80 [dB]	12.45	8.157	14.96	19.2	22.96	19.42	20.08	21.6	20.1	17.6	4.653
D50 [%]	88.52	37.3	82.03	92.4	97.62	94.81	92.91	95.62	94.69	92.43	62.2
TS [ms]	32.8	61.08	35.83	19.63	19.55	20.05	19.61	11.27	17.55	16.09	116.5
EDT [s]	0.3805	0.3956	0.2979	0.2011	0.3303	--	0.2873	0.314	--	0.3634	1.734
RT20 [s]	--	0.3541	0.2699	0.2586	0.2547	0.3091	0.2472	0.2575	0.2685	0.2968	--
r RT20	--	0.9873	0.971	0.9751	0.9031	0.9555	0.9752	0.9824	0.9746	0.9897	--
RT30 [s]	--	0.42	0.2933	0.2573	0.2506	0.261	0.234	0.2446	0.2779	0.3294	--
r RT30	--	0.9806	0.9849	0.9832	0.9696	0.9678	0.9867	0.9908	0.9901	0.9924	--

ROOM C - Abs0.4 - Position 4

Rectilinear Mesh

Band	Lin	31.5	63	125	250	500	1K	2K	4K	8K	16K
C50 [dB]	0.1194	1.173	8.955	16.53	25.73	29.69	26.38	27.25	23.72	3.835	-1.028
C80 [dB]	1.369	8.211	18.51	27.91	36.03	39.35	40.84	38.64	32.89	5.149	0.4358
D50 [%]	50.69	56.71	88.72	97.82	99.73	99.89	99.77	99.81	99.58	70.75	44.11
TS [ms]	233.5	55.35	28.19	16.47	9.01	7.42	6.825	5.92	5.84	124.5	251.8
EDT [s]	6.819	0.3779	0.2408	0.1443	0.1024	0.1109	--	--	--	--	6.601
RT20 [s]	--	0.7	0.216	0.1662	0.1353	0.123	0.123	0.1557	0.1637	--	--
r RT20	--	0.9869	0.9912	0.9806	0.9562	0.8909	0.9446	0.8621	0.9369	--	--
RT30 [s]	--	0.7743	0.2466	0.1795	0.1368	0.1177	0.142	0.144	0.1682	--	--
r RT30	--	0.9916	0.985	0.9914	0.9814	0.9643	0.9684	0.9541	0.972	--	--

Triangular Mesh

Band	Lin	31.5	63	125	250	500	1K	2K	4K	8K	16K
C50 [dB]	9.584	-3.35	3.99	12.91	14.09	15.85	12.69	12.99	12.92	11.89	1.534
C80 [dB]	12.1	2.733	14.95	16.86	19.49	19.52	19.25	19.6	18.63	16.9	2.696
D50 [%]	90.09	31.62	71.48	95.13	96.25	97.47	94.9	95.22	95.14	93.93	58.74
TS [ms]	36.54	68.76	38.78	21.78	17.49	14.19	18.13	13.79	13.48	15.82	184.9
EDT [s]	0.3265	0.5652	0.3394	0.1573	0.2726	0.2261	0.2036	0.2568	0.2362	0.2722	6.138
RT20 [s]	6.314	0.6522	0.1937	0.3188	0.2483	0.3036	0.291	0.3343	0.319	0.3375	--
r RT20	0.9114	0.9044	0.9899	0.9614	0.9761	0.9685	0.9845	0.98	0.9926	0.9931	--
RT30 [s]	--	0.7508	0.2096	0.294	0.235	0.2941	0.3277	0.3673	0.3335	0.3492	--
r RT30	--	0.9713	0.9894	0.9799	0.9904	0.9893	0.9895	0.9898	0.9939	0.9973	--

7.16 Room C – AbsComplex

ROOM C – AbsComplex - Position 1

Rectilinear Mesh

Band	Lin	31.5	63	125	250	500	1K	2K	4K	8K	16K
C50 [dB]	4.566	2.158	10.05	20.73	17.62	24.49	24.33	19.33	16.49	6.86	4.048
C80 [dB]	4.914	11.84	19.86	30.12	28.67	34.35	33.59	28.64	25.27	7.406	4.435
D50 [%]	74.11	62.17	91.01	99.16	98.3	99.65	99.63	98.85	97.8	82.91	71.75
TS [ms]	110.6	51.16	25.96	16.11	12.64	6.999	5.562	6.713	6.447	64.67	114.7
EDT [s]	3.775	0.3224	0.1673	0.1095	0.1749	0.09238	0.09959	0.1515	0.1326	1.42	3.583

RT20 [s]	6.208	0.6788	0.2342	0.1556	0.1762	0.1347	0.1465	0.205	0.2707	6.224	6.104
r RT20	0.9754	0.9623	0.9763	0.9606	0.9714	0.9785	0.9721	0.9625	0.9609	0.9771	0.9755
RT30 [s]	--	0.7767	0.2716	0.1655	0.1803	0.1563	0.168	0.2019	0.2584	--	--
r RT30	--	0.9849	0.9778	0.9856	0.9885	0.9812	0.9785	0.9816	0.9872	--	--

Triangular Mesh

Band	Lin	31.5	63	125	250	500	1K	2K	4K	8K	16K
C50 [dB]	9.176	0.07988	3.175	11.75	6.93	9.993	14.44	11.4	12.85	11.63	0.0265
C80 [dB]	11.76	11.8	14.65	17.39	16.22	15.56	20.04	17.66	17.91	16.43	1.853
D50 [%]	89.21	49.54	67.5	93.73	83.14	90.9	96.53	93.25	95.07	93.57	50.15
TS [ms]	36.13	53.84	37.31	22.69	29.99	19.58	11.11	14.11	13.79	15.05	198.5
EDT [s]	0.3731	0.3708	0.4241	0.2162	0.3502	0.2833	0.2187	0.2752	0.2833	0.2896	4.914
RT20 [s]	5.974	0.6006	0.227	0.2879	0.2607	0.3239	0.3009	0.2982	0.3323	0.4477	--
r RT20	0.9207	0.9267	0.8867	0.9898	0.9865	0.9914	0.9904	0.9929	0.985	0.9796	--
RT30 [s]	--	0.6927	0.2568	0.2717	0.301	0.3335	0.2996	0.3079	0.3696	0.4943	--
r RT30	--	0.9747	0.9298	0.9883	0.9871	0.9955	0.9948	0.9933	0.9902	0.9905	--

ROOM C – AbsComplex - Position 2

Rectilinear Mesh

Band	Lin	31.5	63	125	250	500	1K	2K	4K	8K	16K
C50 [dB]	7.72	1.648	10.15	22.79	25.25	29.84	32.05	26.52	22.59	9.603	6.885
C80 [dB]	9.89	12.3	15.47	32.	39.54	43.35	43.81	37.87	33.31	12.38	9.387
D50 [%]	85.54	59.38	91.2	99.48	99.7	99.9	99.94	99.78	99.45	90.13	82.99
TS [ms]	60.3	50.76	27.44	18.16	9.6	5.343	3.443	4.673	6.037	34.33	63.61
EDT [s]	0.7461	0.3248	0.1738	0.193	0.1652	0.03602	0.0275	--	--	0.5782	0.9458
RT20 [s]	8.143	0.5777	0.3379	0.09375	0.1252	0.1445	0.1934	--	0.1733	8.019	8.019
r RT20	0.9601	0.9711	0.989	0.9746	0.9438	0.96	0.8759	--	0.9015	0.9016	0.9614
RT30 [s]	--	0.6064	0.3584	0.1362	0.1156	0.1268	0.1368	0.1474	0.1795	--	--
r RT30	--	0.9889	0.9959	0.9463	0.9815	0.9812	0.9465	0.9512	0.9598	--	--

Triangular Mesh

Band	Lin	31.5	63	125	250	500	1K	2K	4K	8K	16K
C50 [dB]	10.16	0.2033	7.756	12.37	11.13	12.07	15.43	15.28	12.86	11.15	2.44
C80 [dB]	13.55	11.81	12.81	18.32	18.09	19.86	21.27	24.62	20.68	16.76	4.307
D50 [%]	91.22	51.17	85.64	94.53	92.85	94.15	97.22	97.12	95.07	92.88	63.69
TS [ms]	23.39	52.64	30.46	26.77	22.13	15.84	7.999	11.04	11.44	11.85	119.5
EDT [s]	0.3797	0.3576	0.2489	0.2653	0.3258	0.3063	--	--	--	--	2.209
RT20 [s]	--	0.3721	0.3821	0.2733	0.2852	0.2649	0.3003	0.2147	0.2686	0.3893	6.936
r RT20	--	0.9566	0.9921	0.9718	0.969	0.9903	0.986	0.9806	0.9818	0.9916	0.9602
RT30 [s]	--	0.5642	0.3783	0.2934	0.2753	0.2689	0.2871	0.2296	0.2746	0.4027	--
r RT30	--	0.9466	0.9975	0.9886	0.9881	0.9924	0.9907	0.9891	0.9912	0.9966	--

ROOM C – AbsComplex - Position 3

Rectilinear Mesh

Band	Lin	31.5	63	125	250	500	1K	2K	4K	8K	16K
C50 [dB]	1.144	0.4395	13.89	20.97	24.54	21.9	17.77	19.19	15.66	4.388	-0.695
C80 [dB]	2.033	13.	19.46	30.28	35.45	33.68	28.08	29.88	25.09	5.481	0.5205
D50 [%]	56.55	52.53	96.07	99.21	99.65	99.36	98.36	98.81	97.36	73.31	46.01
TS [ms]	207.6	53.26	26.37	14.2	9.797	8.811	12.24	5.85	6.833	107.3	239.1
EDT [s]	5.003	0.3692	0.1828	0.1233	0.102	0.2021	--	--	--	2.36	5.827

RT20 [s]	--	0.5744	0.2256	0.1425	0.1186	0.1613	--	0.218	0.2774	8.271	--
r RT20	--	0.8989	0.9483	0.9661	0.9516	0.8907	--	0.851	0.8803	0.9163	--
RT30 [s]	--	0.6426	0.2397	0.1748	0.1395	0.1669	0.1864	0.2053	0.2676	--	--
r RT30	--	0.974	0.9759	0.9783	0.9678	0.9458	0.911	0.9303	0.9652	--	--

Triangular Mesh

Band	Lin	31.5	63	125	250	500	1K	2K	4K	8K	16K
C50 [dB]	9.217	-2.512	7.33	13.31	14.55	10.73	8.38	13.43	12.98	11.31	1.801
C80 [dB]	12.34	8.078	15.51	18.48	20.55	16.77	16.27	20.26	18.22	16.49	4.181
D50 [%]	89.31	35.93	84.39	95.54	96.61	92.21	87.32	95.65	95.21	93.11	60.22
TS [ms]	30.42	61.27	34.63	18.85	19.16	24.1	26.73	8.525	15.21	14.73	127.2
EDT [s]	0.3885	0.3971	0.2852	0.1759	0.3083	--	0.3084	--	--	0.3638	2.052
RT20 [s]	--	0.3331	0.2287	0.2953	0.2981	0.324	0.289	0.3308	0.3834	0.4418	--
r RT20	--	0.9843	0.9618	0.9728	0.9192	0.9757	0.9814	0.9724	0.9481	0.9738	--
RT30 [s]	--	0.4286	0.3069	0.279	0.2945	0.3179	0.2996	0.3318	0.3882	0.4875	--
r RT30	--	0.9694	0.9575	0.9893	0.976	0.9888	0.9882	0.9838	0.9794	0.9884	--

ROOM C – AbsComplex - Position 4

Rectilinear Mesh

Band	Lin	31.5	63	125	250	500	1K	2K	4K	8K	16K
C50 [dB]	0.5288	0.1264	8.682	14.78	25.06	29.83	27.84	24.06	19.03	4.019	-1.108
C80 [dB]	1.721	7.475	18.39	26.72	32.78	38.35	36.75	31.72	25.93	5.445	0.3108
D50 [%]	53.04	50.73	88.07	96.78	99.69	99.9	99.84	99.61	98.76	71.62	43.66
TS [ms]	222.6	57.46	28.88	19.67	9.081	8.163	6.691	7.718	8.462	114.1	252.3
EDT [s]	6.783	0.4022	0.2414	0.1583	0.09417	0.1208	0.1173	--	--	--	6.478
RT20 [s]	--	0.71	0.2178	0.1683	0.143	--	0.1351	0.1709	0.2327	--	--
r RT20	--	0.9816	0.9924	0.9823	0.9202	--	0.906	0.8943	0.9345	--	--
RT30 [s]	--	0.7954	0.2289	0.1816	0.1609	0.1479	0.1615	0.1846	0.2277	--	--
r RT30	--	0.9905	0.9942	0.9915	0.9682	0.9128	0.929	0.9502	0.9709	--	--

Triangular Mesh

Band	Lin	31.5	63	125	250	500	1K	2K	4K	8K	16K
C50 [dB]	8.942	-3.19	3.589	10.33	12.5	15.4	14.54	13.29	12.25	10.8	1.24
C80 [dB]	11.52	2.421	15.2	15.18	17.32	19.17	20.52	20.35	17.81	14.75	2.792
D50 [%]	88.69	32.42	69.56	91.51	94.68	97.2	96.6	95.53	94.38	92.32	57.09
TS [ms]	36.45	69.2	39.27	24.9	18.9	14.38	18.17	13.86	14.22	17.45	167.5
EDT [s]	0.3725	0.5906	0.3448	0.2005	0.3137	0.2298	0.2008	0.2791	0.255	0.3134	4.797
RT20 [s]	5.779	0.6235	0.2152	0.3013	0.2638	0.3194	0.2936	0.273	0.338	0.4453	--
r RT20	0.9066	0.862	0.9747	0.9707	0.9757	0.967	0.9653	0.9849	0.9886	0.9923	--
RT30 [s]	--	0.7246	0.2124	0.2884	0.2974	0.2994	0.3083	0.2857	0.3471	0.4571	--
r RT30	--	0.9584	0.9859	0.9878	0.9761	0.9865	0.9875	0.9923	0.9931	0.9972	--
RTU [s]	--	--	0.2704	0.3202	0.3167	0.3453	0.3181	0.3017	0.3638	0.7157	--

7.17 Room D – Abs0.9

ROOM D - Abs0.9 - Position 1

Rectilinear Mesh

Band	Lin	31.5	63	125	250	500	1K	2K	4K	8K	16K
C50 [dB]	-2.267	3.801	0.09028	-0.9732	-2.046	0.00250	1.939	0.7104	-0.1825	-1.919	-2.878
C80 [dB]	-0.9155	7.795	1.292	1.307	1.885	2.1	4.297	4.135	2.666	-0.3809	-1.789

D50 [%]	37.24	70.58	50.52	44.42	38.43	50.01	60.98	54.08	48.95	39.13	34.01
TS [ms]	320.9	55.05	89.02	78.93	73.09	74.96	55.5	62.51	79.55	211.5	365.
EDT [s]	7.18	0.462	1.145	1.16	0.7107	1.017	0.9091	0.921	1.209	3.345	7.732
RT20 [s]	--	1.214	1.025	1.056	0.9402	0.8828	0.9066	1.028	1.342	9.599	--
r RT20	--	0.9945	0.9924	0.9905	0.9856	0.9967	0.997	0.9977	0.9942	0.968	--
RT30 [s]	--	1.797	1.065	1.023	0.9093	0.8265	0.9304	1.069	1.47	--	--
r RT30	--	0.943	0.9948	0.9954	0.994	0.9963	0.9985	0.9981	0.995	--	--

Triangular Mesh

Band	Lin	31.5	63	125	250	500	1K	2K	4K	8K	16K
C50 [dB]	-4.036	1.375	-4.595	-5.819	-5.289	-4.401	-2.918	-4.354	-3.804	-4.073	-7.091
C80 [dB]	-1.956	3.615	-3.528	-3.823	-1.871	-2.624	-1.034	-1.602	-1.945	-1.895	-5.019
D50 [%]	28.31	57.85	25.77	20.75	22.83	26.63	33.81	26.84	29.4	28.14	16.34
TS [ms]	175.	102.5	180.7	179.2	135.9	151.4	127.9	141.3	157.9	172.6	357.6
EDT [s]	2.406	1.891	2.269	2.41	1.875	1.911	1.811	1.911	2.155	2.458	5.286
RT20 [s]	4.271	2.49	2.362	2.096	2.156	1.973	1.926	2.067	2.619	2.894	--
r RT20	0.968	0.9991	0.9964	0.996	0.9922	0.9949	0.9981	0.9995	0.9971	0.9977	--
RT30 [s]	--	2.558	2.411	2.109	2.244	1.972	1.988	2.228	2.921	3.103	--
r RT30	--	0.9988	0.9981	0.9971	0.9959	0.9983	0.9986	0.9972	0.9945	0.9974	--

ROOM D - Abs0.9 - Position 2

Rectilinear Mesh

Band	Lin	31.5	63	125	250	500	1K	2K	4K	8K	16K
C50 [dB]	0.1407	-5.37	7.442	1.934	2.212	0.09834	3.491	2.84	1.856	0.4291	0.6624
C80 [dB]	2.051	-0.9047	8.938	5.18	3.931	3.563	6.453	5.338	4.233	2.305	1.388
D50 [%]	50.81	22.5	84.73	60.95	62.47	50.57	69.08	65.79	60.52	52.47	46.19
TS [ms]	240.5	121.5	45.24	58.23	61.69	61.2	42.67	50.23	61.81	162.1	279.3
EDT [s]	6.26	1.404	--	0.7342	0.7975	0.749	0.9171	0.9735	1.107	3.024	7.861
RT20 [s]	--	1.194	1.064	1.166	0.777	0.827	0.962	1.006	1.31	9.03	--
r RT20	--	0.977	0.9686	0.9724	0.9964	0.9942	0.9983	0.9988	0.9978	0.9848	--
RT30 [s]	--	1.138	1.023	1.099	0.9302	0.8361	0.9547	1.063	1.469	--	--
r RT30	--	0.9874	0.9862	0.9878	0.9855	0.9975	0.9991	0.9981	0.9949	--	--

Triangular Mesh

Band	Lin	31.5	63	125	250	500	1K	2K	4K	8K	16K
C50 [dB]	-2.191	-9.116	2.125	-2.054	-1.446	-3.219	-1.499	-0.5548	-1.937	-2.922	-3.941
C80 [dB]	-0.4679	-5.485	2.785	0.3091	-0.2339	-0.3329	0.2294	0.7452	0.2997	-1.299	-2.543
D50 [%]	37.65	10.92	61.99	38.39	41.75	32.27	41.45	46.81	39.03	33.79	28.75
TS [ms]	145.6	218.2	108.1	138.3	124.8	118.2	120.1	117.8	129.8	146.5	286.
EDT [s]	2.221	2.422	2.063	2.53	1.642	1.551	1.975	1.959	2.012	2.186	4.614
RT20 [s]	3.844	2.443	2.073	2.392	2.259	2.067	1.909	2.099	2.777	2.889	--
r RT20	0.9748	0.9904	0.9897	0.9932	0.9946	0.9966	0.9991	0.998	0.9968	0.9955	--
RT30 [s]	--	2.46	2.141	2.374	2.113	2.103	1.927	2.217	2.871	3.18	--
r RT30	--	0.9956	0.9961	0.9975	0.9966	0.9987	0.9996	0.9981	0.9985	0.9953	--

ROOM D - Abs0.9 - Position 3

Rectilinear Mesh

Band	Lin	31.5	63	125	250	500	1K	2K	4K	8K	16K
C50 [dB]	-5.408	-6.516	-2.111	1.846	0.7601	1.587	-2.38	0.9892	0.4582	-4.786	-8.024
C80 [dB]	-2.649	-2.477	3.121	4.225	3.816	3.302	1.966	3.784	2.737	-1.719	-4.175

D50 [%]	22.35	18.24	38.08	60.47	54.36	59.04	36.63	55.67	52.63	24.94	13.61
TS [ms]	385.9	149.6	90.85	57.57	65.3	72.62	84.29	63.42	76.59	242.5	438.3
EDT [s]	8.817	1.734	1.299	0.9768	0.7971	1.005	0.9536	1.149	1.162	3.452	8.869
RT20 [s]	--	1.228	1.015	1.122	0.9093	0.9024	0.955	1.033	1.374	--	--
r RT20	--	0.9978	0.9864	0.9523	0.9827	0.996	0.9957	0.9992	0.9958	--	--
RT30 [s]	--	1.185	0.9865	1.046	0.9667	0.8917	0.9661	1.063	1.526	--	--
r RT30	--	0.9987	0.9904	0.9805	0.9913	0.998	0.9983	0.9992	0.9944	--	--

Triangular Mesh

Band	Lin	31.5	63	125	250	500	1K	2K	4K	8K	16K
C50 [dB]	-4.244	-9.906	-6.551	-2.847	-3.353	-2.512	-5.785	-5.122	-3.59	-3.842	-6.69
C80 [dB]	-2.277	-6.2	-2.457	-1.027	-0.9111	-1.281	-2.165	-2.398	-1.76	-2.036	-4.299
D50 [%]	27.35	9.271	18.12	34.17	31.6	35.93	20.88	23.52	30.44	29.22	17.65
TS [ms]	182.7	250.	183.5	146.8	140.7	148.9	159.8	158.3	158.4	167.6	338.6
EDT [s]	2.481	2.789	2.189	2.548	1.971	2.039	2.006	2.174	2.196	2.358	4.972
RT20 [s]	4.379	2.386	2.267	2.141	2.103	2.019	2.026	2.009	2.78	2.94	7.957
r RT20	0.9729	0.9998	0.9919	0.9857	0.9957	0.9963	0.9993	0.9995	0.9972	0.9957	0.9907
RT30 [s]	--	2.393	2.292	2.123	2.018	2.023	2.002	2.09	2.971	3.199	--
r RT30	--	0.9999	0.9964	0.9943	0.9974	0.9985	0.9995	0.9991	0.9972	0.996	--

ROOM D - Abs0.9 - Position 4

Rectilinear Mesh

Band	Lin	31.5	63	125	250	500	1K	2K	4K	8K	16K
C50 [dB]	-4.347	-8.599	0.2386	-2.222	0.6037	2.795	0.1553	-0.3231	0.1243	-3.486	-5.829
C80 [dB]	-2.053	-5.918	2.565	-0.5648	2.703	4.918	3.811	2.967	3.092	-0.776	-3.805
D50 [%]	26.88	12.13	51.37	37.48	53.47	65.56	50.89	48.14	50.72	30.95	20.72
TS [ms]	370.9	141.7	75.06	95.86	66.2	55.33	67.9	65.36	77.13	233.5	429.5
EDT [s]	7.72	1.204	0.8457	1.153	0.9946	0.9686	0.8922	0.9446	1.185	3.799	8.035
RT20 [s]	--	1.236	1.096	0.924	0.9157	0.9189	0.9229	0.9989	1.4	--	--
r RT20	--	0.9678	0.9859	0.9926	0.994	0.9902	0.9981	0.9949	0.9985	--	--
RT30 [s]	--	1.197	1.143	0.9355	0.9585	0.8806	0.9594	1.043	1.477	--	--
r RT30	--	0.9866	0.9938	0.9942	0.9969	0.9949	0.9978	0.9975	0.9979	--	--

Triangular Mesh

Band	Lin	31.5	63	125	250	500	1K	2K	4K	8K	16K
C50 [dB]	-4.308	-12.55	-3.588	-7.197	-3.954	-1.975	-4.366	-3.703	-3.972	-4.449	-6.141
C80 [dB]	-2.04	-9.66	-1.62	-5.719	-1.767	-0.4385	-1.512	-1.183	-2.012	-2.044	-4.284
D50 [%]	27.05	5.267	30.45	16.01	28.69	38.82	26.79	29.89	28.61	26.42	19.56
TS [ms]	173.6	231.5	151.5	187.2	144.9	127.	151.	138.7	155.8	169.3	347.8
EDT [s]	2.394	2.598	2.197	2.1	1.939	1.84	2.05	1.998	2.218	2.364	5.247
RT20 [s]	4.312	2.525	2.29	2.114	2.149	2.12	1.889	2.18	2.636	2.958	--
r RT20	0.9689	0.9904	0.9949	0.9965	0.9965	0.9952	0.9985	0.9996	0.9972	0.9987	--
RT30 [s]	--	2.517	2.393	2.17	2.082	2.073	2.	2.209	2.92	3.12	--
r RT30	--	0.9958	0.9971	0.9981	0.9983	0.9982	0.998	0.9992	0.9945	0.9984	--

7.18 Room D – Abs0.4

ROOM D - Abs0.4 - Position 1

Rectilinear Mesh

Band	Lin	31.5	63	125	250	500	1K	2K	4K	8K	16K
C50 [dB]	4.901	4.071	14.16	19.8	20.46	21.49	22.12	20.63	18.65	7.31	4.57
C80 [dB]	5.293	12.11	16.93	33.05	32.98	32.59	33.74	29.08	26.77	7.931	5.036
D50 [%]	75.55	71.86	96.31	98.96	99.11	99.29	99.39	99.14	98.65	84.33	74.12
TS [ms]	104.7	45.54	28.1	13.81	13.21	7.958	5.822	6.332	6.055	60.	104.1
EDT [s]	3.546	0.3043	0.1939	0.08969	--	--	--	--	--	1.441	3.336
RT20 [s]	--	0.5664	0.3497	0.1757	0.1482	0.1601	0.1534	0.1712	0.2099	5.932	6.108
r RT20	--	0.9676	0.9386	0.9067	0.9698	0.9833	0.9735	0.9698	0.9797	0.9745	0.9884
RT30 [s]	--	0.7326	0.3484	0.1444	0.1349	0.1527	0.1528	0.1798	0.2071	--	--
r RT30	--	0.9665	0.9853	0.9572	0.9798	0.9914	0.9904	0.9874	0.9912	--	--

Triangular Mesh

Band	Lin	31.5	63	125	250	500	1K	2K	4K	8K	16K
C50 [dB]	8.228	4.854	11.25	10.11	7.599	9.762	11.12	9.027	10.12	10.21	-0.097
C80 [dB]	11.14	12.61	12.98	16.15	13.83	15.73	16.5	13.64	15.01	15.14	1.583
D50 [%]	86.93	75.36	93.02	91.12	85.19	90.45	92.83	88.88	91.13	91.29	49.44
TS [ms]	38.33	42.8	33.82	20.77	27.64	22.9	15.31	18.26	16.7	17.18	210.1
EDT [s]	0.4263	0.2943	0.2142	0.2662	0.336	0.3177	0.3082	0.3666	0.335	0.3416	5.34
RT20 [s]	5.908	0.5176	0.4689	0.3198	0.2575	0.305	0.3274	0.4086	0.4199	0.4001	--
r RT20	0.9251	0.9554	0.9335	0.987	0.9816	0.9896	0.9935	0.9928	0.9892	0.9963	--
RT30 [s]	--	0.6013	0.4018	0.3323	0.2606	0.3182	0.3181	0.4064	0.4558	0.4246	--
r RT30	--	0.9814	0.9741	0.9912	0.9913	0.9956	0.9958	0.9964	0.993	0.9967	--

ROOM D - Abs0.4 - Position 2

Rectilinear Mesh

Band	Lin	31.5	63	125	250	500	1K	2K	4K	8K	16K
C50 [dB]	7.988	0.6944	15.32	17.91	23.91	24.74	28.48	23.27	23.22	9.803	7.415
C80 [dB]	10.42	11.66	18.18	30.52	35.71	39.27	42.77	36.19	31.52	12.93	10.13
D50 [%]	86.29	53.99	97.15	98.41	99.6	99.67	99.86	99.53	99.53	90.53	84.65
TS [ms]	60.13	54.14	25.02	14.07	8.676	5.557	3.927	4.15	5.663	33.99	60.94
EDT [s]	0.7998	0.3556	0.1554	0.0863	--	0.04189	0.02181	0.02237	--	--	--
RT20 [s]	7.739	0.6486	0.3155	0.1853	0.178	0.1728	--	0.1891	0.1764	7.816	7.557
r RT20	0.9366	0.9686	0.8997	0.9749	0.8752	0.9158	--	0.8883	0.8771	0.9047	0.9381
RT30 [s]	--	0.6787	0.324	0.1727	0.1348	0.1497	0.1414	0.1735	0.1749	--	--
r RT30	--	0.991	0.9765	0.9905	0.9585	0.9694	0.9371	0.9279	0.9469	--	--

Triangular Mesh

Band	Lin	31.5	63	125	250	500	1K	2K	4K	8K	16K
C50 [dB]	10.22	-0.8644	14.88	10.32	12.48	10.44	15.09	11.72	11.47	11.69	3.014
C80 [dB]	13.	7.897	18.97	17.98	16.35	16.67	22.17	17.96	16.27	15.27	4.317
D50 [%]	91.32	45.04	96.85	91.49	94.65	91.71	97.	93.69	93.35	93.65	66.69
TS [ms]	21.84	61.91	26.	21.66	20.71	16.55	9.268	13.44	14.1	12.28	105.9
EDT [s]	--	0.4842	0.1664	0.3041	--	--	--	--	--	--	1.818
RT20 [s]	--	0.6363	0.2717	0.2857	0.2458	0.2851	0.2797	0.3173	0.3744	0.4117	--
r RT20	--	0.9725	0.9021	0.9797	0.9538	0.959	0.9712	0.9729	0.9837	0.9888	--
RT30 [s]	--	0.6814	0.2665	0.2575	0.2536	0.2705	0.2769	0.3151	0.3735	0.4199	--

r RT30	--	0.9903	0.9735	0.9825	0.9853	0.983	0.9877	0.9888	0.992	0.995	--
--------	----	--------	--------	--------	--------	-------	--------	--------	-------	-------	----

ROOM D - Abs0.4 - Position 3

Rectilinear Mesh

Band	Lin	31.5	63	125	250	500	1K	2K	4K	8K	16K
C50 [dB]	1.804	1.877	12.08	19.27	22.2	24.33	23.72	22.34	18.99	5.072	0.1072
C80 [dB]	2.815	11.45	21.09	28.66	34.16	33.25	39.22	37.32	26.95	6.544	1.603
D50 [%]	60.24	60.64	94.17	98.83	99.4	99.63	99.58	99.42	98.75	76.27	50.62
TS [ms]	190.7	51.47	27.08	14.41	9.952	7.911	5.503	7.446	8.357	90.44	211.2
EDT [s]	5.364	0.3433	0.1912	0.111	--	--	--	--	--	1.304	5.067
RT20 [s]	--	0.666	0.217	0.1745	0.1561	--	0.1533	0.1708	0.2189	--	--
r RT20	--	0.9746	0.9615	0.9892	0.8621	--	0.8611	0.8884	0.923	--	--
RT30 [s]	--	0.7112	0.272	0.1772	0.1612	0.1589	0.1716	0.1707	0.2024	--	--
r RT30	--	0.9911	0.9699	0.9945	0.9364	0.9062	0.9201	0.8991	0.9573	--	--

Triangular Mesh

Band	Lin	31.5	63	125	250	500	1K	2K	4K	8K	16K
C50 [dB]	7.946	-0.1081	5.431	12.65	10.82	12.35	8.47	10.77	10.37	9.567	1.777
C80 [dB]	11.85	6.475	18.08	17.15	16.73	17.17	17.61	18.66	17.21	14.53	4.997
D50 [%]	86.17	49.38	77.74	94.85	92.35	94.5	87.55	92.27	91.6	90.05	60.09
TS [ms]	32.32	62.63	36.03	18.43	21.35	23.48	22.03	13.14	18.44	19.06	104.3
EDT [s]	0.4336	0.5324	0.3361	0.1624	--	--	0.3828	0.4014	--	--	1.458
RT20 [s]	--	0.7248	0.2376	0.3483	0.2365	0.3023	0.2475	0.3013	0.3216	0.3566	--
r RT20	--	0.9952	0.9297	0.9732	0.9333	0.9469	0.9778	0.9871	0.9746	0.991	--
RT30 [s]	--	0.7462	0.3525	0.298	0.2367	0.2935	0.2572	0.2926	0.3256	0.381	--
r RT30	--	0.9981	0.9136	0.9782	0.9739	0.9752	0.9884	0.9919	0.9896	0.9954	--

ROOM D - Abs0.4 - Position 4

Rectilinear Mesh

Band	Lin	31.5	63	125	250	500	1K	2K	4K	8K	16K
C50 [dB]	-0.2849	4.736	13.95	22.44	23.86	21.82	19.52	20.62	18.19	3.219	-1.557
C80 [dB]	1.322	10.85	17.77	31.41	35.98	33.49	31.28	30.66	27.03	4.989	0.3985
D50 [%]	48.36	74.85	96.13	99.43	99.59	99.35	98.89	99.14	98.5	67.73	41.13
TS [ms]	269.7	45.34	29.68	14.47	9.053	7.572	7.179	6.135	7.107	144.7	290.5
EDT [s]	8.779	0.2901	0.2113	0.1316	0.1212	0.141	--	--	--	--	8.528
RT20 [s]	--	0.5758	0.2822	0.1287	0.1399	0.1513	0.1663	0.1714	0.2025	6.302	--
r RT20	--	0.9743	0.9446	0.9735	0.9879	0.9685	0.9729	0.9652	0.9531	0.9219	--
RT30 [s]	--	--	0.2972	0.1565	0.1328	0.1494	0.1593	0.1656	0.1951	--	--
r RT30	--	--	0.9825	0.9752	0.9913	0.9812	0.9821	0.9778	0.9819	--	--

Triangular Mesh

Band	Lin	31.5	63	125	250	500	1K	2K	4K	8K	16K
C50 [dB]	7.868	0.8903	8.43	12.27	12.69	11.85	7.773	9.393	9.896	9.137	1.993
C80 [dB]	11.	5.033	12.42	14.48	17.42	17.65	14.39	14.75	14.52	14.3	3.034
D50 [%]	85.96	55.11	87.45	94.4	94.89	93.87	85.69	89.69	90.71	89.13	61.27
TS [ms]	39.6	60.68	36.51	23.82	16.09	16.4	25.44	16.11	16.91	18.6	181.1
EDT [s]	0.4208	0.6264	0.245	0.2374	0.2359	0.2325	0.3313	0.3822	0.3049	0.3554	5.697
RT20 [s]	6.972	0.5885	0.3353	0.4005	0.344	0.3198	0.3442	0.4299	0.3771	0.4167	--
r RT20	0.8951	0.9794	0.9798	0.9644	0.9693	0.9706	0.9851	0.9857	0.9908	0.9961	--
RT30 [s]	--	0.7582	0.2999	0.3706	0.3319	0.3198	0.3637	0.4474	0.4397	0.4111	--

r RT30	--	0.9726	0.9822	0.9783	0.9852	0.9836	0.9914	0.9936	0.9859	0.9986	--
--------	----	--------	--------	--------	--------	--------	--------	--------	--------	--------	----

7.19 Room D – AbsComplex

ROOM D – AbsComplex - Position 1

Rectilinear Mesh

Band	Lin	31.5	63	125	250	500	1K	2K	4K	8K	16K
C50 [dB]	4.708	4.527	14.61	20.9	17.26	23.38	23.99	18.35	16.46	6.958	4.245
C80 [dB]	5.088	10.94	16.6	36.41	27.12	30.24	29.35	23.01	20.02	7.569	4.679
D50 [%]	74.73	73.93	96.66	99.19	98.15	99.54	99.6	98.56	97.79	83.23	72.66
TS [ms]	111.1	46.02	28.74	15.31	14.46	6.514	7.073	8.287	7.686	63.19	112.5
EDT [s]	3.792	0.3015	0.1965	0.1006	0.1697	--	--	--	--	1.456	3.551
RT20 [s]	--	0.6093	0.3397	0.156	0.1651	0.1792	0.1488	0.2202	0.2935	6.044	--
r RT20	--	0.9771	0.9282	0.905	0.9718	0.9529	0.9568	0.9641	0.9735	0.9775	--
RT30 [s]	--	0.7854	0.3542	0.119	0.1772	0.1788	0.1705	0.2212	0.2793	--	--
r RT30	--	0.9638	0.9815	0.9419	0.9815	0.9803	0.9618	0.979	0.9878	--	--

Triangular Mesh

Band	Lin	31.5	63	125	250	500	1K	2K	4K	8K	16K
C50 [dB]	8.312	5.036	10.32	9.131	5.645	9.439	12.71	9.295	10.52	10.22	0.0154
C80 [dB]	10.91	11.15	11.2	14.66	11.13	13.44	16.87	15.14	14.15	14.12	1.757
D50 [%]	87.15	76.13	91.51	89.12	78.58	89.78	94.91	89.48	91.85	91.31	50.09
TS [ms]	36.12	44.07	35.33	24.31	33.13	23.51	14.31	17.33	16.18	17.77	186.3
EDT [s]	0.4439	0.2928	0.2191	0.3052	0.3912	0.3431	0.2765	0.363	0.3423	0.3785	4.381
RT20 [s]	5.54	0.6323	0.4423	0.3702	0.3025	0.3413	0.3288	0.3492	0.4172	0.5376	--
r RT20	0.8942	0.9755	0.9243	0.9845	0.9883	0.9896	0.9908	0.992	0.9927	0.9864	--
RT30 [s]	--	0.6816	0.4165	0.3665	0.3562	0.3606	0.3295	0.3333	0.4149	0.5527	--
r RT30	--	0.9898	0.9796	0.9905	0.9832	0.995	0.9962	0.9957	0.9971	0.9958	--

ROOM D – AbsComplex - Position 2

Rectilinear Mesh

Band	Lin	31.5	63	125	250	500	1K	2K	4K	8K	16K
C50 [dB]	7.744	0.7554	12.34	18.61	21.31	25.44	28.17	25.54	22.58	9.402	7.062
C80 [dB]	10.11	12.3	16.34	31.58	34.47	38.13	37.66	32.33	26.93	12.56	9.646
D50 [%]	85.61	54.34	94.49	98.64	99.27	99.71	99.85	99.72	99.45	89.71	83.56
TS [ms]	63.78	53.55	26.74	17.24	11.6	5.518	3.346	5.236	6.316	35.86	66.39
EDT [s]	0.7733	0.3476	0.1676	0.1937	--	0.03569	0.0273	--	--	--	0.8842
RT20 [s]	7.587	0.6326	0.3076	0.1439	0.1445	0.1851	--	--	0.1947	7.674	7.422
r RT20	0.9353	0.9592	0.9598	0.9364	0.9042	0.9204	--	--	0.8948	0.9115	0.938
RT30 [s]	--	0.6615	0.3186	0.1385	0.1292	0.1469	0.1608	0.162	0.1949	--	--
r RT30	--	0.9883	0.9877	0.9802	0.9709	0.9708	0.9213	0.933	0.9356	--	--

Triangular Mesh

Band	Lin	31.5	63	125	250	500	1K	2K	4K	8K	16K
C50 [dB]	10.48	-0.8444	14.37	9.476	11.2	10.15	14.02	14.79	12.07	11.52	3.301
C80 [dB]	13.03	8.956	18.02	15.28	16.18	15.82	19.86	20.06	17.71	13.89	4.918
D50 [%]	91.78	45.15	96.48	89.86	92.95	91.2	96.19	96.78	94.15	93.42	68.14
TS [ms]	20.73	60.78	26.4	27.82	24.66	17.16	8.529	12.35	13.16	12.6	93.7
EDT [s]	--	0.3804	0.1662	0.3454	--	--	--	--	--	--	1.598
RT20 [s]	--	0.693	0.3071	0.3154	0.2992	0.3059	0.3357	0.2478	0.3223	0.4431	7.308

r RT20	--	0.9832	0.9189	0.9743	0.9791	0.9714	0.9735	0.9667	0.9818	0.9867	0.9523
RT30 [s]	--	0.7055	0.2914	0.3518	0.3469	0.3098	0.3184	0.2577	0.3227	0.4496	--
r RT30	--	0.9952	0.968	0.9864	0.9825	0.9876	0.9912	0.9881	0.9931	0.995	--

ROOM D – AbsComplex - Position 3

Rectilinear Mesh

Band	Lin	31.5	63	125	250	500	1K	2K	4K	8K	16K
C50 [dB]	1.441	2.823	11.78	19.92	23.56	23.33	18.16	20.27	16.02	4.348	-0.621
C80 [dB]	2.332	10.59	20.42	31.1	32.27	30.33	28.85	31.22	20.63	5.514	0.7514
D50 [%]	58.22	65.7	93.77	98.99	99.56	99.54	98.5	99.07	97.56	73.13	46.43
TS [ms]	197.6	49.69	27.8	14.48	8.741	10.34	15.19	6.624	7.989	99.22	226.3
EDT [s]	5.445	0.3284	0.1907	0.1183	0.07502	0.3082	--	--	--	1.644	5.174
RT20 [s]	--	0.6651	0.248	0.1441	0.155	0.1484	--	--	0.3258	--	--
r RT20	--	0.9838	0.944	0.9663	0.9655	0.8973	--	--	0.8904	--	--
RT30 [s]	--	0.7237	0.2869	0.1587	0.1744	0.1818	0.207	0.2243	0.286	--	--
r RT30	--	0.9935	0.9729	0.986	0.9665	0.9289	0.8959	0.9218	0.9467	--	--

Triangular Mesh

Band	Lin	31.5	63	125	250	500	1K	2K	4K	8K	16K
C50 [dB]	8.787	-0.2927	5.325	11.03	9.76	11.23	7.277	11.61	11.38	10.98	1.612
C80 [dB]	11.97	5.8	18.67	17.1	15.17	15.34	14.7	18.5	16.62	14.2	4.784
D50 [%]	88.32	48.32	77.32	92.68	90.44	92.99	84.23	93.54	93.22	92.61	59.18
TS [ms]	29.68	65.11	36.49	19.94	20.74	27.11	32.38	9.568	16.63	16.9	112.9
EDT [s]	0.4385	0.5918	0.337	0.1795	0.3659	--	0.3589	--	--	--	1.701
RT20 [s]	--	0.7529	--	0.3725	0.2923	0.3775	0.3172	0.394	0.4054	0.5203	--
r RT20	--	0.9971	--	0.9755	0.9589	0.9589	0.979	0.9662	0.9618	0.9673	--
RT30 [s]	--	0.7506	0.3657	0.3318	0.3439	0.3733	0.3392	0.3694	0.4103	0.5502	--
r RT30	--	0.999	0.8923	0.9878	0.9732	0.9876	0.9873	0.9838	0.9772	0.9897	--

ROOM D – AbsComplex - Position 4

Rectilinear Mesh

Band	Lin	31.5	63	125	250	500	1K	2K	4K	8K	16K
C50 [dB]	0.3038	4.207	13.72	18.5	23.05	24.55	23.05	19.4	16.01	3.577	-1.41
C80 [dB]	1.865	8.47	16.95	27.68	31.81	31.99	29.88	25.07	20.72	5.546	0.444
D50 [%]	51.75	72.49	95.92	98.61	99.51	99.65	99.51	98.86	97.55	69.5	41.95
TS [ms]	244.7	48.36	30.81	18.31	8.806	7.495	6.802	7.818	9.638	122.9	277.3
EDT [s]	8.529	0.406	0.2115	0.1779	0.08479	0.1269	--	--	--	--	8.253
RT20 [s]	--	0.5847	0.2962	0.1429	0.1751	0.143	0.1566	0.1796	0.2597	6.449	--
r RT20	--	0.9865	0.9357	0.9369	0.9484	0.9432	0.9609	0.9452	0.951	0.9269	--
RT30 [s]	--	0.9959	0.3144	0.1683	0.1621	0.158	0.164	0.2119	0.2498	--	--
r RT30	--	0.9135	0.9806	0.9765	0.968	0.9651	0.966	0.9697	0.9788	--	--

Triangular Mesh

Band	Lin	31.5	63	125	250	500	1K	2K	4K	8K	16K
C50 [dB]	7.501	1.199	7.774	10.12	10.8	12.43	9.609	9.698	9.691	8.465	1.836
C80 [dB]	10.33	4.918	11.66	13.42	14.86	17.44	16.	15.03	13.62	12.39	3.044
D50 [%]	84.9	56.86	85.69	91.13	92.32	94.6	90.14	90.32	90.3	87.54	60.42
TS [ms]	39.15	61.83	37.92	27.34	17.9	16.38	24.3	15.05	17.39	20.02	166.4
EDT [s]	0.4609	0.6858	0.2698	0.2673	0.3351	0.2445	0.2836	0.3954	0.327	0.4101	4.597
RT20 [s]	6.403	0.661	0.346	0.4003	0.3964	0.3076	0.3274	0.3385	0.3867	0.5172	--

Appendix B Octave Band Acoustical Parameters

r RT20	0.8818	0.9883	0.9856	0.9852	0.9811	0.9804	0.9701	0.9879	0.9902	0.9969	--
RT30 [s]	--	0.731	0.3479	0.3801	0.3748	0.3436	0.3437	0.3277	0.3887	0.5186	--
r RT30	--	0.9915	0.9838	0.9893	0.9917	0.9873	0.9865	0.9949	0.9954	0.9986	--

Appendix C Guide To Audio CD

Appendix E refers the reader to the Audio CD that can be found on the inside back cover of this thesis. This CD contains examples of a number of different audio samples each having been convolved with a selection of *WaveVerb* RIR measurements (from Room D) as discussed in Chapter 6.7. What follows is a track listing of the CD describing the contents in terms of which audio sample has been used as the source sound, together with a list of which RIRs have been used to process it.

1. Original Sample - Recorded Anechoic Speech (female).

2. Rectilinear Mesh:	Abs0.9	Position 1
3. Triangular Mesh:	Abs0.9	Position 1
4. Rectilinear Mesh:	Abs0.9	Position 2
5. Triangular Mesh:	Abs0.9	Position 2
6. Rectilinear Mesh:	Abs0.9	Position 3
7. Triangular Mesh:	Abs0.9	Position 3
8. Rectilinear Mesh:	Abs0.9	Position 4
9. Triangular Mesh:	Abs0.9	Position 4
10. Rectilinear Mesh:	Abs0.4	Position 1
11. Triangular Mesh:	Abs0.4	Position 1
12. Rectilinear Mesh:	Abs0.4	Position 2
13. Triangular Mesh:	Abs0.4	Position 2
14. Rectilinear Mesh:	Abs0.4	Position 3
15. Triangular Mesh:	Abs0.4	Position 3
16. Rectilinear Mesh:	Abs0.4	Position 4
17. Triangular Mesh:	Abs0.4	Position 4
18. Rectilinear Mesh:	AbsComplex	Position 1
19. Triangular Mesh:	AbsComplex	Position 1
20. Rectilinear Mesh:	AbsComplex	Position 2
21. Triangular Mesh:	AbsComplex	Position 2
22. Rectilinear Mesh:	AbsComplex	Position 3
23. Triangular Mesh:	AbsComplex	Position 3
24. Rectilinear Mesh:	AbsComplex	Position 4
25. Triangular Mesh:	AbsComplex	Position 4
26. Triangular Mesh:	AbsComplex	Position 4 – Stereo RIR.

27. Original Sample - Recorded Anechoic Acoustic Guitar

28. Rectilinear Mesh:	Abs0.9	Position 1
29. Triangular Mesh:	Abs0.9	Position 1
30. Rectilinear Mesh:	Abs0.9	Position 2
31. Triangular Mesh:	Abs0.9	Position 2
32. Rectilinear Mesh:	Abs0.9	Position 3
33. Triangular Mesh:	Abs0.9	Position 3
34. Rectilinear Mesh:	Abs0.9	Position 4
35. Triangular Mesh:	Abs0.9	Position 4
36. Rectilinear Mesh:	Abs0.4	Position 1
37. Triangular Mesh:	Abs0.4	Position 1
38. Rectilinear Mesh:	Abs0.4	Position 2
39. Triangular Mesh:	Abs0.4	Position 2
40. Rectilinear Mesh:	Abs0.4	Position 3
41. Triangular Mesh:	Abs0.4	Position 3
42. Rectilinear Mesh:	Abs0.4	Position 4
43. Triangular Mesh:	Abs0.4	Position 4
44. Rectilinear Mesh:	AbsComplex	Position 1
45. Triangular Mesh:	AbsComplex	Position 1
46. Rectilinear Mesh:	AbsComplex	Position 2
47. Triangular Mesh:	AbsComplex	Position 2
48. Rectilinear Mesh:	AbsComplex	Position 3
49. Triangular Mesh:	AbsComplex	Position 3
50. Rectilinear Mesh:	AbsComplex	Position 4
51. Triangular Mesh:	AbsComplex	Position 4
52. Triangular Mesh:	AbsComplex	Position 4 – Stereo RIR.

53. Original Sample – Recording of a Close-Miked Drum Kit

54. Rectilinear Mesh:	Abs0.9	Position 4
55. Triangular Mesh:	Abs0.9	Position 4
56. Rectilinear Mesh:	Abs0.4	Position 4
57. Triangular Mesh:	Abs0.4	Position 4
58. Rectilinear Mesh:	AbsComplex	Position 4
59. Triangular Mesh:	AbsComplex	Position 4
60. Triangular Mesh:	AbsComplex	Position 4 – Stereo RIR.

61. Original Sample – Recording of Close-Miked singing (female)

62. Rectilinear Mesh:	Abs0.9	Position 4
63. Triangular Mesh:	Abs0.9	Position 4
64. Rectilinear Mesh:	Abs0.4	Position 4
65. Triangular Mesh:	Abs0.4	Position 4
66. Rectilinear Mesh:	AbsComplex	Position 4
67. Triangular Mesh:	AbsComplex	Position 4
68. Triangular Mesh:	AbsComplex	Position 4 – Stereo RIR.

69. Original Sample – Recording of Sampled Acoustic Piano

70. Rectilinear Mesh:	Abs0.9	Position 4
71. Triangular Mesh:	Abs0.9	Position 4
72. Rectilinear Mesh:	Abs0.4	Position 4
73. Triangular Mesh:	Abs0.4	Position 4
74. Rectilinear Mesh:	AbsComplex	Position 4
75. Triangular Mesh:	AbsComplex	Position 4
76. Triangular Mesh:	AbsComplex	Position 4 – Stereo RIR.

Appendix D Guide To Data CD

Appendix F refers the reader to the Data CD that can be found on the inside back cover of this thesis. The CD when accessed contains six top-level directories as follows:

- Animations
- C Code
- Case_Study_Audio
- Case_Study_Rect
- Case_Study_Tri
- Vmpeg

Animations

This directory contains two MPEG files, *colour.mpg* and *mesh.mpg*. These two video files are animations of the graphical implementation of the *WaveVerb* system, demonstrating wave propagation, diffraction and interference on the triangular mesh using two different rendering methods. Further details can be found in Chapter 6.2.3.

It should be possible to view these files on any computer platform using the standard Media/Movie player supplied as part of the operating system. A freeware MPEG player is also included on this CD in the *Vmpeg* directory, details of which follow below.

C Code

This directory contains the original commented C source code and Makefiles used in the development of the *WaveVerb* system. The sub-directories contain all the associated additional libraries (*Aiff*, *Fft*, *Utils*, *lib*), and include files (*include*), as well as the full code listing for the Analysis Module (*Analysis_Module*), and the triangular mesh implementation with graphical visualisation and interaction using OpenGL (*WV_TriGL*).

Case_Study_Audio

This directory contains the WAV files used in the Case Study presented in Chapters 6.3-6.7. The hierarchical sub-directories are organised according to Room (*A*, *B*, *C*, *D*), Absorption Conditions (*Abs0.4*, *Abs0.9*, *AbsComplex*), and Position (*1*, *2*, *3*, *4*). Each *Position* directory contains a stereo WAV file, *compare.wav*, that has the RIR measured from the rectilinear mesh on the left channel and the RIR measured from the triangular mesh on the right channel.

The Room D cases also contain a stereo RIR file that is the same as *compare.wav* but with noise reduction processing called *compare_nr.wav*. In addition, each of the audio samples detailed in Chapter 6.7 as convolved separately with both of the single channel component RIRs are included in the Room D Position sub-directories.

Finally, there is an additional sub-directory to *Case_Study_Audio* called *Samples* that contains the five original unprocessed sound examples.

Case_Study_Rect

This directory contains the C source code as used by the pre-defined and compiled command line only implementation of the rectilinear waveguide mesh as used in the Case Study presented in Chapters 6.3-6.7. Also included in each case are the resulting measured single channel RIR AIF soundfiles. The hierarchical sub-directories are organised according to Room (*A, B, C, D*), Absorption Conditions (*Abs0.4, Abs0.9, Abs1.0, AbsComplex*), and Position (*1, 2, 3, 4*).

Case_Study_Tri

This directory contains the C source code as used by the pre-defined and compiled command line only implementation of the triangular waveguide mesh as used in the Case Study presented in Chapters 6.3-6.7. Also included in each case are the resulting measured RIR AIF soundfiles (in single channel mono, two channel stereo or four channel B-format as appropriate). The hierarchical sub-directories are organised according to Room (*A, B, C, D*), Absorption Conditions (*Abs0.4, Abs0.9, Abs1.0, AbsComplex*), and Position (*1, 2, 3, 4*).

Vmpeg

This is a freeware MPEG player for Microsoft Windows based PCs. It should be possible to run this application directly from this Data CD. If not copy the entire contents of the *Vmpeg* directory to a temporary directory on your local machine and run the application from the hard disk. To play the MPEG movies presented in the *Animations* directory do the following:

1. Double-click on the **Vmpegwin.exe** filename or icon.
2. Click on the **Configure** Menu on the Transport/Controls Window and select the **Video...** option from the drop down menu.
3. Set **Display** to **24 bit**.
4. Set **Frames** to **fps** and enter **12** in the associated dialogue box.
5. Click on the **OK** button.
6. Go to the **File** Menu on the Transport/Controls Window and select the **Open...** option from the drop down menu.

7. Locate and select either of the animation MPEG *.mpg* files, and then Click on the **OK** button.
8. Click on the **Play** Button on the Transport/Controls Window to view the file.

Additional help can be found from the **Help** menu on the Transport/Controls Window or in the *Readme.txt* file in the Vmpeg directory on the Data CD.

Appendix E CD-1, Audio

Please refer to the Audio CD, labelled CD-1 that can be found on the inside back cover of this thesis, and the accompanying track listing that can be found in Appendix C.

[Please Note – A copy of the original accompanying Audio CD is available on request – Email dtm3@ohm.york.ac.uk for details]

Appendix F CD-2, Data

Please refer to the Data CD, labelled CD-2 that can be found on the inside back cover of this thesis, and the accompanying guide that can be found in Appendix D.

[Please Note – A copy of the original accompanying Data CD is available on request – Email dtm3@ohm.york.ac.uk for details]

Glossary

The meanings, within the context of this thesis, of the abbreviations and technical terms used are defined below. Derived and adapted from [Dodge and Jerse, 1985] and [Everest, 1994].

Terms and Abbreviations

AIFF/AIF	A standardised audio file format.
absorption	In acoustics, the changing of sound energy to heat.
absorption coefficient	The fraction of sound energy that is absorbed at any surface. It ranges between 0 and 1 and varies with the frequency and angle of incidence of the sound.
acoustics	The study of the physics of sound. It can also refer to the effect a given environment has on a sound – an environmental context.
aliasing	In a digital sound system, the reflection of frequencies higher than the Nyquist frequency to lower frequencies. An <i>aliased</i> frequency is one which, after reflection, is indistinguishable from a lower, un-reflected frequency.
algorithm	A step-by-step procedure for accomplishing a task. Each step must be defined unambiguously and there must be a clear path to the completion of the algorithm. Most algorithms can be translated into a programming language and executed on a computer.
amplitude	The instantaneous magnitude of an oscillating quantity. In digital audio, amplitude describes the value of the largest sample of a signal. In acoustics, the peak amount of atmospheric displacement of a sound, measured in units of pressure (Newtons per square meter).
anechoic	Without echo.
array	A collection of values stored in a computer in tabular form. An array can have one or more dimensions.
attenuation	The reduction of the amplitude component of the sound.
bandwidth	(1) A measure of the width of the passband or stopband of a filter. (2) A measure of the width of the resonance or frequency region occupied by the spectrum of a signal.
BEM	Boundary Element Method.

binaural	Pertaining to two ears or to a recording system in which a dummy head is used with a microphone placed at each ear position.
BRIR	Binaural Room Impulse Response. The RIR measured at the entrance of the ear canals of the listener.
CAD	Computer Aided Design.
CD	Compact Disc.
component	A part of a whole. A frequency component is a single frequency found in the spectrum of a signal.
continuous	When referring to a signal, relates to the fact that the information it carries may at any instant take any value within the limits of the system.
CPU	Central Processing Unit.
dB	Decibel. The bel is the logarithm of the ratio of two powers and the decibel is one tenth of a bel.
decay	That portion of the envelope of a tone in which the amplitude decreases from its steady state value to zero.
delay line	A digital device that delays one signal with respect to another.
DFT	Discrete Fourier Transform. The implementation of a Fourier Analysis for a finite-length digital sequence.
diffraction	The distortion of a wavefront caused by the presence of an obstacle in the soundfield.
dispersion	The characteristic of a medium such that the velocity of a propagating wave is dependent upon its frequency.
digital	Characteristic of a system or device that handles information in numerical quantities.
discrete	Discontinuous. For example, a digital signal is discrete in that it is comprised of values at specific points in time and is undefined elsewhere.
DSP	Digital Signal Processor/Processing.
FEM	Finite Element Method.
FDTD	Finite Difference Time Domain.
FFT	Fast Fourier Transform. An optimized and computationally more efficient implementation of the DFT.
FIR	Finite Impulse Response, a class of digital filter.
Fourier Analysis	Mathematical representation of a waveform as an infinite series of sine wave components, allowing the spectral content of the waveform to be determined and analysed.

filter	A device that passes certain frequencies and attenuates others.
frequency	The rate of repetition of a periodic waveform. Expressed in Hertz = cycles per second.
frequency response	The changes in the sensitivity of a system with respect to frequency.
gain	In a device, the ratio of output amplitude to input amplitude. When the gain is larger than one, amplification exists.
HRTF	Head Related Transfer Function, see BRIR.
IIR	Infinite Impulse Response, a class of digital filter.
ISO	The International Organization for Standardization. A worldwide federation of national standards bodies from some 130 countries.
ISO3382	International standard number 3382, on measuring the reverberation time of rooms from a RIR with reference to other acoustical parameters.
impedance	The opposition to the flow of a signal.
impulse	A waveform with significant amplitude only during a relatively brief portion of its period. An impulse has a very rich spectrum.
interface	The boundary or means of connection between two or more elements in a computer system. An interface can be between hardware devices, pieces of software or a user and a computer system.
interference	The combination of two or more signals results in an interaction called interference that can be constructive or destructive.
linear	(1) Characteristic of a phenomenon which always changes by the same amount over a given interval in time. (2) Characteristic of a system in which the doubling of the amplitude of the input signal results in an associated doubling in amplitude of the output signal.
localisation	The process of synthesizing cues that create the auditory illusion of the placement in space of a sound source.
MIDI	Musical Instrument Digital Interface, a standard communications protocol (generally) between electronic musical instruments.
mode	A room resonance, having their greatest effect at low frequencies and for small rooms.

MPEG	Motion Picture Expert Group. Have defined a number of standards for video and audio with particular regard to compression and decompression formats and algorithms.
noise	Generally a random signal of an electrical or acoustic nature, usually being an undesirable property.
Nyquist Frequency	The highest frequency of a signal that can be accurately represented by a discrete digital system, equal to half of the sampling frequency.
octave	The musical interval between two frequencies having a ratio of 2:1.
PC	Personal Computer.
Pentium MMX	A family of CPUs used as the main host processor in a PC. The Pentium MMX CPU is made by, and is a trademark of, the Intel Corporation.
phase	A means of comparing the relative position in time of two waveforms or of marking a specific point on a waveform.
pitch	A subjective term for the perceived frequency of a sound.
psychoacoustics	The study of the way humans perceive sound. It includes such subjective responses to sound as pitch, loudness, duration, timbre, and apparent location.
real-time	Characteristic of a process in which data is processed at the same rate as it is taken in or used.
resonance	A natural periodicity, or the reinforcement associated with this with this periodicity.
reverb	Abbreviation of reverberation; a term usually associated with audio processors designed to enhance an audio signal by adding a reverberant effect.
reverberation	The smooth and gradual decay of sound in an enclosed space after the original source has stopped. This is due to multiple overlapping sound reflections from the boundaries.
reverberation time	The time required for the sound in an enclosed space to decay by 60 dB from its initial level.
RIR	Room Impulse Response. The natural response of the soundfield in an enclosed space when excited by an impulsive sound source.
RFR	The frequency spectrum of a RIR.
room mode	The normal modes of vibration of an enclosed space. See mode.

RT_{60}	Reverberation time.
sampling	The process of representing a waveform by measuring its value at equally spaced, discrete points in time.
SMPTE	The Society of Motion Picture and Television Engineers.
signal	A temporal phenomenon that carries information.
signal processor	A device that modifies a signal passing through it.
spectrum	The representation of the distribution of energy of a signal in terms of its frequency components.
specular	A class of reflection where the angle of incidence equals the angle of reflection, differing from a diffuse reflection, where the sound wave energy is spread out in time and direction.
standing wave	A resonance condition in an enclosed space in which sound waves travelling in one direction interact with those travelling in the opposite direction resulting in a stable condition.
steady state response	The response of a filter to a constant signal.
stereo	A stereophonic system with two audio channels.
TDS	Time-delay spectrometry, a method for obtaining anechoic results in reverberant spaces.
timbre	The quality of a sound, related to its harmonic structure.
time domain	A way of characterising a signal in terms of its amplitude fluctuations against time. The representation of a signal in the time domain is called its waveform.
transaural	An enhanced stereo playback system where the signal from each loudspeaker is delivered to one ear rather than both using cross-talk cancellation.
transducer	A device that converts energy from one form into another. For example, mechanical energy, such as a sound wave can be transduced into electrical signals using a microphone.
transient	A short-lived signal, or aspect of a signal.
waveform	The continuous sequence of displacement or pressure (or any other appropriate variable) differences making up one or more complete cycles of a complex vibration or wave.
WAV	A standardised audio file format.

References

- [Adey et al, 2000] R. A. Adey, S. M. Niku, J. Baynham and P. Burns, “Acoustic diagnostic analysis using Boundary Elements”, <http://www.beasy.com>, Computational Mechanics Publications, BEASY, Southampton, England.
- [Aird, 1999] M. L. Aird, “Physical Modelling Of Percussion Instruments Using Digital Waveguide Meshes”, unpublished manuscript, 1999.
- [Akhtarzad and Johns, 1975] S. Akhtarzad and P. B. Johns, “The Solution of Maxwell’s Equations in 3 Space Dimensions and Time by the TLM Method of Numerical Analysis”, *Proceedings of the IEE*, Vol. 122, No. 12, pp. 1344-1348, 1975.
- [Ando, 1985] Y. Ando, “Concert Hall Acoustics”, Springer-Verlag, Berlin, 1985.
- [Ballan et al, 1994] O. Ballan, L. Mozzoni and D. Rocchesso, “Sound Spatialisation in Real Time by First Reflection Simulation”, *Proceedings of the International Computer Music Conference*, pp. 475-476, Denmark, 1994.
- [Barron, 1993] M. Barron, “Auditorium Acoustics and Architectural Design”, E & FN Spon, An Imprint of Chapman & Hall, London, 1993.
- [Bamford and Vanderkooy, 1995] J. S. Bamford and J. Vanderkooy, “Ambisonic Sound for Us”, *Presented at the 99th Audio Engineering Society Convention*, October 1995, Preprint 4138 (O-4), 1995.
- [Begault, 1991] D. R. Begault, “Challenges to the Successful Implementation of 3-D Sound”, *Journal of the Audio Engineering Society*, Vol. 39, No. 11, pp. 864-870, Nov 1991.
- [Begault, 1994] D. R. Begault, “3-D Sound for Virtual Reality and Multimedia”, AP Professional, Academic Press Limited, London, 1994.
- [Beranek 1962] Leo L. Beranek, “Music, Acoustics and Architecture”, John Wiley and Sons Inc, New York, 1962.

-
- [Botteldooren, 1995] D. Botteldooren, “Finite-difference time-domain simulation of low-frequency room acoustic problems”, *Journal of the Acoustical Society of America*, Vol. 98, No. 6, pp. 3302-3308, December 1995.
- [Brillouin, 1953] L. Brillouin, “Wave Propagation in Periodic Structures: Electric Filters and Crystal Lattices”, Second Edition, Dover Publications, Inc. New York, 1953.
- [Campos, 1999] G. Campos, “Three-Dimensional Waveguide Mesh Modelling for Room Acoustic Simulation: MPhil/DPhil Transfer Report”, Department of Electronics, University of York, unpublished, April 1999.
- [Davis and Jones, 1989] G. Davis and R. Jones, “Yamaha Sound Reinforcement Handbook”, Hal Leonard Publishing, Milwaukee, 1989.
- [De Poli and Rocchesso, 1998] G. De Poli and D. Rocchesso, “Tutorial Article: Physically Based Sound Modelling”, *Organised Sound*, Vol. 3, No.1, pp. 61-76, 1998.
- [Dhillon, 1994] N. S. Dhillon, “Cellular Approach for Modelling Room Acoustics: A Framework for Implementation Based on the Ray Tracing Algorithm”, Master of Science Thesis, Dept. of Electrical Engineering, University of Wisconsin, Madison, USA, <http://home1.gte.net/dhillon/camra/index.html>, 1994.
- [Dodge and Jerse, 1985] C. Dodge and T. A. Jerse, “Computer Music - Synthesis, Composition, and Performance”, Schirmer, New York, 1985.
- [Everest, 1994] F. A. Everest, “The Master Handbook of Acoustics, 3rd Edition”, TAB Books, McGraw-Hill Inc, Blue Ridge Summit, PA, 1994.
- [Farina, 1995] A. Farina, “RAMSETE - a new Pyramid Tracer for medium and large scale acoustic problems”, *Proceedings of EURO-NOISE 95 Conference*, Lyon, France, 21-23, March 1995; http://pcangelo.ramsete.com/list_pub.htm
- [Farina and Righini, 1999] A. Farina and F. Righini, “AURORA 3.0 Home Page, Software auralization on a standard multi-media PC”, <http://pcfarina.eng.unipr.it/aurora/>, 1999.
- [Fontana and Rocchesso, 1995] F. Fontana and D. Rocchesso, “A New Formulation of the 2D-Waveguide Mesh for Percussion Instruments”, *Proceedings of the XI Colloquium on Musical Informatics*, pp. 27-30, Bologna, Italy, November 1995.

-
- [Fontana and Rocchesso, 1999] F. Fontana and D. Rocchesso, “Signal-Theoretic Characterization of Waveguide Mesh Geometries for Models of Two-Dimensional Wave Propagation in Elastic Media”, Submitted to *The IEEE Transactions on Speech and Audio*, 1999.
- [Geest and McCulloch, 1998] “The Virtual Room: Deriving Acoustic Characteristics By Modelling”, *Proceedings of the Institute of Acoustics - Reproduced Sound 14*, Vol. 20, Part 5, pp. 169-180, 1998.
- [Gerzon, 1992] M. A. Gerzon, “General Metatheory of Auditory Localisation”, *Presented at the 92nd Audio Engineering Society Convention*, March 1992, Preprint 3306, 1992.
- [Hibbitt et al. 1999] Hibbitt, Karlsson & Sorensen, Inc, “ABAQUS Home Page - Finite Element Analysis Products”, <http://www.hks.com>, 1999.
- [Howard and Angus, 1996] D. M. Howard and J. A. S. Angus, “Acoustics and Psychoacoustics”, Focal Press, Butterworth-Heinemann, Oxford, 1996.
- [Hugonnet and Walder, 1998] C. Hugonnet and P. Walder, “Stereophonic Sound Recording Theory and Practice”, John Wiley and Sons Ltd, Chichester, England, 1998.
- [Huopaniemi et al, 1997] J. Huopaniemi, L. Savioja and M. Karjalainen, “Modelling of Reflections and Air Absorption in Acoustical Spaces – A Digital Filter Design Approach”, *Proceedings of the 1997 IEEE Workshop on Applications of Signal Processing to Audio and Acoustics (WASPAA'97)*, Session 5.2, Mohonk Mountain House, New Paltz, New York, Oct. 19-22,1997; <http://www.acoustics.hut.fi/~ruba/pubs/>
- [ISO3382, 1997] International Standard 3382, “Acoustics – Measurement of reverberation time of rooms with reference to other acoustical parameters”, ISO, Second Edition, 1997.
- [Johns and Beurle, 1971] P. B. Johns and R. L. Beurle, “Numerical Solution of 2-dimensional Scattering Problems Using a Transmission-Line Matrix”, *Proceedings of the IEE*, Vol. 118, No. 9, pp. 1203-1208, September, 1971.
- [Kleiner et al, 1993] M. Kleiner, B. Dalenbäck and P. Svensson “Auralisation - an Overview”, *Journal of the Audio Engineering Society*, Vol. 41, No. 11, pp. 861-875, Nov 1993.

-
- [Krokstad et al, 1968] A. Krokstad, S. Strøm and S. Sørsdal, “Calculating the Acoustical Room Response by the Use of a Ray Tracing Technique”, *Journal of Sound Vibration*, Vol. 8, No. 1, pp. 118-125, 1968.
- [Laird et al, 1998] J. Laird, P. Masri and C. N. Canagarajah, “Efficient and Accurate Synthesis of Circular Membranes Using Digital Waveguides”, *Proceedings of the IEE Colloquium on Audio and music technology: The creative challenge of DSP*, IEE Digest 98/470, pp. 12/1-12/6, 1998.
- [Laird, 1999] J. Laird, “Derivation of the phase delay caused by a 2D Triangular Digital Waveguide Mesh”, unpublished manuscript, 1999.
- [Laird et al, 1999] J. Laird, P. Masri and C. N. Canagarajah, “Modelling Diffusion at the Boundary of a Digital Waveguide Mesh”, *Proceedings of the International Computer Music Conference*, pp. 492-495, Hong Kong, 1999.
- [Lake Technology Ltd, 1999] Lake Technology Limited, “Lake DSP Homepage”, <http://www.lakedsp.com/index.htm>, 1999.
- [Lynn and Fuerst, 1996] P. A. Lynn and W. Fuerst, “Introductory Digital Signal Processing With Computer Applications, Revised Edition”, John Wiley and Sons Ltd, Chichester, England, 1996.
- [MacDonald, 1995] A. MacDonald, “Performance Practice in the Presentation of Electroacoustic Music”, *Computer Music Journal*, Vol. 19, No. 4, pp. 88-92, 1995.
- [Malham, 1998] D.G. Malham, “Sound Spatialisation”, *1998 Workshop on Digital Audio Effects (DAFX98)*, pp. 62-70, November 19-21, 1998, Barcelona, Spain.
- [Malham and Myatt, 1995] D. G. Malham and A. Myatt, “3-D Sound Spatialisation Using Ambisonic Techniques”, *Computer Music Journal*, Vol. 19, No. 2, pp. 58-70, 1995.
- [Markel and Gray, 1976] J.D. Markel and A.H. Gray, “Linear Prediction of Speech”, Springer-Verlag, Berlin, 1976.
- [Moorer, 1979] J. A. Moorer, “About this Reverberation Business”, *Computer Music Journal*, Vol. 3, No. 2, pp. 13-27, 1979.

-
- [Murphy and Howard, 1998a] D.T. Murphy and D.M. Howard, “A multi-channel spatial simulation system for computer music applications”, *Proceedings of the 1998 Institute of Acoustics Conference, Reproduced Sound 14*, pp. 161-168, Oct 22-25, 1998, Windermere, England, Vol. 20: Part 5 (1998).
- [Murphy and Howard, 1998b] D.T. Murphy and D.M. Howard, “Modelling and directionally encoding the acoustics of a room”, *Electronics Letters*, Vol. 34, No. 9, 1998, pp. 864-865.
- [Murphy and Howard, 1999a] D.T. Murphy and D.M. Howard, “Physically modelling the acoustics of a room using a digital waveguide mesh”, *Proceedings of the 25th Euromicro Conference*, Milan, pp. 82-89, Italy, Sept. 8-10, 1999.
- [Murphy and Howard, 1999b] D.T. Murphy and D.M. Howard, “The WaveVerb Multi-Channel Room Acoustics Modelling System”, *Proceedings of the International Computer Music Conference, Hong Kong*, pp. 472-475, Oct. 22-27, 1999.
- [Murphy et al, 1998] D.T. Murphy, D.M. Howard and A.M. Tyrrell, “Multi-channel reverberation for computer music applications”, *Proceedings of the 1998 IEEE Workshop on Signal Processing Systems*, pp. 210-219, Oct 8-10, 1998, Boston, USA.
- [Naylor, 1993] G. M. Naylor, “ODEON - Another Hybrid Room Acoustical Model”, *Applied Acoustics*, Vol. 38, pp. 131-143, 1993.
- [Niku et al, 2000], S. M. Niku, R. A. Adey and T. R. Bridges, “Application of BEASY to Industrial and Environmental Acoustics”, <http://www.beasy.com>, Computational Mechanics Publications, BEASY, Southampton, England.
- [Physics Review, 1996a] “Listening Posts”, *Physics Review*, Vol. 6, No. 2, pp. 34, November 1996 – No Author Name Supplied.
- [Physics Review, 1996b] “The Secret of Acoustics”, *Physics Review*, Vol. 6, No. 2, pp. 7, November 1996 – No Author Name Supplied.
- [Pomeroy and Jaycocks, 1996] S. C. Pomeroy and R. Jaycocks, “Propagation, Scattering and Moving Objects Modelled Using the Transmission Line Matrix Method (TLM)”, *Proceedings of the Institute of Acoustics*, Vol. 18, Part 10, pp. 123-129, 1996.

-
- [Rabiner and Schafer, 1978] L. Rabiner and R. W. Schafer, “Digital Processing of Speech Signals”, Prentice Hall Engineering, Georgia Institute of Technology, Englewood Cliffs, New Jersey, 1978.
- [Rayleigh, 1945] Rayleigh, “The Theory of Sound”, Volume II, Macmillan Company 1896, Reprinted Dover Publications, New York, 1945.
- [Reilly and McGrath, 1995] A. Reilly and D. McGrath, “Convolution Processing for Realistic Reverberation”, *Audio Engineering Society Preprint No. 3977(13)*, 98th AES Convention, Feb 1995.
- [Rife and Vanderkooy, 1989] D. D. Rife and J. Vanderkooy, “Transfer-Function Measurement with Maximum-Length Sequences”, *Journal of the Audio Engineering Society*, Vol. 37, No. 6, pp. 419-444, Jun 1989.
- [Riley, 1994] R. Riley, “Famous Names, How to Choose and Use a Professional Recording Studio”, *Future Music*, Supplement, pp. 14-15, June 1994.
- [Roads, 1995] C. Roads, “The Computer Music Tutorial”, Cambridge, MIT Press, 1995.
- [Robjohns, 1999] H. Robjohns, “In A Space: Preview: The technology behind Sony’s DRE 777 Sampling Reverb”, *Sound On Sound*, Vol. 14, No. 8, pp. 108-110, June 1999.
- [Rossiter et al, 1996] D. Rossiter, A. Horner, G. Baciú, “Visualization and Manipulation of 3D Digital Waveguide Structures for Sound Experimentation”, *Proceeding of the International Computer Music Conference*, pp. 43-46, Hong Kong, 1996.
- [Sabine, 1964] W. C. Sabine, “Collected Papers on Acoustics”, Dover Publications Inc, New York, 1964.
- [Savioja, 1997] L. Savioja, “Derivation of 1D termination boundary conditions on the rectilinear digital waveguide mesh”, unpublished manuscript, 1997.
- [Savioja et al. 1994] L. Savioja, T. J. Rinne and T. Takala, “Simulation of Room Acoustics with a 3-D Finite Difference Mesh”, *Proceedings of the International Computer Music Conference*, pp. 463-466, Denmark, 1994.

-
- [Savioja et al. 1995] L. Savioja, J. Backman, A. Järvinen and T. Takala, “Waveguide Mesh Method for Low-Frequency Simulation of Room Acoustics”, *Proceedings of the International Congress on Acoustics*, Trondheim, Norway, Vol. 2, pp. 637-641, June 26-30, 1995.
- [Savioja et al. 1996a] L. Savioja, A. Järvinen, K. Melkas and K. Saarinen, “Determination of the Low Frequency Behaviour of an IEC Listening Room”, *Proceedings of the Nordic Acoustical Meeting*, Helsinki, Finland, pp. 55-58, June 12-14, 1996.
- [Savioja et al. 1996b] L. Savioja, M. Karjalainen and T. Takala, “DSP Formulation of a Finite Difference Method for Room Acoustics Simulation”, *Proceedings of NORSIG’96 IEEE Nordic Signal Processing Symposium*, pp. 455-458, Espoo, Finland, Sept 24-27, 1996.
- [Savioja and Välimäki, 1996] L. Savioja and V. Välimäki, “The Bilinearly Deinterpolated Waveguide Mesh”, *Proceedings of NORSIG’96 IEEE Nordic Signal Processing Symposium*, pp. 443-446, Espoo, Finland, Sept 24-27, 1996.
- [Savioja and Välimäki, 1999a] L. Savioja and V. Välimäki, “Reduction of the Dispersion Error in the Interpolated Digital Waveguide Mesh Using Frequency Warping”, *Proceedings of IEEE International Conference on Acoustics, Speech, and Signal Processing (ICASSP’99)*, Vol. 2, pp. 973-976, Phoenix, Arizona, March 15-19, 1999.
- [Savioja and Välimäki, 1999b] L. Savioja and V. Välimäki, “Reduction of the dispersion error in the triangular digital waveguide mesh using frequency warping”, *IEEE Signal Processing Letters*, Vol. 6, No. 3, pp. 58-60, Mar. 1999.
- [Schroeder and Logan, 1961] M. R. Schroeder and B. F. Logan, “‘Colorless’ Artificial Reverberation”, *Journal of the Audio Engineering Society*, Vol. 9, No. 3, pp. 192-197, Jul 1961.
- [Schroeder, 1962] M. R. Schroeder, “Natural Sounding Artificial Reverberation”, *Journal of the Audio Engineering Society*, Vol. 10, No. 3, pp. 219-223, Jul 1962.
- [Scott, 1998] D. Scott, “Audio and Musical Applications for Silicon Graphics Systems: Performance Hints for Signal Processing Applications”,
<http://reality.sgi.com/dscott/audio.apps/dev/sp.html>, 1998.

-
- [Smith, 1992] J. O. Smith, “Physical modelling using digital waveguides”, *Computer Music Journal*, Vol. 16, No. 4, pp. 74-87, Winter 1992.
- [Stephenson, 1990] U. Stephenson, “Comparison of the Mirror Image Source Method and the Sound Particle Simulation Method”, *Applied Acoustics*, No. 29, pp. 35-72, 1990.
- [Syntrillium, 1999] Syntrillium Software Corporation, “Cool Edit Pro Homepage”, <http://www.syntrillium.com/cep/index.html>, 1999.
- [Todoroff, 1995] T. Todoroff “Real-Time Granular Morphing and Spatialisation of Sounds With Gestural Control Within MAX/FTS”, *Proceedings of the International Computer Music Conference*, pp. 315-318, 1995.
- [Tronchin and Farina, 1997] L. Tronchin and A. Farina, “Acoustics of the Former Teatro “La Fenice” in Venice”, *Journal of the Audio Engineering Society*, Vol. 45, No. 12, pp. 1051-1062, Dec. 1997.
- [Välämäki et al, 1996] V. Välämäki, R. Hänninen, and M. Karjalainen, “An improved digital waveguide model of a Flute: implementation issues”, *Proceedings of the International Computer Music Conference 1996*, pp. 1-4, Hong Kong, Aug 19-24, 1996.
- [Van Duyne and Smith, 1993] S. A. Van Duyne and J. O. Smith III, “Physical Modeling with the 2-D Digital Waveguide Mesh”, *Proceedings of the International Computer Music Conference*, pp. 40-47, Tokyo, Japan, 1993.
- [Van Duyne et al, 1994] S. A. Van Duyne, J. R. Pierce, and J. O. Smith III, “Travelling Wave Implementation of A Lossless Mode-Coupling Filter and The Wave Digital Hammer”, *Proceedings of the International Computer Music Conference*, pp. 411-418, Denmark, 1994.
- [Van Duyne and Smith, 1994] S. A. Van Duyne and J. O. Smith III, “A Simplified Approach to Modelling Dispersion Caused by Stiffness in Strings and Plates”, *Proceedings of the International Computer Music Conference*, pp. 407-410, Denmark, 1994.
- [Van Duyne and Smith, 1995] S. A. Van Duyne and J. O. Smith III, “The Tetrahedral Digital Waveguide Mesh”, *Proceedings of the IEEE Workshop on the Application of Signal Processing to Audio and Acoustics*, pp. 1-4, Mohonk, 1995.

-
- [Van Duyne and Smith, 1996] S. A. Van Duyne and J. O. Smith III, “The 3D Tetrahedral Digital Waveguide Mesh with Musical Applications”, *Proceedings of the International Computer Music Conference*, pp. 9-16, Hong Kong, 1996.
- [Wadhams, 1990] W. Wadhams, “Sound Advice - The Musician's Guide to the Recording Studio”, Schirmer, New York, 1990.
- [Wang, 1994] J. Wang, “Architectural acoustics in China – Past and present”, *Proceedings of the Acoustical Society of America, Wallace Clement Sabine Centennial Symposium*, Cambridge, Massachusetts, pp. 21-24, 5-7 June, 1994.
- [White, 1995a] P. White, “Right On - Scott Willing of QSound Labs”, *Sound on Sound*, Vol. 11, No. 1, Nov 1995; http://www.sospubs.co.uk/sos/1995_articles/nov95/qsound.html
- [White, 1995b] P. White, “Beyond the Boundary: All About The Boundary Effect”, *Sound on Sound*, Vol. 11, No. 2, pp. 42-23, December 1995.
- [Wishart, 1996] T. Wishart, “On Sonic Art”, Harwood Academic, Amsterdam, 1996.
- [Woo et al, 1997] M. Woo, J. Neider and T. Davis, “OpenGL Programming Guide, 2nd Edition: The Official Guide to Learning OpenGL, Version 1.1”, Addison-Wesley, Reading, Massachusetts, 1997.
- [Woram, 1989] J. M. Woram, “Sound Recording Handbook”, Howard W Sams and Company, Indianapolis, 1989.
- [Wright, 1995] J. R. Wright, “An Exact Model of Acoustic Radiation in Enclosed Spaces”, *Journal of the Audio Engineering Society*, Vol. 43, No. 10, pp. 813-820, October 1995.
- [Wright, 1998] J. R. Wright, “Seeing Sound”, *Proceedings of the Institute of Acoustics – Reproduced Sound 14*, Vol. 20, Part 5, pp. 147-150, 1998.
